Synthesis of hybrid magnetic carbon nanocomposites for catalytic wet peroxide oxidation

Rui S. Ribeiro

Dissertation presented for the Ph.D. degree in the
Doctoral Program in Chemical and Biological Engineering at the Faculty of Engineering, University of Porto, Portugal

Supervisor: **Joaquim L. Faria**
Co-supervisors: **Helder T. Gomes**
Adrián M.T. Silva

Associate Laboratory LSRE-LCM
Department of Chemical Engineering
Faculty of Engineering, University of Porto
Portugal

July, 2018

“It is far better to light the candle than to curse the darkness”

- William L. Watkinson

PREFACE

- People need water as they need oxygen; without it, life could not exist.

Water has always been intrinsically connected with all aspects of the human development. However, since humans started to settle down and form population clusters, including cities, the ability of natural water purification processes to promote wastewater recycling has been surpassed by the potable water requirements for human activities. Nowadays, with the increasing scarcity of clean water sources, and the dramatic rise of the world population, artificial water management methods became of utmost importance, namely for wastewater treatment and reuse. Consequently, there is a clear demand for further action in the water sector worldwide, Portugal included. As a young researcher I want to do something in this regard.

In a broad perspective, through the Ph.D. studies herein presented —performed from July, 2014 to June, 2018— I was able to participate in the settling of an alternative technology for the treatment of recalcitrant organic pollutants typically not treatable by conventional means of water treatment. This Ph.D. dissertation can therefore be considered a first step to achieve my long-term career purpose.

International research articles are easier disseminated and accessible to a larger part of the scientific community when compared to Ph.D. dissertations, while also allowing an ongoing evaluation of the work progress. Bearing this in mind, publishing research articles during the period of these Ph.D. studies was considered the most suitable pathway to achieve my personal and scientific goals. As a result of this approach, this Ph.D. dissertation gathers the most significant findings arising from the tasks I have performed during all the steps involved in the preparation of 7 scientific articles published in international peer reviewed ISI indexed journals:

Rui S. Ribeiro, Adrián M.T. Silva, José L. Figueiredo, Joaquim L. Faria, Helder T. Gomes, Catalytic wet peroxide oxidation: a route towards the application of hybrid magnetic carbon nanocomposites for the degradation of organic pollutants. A review, Appl. Catal. B 187 (2016) 428-460
DOI: 10.1016/j.apcatb.2016.01.033

Rui S. Ribeiro, Adrián M.T. Silva, Maria T. Pinho, José L. Figueiredo, Joaquim L. Faria, Helder T. Gomes, Development of glycerol-based metal-free carbon materials for environmental catalytic applications, Catal. Today 240, Part A (2015) 61-66
DOI: 10.1016/j.cattod.2014.03.048

Rui S. Ribeiro, Adrián M.T. Silva, Luisa M. Pastrana-Martínez, José L. Figueiredo, Joaquim L. Faria, Helder T. Gomes, Graphene-based materials for the catalytic wet peroxide oxidation of highly concentrated 4-nitrophenol solutions, Catal. Today 249 (2015) 204-212
DOI: 10.1016/j.cattod.2014.10.004

Rui S. Ribeiro, Adrián M.T. Silva, José L. Figueiredo, Joaquim L. Faria, Helder T. Gomes, The role of cobalt in bimetallic iron-cobalt magnetic carbon xerogels developed for catalytic wet peroxide oxidation, Catal. Today 296 (2017) 66-75
DOI: 10.1016/j.cattod.2017.06.023

Rui S. Ribeiro, Adrián M.T. Silva, Pedro B. Tavares, José L. Figueiredo, Joaquim L. Faria, Helder T. Gomes, Hybrid magnetic graphitic nanocomposites for catalytic wet peroxide oxidation applications, Catal. Today 280 (2017) 184-191
DOI: 10.1016/j.cattod.2016.04.040

Rui S. Ribeiro, Zacharias Frontistis, Dionissios Mantzavinos, Danae Venieri, Maria Antonopoulou, Ioannis K. Konstantinou, Adrián M.T. Silva, Joaquim L. Faria, Helder T. Gomes, Magnetic carbon xerogels for the catalytic wet peroxide oxidation of sulfamethoxazole in environmentally relevant water matrices, Appl. Catal. B 199 (2016) 170-186
DOI: 10.1016/j.apcatb.2016.06.021

Rui S. Ribeiro, Raquel O. Rodrigues, Adrián M.T. Silva, Pedro B. Tavares, Ana M.C. Carvalho, José L. Figueiredo, Joaquim L. Faria, Helder T. Gomes, Hybrid magnetic graphitic nanocomposites towards catalytic wet peroxide oxidation of the liquid effluent from a mechanical biological treatment plant for municipal solid waste, Appl. Catal. B 219 (2017) 645-657
DOI: 10.1016/j.apcatb.2017.08.013

ACKNOWLEDGMENTS

I would like to express my heartfelt gratitude towards my supervisors for their overwhelming support, encouragement and mentorship throughout all the work, while at the same time, they have provided me a great deal of autonomy and the chance to develop my independent thinking skills. In particular, I thank Professor Joaquim L. Faria for the insightful advices and the long-term perspective he instilled me; I thank Professor Helder T. Gomes for the friendship, patience and for being always available; and I thank Doctor Adrián M.T. Silva for the countless insightful comments but, most of all, for being a role model as both a passionate and a successful young researcher - inspiring me to pursue a career in scientific research.

I thank FCT - Fundação para a Ciência e a Tecnologia, for the individual Ph.D. grant SFRH/BD/94177/2013, with financing from the European Social Fund (through POPH and QREN) and by national funds through FCT and MCTES - Ministério da Ciência, Tecnologia e Ensino Superior.

I am also very grateful to the co-authors of the research articles published during the period of these Ph.D. studies, for their important contribution towards the overall study, namely Professors Danae Venieri, Dionissios Mantzavinos, Ioannis Konstantinou, José L. Figueiredo and Pedro B. Tavares, Doctors Luisa Pastrana-Martínez, Maria Antonopoulou and Zacharias Frontistis, and Mss. Ana M.C. Carvalho, Maria T. Pinho and Raquel O. Rodrigues.

I also thank Professor Dionissios Mantzavinos, Doctor Zacharias Frontistis and COST - European Cooperation in Science and Technology, through the COST Action ES1403: New and emerging challenges and opportunities in wastewater reuse (NEREUS), for the opportunity to perform a short-term scientific mission for advanced training at the University of Patras, Greece. This experience contributed immensely to this thesis and to my personal enrichment.

I acknowledge the role of the Associate Laboratory LSRE-LCM, both located at the Faculty of Engineering, University of Porto (FEUP), and at the Polytechnic Institute of Bragança (IPB), for providing the facilities, services and resources required to conduct this study. Specifically, this work was financially supported by: Project POCI-01-0145-FEDER-006984 – Associate Laboratory LSRE-LCM funded by FEDER through COMPETE2020 —Programa Operacional Competitividade e Internacionalização (POCI)— and by national funds through FCT.

I also thank Maria João Afonso and Professor Olga Ferreira for all the technical support I was given at the *Laboratório de Processos Químicos*, Polytechnic Institute of Bragança; and David Cabral for the support regarding atomic absorption spectroscopy analysis.

On a personal basis, I thank my parents - Eduarda and Justino, and my sister - Joana, to whom I owe everything I have achieved and everything I turned out to be.

Raquel, thank you very much for your love, friendship, and unconditional support, and for providing me the strength, confidence and motivation required to keep pushing forward regardless of all the difficulties, problems and obstacles I found ever since you have come into my life. Thank you very much for the endless discussions we engaged in, which contributed a great deal to improve the quality of this thesis; you know what I mean!

ABSTRACT

Catalyst design plays a crucial role in catalytic wet peroxide oxidation (CWPO), since this water treatment technology relies on the catalytic decomposition of hydrogen peroxide (H_2O_2) via formation of hydroxyl radicals ($HO^{\bullet}$), which are very powerful and effective oxidants for the destruction of a huge range of recalcitrant organic pollutants. Several motivations have prompted the present Ph.D. studies on the synthesis and application of hybrid magnetic carbon nanocomposites in CWPO. Among these, a special focus was given to the synergies that can arise from the combination of highly active and magnetically separable iron species with the easily tuned properties of carbon-based materials. Bearing this in mind, the main objective of my studies was the synthesis of hybrid magnetic carbon nanocomposites with high activity and stability characteristics for the CWPO of organic pollutants typically untreatable by conventional biological means.

The first stage was devoted to the study of metal-free carbon materials. The results obtained highlighted the importance of the interplay between chemical and textural properties when developing efficient carbon-based catalysts for CWPO. Also of relevance were the adsorptive interactions between the pollutant molecules and the surface of the catalysts, when seeking for highly efficient CWPO applications.

Within the hybrid magnetic carbon composites, carbon structures decorated with magnetic particles were initially studied. For that purpose, magnetic carbon xerogels consisting of interconnected carbon microspheres with iron and/or cobalt microparticles embedded in their structure were prepared by inclusion of metal precursors during the sol-gel polymerization of resorcinol and formaldehyde, followed by thermal annealing. The results revealed a clear synergy arising from the simultaneous inclusion of iron and cobalt species within carbon frameworks, which was ascribed to (i) the enhanced accessibility to the active iron species at the surface of the catalyst promoted by the simultaneous incorporation of cobalt, (ii) the ability of metallic Co to catalyse H_2O_2 decomposition via $HO^{\bullet}$ radicals formation, and (iii) the efficient reduction of Fe^{3+} to Fe^{2+} promoted by metallic Co on the surface of the bimetallic catalyst.

Hybrid structures were considered afterwards in which the magnetic phase is protected against the environment by a carbonaceous shell. For that purpose, a hybrid magnetic graphitic nanocomposite, composed by a magnetite core and a graphitic shell, was synthesized by hierarchical co-assembly of magnetite nanoparticles and carbon precursors, followed by thermal annealing. It was found that the encapsulation of magnetite nanoparticles within carbon frameworks (iv) enhances the catalytic activity in CWPO when

compared to bare magnetite, while (v) strongly limiting the leaching of iron species to the treated water.

A high-performance hybrid magnetic graphitic nanocomposite, composed by a cobalt ferrite core and a graphitic shell ($CoFe_2O_4$/MGNC), was then prepared based on the findings previously obtained. The positive effects described in (ii) to (iv) were in this way potentially combined in the same nanocomposite. The application of this new generation catalyst enabled the treatment of a liquid effluent from a mechanical biological treatment plant for municipal solid waste, regardless of its very high pollutant load. In addition, a magnetic separation system was developed for the *in-situ* recovery of $CoFe_2O_4$/MGNC after the CWPO reaction stage. This approach allowed demonstrating the high stability of $CoFe_2O_4$/MGNC for CWPO, through a series of five CWPO reaction/magnetic separation sequential experiments performed in the same vessel.

Although the works reported followed a current trend towards the application of CWPO under intensified conditions (i.e., with higher pollutant concentrations and lower catalyst loads), the ability of this water treatment technology for the elimination of contaminants of emerging concern was also evaluated. Specifically, the ability of CWPO for the degradation of the antimicrobial agent sulfamethoxazole in secondary treated wastewater was shown in a case-study performed during a short-term scientific mission for advanced training at the University of Patras, Greece, under the framework of COST Action ES1403: NEREUS.

Summarizing, the knowledge on the surface reactions and interactions involved when CWPO is carried out in the presence of hybrid magnetic carbon nanocomposites, is the main contribution of my Ph.D. dissertation. This knowledge is fundamental for the design of materials with potential effectiveness for real-scale applications.

RESUMO

O desenvolvimento de catalisadores é crucial para a oxidação húmida catalítica com peróxido de hidrogénio (*catalytic wet peroxide oxidation* - CWPO), dado que esta tecnologia de tratamento de águas tem como base a decomposição catalítica de peróxido de hidrogénio (H_2O_2) via formação de radicais hidroxilo ($HO^{\bullet}$) —espécies com forte carater oxidante e capazes de promover a degradação de uma enorme variedade de poluentes orgânicos recalcitrantes. Foram várias as motivações que estiveram na origem destes estudos de doutoramento dedicados à síntese de compósitos nanoestruturados, contendo nanomateriais magnéticos e materiais de carbono, para aplicação em CWPO. Entre estas, foi dada particular atenção às sinergias que poderão resultar da combinação de espécies de ferro com elevada atividade e propriedades magnéticas, com materiais de carbono possuindo propriedades facilmente ajustadas. Tendo isto em consideração, o principal objetivo destes estudos centrou-se na síntese de compósitos nanoestruturados, contendo nanomateriais magnéticos e materiais de carbono, com elevada atividade e estabilidade para a CWPO de poluentes orgânicos não passiveis de tratamento por métodos biológicos convencionais.

A primeira etapa incidiu no estudo de materiais de carbono sem metais. Os resultados obtidos salientaram a necessidade de manter um equilíbrio entre as propriedades químicas e estruturais quando se pretende desenvolver materiais à base de carbono com elevada eficiência para CWPO. Também relevantes são as interações entre as moléculas de poluente e a superfície dos catalisadores (adsorção), quando se pretende aplicações de CWPO com elevada eficiência.

Entre os compósitos estruturados, o estudo iniciou-se com estruturas de carbono decoradas com partículas magnéticas. Para esse propósito foram preparados xerogéis de carbono magnéticos com microesferas de ferro e/ou cobalto embutidas na sua estrutura, resultantes da inclusão a partir de precursores metálicos durante a polimerização sol-gel do resorcinol com o formaldeído, seguida de redução térmica. Os resultados obtidos revelaram que a incorporação simultânea de espécies de ferro e de cobalto na estrutura de carbono origina a uma clara sinergia, como resultado (i) da maior acessibilidade aos centros ativos de ferro presentes na superfície do catalisador, promovida pela incorporação simultânea de cobalto, (ii) da capacidade do Co metálico catalisar a decomposição de H_2O_2 via formação de radicais $HO^{\bullet}$, e (iii) da redução eficiente de Fe^{3+} a Fe^{2+} promovida pelo Co metálico existente à superfície do catalisador bimetálico.

De seguida foram utilizadas estruturas híbridas, em que a fase magnética é protegida por um recobrimento de carbono. Para esse propósito foi preparado um híbrido magnético à base

de um nanocompósito grafítico, com núcleo de magnetite revestido de material grafítico, através da associação hierárquica de nanopartículas de magnetite a precursores de carbono, seguida de redução térmica. Verificou-se que (iv) a atividade catalítica da magnetite é melhorada pela sua encapsulação na estrutura de carbono, ao mesmo tempo que (v) a lixiviação de ferro para a água tratada é fortemente contida.

Com base nos resultados obtidos anteriormente, foi preparado um híbrido magnético à base de um nanocompósito grafítico de elevada performance, composto por núcleo de ferrite de cobalto e um revestimento de material grafítico ($CoFe_2O_4$/MGNC). Desta forma, os efeitos positivos descritos nos pontos (ii) a (iv) foram potencialmente combinados no mesmo nanocompósito. A aplicação deste catalisador de última geração permitiu efetuar o tratamento de um efluente líquido de uma unidade de tratamento mecânico e biológico de resíduos sólidos urbanos, apesar da sua elevada carga poluente. Para além disso, foi desenvolvido um sistema de separação magnética para a recuperação *in-situ* do $CoFe_2O_4$/MGNC após a etapa de reação de CWPO. Esta abordagem permitiu a demonstração da elevada estabilidade do $CoFe_2O_4$/MGNC em CWPO, nomeadamente através de uma série de cinco experiências sequenciais de reação CWPO/separação magnética realizada no mesmo recipiente.

Embora os trabalhos reportados sigam uma tendência corrente para a aplicação da CWPO sob condições intensivas (i.e., com maiores concentrações de poluente e menores cargas de catalisador), também foi avaliada a capacidade desta tecnologia de tratamento de águas na eliminação de poluentes de preocupação emergente. Concretamente, foi demonstrada a capacidade da CWPO promover a degradação do agente antimicrobiano sulfametoxazol, presente em água residual tratada por métodos biológicos convencionais, num estudo efetuado durante uma missão científica de curta duração para formação avançada realizada na Universidade de Patras, Grécia, no âmbito da Ação COST ES1403: NEREUS.

Em suma, a contribuição para o conhecimento das reações e das interações superficiais envolvidas quando a CWPO é levada a cabo na presença de compósitos nanoestruturados, contendo materiais magnéticos e de carbono, é o principal contributo da minha dissertação de doutoramento. Este conhecimento é fundamental na criação de materiais potencialmente eficazes para aplicações à escala real.

TABLE OF CONTENTS

LIST OF FIGURES

LIST OF TABLES

GLOSSARY

Most used abbreviations

2-NP	2-nitrophenol
4-NP	4-nitrophenol
AC	Activated carbon
AOP	Advanced oxidation processes
ARB&ARG	Antibiotic resistant bacteria and/or resistance genes
$Aromaticity_{app}$	Apparent aromaticity
BOD_5	5-Day biochemical oxygen demand
$BOD_{5,\ app}$	Apparent 5-day biochemical oxygen demand
CNT	Carbon nanotubes
COD	Chemical oxygen demand
COD_{app}	Apparent chemical oxygen demand
CWPO	Catalytic wet peroxide oxidation
DOC	Dissolved organic carbon
d_{pore}	Average pore diameter
$d_{Removal}$	Difference in the pollutant percent removal between catalytic wet peroxide oxidation and pure adsorption experiments
E	Reaction potential at 25 ºC
E^0	Standard reduction potential at 25 ºC
E_a	Apparent activation energy
EDS	Energy dispersive spectroscopy
FTIR	Fourier transform infrared spectroscopy
FWHM	Full width at half maximum
HA	Humic acid
HPLC	High performance liquid chromatography
k_{app}	Apparent first order reaction rate constant
MBT	Mechanical biological treatment
MGNC	Magnetic graphitic nanocomposite
MHA	Muller Hinton agar
MSW	Municipal solid waste
MWCNT	Multiwalled carbon nanotubes
NB	Nutrient broth

$\eta_{H_2O_2}$	Total organic carbon removal per unit of hydrogen peroxide decomposed
PCA	Plate count agar
pH_{PZC}	pH at the point of zero charge
p*k*a	Acid dissociation constant
S_{BET}	Specific surface area
SEM	Scanning electron microscopy
S_{meso}	Non-microporous specific surface area
SMX	Sulfamethoxazole
tBuOH	*tert*-Butanol
TEM	Transmission electron microscopy
TGA	Thermogravimetric analysis
TOC	Total organic carbon
TPD	Temperature programmed desorption
V_{micro}	Micropore volume
V_{total}	Total pore volume
$X_{H_2O_2}$	Hydrogen peroxide conversion
XPS	X-Ray photoelectron spectroscopy
XRD	X-Ray diffraction
X_{TOC}	Total organic carbon conversion

Key materials

$CoFe_2O_4$/MGNC	Hybrid magnetic graphitic nanocomposite composed by a cobalt ferrite core and a graphitic shell
CX	Carbon xerogel
CX/Co	Monometallic magnetic carbon xerogel with cobalt species embedded in its structure
CX/CoFe	Bimetallic magnetic carbon xerogel with iron and cobalt species embedded in its structure
CX/Fe	Monometallic magnetic carbon xerogel with iron species embedded in its structure
Fe_3O_4/MGNC	Hybrid magnetic graphitic nanocomposite composed by a magnetite core and a graphitic shell
GBCM	Glycerol-based carbon material
$GBCM_{150}$	Glycerol-based carbon material obtained after activation under oxidative atmosphere at 150 ºC
$GBCM_{200}$	Glycerol-based carbon material obtained after activation under oxidative atmosphere at 200 ºC
$GBCM_{300}$	Glycerol-based carbon material obtained after activation under oxidative atmosphere at 300 ºC
$GBCM_{350}$	Glycerol-based carbon material obtained after activation under oxidative atmosphere at 350 ºC
GO	Graphene oxide
rGO	Reduced graphene oxide
rGOG	Reduced graphene oxide prepared from graphene oxide using glucose as reducing agent
rGOH	Reduced graphene oxide prepared from graphene oxide using hydrazine as reducing agent
rGOV	Reduced graphene oxide prepared from graphene oxide using vitamin C as reducing agent

PART I: INTRODUCTION

A broad introduction to these Ph.D. studies is initially provided in Part I, including the description of:

- The thesis structure, in Chapter 1;

- The relevance and motivation, and main objectives of these studies, in Chapters 2 and 3, respectively;

- The main experimental methods employed for the synthesis, characterization and application of the carbon-based catalysts in CWPO, in Chapter 4.

1. THESIS OUTLINE

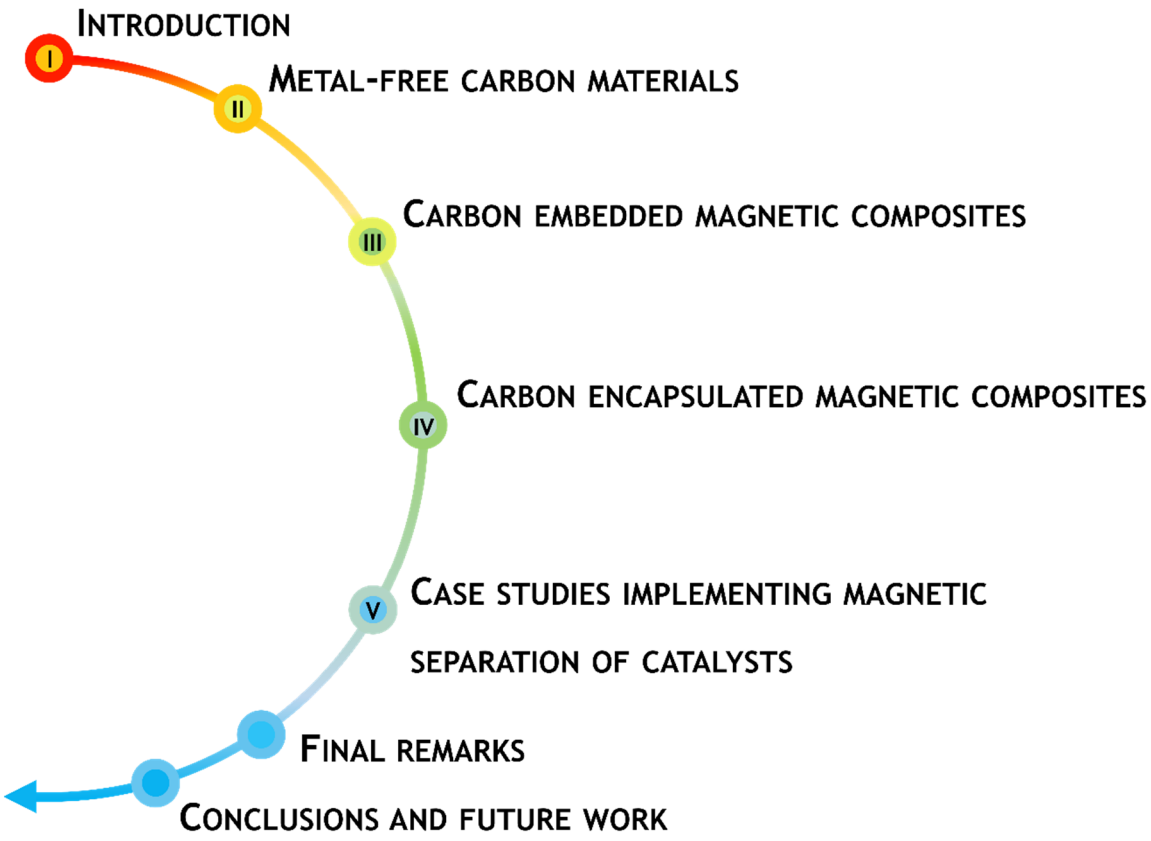

This Ph.D. dissertation is structured in five Parts, divided into ten Chapters. Final remarks, conclusions and future work are provided afterwards.

Part I provides a broad Introduction, organized under Relevance and motivation (Chapter 2), Objectives (Chapter 3) and Materials and methods (Chapter 4), in addition to the Thesis outline herein presented (Chapter 1).

Part II is devoted to the study into how specific properties of Metal-free carbon materials affect their performance in catalytic wet peroxide oxidation (CWPO), including Glycerol-based carbon materials (Chapter 5) and Graphene-based materials (Chapter 6).

Part III and Part IV are fully devoted to the preparation, characterization and application of hybrid magnetic carbon nanocomposites in CWPO. Carbon embedded magnetic composites are addressed in Part III, through the detailed study of catalytic reactions occurring at the surface of Magnetic carbon xerogels (Chapter 7). Part IV is devoted to Carbon encapsulated magnetic composites, particularly to the study of the effects arising from the inclusion of magnetite nanoparticles in a graphitic structure during the synthesis of Hybrid magnetic graphitic nanocomposites (Chapter 8).

Case studies implementing magnetic separation of catalysts are shown in Part V. These include the application of Magnetic carbon xerogels for the CWPO of sulfamethoxazole in environmentally relevant water matrices (Chapter 9), and Hybrid magnetic graphitic nanocomposites towards CWPO of the liquid effluent from a mechanical biological treatment plant for municipal solid waste (Chapter 10).

Final remarks on these Ph.D. studies are gathered after Part V, followed by the main Conclusions and suggestions for Future Work.

Supplementary information to this Ph.D. dissertation is provided in the Appendices. Lists with the most significant Publications and Communications in scientific meetings resulting from these Ph.D. studies are included in Appendix D, and Appendix E, respectively.

The Ph.D. studies were carried out at the Associate Laboratory LSRE-LCM, except those shown in Chapter 9 related to the work performed during a short-term scientific mission for advanced training at the University of Patras, Greece, under the framework of European Cooperation in Science and Technology (COST) Action ES1403: New and emerging challenges and opportunities in wastewater reuse (NEREUS).

2. RELEVANCE AND MOTIVATION

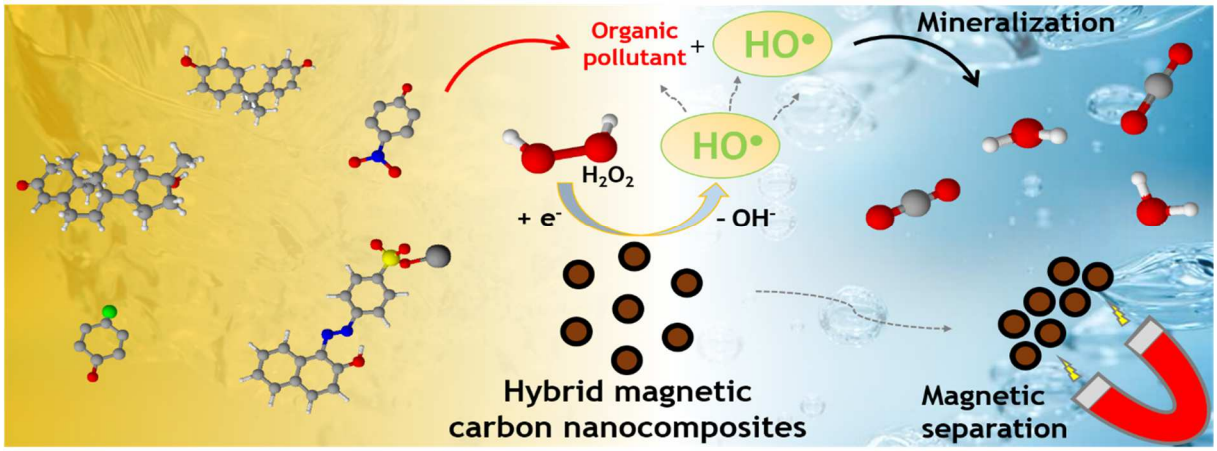

1

[1] Adapted from the graphical abstract of: Rui S. Ribeiro, Adrián M.T. Silva, José L. Figueiredo, Joaquim L. Faria, Helder T. Gomes, Catalytic wet peroxide oxidation: a route towards the application of hybrid magnetic carbon nanocomposites for the degradation of organic pollutants. A review, Appl. Catal. B 187 (2016) 428-460 DOI: 10.1016/j.apcatb.2016.01.033

Wastewater treatment, and even reuse, became of utmost importance with the increasing scarcity of clean water sources. Therefore, the development of efficient and economically viable technologies is presently of high priority in the policy agendas of European Union (EU) member states and many other countries around the world [1]. These technologies should be able to meet the increasingly demanding quality criteria for sustainable and safe urban water cycles and comply with the use of treated wastewater as a reliable alternative of water source. Accordingly, the development of efficient technologies capable of degrading toxic, persistent and bio-recalcitrant organic pollutants, as those commonly associated to negative impacts on conventional biological wastewater treatment processes, is needed. For instance, endocrine disrupting compounds, many types of pharmaceutical drugs including antibiotics, disinfection by-products, personal care products, metabolites, transformation products, pesticides, surfactants and biocides, that can be treated by the so called advanced oxidation processes (AOP), have received a great deal of attention from the scientific community [1].

Among the AOP, catalytic wet peroxide oxidation (CWPO) is recognized as a relatively low cost technology [2], since it operates with simple equipment and under mild conditions (e.g., at atmospheric pressure and low to moderate temperatures) [3]. CWPO employs hydrogen peroxide (H_2O_2) as oxidation source and a suitable catalyst to promote its partial decomposition to hydroxyl radicals ($HO^{\bullet}$) —highly oxidizing species able to efficiently degrade most of the organic pollutants present in aqueous phase [4, 5]. Moreover, H_2O_2 is well-established as an environmentally-friendly agent, since its total decomposition products are oxygen and water, rendering CWPO-based water treatment technologies further attractive from an environmental point of view [3].

However, further optimization of catalyst design is still required in order to bring CWPO to the forefront of the most efficient AOP technologies. Bearing this in mind, the background, main developments, and mechanistic aspects of the CWPO process, specially related with the application of carbon-based catalysts, are presented in the following Sections. Under this context, the current research trend towards the application of hybrid magnetic carbon nanocomposites in CWPO is discussed based on the bibliometric analysis given in Figure 2.1. Afterwards, the main synthesis techniques used for the preparation of hybrid magnetic carbon nanocomposites are briefly presented. The criteria employed for the selection of nitrophenols as aqueous model systems for this Ph.D. dissertation are also described. In addition, all the aqueous model systems and real waste waters used in previous studies on the application of carbon-based catalysts in CWPO are listed in Table 2.1.

2.1. Catalytic wet peroxide oxidation: background, motivations and mechanistic aspects

A route towards the application of hybrid magnetic carbon nanocomposites for the CWPO of organic pollutants is presented in the following Sections. In addition, the established main reaction mechanisms involved in the process are discussed.

2.1.1. The Fenton process

The catalytic oxidation of organic compounds using H_2O_2 as oxidant was first reported in the late 19th century, when the British researcher Henry John H. Fenton published his study on the oxidation of tartaric acid in the presence of iron salts [6]. In that study, it was demonstrated that tartaric acid can be oxidized by the interaction of small amounts of ferrous ion (Fe^{2+}) with distinct oxidizing agents, H_2O_2 leading to the best results. Fenton concluded that Fe^{2+} takes part in the reaction as catalyst, with a very small amount being enough to promote the complete degradation of an almost unlimited quantity of tartaric acid without being consumed.

In the 1930s, Fritz Haber and Joseph J. Weiss brought further insights on the phenomenon reported by Fenton, concluding that $HO^{\bullet}$ radicals —generated from the reaction of H_2O_2 with the superoxide radical anion ($O_2^{\bullet-}$), the Haber-Weiss reaction, as described by Eq. 2.1 [7]— were actually the active species responsible for the oxidation of tartaric acid, and not H_2O_2 itself. According to a subsequent work of these authors, the interaction between H_2O_2 and

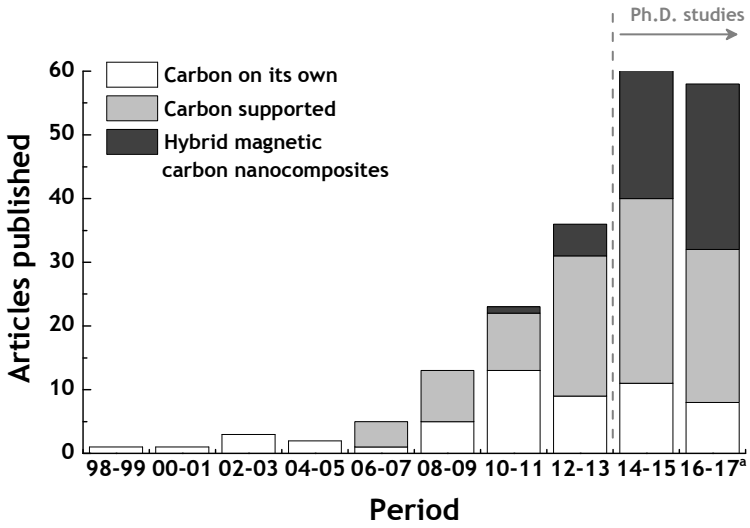

Figure 2.1. Evolution of Scopus's indexed original research articles dealing with the application of carbon-based materials in CWPO processes, including the research articles resulting from the present Ph.D. studies (approximate duration period indicated by the horizontal dashed line). [a] Data collected from Scopus in November, 2017, using the following queries: "catalytic wet peroxide oxidation" and "Fenton".

Table 2.1. List of organic pollutants employed for the application of carbon-based catalysts in CWPO processes, including the research articles resulting from the present Ph.D. studies. Some articles are reported more than once, corresponding to studies performed with more than one organic pollutant

Class	Pollutant	CAS registry number	Articles published[a]	Reference(s)
Dyes	Methylene blue	61-73-4	31	[8-38]
	Orange II	633-96-5	21	[21, 39-57]
	Methyl orange	547-58-0	8	[20, 58-64]
	Rhodamine B	81-88-9	5	[65-69]
	Chromotrope 2R	4197-07-3	3	[54, 70, 71]
	Other	Not applicable	22	[8, 9, 72-91]
	Total		90	
Phenolic compounds	Phenol	108-95-2	38	[9, 92-128]
	4-nitrophenol	100-02-7	9	[128-136]
	Bisphenol A	80-05-7	8	[137-144]
	4-chlorophenol	106-48-9	6	[145-150]
	m-cresol	108-39-4	5	[151-155]
	Other	Not applicable	7	[9, 156-161]
	Total		73	
Real waste waters	Textile	Not applicable	8	[162-169]
	Other	Not applicable	11	[136, 170-179]
	Total		19	
Pharmaceuticals	17α-methyltestosterone	58-18-4	2	[180, 181]
	Ciprofloxacin	85721-33-1	2	[182, 183]
	Sulfamethazine	57-68-1	2	[184, 185]
	Other	Not applicable	4	[186-189]
	Total		10	
Herbicides	Amitrole	61-82-5	1	[190]
	Paraquat	1910-42-5	1	[191]
	Total		2	
Other		Not applicable	12	[107, 120, 122, 156, 192-199]
Absence of pollutant[b]		Not applicable	10	[200-209]

[a] Data collected from Scopus in November, 2017; [b] studies reporting only the H_2O_2 catalytic decomposition in the absence of an organic pollutant.

Fe^{2+} in acidic media results in the decomposition of H_2O_2 through the oxidation of Fe^{2+} to ferric ion (Fe^{3+}), with the formation of hydroxide ions (OH^-) and $HO^\bullet$, as described by Eq. 2.2 [210].

$$H_2O_2 + O_2^{\bullet-} \rightleftarrows OH^- + HO^\bullet + O_2 \quad \textbf{(2.1)}$$

$$H_2O_2 + Fe^{2+} \rightleftarrows OH^- + HO^\bullet + Fe^{3+} \quad \textbf{(2.2)}$$

The participation of Fe^{2+} as catalyst in the oxidation process was finally demonstrated in

the 1950s, in two studies reported by Barb et al. [211, 212]. These authors proposed a two-step mechanism in which Fe^{2+} is regenerated from the Fe^{3+} formed in the reaction described by Eq. 2.2:

- in the first step, H_2O_2 reacts with $HO^{\bullet}$ in solution, resulting in the formation of hydroperoxyl radicals ($HOO^{\bullet}$) and water, as described by Eq. 2.3;
- in the second step, $HOO^{\bullet}$ reduces Fe^{3+}, regenerating Fe^{2+} and closing the catalytic cycle, as described by Eq. 2.4.

$$H_2O_2 + HO^{\bullet} \rightarrow HOO^{\bullet} + H_2O \quad \textbf{(2.3)}$$

$$Fe^{3+} + HOO^{\bullet} \rightarrow O_2 + H^{+} + Fe^{2+} \quad \textbf{(2.4)}$$

In recognition for the major contribution made by Fenton, the reported oxidation process in which homogeneous Fe^{2+} is used as catalyst is known as the Fenton process. Nowadays, it is widely known that $HO^{\bullet}$ radicals are powerful oxidants (standard reduction potential between +2.8 V and +2.0 V at pH 0 and 14, respectively) and serve as effective species in the destruction of a large range of organic pollutants [4, 5]. It is also accepted that the regeneration of Fe^{2+} from Fe^{3+} is mainly accomplished through the reaction of Fe^{3+} with H_2O_2, as described by Eq. 2.5 [213]. Nevertheless, the Fenton process includes several other reactions, such as non-efficient parasitic reactions, resulting in a complex mechanism recently summarized by Munoz et al. [213].

Some drawbacks leading to the increase of operating costs are commonly associated to the Fenton process. One of them is the need for a complicated final separation step for the recovery or elimination of the Fe^{2+}/Fe^{3+} ions, in many cases found in amounts exceeding the limits allowed by EU Directives for discharge of treated water into natural receiving water bodies (2 mg L^{-1} in Portugal [214]), which in turn leads to the undesired production of large amounts of iron sludge in the form of $Fe(OH)_3$ [213, 215]. In this case, the costs associated to the subsequent treatment and disposal of the iron sludge may represent up to 50% of the total operating costs [213]. In addition, the Fenton process operates under pH values in the range 2.5-4.0 [216], originating acidic solutions which need neutralisation before being discharged into natural water courses. A tentative solution to overcome these constraints is the use of supported heterogeneous catalysts, whose advantages and disadvantages are discussed in the following Section.

$$Fe^{3+} + H_2O_2 \rightarrow Fe^{2+} + HOO^{\bullet} + H^{+} \quad \textbf{(2.5)}$$

2.1.2. Carbon-supported metal catalysts

Very distinct materials such as alumina, silica, mesoporous molecular sieves, zeolites, pillared clays, ion-exchange resins and nanometric diamonds have been used to support transition metals, mainly iron [5, 116, 213, 217-223]. Nevertheless, the advantages of using

carbon materials as supports of highly dispersed metal particles are widely recognized. Since the first review on the subject by Ehrburger in 1984 [224], the application of carbon materials as catalyst supports has been subject of several other comprehensive reviews [225-231], reflecting the increasing interest of the scientific community on this type of materials. This interest may be attributed to some specific properties of carbon materials, such as: (i) stability in acidic/basic media; (ii) high specific surface area, leading to high dispersion and stability of the metal phases; (iii) possibility to control, to some extent, the porosity and the surface chemistry, improving diffusion of reactants and products to and from the surface, and increasing metal dispersion by controlling polarity and hydrophobicity; (iv) easy recovery of expensive metal phases by burning away the carbon support; and (v) structural stability at high temperatures [231-233]. In addition, carbon materials are usually cheaper than other conventional catalyst supports [231].

Carbon-supported metal catalysts are typically prepared by techniques similar to those used with other supports, the most widely used being impregnation [231, 232]. Nevertheless, several other methods have also been employed for the preparation of carbon supported metal catalysts, such as precipitation or co-precipitation, liquid-phase reduction, chemical vapour deposition and physical vapour deposition [231]. Given the wide range of methods available for the preparation of supported metal catalysts and the interesting features of carbon materials, their application as supports for Fe species is the most straightforward tentative solution to overcome the drawbacks reported previously on the use of homogeneous Fe^{2+} catalysts in the Fenton process. In this way, it may be expected that the separation of the heterogeneous catalyst from the final treated waters becomes easier, since the active phase is immobilised on the surface of a support. Fe catalysts supported on carbon materials have been extensively used in several studies devoted to the catalytic oxidation of different compounds using H_2O_2 as oxidant [18-28, 44-51, 58-62, 67-69, 76-84, 101-110, 112-119, 133, 140-144, 148, 149, 164-166, 173-178, 182, 183, 185, 190, 191, 195-199, 202, 203], i.e., CWPO – Catalytic Wet Peroxide Oxidation. It should be noted that the term CWPO has been introduced to distinguish between the typical Fenton process and the processes involving heterogeneous supported catalysts, or even other homogeneous catalysts because alternative metals have also been found as active species for CWPO applications, when presenting multiple possible oxidation states (e.g., M^{n+} and $M^{(n+1)+}$, where M represents the metal) [222]. Thus, the main catalytic reactions described by Eqs. 2.2 and 2.5 can be replaced by more general reactions, as described by Eqs. 2.6 and 2.7. Accordingly, other metal catalysts have been supported on carbon structures in order to be employed in CWPO, namely gold [10, 96, 99, 137, 209], copper [17, 30, 86, 111, 192], cobalt [51, 162, 163], nickel [51] and manganese [100].

$$H_2O_2 + M^{n+} \rightleftarrows OH^- + HO^\bullet + M^{(n+1)+} \quad \textbf{(2.6)}$$

$$M^{(n+1)+} + H_2O_2 \rightarrow M^{n+} + HOO^\bullet + H^+ \quad \textbf{(2.7)}$$

Although supported catalysts facilitates the final separation step, this alternative poses other difficulties, namely the loss of catalyst activity due to metal leaching. Some illustrative examples of this catalyst deactivation phenomenon that typically occurs during CWPO of organic pollutants in aqueous phase are shown in Table 2.2.

A carbon-supported Fe catalyst was prepared by Zazo et al. [116] and subsequently tested in the CWPO of phenol. As observed, complete removal of the initial phenol content was obtained in CWPO experiments performed during 4 h at 30 ºC and pH = 3 (*cf*. Table 2.2). Nevertheless, an iron leaching of 2.40 mg L^{-1} was determined at the end of the process. In addition, due to the iron leaching, the authors concluded that this supported catalyst would undergo a significant loss of activity when subjected to continuous mode experiments [116]. Likewise, two distinct carbon materials were used as supports in the study reported by Ramirez et al. [44], namely an activated carbon and a carbon aerogel. The iron leaching in the CWPO of Orange II at 30 ºC and pH = 3 was 0.87 mg L^{-1} and 0.97 mg L^{-1}, with the activated carbon and the carbon aerogel support, respectively (*cf*. Table 2.2). The authors concluded that iron leached from the support leads to a progressive deactivation in consecutive reaction cycles, which is an important limitation for their industrial application [44]. Carbon nanotubes and carbon nanofibers have also been used as supports for Fe species in CWPO applications. Rodríguez et al. [50] also reported the use of supported Fe catalysts prepared by incipient-wetness impregnation, this time using carbon nanotubes, carbon nanofibers and activated carbon as supports. The three catalysts lead to high removals of Orange II in CWPO experiments performed at 30 ºC and pH = 3 (*cf*. Table 2.2). However, very high levels of iron leaching were determined in the treated waters, limiting the stability and durability of the catalysts.

So far, it has been shown that most of the carbon-supported metal catalysts do not exhibit suitable stability for CWPO applications, mainly as a result of metal leaching. At the same time, since the report of Lücking et al. in 1998 [145], different carbon materials have been recognized as active metal-free catalysts for CWPO. In this way, active metals are not required to promote the generation of $HO^\bullet$, thus avoiding the need for a metal separation step at the end of the CWPO treatment. The application of carbon materials directly as catalysts in CWPO processes will be discussed in detail in the next Section.

Table 2.2. Representative examples on the use of carbon-supported metal catalysts in CWPO processes: description of the catalyst, operating conditions and catalytic performance of each catalyst (pollutant removal and iron leached to the treated waters)

Authors	Catalyst	Operating conditions	Pollutant	H_2O_2 stoichiometric ratio[a]	Pollutant removal	$[Fe]_{leaching}$ (mg L^{-1})
Zazo et al., 2006 [116]	Fe (4 wt.%) supported on a commercial activated carbon by incipient-wetness impregnation with an iron nitrate solution, followed by calcination at 200 ºC for 4 h	Batch experiments [Catalyst] = 0.5 g L^{-1} $[H_2O_2]_0$ = 0.50 g L^{-1} T = 50 ºC; pH_0 = 3 t = 4 h	Phenol (100 mg L^{-1})	1.0	100.0% (50.0 mg g^{-1} h^{-1})	2.40
	Same activated carbon, in the absence of Fe				58.0% (29.0 mg g^{-1} h^{-1})	Not addressed
Ramirez et al., 2007 [44]	Fe (7 wt.%) supported on activated carbon (prepared by carbonization of olive stones) by incipient-wetness impregnation with a ferrous acetate solution, followed by annealing under N_2 atmosphere at 200 ºC for 2 h	Batch experiments [Catalyst] = 0.2 g L^{-1} $[H_2O_2]_0$ = 0.20 g L^{-1} T = 30 ºC; pH_0 = 3 t = 4 h	Orange II (35 mg L^{-1})	1.3	98.0% (42.9 mg g^{-1} h^{-1})	0.87
	Same activated carbon, in the absence of Fe	Same conditions as above, except that: t = 35 h			98.0% (4.90 mg g^{-1} h^{-1})	Not addressed
	Fe (7 wt.%) supported on carbon aerogel (prepared by polymerization of an organic resorcinol-formaldehyde solution) by incipient-wetness impregnation with a ferrous acetate solution, followed by annealing under N_2 atmosphere at 200 ºC for 2 h	t = 4 h			98.0% (42.9 mg g^{-1} h^{-1})	0.97
	Same carbon aerogel, in the absence of Fe	t = 15 h			98.0% (9.33 mg g^{-1} h^{-1})	Not addressed
Rodríguez et al., 2010 [50]	Fe (5 wt.%) supported on carbon nanotubes (prepared by chemical vapour deposition) by incipient-wetness impregnation with an unknown Fe precursor, followed by heating under N_2 atmosphere at 350 ºC for 4 h	Batch experiments [Catalyst] = 2.0 g L^{-1} $[H_2O_2]_0$ = 0.35g L^{-1} T = 30 ºC; pH_0 = 3 t = 2 h	Orange II (66 mg L^{-1})	1.2	94.0% (15.5 mg g^{-1} h^{-1})	25.2
	Fe (5 wt.%) supported on commercial carbon nanofibers (origin not specified) by using the same incipient-wetness impregnation procedure as described above				100.0% (16.5 mg g^{-1} h^{-1})	22.7
	Fe (5 wt.%) supported on a commercial activated carbon by using the same incipient-wetness impregnation procedure as described above				94.0% (16.2 mg g^{-1} h^{-1})	50.1

[a] Obtained by dividing the amount of H_2O_2 employed by the stoichiometric amount needed for the complete mineralization of the pollutant considered.

2.1.3. Carbon materials as catalysts on their own

The application of carbon materials directly as catalysts was recognized a long time ago [234]. Back in 1969, Robert W. Coughlin noticed the increasing importance of carbons in several catalytic processes, which was ascribed to some of their properties, such as crystalline structure, microscopic physical structure, electronic properties and surface chemistry, as well as to the presence of impurities [234]. Since then, the use of carbon materials as catalysts on their own has been the subject of several studies, in parallel with the development of new types of nanostructured carbon materials [232]. Comprehensive reviews on the subject with extensive detail may be found in the book published in 2009 by Serp and Figueiredo [231] and in the book published in 2015 by Serp and Machado [235].

In the particular case of CWPO, carbon materials (without any supported metal phase) were first reported as active and stable catalysts by Lücking et al., in 1998 [145]. This study seems to report for the first time the application of carbon supported catalysts in CWPO. At that time, the authors highlighted the difficulty to retain homogeneous catalysts in the process as the main disadvantage on the use of iron salts directly in solution (in the Fenton process), and the leaching of the metal phase from the support material as the main disadvantage of the application of supported metal catalysts in CWPO. Bearing this in mind, Lücking et al. [145] compared the performances of distinct materials in the CWPO of 4-chlorophenol, at pH = 3, namely iron powder, iron supported on activated carbon, graphite and three activated carbons of different origins (without any supported metal phase). As summarized in Table 2.3, the results have shown that both iron powder and iron supported on activated carbon catalysts owe their activity to the Fe ions leached to the solution (300 and 56.0 mg L^{-1}, respectively, in batch experiments), which subsequently act as homogeneous catalysts; on the opposite, both activated carbon and graphite were found to act as heterogeneous catalysts in the decomposition of H_2O_2 and in the oxidation of 4-chlorophenol [145]. In support of this observation, graphite revealed much higher activity in the CWPO of 4-chlorophenol in comparison with homogeneous Fe^{2+} (1 mg L^{-1}, twice the amount leached to the treated water when graphite was used as catalyst) [145].

The results reported by Lücking et al. [145] prompted the scientific community to further explore the use of carbon materials without any supported metal phase in CWPO. Since the ability of carbon materials to selectively decompose H_2O_2 into $HO^{\bullet}$ radicals is of major importance to the global performance of the process, this reaction was also subject of specific research.

Table 2.3. Summary of the comparative study reported by Lücking et al., in 1998 [145], in which carbon materials without any supported metal phase were first shown as active and stable catalysts for CWPO. Data include description of the catalyst, operating conditions and catalytic performance of each catalyst [pollutant removal in terms of dissolved organic carbon (DOC) and iron leached to the treated waters]

Authors	Catalyst	Operating conditions	Pollutant	H_2O_2 stoichiometric ratio[a]	Pollutant removal[b]	$[Fe]_{leaching}$ (mg L^{-1})
Lücking et al., 1998 [145]	Iron powder (95 wt.% Fe, Isocommerz VE Außen- und Binnenhandelsbetrieb BT Herzberg/E)	Batch experiments [Catalyst] = 1.0 g L^{-1} $[H_2O_2]_0$ = 5.30 g L^{-1} T = 30 ºC; pH_0 = 3 t = 6 h	4-chlorophenol (1000 mg L^{-1})	1.2	64.0%	300
	Graphite (99.8 wt.% C, Laborchemie Apolda GmbH)	Same conditions as above, except that t = 96 h			30.0%	0.50
	Homogeneous Fe^{2+} (for comparison purposes)	Same conditions as above, except that [catalyst] = 1 mg L^{-1} and t = 144 h			8.0%	Not applicable
	Activated carbon (RFZ1, from Norit), followed by impregnation with iron hydroxide (ash content ca. 15-20 wt.%)	Batch and continuous experiments [Catalyst] = 1.0 g L^{-1} $[H_2O_2]_0$ = 5.30 g L^{-1} T = 30 ºC (batch) T = 20 ºC (continuous) pH_0 = 3 t = 800 h (batch) t = 160 d (continuous	4-chlorophenol (1000 mg L^{-1})	1.2	80.9% (batch) 41.0% (continuous, 32 d) 17.0% (continuous, 160 d)	56.0 (batch) 14.8 (continuous, 32 d) 0.32 (continuous, 160 d)
	Activated carbon (F-300, from Chemviron Carbon)				70.1% (batch) 18.0% (continuous, 32 d) 8.0% (continuous, 160 d)	< 2.00[c] (batch) 0.46 (continuous, 32 d) 0.18 (continuous, 160 d)
	Activated carbon (Darco GCW, from Norit)				65.7% (batch) 15.0% (continuous, 32 d) 10.0% (continuous, 160 d)	< 2.00[c] (batch) 0.48 (continuous, 32 d) 0.20 (continuous, 160 d)
	Activated carbon (ROW 0.8, from Norit)				72.2% (batch) 13.0% (continuous, 32 d) 6.0% (continuous, 160 d)	< 2.00[c] (batch) 0.12 (continuous, 32 d) 0.11 (continuous, 160 d)

[a] Obtained by dividing the amount of H_2O_2 employed by the stoichiometric amount needed for the complete mineralization of the pollutant considered; [b] Dissolved organic carbon (DOC) removal; [c] Not specified.

2.1.3.1.Mechanism for the decomposition of H_2O_2 in the presence of carbon materials

In a previous publication, our group proposed a mechanism for the decomposition of H_2O_2 when carbon materials are used as catalysts [207], based on experimental results and on other findings reported in the literature [2, 200, 203, 205, 236-244]. The proposed mechanism, given in Table 2.4, consists of the following steps:

- [H_2O_2] decomposes via $HO^{\bullet}$ formation, with the participation of reduced active sites [AS], i.e., electron donor sites existing at the carbon surface (e.g. basic oxygen containing groups, such as chromene and pyrone, basic nitrogen containing functionalities or delocalized π-electrons at the carbon basal planes), as described by Eq. 2.8;
- [H_2O_2] adsorbed over the oxidized active sites [AS^+], i.e., electron acceptor sites, decomposes to $HOO^{\bullet}$ and H^+, regenerating [AS], as described by Eq. 2.9;
- Adsorbed $HOO^{\bullet}$ and H^+ produce atomic oxygen (which may remain trapped in the surface and accounts for the formation of carbon surface oxides) and water when in contact with reducing active sites [AS] existing at the carbon surface, as described by Eq. 2.10;
- Due to self-annihilation, H_2O_2 in the bulk can be decomposed to $HOO^{\bullet}$, $HO^{\bullet}$, O_2 and water, by reaction with $HOO^{\bullet}$, $HO^{\bullet}$ and $O_2^{\bullet-}$, as described by Eqs. 2.12–2.14. Due to the low bimolecular reaction rate, Eqs. 2.13 and 2.14 will have a negligible contribution to this self-annihilation process. H_2O_2 in the bulk may also be decomposed by dissociation as a weak acid, as described by Eq. 2.11;
- Finally, the radicals $HO^{\bullet}$, $HOO^{\bullet}$ and $O_2^{\bullet-}$ can react with themselves resulting mainly in O_2, water and some minor amounts of regenerated H_2O_2 (Eqs. 2.15–2.21).

Most of the reactions given in Table 2.4 are widely accepted in AOP [245, 246], in addition to the catalytic surface reactions described by Eqs. 2.8–2.10. In particular, the mechanism of H_2O_2 decomposition for CWPO applications is especially relevant when leading to the formation of $HO^{\bullet}$, since these species present higher redox potential (2.80 V) than that of $HOO^{\bullet}$ (1.70 V) or H_2O_2 itself (1.77 V) [247].

Since the report of Lücking et al. [145], very distinct materials such as activated carbons [8, 9, 40, 55, 70-72, 85, 97, 98, 121-124, 150, 151, 156, 158, 167-170, 179, 191, 193, 200, 201, 204-208], graphite [92, 95, 120, 171, 208], carbon nanotubes [75, 94, 113, 160, 206], sludge-derived carbon materials [74, 152-155], carbon blacks [95, 125, 208], activated carbon xerogels [54, 63, 130], graphene-based materials [52, 93, 206], carbon aerogels [51], and others [120, 131, 172], have been reported as active catalysts for CWPO. Nevertheless, despite all the significant improvements that have been made, especially in recent years, carbon materials, when used as catalysts on their own, still show lower performances in CWPO when compared with metal-based catalysts [51, 55, 113, 120, 191, 203]. At the same

Table 2.4. Reaction mechanisms for H_2O_2 decomposition. Adapted from [207]

Reaction			Comment/ Rate constant	
$[H_2O_2 + AS]$	→	$HO^{\bullet} + OH^- + [AS^+]$	Catalytic surface reaction [207]	**(2.8)**
$[H_2O_2 + AS^+]$	→	$[HOO^{\bullet} + H^+ + AS]$	Catalytic surface reaction [207]	**(2.9)**
$[HOO^{\bullet} + H^+ + AS]$	→	$H_2O + [O^{\bullet} + AS^+]$	Catalytic surface reaction [207]	**(2.10)**
H_2O_2	⇄	$H^+ + HO_2^-$	pKa = 11.75 [240]	**(2.11)**
$H_2O_2 + HO^{\bullet}$	→	$H_2O + HOO^{\bullet}$	2.7×10^7 M^{-1} s^{-1} [237]	**(2.12)**
$H_2O_2 + HOO^{\bullet}$	→	$HO^{\bullet} + H_2O + O_2$	3 M^{-1} s^{-1} [241]	**(2.13)**
$H_2O_2 + O_2^{\bullet -}$	→	$HO^{\bullet} + OH^- + O_2$	0.13 M^{-1} s^{-1} [244]	**(2.14)**
$HOO^{\bullet}$	⇄	$O_2^{\bullet -} + H^+$	pKa = 4.8 [236]	**(2.15)**
$HO_2^- + HO^{\bullet}$	→	$HOO^{\bullet} + OH^-$	7.5×10^9 M^{-1} s^{-1} [238]	**(2.16)**
$HO^{\bullet} + HOO^{\bullet}$	→	$H_2O + O_2$	6.6×10^9 M^{-1} s^{-1} [239]	**(2.17)**
$HO^{\bullet} + HO^{\bullet}$	→	H_2O_2	5.5×10^9 M^{-1} s^{-1} [237]	**(2.18)**
$HOO^{\bullet} + HOO^{\bullet}$	→	$H_2O_2 + O_2$	8.3×10^5 M^{-1} s^{-1} [236]	**(2.19)**
$HO^{\bullet} + O_2^{\bullet -}$	→	$OH^- + O_2$	8×10^9 M^{-1} s^{-1} [243]	**(2.20)**
$HOO^{\bullet} + O_2^{\bullet -}$	→	$HO_2^- + O_2$	9.7×10^7 M^{-1} s^{-1} [236]	**(2.21)**

time, carbon materials with metals within their structure, arising from the synthesis precursors and procedures considered, have been shown to be active and stable catalysts in CWPO, revealing low leaching levels [94, 145, 160, 171]. Other authors have also suggested the preparation of carbon materials with iron within the carbonaceous structure, as suitable catalysts for CWPO with limited iron leaching [44]. Bearing this in mind, the synthesis of highly stable carbon-based nanostructured composites (resistant to leaching phenomena) containing metallic nanomaterials (e.g. iron, cobalt, nickel and/or their alloys, and/or ferrite), may be considered the next step in the evolution of catalysts for CWPO. In this way, the possible synergistic effects that can arise from the combination of the high catalytic activity of iron or other metal species with the proven catalytic properties of carbon-based materials in CWPO could be explored, but always simultaneously assessing catalyst stability. The magnetic properties of these nanostructured materials would be an additional advantage to the process, enabling *in-situ* magnetic separation, thus avoiding typical systems for separation of the homogeneous, or even of the non-magnetic heterogeneous powders used as catalysts in CWPO.

2.2. Hybrid magnetic carbon nanocomposites

Hybrid magnetic carbon nanocomposites are composed of carbon nanostructures (mainly sp^2-hybridized aromatic carbon atoms) of various dimensionalities (e.g., 0D fullerene, 1D carbon nanotubes and 2D graphene sheets) and magnetic nanoparticles [248]. As shown in Figure 2.2, two general classes of these type of hybrid materials are usually considered: (i)

carbon nanostructures decorated with magnetic nanoparticles, in which the magnetic material is embedded or linked to the carbon structure, without being protected against the environment by a carbonaceous shell, and (ii) carbon encapsulated magnetic nanoparticles, which are core-shell structures with a carbonaceous shell and a core made of magnetic materials [248]. Several techniques for the synthesis of carbon-based nanostructured composites containing magnetic nanomaterials have been explored and improved in recent years [248, 249], as described in a recent review [249] and summarized in Figure 2.3. Methods such as (i) filling process, (ii) template-based synthesis, (iii) chemical vapour deposition, (iv) hydrothermal/solvothermal method, (v) pyrolysis procedure, (vi) sol-gel process, (vii) detonation induced reaction and (viii) self-assembly method, have led to considerable progress and unprecedented prospects for the use of these types of materials in several applications. In particular, these developments opened a window of opportunity, not only for the investigation of their catalytic properties in CWPO, but also for the development of *in-situ* magnetic separation systems.

Several hybrid magnetic composites in which the magnetic material is embedded in the carbon structure have been reported as highly active and efficient catalysts for CWPO applications. The possible synergistic effects that have been claimed regarding the application of carbon nanostructures decorated with magnetic nanoparticles in CWPO were initially evidenced in the study performed by Hu et al. in 2011 [180], which seems to be first reporting the application of this type of nanostructured composites in CWPO processes. Specifically, the high catalytic activity of magnetite (Fe_3O_4) for the CWPO of 17α-methyltestosterone was increased when this magnetic material was grown on the surface of multiwalled carbon nanotubes [180]. Since the report of Hu et al. [180], graphene-based materials [13, 29, 31, 33, 35, 36, 39, 41-43, 65, 66, 89, 90, 127, 157, 184], carbon nanotubes [16, 38, 53, 64, 73, 91, 128, 132, 139, 161, 180, 181, 194], graphitic materials [87, 186], carbon nanofibers [37, 57], and others [11, 14, 34, 56, 138, 187, 189], have been reported as active and efficient catalysts for CWPO when decorated with magnetic nanoparticles. Carbon encapsulated magnetic nanoparticles have also been employed in CWPO. In this case, the first study was reported in 2014, by Zhang et al. [15]. Briefly, Fe_3O_4 was prepared by

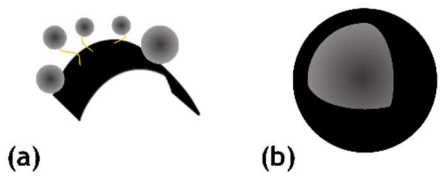

Figure 2.2. Representation of the two general classes of nanostructured hybrid magnetic carbon materials: (a) carbon nanostructures decorated with magnetic nanoparticles —chains correspond to optional molecular linkers, and (b) carbon encapsulated magnetic nanoparticles. The carbon material is shown in black, whereas magnetic particles are represented by grey spheres. Adapted from [248].

co-precipitation; then, hydrothermal dehydrogenation of glucose was adopted in order to coat the Fe_3O_4 cores with a faintly distinguished carbon layer. At that time the authors concluded that carbon encapsulation enhances the catalytic activity of the bare Fe_3O_4 cores [15]. Since the report of Zhang et al. [15], six studies on the synthesis of carbon encapsulated magnetic nanoparticles for CWPO applications have been reported [12, 32, 88, 126, 146, 147] —five out of which were published since the beginning of these Ph.D. studies.

2.3. Nitrophenols as aqueous model systems

Nitrophenols are man-made, toxic and bio-recalcitrant chemical compounds, containing at least one nitro group (-NO_2) attached to an aromatic ring [250-254]. Therefore, their presence can have a negative impact on conventional biological wastewater treatment processes. The main sources of nitrophenols are industrial manufacturing and processing activities, with the subsequent disposal into water matrices [252]. 2-nitrophenol (2-NP) and 4-nitrophenol (4-NP) possess very similar properties (*cf.* Table 2.5). Indeed, the manufacture of one isomer usually leads to the formation of residual amounts of the other [252]. Nevertheless, 2-NP is used mainly for the production of dyes, paints, rubber chemicals and fungicides; while 4-NP is used mainly in the drugs, fungicides, dyes and leather industries [252].

Small amounts of 2-NP and 4-NP have been found in natural water bodies, which poses a risk of human exposure through drinking water, possibly leading to several negative health effects [252]. The release of industrial waste waters into publicly owned wastewater treatment plants (WWTP) is partially responsible for this phenomenon, in addition to the

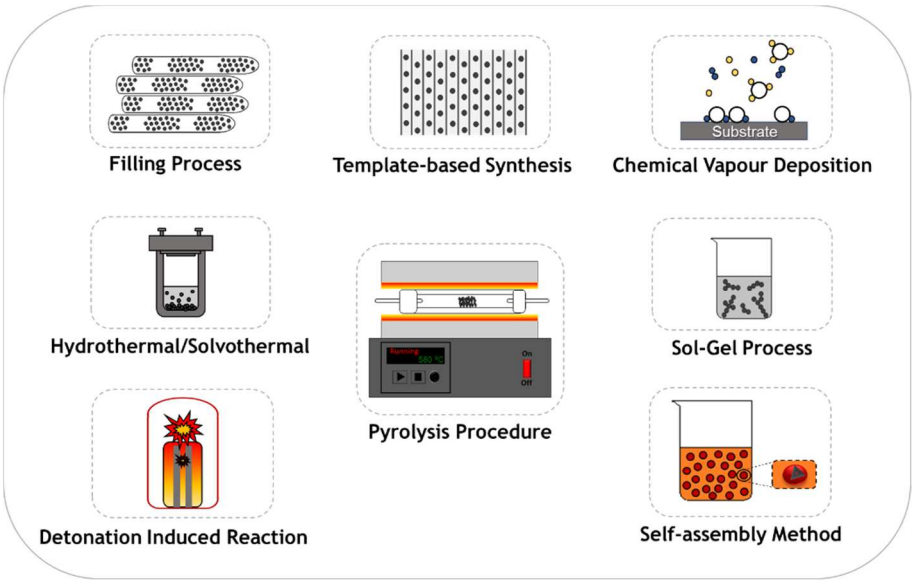

Figure 2.3. Main synthesis techniques used for the preparation of hybrid magnetic carbon nanocomposites.

Table 2.5. Identification, and physical and chemical properties of 2-nitrophenol and 4-nitrophenol. Adapted from [252]

Characteristic/ property	2-nitrophenol (2-NP)	4-nitrophenol (4-NP)
CAS registry number	88-75-5	100-02-7
Chemical formula	$C_6H_5NO_3$	$C_6H_5NO_3$
Chemical structure	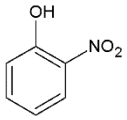	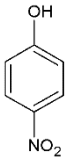
Molecular weight	139.11 g mol^{-1}	139.11 g mol^{-1}
Colour	Light yellow	Colourless to light yellow
Melting/boiling point	44-45 ºC/ 216 ºC	113-114 ºC/ 297 ºC
Acid dissociation constant (p*K*a)	7.21-7.23	7.08-7.18
Solubility in distilled water at 25 ºC	1400-2100 mg L^{-1}	16000 mg L^{-1}

degradation of the products containing nitrophenols in their formulation [252].

Data available on the environmental fate of nitrophenols clearly indicates that both 2-NP and 4-NP undergo chemical oxidation in natural surface waters due to reaction with sunlight-induced HO• radicals [252, 254]. This knowledge opens future prospects for the application of AOPs for the treatment of industrial waste waters containing nitrophenols, such as CWPO.

Bearing this in mind, 2-NP and 4-NP can be regarded as suitable aqueous model systems of refractory organic pollutants typically not treatable by conventional biological technologies.

References

[1] D. Fatta-Kassinos, C. Manaia, T.U. Berendonk, E. Cytryn, J. Bayona, B. Chefetz, J. Slobodnik, N. Kreuzinger, L. Rizzo, S. Malato, L. Lundy, A. Ledin, COST Action ES1403: New and Emerging challenges and opportunities in wastewater REUSe (NEREUS), Environ. Sci. Pollut. Res. 22 (2015) 7183-7186.

[2] J.J. Pignatello, E. Oliveros, A. MacKay, Advanced oxidation processes for organic contaminant destruction based on the Fenton reaction and related chemistry, Crit. Rev. Environ. Sci. Technol. 36 (2006) 1-84.

[3] C.W. Jones, Applications of hydrogen peroxide and derivatives, The Royal Society of Chemistry, Cambridge, UK, 1999.

[4] P.R. Gogate, A.B. Pandit, A review of imperative technologies for wastewater treatment I: oxidation technologies at ambient conditions, Adv. Environ. Res. 8 (2004) 501-551.

[5] S. Navalon, M. Alvaro, H. Garcia, Heterogeneous Fenton catalysts based on clays, silicas and zeolites, Appl. Catal. B 99 (2010) 1-26.

[6] H.J.H. Fenton, Oxidation of tartaric acid in presence of iron, J. Chem. Soc., Trans. 65 (1894) 899-910.

[7] F. Haber, J. Weiss, Über die katalyse des hydroperoxydes, Naturwissenschaften 20 (1932) 948-950.

[8] V.P. Santos, M.F.R. Pereira, P.C.C. Faria, J.J.M. Órfão, Decolourisation of dye solutions by oxidation with H_2O_2 in the presence of modified activated carbons, J. Hazard. Mater. 162 (2009) 736-742.

[9] L.C.A. Oliveira, C.N. Silva, M.I. Yoshida, R.M. Lago, The effect of H_2 treatment on the activity of activated carbon for the oxidation of organic contaminants in water and the H_2O_2 decomposition, Carbon 42 (2004) 2279-2284.

[10] E. Lorençon, D.C. Ferreira, R.R. Resende, K. Krambrock, Amphiphilic gold nanoparticles supported on carbon nanotubes: catalysts for the oxidation of lipophilic compounds by wet peroxide in biphasic systems, Appl. Catal. A 505 (2015) 566-574.

[11] C. Bao, H. Zhang, L. Zhou, Y. Shao, J. Ma, Q. Wu, Preparation of copper doped magnetic porous carbon for removal of methylene blue by a heterogeneous Fenton-like reaction, RSC Adv. 5 (2015) 72423-72432.

[12] Y. Shao, L. Zhou, C. Bao, J. Ma, A facile approach to the fabrication of rattle-type magnetic carbon nanospheres for removal of methylene blue in water, Carbon 89 (2015) 378-391.

[13] B. Yang, Z. Tian, L. Zhang, Y. Guo, S. Yan, Enhanced heterogeneous Fenton degradation of methylene blue by nanoscale zero valent iron (nZVI) assembled on magnetic Fe_3O_4/reduced graphene oxide, J. Water Process Eng. 5 (2015) 101-111.

[14] J.C. Tristão, F.G. de Mendonça, R.M. Lago, J.D. Ardisson, Controlled formation of reactive Fe particles dispersed in a carbon matrix active for the oxidation of aqueous contaminants with H_2O_2, Environ. Sci. Pollut. Res. 22 (2015) 856-863.

[15] X. Zhang, M. He, J.-H. Liu, R. Liao, L. Zhao, J. Xie, R. Wang, S.-T. Yang, H. Wang, Y. Liu, Fe_3O_4@C nanoparticles as high-performance Fenton-like catalyst for dye decoloration, Chin. Sci. Bull. 59 (2014) 3406-3412.

[16] H. Wang, H. Jiang, S. Wang, W. Shi, J. He, H. Liu, Y. Huang, Fe_3O_4-MWCNT magnetic nanocomposites as efficient peroxidase mimic catalysts in a Fenton-like reaction for water purification without pH limitation, RSC Adv. 4 (2014) 45809-45815.

[17] J. Qian, K. Wang, Q. Guan, H. Li, H. Xu, Q. Liu, W. Liu, B. Qiu, Enhanced wet hydrogen peroxide catalytic oxidation performances based on CuS nanocrystals/reduced graphene oxide composites, Appl. Surf. Sci. 288 (2014) 633-640.

[18] J. Ma, L. Zhou, W. Dan, H. Zhang, Y. Shao, C. Bao, L. Jing, Novel magnetic porous carbon spheres derived from chelating resin as a heterogeneous Fenton catalyst for the

removal of methylene blue from aqueous solution, J. Colloid Interface Sci. 446 (2015) 298-306.
[19] L. Zhou, Y. Shao, J. Liu, Z. Ye, H. Zhang, J. Ma, Y. Jia, W. Gao, Y. Li, Preparation and characterization of magnetic porous carbon microspheres for removal of methylene blue by a heterogeneous Fenton reaction, ACS Appl. Mater. Interfaces 6 (2014) 7275-7285.
[20] W. Li, T. Sun, F. Li, Highly efficient iron nanocatalyst stabilized by double-walled carbon nanotubes and mixed metal oxides for degradation of cationic and anionic dyes by a Fenton-like process, Ind. Eng. Chem. Res. 53 (2014) 18095-18103.
[21] Y.C. Lee, S.J. Chang, M.H. Choi, T.J. Jeon, T. Ryu, Y.S. Huh, Self-assembled graphene oxide with organo-building blocks of Fe-aminoclay for heterogeneous Fenton-like reaction at near-neutral pH: a batch experiment, Appl. Catal. B 142-143 (2013) 494-503.
[22] S.B. Lima, S.M.S. Borges, M. Do Carmo Rangel, S.G. Marchetti, Effect of iron content on the catalytic properties of activated carbon-supported magnetite derived from biomass, J. Braz. Chem. Soc. 24 (2013) 344-354.
[23] M. Gonçalves, M.C. Guerreiro, L.C.A. Oliveira, C.S. Castro, A friendly environmental material: iron oxide dispersed over activated carbon from coffee husk for organic pollutants removal, J. Environ. Manage. 127 (2013) 206-211.
[24] C.S. Castro, M.C. Guerreiro, L.C.A. Oliveira, M. Gonçalves, A.S. Anastácio, M. Nazzarro, Iron oxide dispersed over activated carbon: support influence on the oxidation of the model molecule methylene blue, Appl. Catal. A 367 (2009) 53-58.
[25] M. Wang, L. Zhang, X. Fan, Y. Zhou, L. Chen, Q. Kong, J. Shi, A unique route to fabricate mesoporous carbon with abundant ferric species as a heterogeneous Fenton catalyst under neutral conditions, RSC Adv. 5 (2015) 101241-101246.
[26] C. Zheng, X. Cheng, C. Yang, C. Zhang, H. Li, L. Kan, J. Xia, X. Sun, Hydrophilic modification of ordered mesoporous carbon supported Fe nanoparticles with enhanced adsorption and heterogeneous Fenton-like oxidation performance, RSC Adv. 5 (2015) 98842-98852.
[27] L. Zhou, J. Ma, H. Zhang, Y. Shao, Y. Li, Fabrication of magnetic carbon composites from peanut shells and its application as a heterogeneous Fenton catalyst in removal of methylene blue, Appl. Surf. Sci. 324 (2015) 490-498.
[28] L.A. Silva, S.M.S. Borges, P.N. Paulino, M.A. Fraga, S.T. Oliva, S.G. Marchetti, M.C. Rangel, Methylene blue oxidation over iron oxide supported on activated carbon derived from peanut hulls, Catal. Today 289 (2017) 237-248.
[29] W. Liu, J. Qian, K. Wang, H. Xu, D. Jiang, Q. Liu, X. Yang, H. Li, Magnetically separable Fe_3O_4 nanoparticles-decorated reduced graphene oxide nanocomposite for catalytic wet hydrogen peroxide oxidation, J. Inorg. Organomet. Polym. Mater. 23 (2013) 907-916.

[30] G. Nie, Z. Li, X. Lu, J. Lei, C. Zhang, C. Wang, Fabrication of polyacrylonitrile/CuS composite nanofibers and their recycled application in catalysis for dye degradation, Appl. Surf. Sci. 284 (2013) 595-600.

[31] H.P. Bi, L.Z. Liu, J.J. Ding, G.Y. He, H.Q. Chen, X. Wang, Preparation and catalytic property of Cu-graphene Fenton-like catalyst, Chin. J. Inorg. Chem. 30 (2014) 2347-2352.

[32] R. Wang, X. Liu, R. Wu, B. Yu, H. Li, X. Zhang, J. Xie, S.-T. Yang, $Fe_3O_4/SiO_2/C$ nanocomposite as a high-performance Fenton-like catalyst in a neutral environment, RSC Adv. 6 (2016) 8594-8600.

[33] Q. Wu, H. Zhang, L. Zhou, C. Bao, H. Zhu, Y. Zhang, Synthesis and application of $rGO/CoFe_2O_4$ composite for catalytic degradation of methylene blue on heterogeneous Fenton-like oxidation, J. Taiwan Inst. Chem. Eng. 67 (2016) 484-494.

[34] F. Xue, S.T. Yang, X. Jin, T. Li, R. Wang, X. Liu, Y. Bai, L. Chen, Z. Ming, H. Yang, One-pot modification of Fe_3O_4 to prepare $Fe_3O_4/SiO_2/C$ nanoparticles and their catalytic activity in Fenton-like process for dye decolouration, Micro Nano Lett. 11 (2016) 675-679.

[35] J. Zhang, T. Yao, C. Guan, N. Zhang, H. Zhang, X. Zhang, J. Wu, One-pot preparation of ternary reduced graphene oxide nanosheets/Fe_2O_3/polypyrrole hydrogels as efficient Fenton catalysts, J. Colloid Interface Sci. 505 (2017) 130-138.

[36] Y. Hua, S. Wang, J. Xiao, C. Cui, C. Wang, Preparation and characterization of Fe_3O_4/gallic acid/graphene oxide magnetic nanocomposites as highly efficient Fenton catalysts, RSC Adv. 7 (2017) 28979-28986.

[37] S.H. Yoo, D. Jang, H.I. Joh, S. Lee, Iron oxide/porous carbon as a heterogeneous Fenton catalyst for fast decomposition of hydrogen peroxide and efficient removal of methylene blue, J. Mater. Chem. A 5 (2017) 748-755.

[38] M. Zhang, K.P. Annamalai, L. Liu, T. Chen, J. Gao, Y. Tao, Multiwalled carbon nanotube-supported $CuCo_2S_4$ as a heterogeneous Fenton-like catalyst with enhanced performance, RSC Adv. 7 (2017) 20724-20731.

[39] N.A. Zubir, C. Yacou, J. Motuzas, X. Zhang, X.S. Zhao, J.C. Diniz da Costa, The sacrificial role of graphene oxide in stabilising a Fenton-like catalyst GO-Fe_3O_4, Chem. Commun. 51 (2015) 9291-9293.

[40] M.T. Pinho, A.M.T. Silva, N.A. Fathy, A.A. Attia, H.T. Gomes, J.L. Faria, Activated carbon xerogel–chitosan composite materials for catalytic wet peroxide oxidation under intensified process conditions, J. Environ. Chem. Eng. 3 (2015) 1243-1251.

[41] N.A. Zubir, C. Yacou, J. Motuzas, X. Zhang, J.C. Diniz da Costa, Structural and functional investigation of graphene oxide–Fe_3O_4 nanocomposites for the heterogeneous Fenton-like reaction, Sci. Rep. 4, Article number: 4594 (2014).

[42] N.A. Zubir, C. Yacou, X. Zhang, J.C. Diniz da Costa, Optimisation of graphene oxide–iron oxide nanocomposite in heterogeneous Fenton-like oxidation of acid orange 7, J. Environ. Chem. Eng. 2 (2014) 1881-1888.
[43] N.A. Zubir, X. Zhang, C. Yacou, J.C. Diniz da Costa, Fenton-like degradation of acid orange 7 using graphene oxide-iron oxide nanocomposite, Sci. Adv. Mater. 6 (2014) 1382-1388.
[44] J.H. Ramirez, F.J. Maldonado-Hódar, A.F. Pérez-Cadenas, C. Moreno-Castilla, C.A. Costa, L.M. Madeira, Azo-dye orange II degradation by heterogeneous Fenton-like reaction using carbon-Fe catalysts, Appl. Catal. B 75 (2007) 312-323.
[45] H. Haham, J. Grinblat, M.T. Sougrati, L. Stievano, S. Margel, Engineering of iron-based magnetic activated carbon fabrics for environmental remediation, Materials 8 (2015) 4593-4607.
[46] F.M. Duarte, F.J. Maldonado-Hódar, L.M. Madeira, New insight about orange II elimination by characterization of spent activated carbon/Fe Fenton-like catalysts, Appl. Catal. B 129 (2013) 264-272.
[47] F.M. Duarte, F.J. Maldonado-Hódar, L.M. Madeira, Influence of the iron precursor in the preparation of heterogeneous Fe/activated carbon Fenton-like catalysts, Appl. Catal. A 458 (2013) 39-47.
[48] Y. Tu, S. Tian, L. Kong, Y. Xiong, Co-catalytic effect of sewage sludge-derived char as the support of Fenton-like catalyst, Chem. Eng. J. 185-186 (2012) 44-51.
[49] F.M. Duarte, F.J. Maldonado-Hódar, L.M. Madeira, Influence of the particle size of activated carbons on their performance as fe supports for developing fenton-like catalysts, Ind. Eng. Chem. Res. 51 (2012) 9218-9226.
[50] A. Rodríguez, G. Ovejero, J.L. Sotelo, M. Mestanza, J. García, Heterogeneous Fenton catalyst supports screening for mono azo dye degradation in contaminated wastewaters, Ind. Eng. Chem. Res. 49 (2010) 498-505.
[51] F.M. Duarte, F.J. Maldonado-Hódar, A.F. Pérez-Cadenas, L.M. Madeira, Fenton-like degradation of azo-dye orange II catalyzed by transition metals on carbon aerogels, Appl. Catal. B 85 (2009) 139-147.
[52] Y. Zhao, W.-F. Chen, C.-F. Yuan, Z.-Y. Zhu, L.-F. Yan, Hydrogenated graphene as metal-free catalyst for Fenton-like reaction, Chin. J. Chem. Phys. 25 (2012) 335-338.
[53] J. Deng, X. Wen, Q. Wang, Solvothermal in situ synthesis of Fe_3O_4-multi-walled carbon nanotubes with enhanced heterogeneous Fenton-like activity, Mater. Res. Bull. 47 (2012) 3369-3376.

[54] R.S. Ribeiro, N.A. Fathy, A.A. Attia, A.M.T. Silva, J.L. Faria, H.T. Gomes, Activated carbon xerogels for the removal of the anionic azo dyes orange II and chromotrope 2R by adsorption and catalytic wet peroxide oxidation, Chem. Eng. J. 195-196 (2012) 112-121.
[55] F. Duarte, F.J. Maldonado-Hódar, L.M. Madeira, Influence of the characteristics of carbon materials on their behaviour as heterogeneous Fenton catalysts for the elimination of the azo dye orange II from aqueous solutions, Appl. Catal. B 103 (2011) 109-115.
[56] L. Kong, Y. Zhu, M. Liu, X. Chang, Y. Xiong, D. Chen, Conversion of Fe-rich waste sludge into nano-flake Fe-SC hybrid Fenton-like catalyst for degradation of AOII, Environ. Pollut. 216 (2016) 568-574.
[57] J. Wang, C. Liu, J. Li, R. Luo, X. Hu, X. Sun, J. Shen, W. Han, L. Wang, *In-situ* incorporation of iron-copper bimetallic particles in electrospun carbon nanofibers as an efficient Fenton catalyst, Appl. Catal. B 207 (2017) 316-325.
[58] Z. Qu, X. Tang, X. Li, K. Chen, D. Ma, Degradation of methyl orange over Fe^{2+} activated sulphonated carbon catalyst, Chin. J. Catal. 30 (2009) 142-146.
[59] S.T.T. Le, T.T. Ngo, W. Khanitchaidecha, A. Nakaruk, Synthesis of iron/GAC catalyst for wastewater treatment using heterogeneous Fenton reaction, Bull. Mater. Sci. 38 (2015) 1039-1042.
[60] C. Yang, D. Wang, Q. Tang, The synthesis of NdFeB magnetic activated carbon and its application in degradation of azo dye methyl orange by Fenton-like process, J. Taiwan Inst. Chem. Eng. 45 (2014) 2584-2589.
[61] T.D. Nguyen, N.H. Phan, M.H. Do, K.T. Ngo, Magnetic Fe_2MO_4 (M:Fe, Mn) activated carbons: fabrication, characterization and heterogeneous Fenton oxidation of methyl orange, J. Hazard. Mater. 185 (2011) 653-661.
[62] M. Arshadi, M.K. Abdolmaleki, F. Mousavinia, A. Khalafi-Nezhad, H. Firouzabadi, A. Gil, Degradation of methyl orange by heterogeneous Fenton-like oxidation on a nano-organometallic compound in the presence of multi-walled carbon nanotubes, Chem. Eng. Res. Des. 112 (2016) 113-121.
[63] N.A. Fathy, S.M. El-Khouly, N.A. Hassan, R.M.S. Awad, Free- and Ni-doped carbon xerogels catalysts for wet peroxide oxidation of methyl orange, J. Water Process Eng. 16 (2017) 21-27.
[64] H.-Y. Xu, T.-N. Shi, H. Zhao, L.-G. Jin, F.-C. Wang, C.-Y. Wang, S.-Y. Qi, Heterogeneous Fenton-like discoloration of methyl orange using Fe_3O_4/MWCNTs as catalyst: process optimization by response surface methodology, Front. Mater. Sci. 10 (2016) 45-55.
[65] Y.H. Chang, Y.F. Yao, H. Luo, L. Cui, L.J. Zhi, Magnetic Fe_3O_4-GO nanocomposites as highly efficient Fenton-like catalyst for the degradation of dyes, Int. J. Nanomanuf. 10 (2014) 132-141.

[66] C. Deng, Y. Xie, W. Wang, Y. Song, Y. Zeng, Heterogeneous Fenton degradation of rhodamine-B by Fe^0 assembled on magnetic reduced graphene oxide, Chin. J. Environ. Eng. 11 (2017) 3499-3506.
[67] S. Guo, N. Yuan, G. Zhang, J.C. Yu, Graphene modified iron sludge derived from homogeneous Fenton process as an efficient heterogeneous Fenton catalyst for degradation of organic pollutants, Microporous Mesoporous Mater. 238 (2017) 62-68.
[68] M. Hou, Y. Guo, X. Chen, M. Xiao, C. Hong, Y. Yao, F. Zhu, W. Wang, Preparation, characterization and catalytic performance of paper mill sludge and municipal wastewater treatment sludge-based catalysts for Fenton-like oxidation of rhodamine B, Desalin. Water Treat. 84 (2017) 190-198.
[69] P.V. Nidheesh, R. Rajan, Removal of rhodamine B from a water medium using hydroxyl and sulphate radicals generated by iron loaded activated carbon, RSC Adv. 6 (2016) 5330-5340.
[70] H.T. Gomes, S.M. Miranda, M.J. Sampaio, A.M.T. Silva, J.L. Faria, Activated carbons treated with sulphuric acid: catalysts for catalytic wet peroxide oxidation, Catal. Today 151 (2010) 153-158.
[71] H.T. Gomes, S.M. Miranda, M.J. Sampaio, J.L. Figueiredo, A.M.T. Silva, J.L. Faria, The role of activated carbons functionalized with thiol and sulfonic acid groups in catalytic wet peroxide oxidation, Appl. Catal. B 106 (2011) 390-397.
[72] L. Dąbek, E. Ozimina, A. Picheta-Oleś, Impact of properties of activated carbons on the speed of removal of selected dyes from solutions in the presence of hydrogen peroxide, Rocz. Ochr. Sr. 13 (2011) 1023-1042.
[73] M.F. Variava, T.L. Church, A.T. Harris, Magnetically recoverable Fe_xO_y–MWNT Fenton's catalysts that show enhanced activity at neutral pH, Appl. Catal. B 123–124 (2012) 200-207.
[74] L. Gu, N. Zhu, H. Guo, S. Huang, Z. Lou, H. Yuan, Adsorption and Fenton-like degradation of naphthalene dye intermediate on sewage sludge derived porous carbon, J. Hazard. Mater. 246–247 (2013) 145-153.
[75] M. Soria-Sánchez, E. Castillejos-López, A. Maroto-Valiente, M.F.R. Pereira, J.J.M. Órfão, A. Guerrero-Ruiz, High efficiency of the cylindrical mesopores of MWCNTs for the catalytic wet peroxide oxidation of C.I. reactive red 241 dissolved in water, Appl. Catal. B 121–122 (2012) 182-189.
[76] G. Ersöz, Fenton-like oxidation of reactive black 5 using rice husk ash based catalyst, Appl. Catal. B 147 (2014) 353-358.
[77] J.C. García, M.P. Castellanos, Á. Uscátegui, J. Fernández, A.M. Pedroza, C.E. Daza, Removal of synthetic dyes by Fenton process using activated carbon-supported Fe_2O_3 obtained from rose remnants, Univ. Sci. 17 (2012) 303-314.

[78] Y. Yao, Y. Mao, B. Zheng, Z. Huang, W. Lu, W. Chen, Anchored iron ligands as an efficient Fenton-like catalyst for removal of dye pollutants at neutral pH, Ind. Eng. Chem. Res. 53 (2014) 8376-8384.
[79] L. Sun, Y. Yao, L. Wang, Y. Mao, Z. Huang, D. Yao, W. Lu, W. Chen, Efficient removal of dyes using activated carbon fibers coupled with 8-hydroxyquinoline ferric as a reusable Fenton-like catalyst, Chem. Eng. J. 240 (2014) 413-419.
[80] J. Wu, G. Lin, P. Li, W. Yin, X. Wang, B. Yang, Heterogeneous Fenton-like degradation of an azo dye reactive brilliant orange by the combination of activated carbon-FeOOH catalyst and H_2O_2, Water Sci. Technol. 67 (2013) 572-578.
[81] L. Wang, Y. Yao, L. Sun, W. Lü, W. Chen, Activation of hydrogen peroxide by activated carbon fibers coupled with Fe(III)-citrate for degradation of dyes at neutral pH, Acta Chim. Sinica 71 (2013) 1633-1638.
[82] I. Mesquita, L.C. Matos, F.M. Duarte, F.J. Maldonado-Hódar, A. Mendes, L.M. Madeira, Treatment of azo dye-containing wastewater by a Fenton-like process in a continuous packed-bed reactor filled with activated carbon, J. Hazard. Mater. 237–238 (2012) 30-37.
[83] J. Ma, Q. Yang, Y. Wen, W. Liu, Fe-g-C_3N_4/graphitized mesoporous carbon composite as an effective Fenton-like catalyst in a wide pH range, Appl. Catal. B 201 (2017) 232-240.
[84] D. Li, J. Zhu, J. Wu, W. Yin, H. Liang, G. Lin, Development of an activated carbon-supported zero-valent iron catalyst (AC-Fe^0) for enhancing degradation of reactive brilliant orange and reducing iron sludge production, Environ. Prog. Sustainable Energy 35 (2016) 949-956.
[85] O. Türgay, G. Ersöz, S. Atalay, J. Forss, U. Welander, The treatment of azo dyes found in textile industry wastewater by anaerobic biological method and chemical oxidation, Sep. Purif. Technol. 79 (2011) 26-33.
[86] J. Liao, L. Li, H. Li, Facile synthesis of graphite film-supported CuO nanowires and their high catalytic performance in oxidation of Congo red, J. Chem. Eng. Jpn. 49 (2016) 771-775.
[87] G. Yuan, G. Zhang, Y. Zhou, F. Yang, Synergetic adsorption and catalytic oxidation performance originating from leafy graphite nanosheet anchored iron(ii) phthalocyanine nanorods for efficient organic dye degradation, RSC Adv. 5 (2015) 26132-26140.
[88] H. Chen, J. Lee, Y. Zheng, Q. Duan, A non-traditional energy transfer process in CWPO heterogeneous reaction for wastewater treatment, Chem. Eng. Res. Des. 114 (2016) 142-147.
[89] N.A. Fathy, S.E. El-Shafey, O.I. El-Shafey, Synthesis of a novel MnO_2@carbon nanotubes-graphene hybrid catalyst (MnO_2@CNT-G) for catalytic oxidation of basic red 18 dye (BR18), J. Water Process Eng. 17 (2017) 95-101.

[90] X. Huang, Y. Niu, W. Hu, Fe/Fe_3C nanoparticles loaded on Fe/N-doped graphene as an efficient heterogeneous Fenton catalyst for degradation of organic pollutants, Colloids Surf. A 518 (2017) 145-150.
[91] N.A. Fathy, S.E. El-Shafey, O.I. El-Shafey, W.S. Mohamed, Oxidative degradation of RB19 dye by a novel γ-MnO_2/MWCNT nanocomposite catalyst with H_2O_2, J. Environ. Chem. Eng. 1 (2013) 858-864.
[92] O.P. Pestunova, O.L. Ogorodnikova, V.N. Parmon, Studies on the phenol wet peroxide oxidation in the presence of solid catalysts, Chem. Sustain. Dev. 11 (2003) 227-232.
[93] J.C. Espinosa, S. Navalón, A. Primo, M. Moral, J.F. Sanz, M. Álvaro, H. García, Graphenes as efficient metal-free Fenton catalysts, Chem. Eur. J. 21 (2015) 11966-11971.
[94] M.T. Pinho, H.T. Gomes, R.S. Ribeiro, J.L. Faria, A.M.T. Silva, Carbon nanotubes as catalysts for catalytic wet peroxide oxidation of highly concentrated phenol solutions: towards process intensification, Appl. Catal. B 165 (2015) 706-714.
[95] C.M. Domínguez, P. Ocón, A. Quintanilla, J.A. Casas, J.J. Rodríguez, Graphite and carbon black materials as catalysts for wet peroxide oxidation, Appl. Catal. B 144 (2014) 599-606.
[96] C.M. Domínguez, A. Quintanilla, J.A. Casas, J.J. Rodriguez, Kinetics of wet peroxide oxidation of phenol with a gold/activated carbon catalyst, Chem. Eng. J. 253 (2014) 486-492.
[97] F. Martínez, I. Pariente, C. Brebou, R. Molina, J.A. Melero, D. Bremner, D. Mantzavinos, Chemical surface modified-activated carbon cloth for catalytic wet peroxide oxidation of phenol, J. Chem. Technol. Biotechnol. 89 (2014) 1182-1188.
[98] C.M. Domínguez, P. Ocón, A. Quintanilla, J.A. Casas, J.J. Rodríguez, Highly efficient application of activated carbon as catalyst for wet peroxide oxidation, Appl. Catal. B 140–141 (2013) 663-670.
[99] A. Quintanilla, S. García-Rodríguez, C.M. Domínguez, S. Blasco, J.A. Casas, J.J. Rodriguez, Supported gold nanoparticle catalysts for wet peroxide oxidation, Appl. Catal. B 111-112 (2012) 81-89.
[100] L. Kong, W. Wei, Q. Zhao, J.Q. Wang, Y. Wan, Active coordinatively unsaturated manganese monoxide-containing mesoporous carbon catalyst in wet peroxide oxidation, ACS Catal. 2 (2012) 2577-2586.
[101] S.A. Messele, O.S.G.P. Soares, J.J.M. Órfão, C. Bengoa, F. Stüber, A. Fortuny, A. Fabregat, J. Font, Effect of activated carbon surface chemistry on the activity of ZVI/AC catalysts for Fenton-like oxidation of phenol, Catal. Today 240 (2015) 73-79.

[102] S.A. Messele, C. Bengoa, F. Stüber, A. Fortuny, A. Fabregat, J. Font, Catalytic wet peroxide oxidation of phenol using nanoscale zero-valent iron supported on activated carbon, Desalin. Water Treat. 57 (2016) 5155–5164.
[103] S.A. Messele, O.S.G.P. Soares, J.J.M. Órfão, F. Stüber, C. Bengoa, A. Fortuny, A. Fabregat, J. Font, Zero-valent iron supported on nitrogen-containing activated carbon for catalytic wet peroxide oxidation of phenol, Appl. Catal. B 154–155 (2014) 329-338.
[104] T. Wanchun, L. Fen, W. Junli, L. Jiehua, L. Xiaoxi, Activated carbon/iron oxide composite material for phenol catalytic degradation from aqueous system, Tech. Equip. Environ. Pollut. Control 5 (2013) 1744-1748.
[105] Y.Z. Yang, Y.P. Li, D.W. Yang, F. Duan, H.B. Cao, Degradation of phenol with a Fe/Cu-catalytic heterogeneous-Fenton process, Huan Jing Ke Xue 34 (2013) 2658-2664.
[106] F. Martínez, M.I. Pariente, J.A. Botas, J.A. Melero, A. Rubalcaba, Influence of preoxidizing treatments on the preparation of iron-containing activated carbons for catalytic wet peroxide oxidation of phenol, J. Chem. Technol. Biotechnol. 87 (2012) 880-886.
[107] J. Chun, H. Lee, S.-H. Lee, S.-W. Hong, J. Lee, C. Lee, J. Lee, Magnetite/mesocellular carbon foam as a magnetically recoverable fenton catalyst for removal of phenol and arsenic, Chemosphere 89 (2012) 1230-1237.
[108] A. Rey, J. Carbajo, C. Adán, M. Faraldos, A. Bahamonde, J.A. Casas, J.J. Rodríguez, Improved mineralization by combined advanced oxidation processes, Chem. Eng. J. 174 (2011) 134-142.
[109] J. Li, J. Gu, H. Li, Y. Liang, Y. Hao, X. Sun, L. Wang, Synthesis of highly ordered Fe-containing mesoporous carbon materials using soft templating routes, Microporous Mesoporous Mater. 128 (2010) 144-149.
[110] R.-M. Liou, S.-H. Chen, C.H. Huang, M.Y. Hung, J.S. Chang, C.L. Lai, Wet hydrogen peroxide catalytic oxidation of phenol with FeAC (iron-embedded activated carbon) catalysts, Water Sci. Technol. 61 (2010) 1489-1498.
[111] R.-M. Liou, S.-H. Chen, CuO impregnated activated carbon for catalytic wet peroxide oxidation of phenol, J. Hazard. Mater. 172 (2009) 498-506.
[112] A. Rey, M. Faraldos, J.A. Casas, J.A. Zazo, A. Bahamonde, J.J. Rodríguez, Catalytic wet peroxide oxidation of phenol over Fe/AC catalysts: influence of iron precursor and activated carbon surface, Appl. Catal. B 86 (2009) 69-77.
[113] Q. Liao, J. Sun, L. Gao, Degradation of phenol by heterogeneous Fenton reaction using multi-walled carbon nanotube supported Fe_2O_3 catalysts, Colloids Surf. A 345 (2009) 95-100.
[114] J.A. Zazo, A.F. Fraile, A. Rey, A. Bahamonde, J.A. Casas, J.J. Rodríguez, Optimizing calcination temperature of Fe/activated carbon catalysts for CWPO, Catal. Today 143 (2009) 341-346.

[115] J.C. Moreno, V.M. Sarria, Á.D. Polo, L. Giraldo, Evaluation of the hydrogen peroxide in the oxidation of phenol with iron supported on activated carbon cloth, Inf. Tecnol. 18 (2007) 67-72.
[116] J.A. Zazo, J.A. Casas, A.F. Mohedano, J.J. Rodríguez, Catalytic wet peroxide oxidation of phenol with a Fe/active carbon catalyst, Appl. Catal. B 65 (2006) 261-268.
[117] X. Liu, H. Yin, A. Lin, Z. Guo, Effective removal of phenol by using activated carbon supported iron prepared under microwave irradiation as a reusable heterogeneous Fenton-like catalyst, J. Environ. Chem. Eng. 5 (2017).
[118] S.A. Messele, O.S.G.P. Soares, J.J.M. Órfão, C. Bengoa, J. Font, Zero-valent iron supported on nitrogen-doped carbon xerogel as catalysts for the oxidation of phenol by Fenton-like system, Environ. Technol. (2017) 1-8.
[119] A. Rey, A.B. Hungria, C.J. Duran-Valle, M. Faraldos, A. Bahamonde, J.A. Casas, J.J. Rodríguez, On the optimization of activated carbon-supported iron catalysts in catalytic wet peroxide oxidation process, Appl. Catal. B 181 (2016) 249-259.
[120] O. Taran, E. Polyanskaya, O. Ogorodnikova, V. Kuznetsov, V. Parmon, M. Besson, C. Descorme, Influence of the morphology and the surface chemistry of carbons on their catalytic performances in the catalytic wet peroxide oxidation of organic contaminants, Appl. Catal. A 387 (2010) 55-66.
[121] A.M. Dehkordi, A.A. Ebrahimi, Catalytic wet peroxide oxidation of phenol in a new two-impinging-jets reactor, Ind. Eng. Chem. Res. 48 (2009) 10619-10626.
[122] Z.G. Meng, J. Wang, L. Fu, F.L. Yang, S.W. Hu, Research on wet peroxide oxidation treating wastewater of phenol and acetone, J. Xi'an Univ. Archit. Technol. 41 (2009) 571-574.
[123] J.M. Britto, S.B.d. Oliveira, D. Rabelo, M.d.C. Rangel, Catalytic wet peroxide oxidation of phenol from industrial wastewater on activated carbon, Catal. Today 133-135 (2008) 582-587.
[124] A. Rey, M. Faraldos, A. Bahamonde, J.A. Casas, J.A. Zazo, J.J. Rodríguez, Role of the activated carbon surface on catalytic wet peroxide oxidation, Ind. Eng. Chem. Res. 47 (2008) 8166-8174.
[125] J.L. Diaz de Tuesta, A. Quintanilla, J.A. Casas, J.J. Rodríguez, P-, B- and N-doped carbon black for the catalytic wet peroxide oxidation of phenol: activity, stability and kinetic studies, Catal. Commun. 102 (2017) 131-135.
[126] A. Mani, T. Kulandaivellu, S. Govindaswamy, A.M. Mohan, Fe_3O_4 nanoparticle-encapsulated mesoporous carbon composite: an efficient heterogeneous Fenton catalyst for phenol degradation, Environ. Sci. Pollut. Res. (2017) 1-11.

[127] P. Wang, X. Zhou, Y. Zhang, L. Yang, K. Zhi, L. Wang, L. Zhang, X. Guo, Unveiling the mechanism of electron transfer facilitated regeneration of active Fe^{2+} by nano-dispersed iron/graphene catalyst for phenol removal, RSC Adv. 7 (2017) 26983-26991.
[128] X. Tian, Y. Liu, W. Chi, Y. Wang, X. Yue, Q. Huang, C. Yu, Catalytic degradation of phenol and *p*-nitrophenol using Fe_3O_4/MWCNT nanocomposites as heterogeneous Fenton-like catalyst, Water Air Soil Pollut. 228 (2017).
[129] R.S. Ribeiro, A.M.T. Silva, L.M. Pastrana-Martínez, J.L. Figueiredo, J.L. Faria, H.T. Gomes, Graphene-based materials for the catalytic wet peroxide oxidation of highly concentrated 4-nitrophenol solutions, Catal. Today 249 (2015) 204–212.
[130] N.A. Fathy, M.A. Shouman, R.M.M. Aboelenin, Nitrogen and phosphorous-doped porous carbon xerogels as metal-free catalysts for environmental catalytic peroxide oxidation of 4-nitrophenol, Asia-Pac. J. Chem. Eng. 11 (2016) 836-845.
[131] M. Martin-Martinez, M.F.F. Barreiro, A.M.T. Silva, J.L. Figueiredo, J.L. Faria, H.T. Gomes, Lignin-based activated carbons as metal-free catalysts for the oxidative degradation of 4-nitrophenol in aqueous solution, Appl. Catal. B 219 (2017) 372-378.
[132] M. Martin-Martinez, R.S. Ribeiro, B.F. Machado, P. Serp, S. Morales-Torres, A.M.T. Silva, J.L. Figueiredo, J.L. Faria, H.T. Gomes, Role of nitrogen doping on the performance of carbon nanotube catalysts: a catalytic wet peroxide oxidation application, ChemCatChem 8 (2016) 2068-2078.
[133] C.S.D. Rodrigues, O.S.G.P. Soares, M.T. Pinho, M.F.R. Pereira, L.M. Madeira, p-Nitrophenol degradation by heterogeneous Fenton's oxidation over activated carbon-based catalysts, Appl. Catal. B 219 (2017) 109-122.
[134] R.S. Ribeiro, A.M.T. Silva, J.L. Figueiredo, J.L. Faria, H.T. Gomes, The role of cobalt in bimetallic iron-cobalt magnetic carbon xerogels developed for catalytic wet peroxide oxidation, Catal. Today 296 (2017) 66-75.
[135] R.S. Ribeiro, A.M.T. Silva, P.B. Tavares, J.L. Figueiredo, J.L. Faria, H.T. Gomes, Hybrid magnetic graphitic nanocomposites for catalytic wet peroxide oxidation applications, Catal. Today 280 (2017) 184-191.
[136] R.S. Ribeiro, R.O. Rodrigues, A.M.T. Silva, P.B. Tavares, A.M.C. Carvalho, J.L. Figueiredo, J.L. Faria, H.T. Gomes, Hybrid magnetic graphitic nanocomposites towards catalytic wet peroxide oxidation of the liquid effluent from a mechanical biological treatment plant for municipal solid waste, Appl. Catal. B 219 (2017) 645-657.
[137] X. Yang, P.F. Tian, C. Zhang, Y.Q. Deng, J. Xu, J. Gong, Y.F. Han, Au/carbon as Fenton-like catalysts for the oxidative degradation of bisphenol A, Appl. Catal. B 134-135 (2013) 145-152.

[138] Y. Wang, H. Zhao, G. Zhao, Iron-copper bimetallic nanoparticles embedded within ordered mesoporous carbon as effective and stable heterogeneous Fenton catalyst for the degradation of organic contaminants, Appl. Catal. B 164 (2015) 396-406.
[139] V. Cleveland, J.-P. Bingham, E. Kan, Heterogeneous Fenton degradation of bisphenol A by carbon nanotube-supported Fe_3O_4, Sep. Purif. Technol. 133 (2014) 388-395.
[140] J.R. Kim, S.G. Huling, E. Kan, Effects of temperature on adsorption and oxidative degradation of bisphenol A in an acid-treated iron-amended granular activated carbon, Chem. Eng. J. 262 (2015) 1260-1267.
[141] D. Zhou, C. Wang, Y. Zhao, Degradation of BPA by heterogeneous Fenton-like action using active carbon-Fe, Chin. J. Environ. Eng. 8 (2014) 5284-5288.
[142] W. Zhou, Z. Cheng, X. Quan, B. Chen, Catalytic wet oxidation of bisphenol A with hydrogen peroxide over Fe/AC catalyst, Huagong Xuebao/CIESC J. 64 (2013) 936-942.
[143] R. Juhola, A. Heponiemi, S. Tuomikoski, T. Hu, T. Vielma, U. Lassi, Preparation of novel Fe catalysts from industrial by-products: catalytic wet peroxide oxidation of bisphenol A, Top. Catal. 60 (2017) 1387-1400.
[144] I.F. Mena, E. Diaz, J.J. Rodriguez, A.F. Mohedano, CWPO of bisphenol A with iron catalysts supported on microporous carbons from grape seeds activation, Chem. Eng. J. 318 (2017) 153-160.
[145] F. Lücking, H. Köser, M. Jank, A. Ritter, Iron powder, graphite and activated carbon as catalysts for the oxidation of 4-chlorophenol with hydrogen peroxide in aqueous solution, Water Res. 32 (1998) 2607-2614.
[146] X. Li, F. Gai, B. Guan, Y. Zhang, Y. Liu, Q. Huo, Fe@C core-shell and Fe@C yolk-shell particles for effective removal of 4-chlorophenol, J. Mater. Chem. A 3 (2015) 3988-3994.
[147] T. Zeng, X. Zhang, S. Wang, Y. Ma, H. Niu, Y. Cai, Assembly of a nanoreactor system with confined magnetite core and shell for enhanced Fenton-like catalysis, Chem. Eur. J. 20 (2014) 6474-6481.
[148] W. Liu, L. Xu, X. Li, C. Shen, S. Rashid, Y. Wen, W. Liu, X. Wu, High-dispersive FeS_2 on graphene oxide for effective degradation of 4-chlorophenol, RSC Adv. 5 (2015) 2449-2456.
[149] F. Duan, Y. Yang, Y. Li, H. Cao, Y. Wang, Y. Zhang, Heterogeneous Fenton-like degradation of 4-chlorophenol using iron/ordered mesoporous carbon catalyst, J. Environ. Sci. 26 (2014) 1171-1179.
[150] H.H. Huang, M.C. Lu, J.N. Chen, C.T. Lee, Catalytic decomposition of hydrogen peroxide and 4-chlorophenol in the presence of modified activated carbons, Chemosphere 51 (2003) 935-943.

[151] Y. Wang, H. Wei, P. Liu, Y. Yu, Y. Zhao, X. Li, W. Jiang, J. Wang, X. Yang, C. Sun, Effect of structural defects on activated carbon catalysts in catalytic wet peroxide oxidation of m-cresol, Catal. Today 258, Part 1 (2015) 120-131.
[152] Y. Yu, H. Wei, L. Yu, T. Zhang, S. Wang, X. Li, J. Wang, C. Sun, Surface modification of sewage sludge derived carbonaceous catalyst for m-cresol catalytic wet peroxide oxidation and degradation mechanism, RSC Adv. 5 (2015) 41867-41876.
[153] Y. Wang, H. Wei, Y. Zhao, W. Sun, C. Sun, The optimization, kinetics and mechanism of m-cresol degradation via catalytic wet peroxide oxidation with sludge-derived carbon catalyst, J. Hazard. Mater. 326 (2017) 36-46.
[154] Y. Wang, H. Wei, Y. Zhao, W. Sun, C. Sun, Low temperature modified sludge-derived carbon catalysts for efficient catalytic wet peroxide oxidation of m-cresol, Green Chem. 19 (2017) 1362-1370.
[155] Y. Yu, H. Wei, L. Yu, W. Wang, Y. Zhao, B. Gu, C. Sun, Sewage-sludge-derived carbonaceous materials for catalytic wet hydrogen peroxide oxidation of m-cresol in batch and continuous reactors, Environ. Technol. 37 (2016) 153-162.
[156] A. Georgi, F.D. Kopinke, Interaction of adsorption and catalytic reactions in water decontamination processes: Part I. Oxidation of organic contaminants with hydrogen peroxide catalyzed by activated carbon, Appl. Catal. B 58 (2005) 9-18.
[157] F. Xiao, W. Li, L. Fang, D. Wang, Synthesis of akageneite (beta-FeOOH)/reduced graphene oxide nanocomposites for oxidative decomposition of 2-chlorophenol by Fenton-like reaction, J. Hazard. Mater. 308 (2016) 11-20.
[158] H.-H. Huang, M.-C. Lu, J.-N. Chen, C.-T. Lee, Influence of surface modification on catalytic activity of activated carbon toward decomposition of hydrogen peroxide and 2-chlorophenol, J. Environ. Sci. Health., Part A 38 (2003) 1233-1246.
[159] R.S. Ribeiro, A.M.T. Silva, M.T. Pinho, J.L. Figueiredo, J.L. Faria, H.T. Gomes, Development of glycerol-based metal-free carbon materials for environmental catalytic applications, Catal. Today 240, Part A (2015) 61-66.
[160] R.S. Ribeiro, A.M.T. Silva, J.L. Figueiredo, J.L. Faria, H.T. Gomes, Removal of 2-nitrophenol by catalytic wet peroxide oxidation using carbon materials with different morphological and chemical properties, Appl. Catal. B 140 (2013) 356-362.
[161] L. Zhou, H. Zhang, L. Ji, Y. Shao, Y. Li, Fe_3O_4/MWCNT as a heterogeneous Fenton catalyst: degradation pathways of tetrabromobisphenol A, RSC Adv. 4 (2014) 24900-24908.
[162] S. Karthikeyan, R. Boopathy, G. Sekaran, In situ generation of hydroxyl radical by cobalt oxide supported porous carbon enhance removal of refractory organics in tannery dyeing wastewater, J. Colloid Interface Sci. 448 (2015) 163-174.

[163] S. Karthikeyan, R.B. Ahamed, M. Velan, G. Sekaran, Synthesis and characterization of Co-NPAC and in situ hydroxyl radical generation for the oxidation of dye laden wastewater from the leather industry, RSC Adv. 4 (2014) 63354-63366.
[164] T.L.P. Dantas, V.P. Mendonça, H.J. José, A.E. Rodrigues, R.F.P.M. Moreira, Treatment of textile wastewater by heterogeneous Fenton process using a new composite Fe_2O_3/carbon, Chem. Eng. J. 118 (2006) 77-82.
[165] F.M. Duarte, V. Morais, F.J. Maldonado-Hódar, L.M. Madeira, Treatment of textile effluents by the heterogeneous Fenton process in a continuous packed-bed reactor using Fe/activated carbon as catalyst, Chem. Eng. J. 232 (2013) 34-41.
[166] Y. Li, H. Fei, Q.-q. Luo, M. Zhang, H.-j. Dai, L. Yin, H.-x. Shi, Preparation of Fe-Cu/activated carbon catalyst and advanced treatment of printing and dyeing wastewater by CWPO, J. Zhejiang Univ. Sci. 6 (2013) 676-680.
[167] S. Karthikeyan, M.E. Priya, R. Boopathy, M. Velan, A.B. Mandal, G. Sekaran, Heterocatalytic Fenton oxidation process for the treatment of tannery effluent: kinetic and thermodynamic studies, Environ. Sci. Pollut. Res. 19 (2012) 1828-1840.
[168] S. Karthikeyan, A. Titus, A. Gnanamani, A.B. Mandal, G. Sekaran, Treatment of textile wastewater by homogeneous and heterogeneous Fenton oxidation processes, Desalination 281 (2011) 438-445.
[169] G. Sekaran, S. Karthikeyan, K. Ramani, B. Ravindran, A. Gnanamani, A.B. Mandal, Heterogeneous Fenton oxidation of dissolved organics in salt-laden wastewater from leather industry without sludge production, Environ. Chem. Lett. 9 (2011) 499-504.
[170] S. Zhang, Y. Han, L. Wang, Y. Chen, P. Zhang, Treatment of hypersaline industrial wastewater from salicylaldehyde production by heterogeneous catalytic wet peroxide oxidation on commercial activated carbon, Chem. Eng. J. 252 (2014) 141-149.
[171] C.M. Domínguez, A. Quintanilla, J.A. Casas, J.J. Rodríguez, Treatment of real winery wastewater by wet oxidation at mild temperature, Sep. Purif. Technol. 129 (2014) 121-128.
[172] A. Quintanilla, C.M. Domínguez, N. Alonso-Morales, M.A. Gllarranz, J.A. Casas, J.J. Rodríguez, A. Rey, Carbon catalysts in humid oxidation processes with hydrogen peroxide: for industrial wastewater treatment, Ingenieria Quimica (Spain) 43 (2011) 120-124.
[173] V. Gosu, B.R. Gurjar, R.Y. Surampalli, T.C. Zhang, NFe_0/GAC-mediated advanced catalytic per-oxidation for pharmaceutical wastewater treatment, J. Environ. Chem. Eng. 2 (2014) 1996-2004.
[174] P. Bautista, Á.F. Mohedano, N. Menéndez, J.A. Casas, J.J. Rodríguez, Catalytic wet peroxide oxidation of cosmetic wastewaters with Fe-bearing catalysts, Catal. Today 151 (2010) 148-152.

[175] J. Zheng, Q. He, D. Zhang, Z. Fang, H. Bao, H. Zhang, Advanced treatment of coking wastewater by Fe^0/GAC-Fenton heterogeneous coupling process, Chin. J. Environ. Eng. 10 (2016) 6983-6987.

[176] H. Zhuang, H. Han, S. Shan, Treatment of British Gas/Lurgi coal gasification wastewater using a novel integration of heterogeneous Fenton oxidation on coal fly ash/sewage sludge carbon composite and anaerobic biological process, Fuel 178 (2016) 155-162.

[177] B. Kakavandi, A.A. Babaei, Heterogeneous Fenton-like oxidation of petrochemical wastewater using a magnetically separable catalyst (MNPs@C): process optimization, reaction kinetics and degradation mechanisms, RSC Adv. 6 (2016) 84999-85011.

[178] H. Zhuang, X. Hong, S. Shan, X. Yuan, Recycling rice straw derived, activated carbon supported, nanoscaled Fe_3O_4 as a highly efficient catalyst for Fenton oxidation of real coal gasification wastewater, RSC Adv. 6 (2016) 95129-95136.

[179] X. Qin, H. Cui, X. Wang, S. Yuan, CWPO treatment of transfer station leachate with activated carbon as catalyst, J. Beijing Univ. Tech. 42 (2016) 1435-1440.

[180] X. Hu, B. Liu, Y. Deng, H. Chen, S. Luo, C. Sun, P. Yang, S. Yang, Adsorption and heterogeneous Fenton degradation of 17α-methyltestosterone on nano Fe_3O_4/MWCNTs in aqueous solution, Appl. Catal. B 107 (2011) 274-283.

[181] X.-b. Hu, Y.-h. Deng, Z.-q. Gao, B.-z. Liu, C. Sun, Transformation and reduction of androgenic activity of 17α-methyltestosterone in Fe_3O_4/MWCNTs–H_2O_2 system, Appl. Catal. B 127 (2012) 167-174.

[182] M. Yang, J. Ma, Y. Sun, X. Xiong, C. Li, Q. Li, J. Chen, Synthesis of carbon nanotubes/FeS Fenton-like catalyst and its catalytic properties, Chem. J. Chinese Univ. 35 (2014) 570-575.

[183] J. Ma, M. Yang, F. Yu, J. Chen, Easy solid-phase synthesis of pH-insensitive heterogeneous CNTs/FeS Fenton-like catalyst for the removal of antibiotics from aqueous solution, J. Colloid Interface Sci. 444 (2015) 24-32.

[184] Z. Wan, J. Hu, J. Wang, Removal of sulfamethazine antibiotics using CeFe-graphene nanocomposite as catalyst by Fenton-like process, J. Environ. Manage. 182 (2016) 284-291.

[185] Z. Wan, J. Wang, Degradation of sulfamethazine using Fe_3O_4-Mn_3O_4/reduced graphene oxide hybrid as Fenton-like catalyst, J. Hazard. Mater. 324 (2017) 653-664.

[186] L. Wang, Q. Zhao, J. Hou, J. Yan, F. Zhang, J. Zhao, H. Ding, Y. Li, L. Ding, One-step solvothermal synthesis of magnetic Fe_3O_4-graphite composite for Fenton-like degradation of levofloxacin, J. Environ. Sci. Health A Tox. Hazard. Subst. Environ. Eng. 51 (2016) 52-62.

[187] N. Jaafarzadeh, B. Kakavandi, A. Takdastan, R.R. Kalantary, M. Azizi, S. Jorfi, Powder activated carbon/Fe_3O_4 hybrid composite as a highly efficient heterogeneous catalyst for

Fenton oxidation of tetracycline: degradation mechanism and kinetic, RSC Adv. 5 (2015) 84718-84728.

[188] R.S. Ribeiro, Z. Frontistis, D. Mantzavinos, D. Venieri, M. Antonopoulou, I. Konstantinou, A.M.T. Silva, J.L. Faria, H.T. Gomes, Magnetic carbon xerogels for the catalytic wet peroxide oxidation of sulfamethoxazole in environmentally relevant water matrices, Appl. Catal. B 199 (2016) 170-186.

[189] M.R. Carrasco-Díaz, E. Castillejos-López, A. Cerpa-Naranjo, M.L. Rojas-Cervantes, On the textural and crystalline properties of Fe-carbon xerogels. Application as Fenton-like catalysts in the oxidation of paracetamol by H_2O_2, Microporous Mesoporous Mater. 237 (2017) 282-293.

[190] M.A. Fontecha-Cámara, M.A. Álvarez-Merino, F. Carrasco-Marín, M.V. López-Ramón, C. Moreno-Castilla, Heterogeneous and homogeneous Fenton processes using activated carbon for the removal of the herbicide amitrole from water, Appl. Catal. B 101 (2011) 425-430.

[191] A. Dhaouadi, N. Adhoum, Heterogeneous catalytic wet peroxide oxidation of paraquat in the presence of modified activated carbon, Appl. Catal. B 97 (2010) 227-235.

[192] Priyanka, V. Subbaramaiah, V.C. Srivastava, I.D. Mall, Catalytic oxidation of nitrobenzene by copper loaded activated carbon, Sep. Purif. Technol. 125 (2014) 284-290.

[193] A.R. Yeddou, B. Nadjemi, F. Halet, A. Ould-Dris, R. Capart, Removal of cyanide in aqueous solution by oxidation with hydrogen peroxide in presence of activated carbon prepared from olive stones, Miner. Eng. 23 (2010) 32-39.

[194] L. Yu, X. Yang, Y. Ye, D. Wang, Efficient removal of atrazine in water with a Fe_3O_4/MWCNTs nanocomposite as a heterogeneous Fenton-like catalyst, RSC Adv. 5 (2015) 46059-46066.

[195] S. Hu, H. Yao, K. Wang, C. Lu, Y. Wu, Intensify removal of nitrobenzene from aqueous solution using nano-zero valent iron/granular activated carbon composite as Fenton-like catalyst, Water Air Soil Pollut. 226 (2015) Article number 155.

[196] S. Karthikeyan, C. Judia Magthalin, M. Mahesh, C. Anandan, G. Sekaran, Synthesis of reactive iron impregnated nanoporous activated carbon and its application in anaerobic biological treatment to enhance biodegradability of ortho-phenylenediamine, J. Chem. Technol. Biotechnol. 90 (2015) 1013-1026.

[197] M. Munoz, C.M. Domínguez, Z.M. de Pedro, A. Quintanilla, J.A. Casas, J.J. Rodríguez, Degradation of imidazolium-based ionic liquids by catalytic wet peroxide oxidation with carbon and magnetic iron catalysts, J. Chem. Technol. Biotechnol. 91 (2016) 2882-2887.

[198] A.A. Morales-Pérez, P. Maravilla, M. Solís-López, R. Schouwenaars, A. Durán-Moreno, R.M. Ramírez-Zamora, Optimization of the synthesis process of an iron oxide nanocatalyst

supported on activated carbon for the inactivation of Ascaris eggs in water using the heterogeneous Fenton-like reaction, Water Sci. Technol. 73 (2016) 1000-1009.
[199] S. Yu, L. Chen, Z. Yan, Graphene/hemin hybrid material as a catalyst for degradation of alkaline lignin with hydrogen peroxide, Bioresources 12 (2017) 2354-2366.
[200] L.B. Khalil, B.S. Girgis, T.A.M. Tawfik, Decomposition of H_2O_2 on activated carbon obtained from olive stones, J. Chem. Technol. Biotechnol. 76 (2001) 1132-1140.
[201] V. Strelko, S. Stavitskaya, N. Tsyba, A. Lysenko, S. Zhuravskii, V. Goba, Directed modification of carbons of varied origin and chemical nature of the surface in order to control their catalytic activity, Russ. J. Appl. Chem. 80 (2007) 389-396.
[202] C. Castro, L. Oliveira, M. Guerreiro, Effect of hydrogen treatment on the catalytic activity of iron oxide based materials dispersed over activated carbon: investigations toward hydrogen peroxide decomposition, Catal. Lett. 133 (2009) 41-48.
[203] A. Rey, A. Bahamonde, J.A. Casas, J.J. Rodríguez, Selectivity of hydrogen peroxide decomposition towards hydroxyl radicals in catalytic wet peroxide oxidation (CWPO) over Fe/AC catalysts, Water Sci. Technol. 61 (2010) 2769-2778.
[204] A. Aguinaco, J.P. Pocostales, J.F. García-Araya, F.J. Beltrán, Decomposition of hydrogen peroxide in the presence of activated carbons with different characteristics, J. Chem. Technol. Biotechnol. 86 (2011) 595-600.
[205] A. Rey, J.A. Zazo, J.A. Casas, A. Bahamonde, J.J. Rodríguez, Influence of the structural and surface characteristics of activated carbon on the catalytic decomposition of hydrogen peroxide, Appl. Catal. A 402 (2011) 146-155.
[206] K.V. Voitko, R.L.D. Whitby, V.M. Gun'ko, O.M. Bakalinska, M.T. Kartel, K. Laszlo, A.B. Cundy, S.V. Mikhalovsky, Morphological and chemical features of nano and macroscale carbons affecting hydrogen peroxide decomposition in aqueous media, J. Colloid Interface Sci. 361 (2011) 129-136.
[207] R.S. Ribeiro, A.M.T. Silva, J.L. Figueiredo, J.L. Faria, H.T. Gomes, The influence of structure and surface chemistry of carbon materials on the decomposition of hydrogen peroxide, Carbon 62 (2013) 97-108.
[208] C.M. Domínguez, A. Quintanilla, P. Ocón, J.A. Casas, J.J. Rodríguez, The use of cyclic voltammetry to assess the activity of carbon materials for hydrogen peroxide decomposition, Carbon 60 (2013) 76-83.
[209] X.J. Yang, P.F. Tian, H.L. Wang, J. Xu, Y.F. Han, Catalytic decomposition of H_2O_2 over a Au/carbon catalyst: a dual intermediate model for the generation of hydroxyl radicals, J. Catal. 336 (2016) 126-132.
[210] F. Haber, J. Weiss, The catalytic decomposition of hydrogen peroxide by iron salts, Proc. R. Soc. Lond. A Math. Phys. Sci. 147 (1934) 332-351.

[211] W.G. Barb, J.H. Baxendale, P. George, K.R. Hargrave, Reactions of ferrous and ferric ions with hydrogen peroxide. Part I.-The ferrous ion reaction, Trans. Faraday Soc. 47 (1951) 462-500.
[212] W.G. Barb, J.H. Baxendale, P. George, K.R. Hargrave, Reactions of ferrous and ferric ions with hydrogen peroxide. Part II.-The ferric ion reaction, Trans. Faraday Soc. 47 (1951) 591-616.
[213] M. Munoz, Z.M. de Pedro, J.A. Casas, J.J. Rodríguez, Preparation of magnetite-based catalysts and their application in heterogeneous Fenton oxidation - A review, Appl. Catal. B 176-177 (2015) 249-265.
[214] Decreto-Lei n.º 236/98 de 1 de agosto, Diário da República - I Série - A, n.º 176 - 1-8-1998.
[215] P.V. Nidheesh, R. Gandhimathi, S.T. Ramesh, Degradation of dyes from aqueous solution by Fenton processes: a review, Environ. Sci. Pollut. Res. 20 (2013) 2099-2132.
[216] J. Barrault, J.M. Tatibouët, N. Papayannakos, Catalytic wet peroxide oxidation of phenol over pillared clays containing iron or copper species, Comptes Rendus de l'Académie des Sciences - Series IIC - Chemistry 3 (2000) 777-783.
[217] M.C. Pereira, L.C.A. Oliveira, E. Murad, Iron oxide catalysts: Fenton and Fenton-like reactions - A review, Clay Miner. 47 (2012) 285-302.
[218] P.V. Nidheesh, Heterogeneous Fenton catalysts for the abatement of organic pollutants from aqueous solution: a review, RSC Adv. 5 (2015) 40552-40577.
[219] S. Rahim Pouran, A.A. Abdul Raman, W.M.A. Wan Daud, Review on the application of modified iron oxides as heterogeneous catalysts in Fenton reactions, J. Cleaner Prod. 64 (2014) 24-35.
[220] M. Muruganandham, R.P.S. Suri, M. Sillanpää, J.J. Wu, B. Ahmmad, S. Balachandran, M. Swaminathan, Recent developments in heterogeneous catalyzed environmental remediation processes, J. Nanosci. Nanotechnol. 14 (2014) 1898-1910.
[221] A. Dhakshinamoorthy, S. Navalon, M. Alvaro, H. Garcia, Metal nanoparticles as heterogeneous Fenton catalysts, ChemSusChem 5 (2012) 46-64.
[222] S. Navalon, A. Dhakshinamoorthy, M. Alvaro, H. Garcia, Heterogeneous Fenton catalysts based on activated carbon and related materials, ChemSusChem 4 (2011) 1712-1730.
[223] S. Navalon, R. Martin, M. Alvaro, H. Garcia, Gold on diamond nanoparticles as a highly efficient Fenton catalyst, Angew. Chem. Int. Ed. 49 (2010) 8403-8407.
[224] P. Ehrburger, Dispersion of small particles on carbon surfaces, Adv. Colloid Interface Sci. 21 (1984) 275–302.

[225] L.R. Radovic, F. Rodríguez-Reinoso, in: P.A. Thrower (Ed.), Chemistry and physics of carbon, Marcel Dekker, New York, 1997, pp. 243-358.
[226] E. Auer, A. Freund, J. Pietsch, T. Tacke, Carbons as supports for industrial precious metal catalysts, Appl. Catal. A 173 (1998) 259-271.
[227] R. Schlögl, in: G. Ertl, H. Knözinger, J. Weitkamp (Eds.), Preparation of Solid Catalysts, Wiley-VCH Verlag GmbH, Weinheim, Germany, 1999, pp. 150-240.
[228] L.R. Radovic, C. Sudhakar, in: H. Marsh, E.A. Heintz, F. Rodríguez-Reinoso (Eds.), Introduction to carbon technologies, University of Alicante Press, Alicante, Spain, 1997, pp. 103-165.
[229] F. Rodríguez-Reinoso, in: J.W. Patrick (Ed.), Porosity in carbons: characterization and applications, Edward Arnold, London, 1995.
[230] F. Rodríguez-Reinoso, The role of carbon materials in heterogeneous catalysis, Carbon 36 (1998) 159-175.
[231] P. Serp, J.L. Figueiredo, Carbon materials for catalysis, John Wiley & Sons, Inc., Hoboken, New Jersey, 2009.
[232] J.L. Figueiredo, Functionalization of porous carbons for catalytic applications, J. Mater. Chem. A 1 (2013) 9351-9364.
[233] P. Serp, M. Corrias, P. Kalck, Carbon nanotubes and nanofibers in catalysis, Appl. Catal. A 253 (2003) 337-358.
[234] R.W. Coughlin, Carbon as adsorbent and catalyst, Ind. Eng. Chem. Prod. Res. Dev. 8 (1969) 12–23.
[235] P. Serp, B.F. Machado, Nanostructured carbon materials for catalysis, The Royal Society of Chemistry, Cambridge, UK, 2015.
[236] B.H.J. Bielski, D.E. Cabelli, R.L. Arudi, A.B. Ross, Reactivity of HO_2/O_2^- radicals in aqueous solution, J. Phys. Chem. Ref. Data 14 (1985) 1041-1100.
[237] G.V. Buxton, C.L. Greenstock, W.P. Helman, A.B. Ross, Critical Review of rate constants for reactions of hydrated electrons, hydrogen atoms and hydroxyl radicals ($HO^•/O^{•-}$) in aqueous solution, J. Phys. Chem. Ref. Data 17 (1988) 513-886.
[238] H. Christensen, K. Sehested, H. Corfitzen, Reactions of hydroxyl radicals with hydrogen peroxide at ambient and elevated temperatures, J. Phys. Chem. 86 (1982) 1588-1590.
[239] A.J. Elliot, G.V. Buxton, Temperature dependence of the reactions OH + O_2^- and OH + HO_2 in water up to 200 ºC, J. Chem. Soc., Faraday Trans. 88 (1992) 2465-2470.
[240] M.G. Evans, N. Uri, The dissociation constant of hydrogen peroxide and the electron affinity of the HO_2 radical, Trans. Faraday Soc. 45 (1949) 224-230.
[241] W.H. Koppenol, J. Butler, J.W. Van Leeuwen, The Haber-Weiss cycle, Photochem. Photobiol. 28 (1978) 655-658.

[242] S.-S. Lin, M.D. Gurol, Catalytic decomposition of hydrogen peroxide on iron oxide: kinetics, mechanism, and implications, Environ. Sci. Technol. 32 (1998) 1417-1423.
[243] K.G. Linden, C.M. Sharpless, S.A. Andrews, K.Z. Atasi, V. Korategere, M. Stefan, I.H.M. Suffet, Innovative UV technologies to oxidize organic and organoleptic chemicals, in: I. Publishing (Ed.), London, 2005, p. Chapter 8.
[244] J. Weinstein, B.H.J. Bielski, Kinetics of the interaction of perhydroxyl and superoxide radicals with hydrogen peroxide. The Haber-Weiss reaction, J. Am. Chem. Soc. 101 (1979) 58-62.
[245] S. Ghafoori, M. Mehrvar, P.K. Chan, Free-radical-induced degradation of aqueous polyethylene oxide by UV/H_2O_2: experimental design, reaction mechanisms, and kinetic modeling, Ind. Eng. Chem. Res. 51 (2012) 14980-14993.
[246] T. Schaefer, J. Schindelka, D. Hoffmann, H. Herrmann, Laboratory kinetic and mechanistic studies on the OH-initiated oxidation of acetone in aqueous solution, J. Phys. Chem. A 116 (2012) 6317-6326.
[247] D.G. Rao, R. Senthilkumar, J.A. Byrne, S. Feroz, Wastewater treatment: advanced processes and technologies, CRC Press and IWA Publishing, London, UK, 2013.
[248] S. Boncel, A.P. Herman, K.Z. Walczak, Magnetic carbon nanostructures in medicine, J. Mater. Chem. 22 (2012) 31-37.
[249] M. Zhu, G. Diao, Review on the progress in synthesis and application of magnetic carbon nanocomposites, Nanoscale 3 (2011) 2748-2767.
[250] K.W. Brown, K.C. Donnelly, An estimation of the risk associated with the organic constituents of hazardous and municipal waste landfill leachates, Hazard. Waste Hazard. Mater. 5 (1988) 1-30.
[251] S. Sporstøl, K. Urdal, H. Drangsholt, N. Gjøs, Description of a method for automated determination of organic pollutants in water, Int. J. Environ. Anal. Chem. 21 (1985) 129-138.
[252] ATSDR, Toxicological profile for nitrophenols, Agency for Toxic Substances and Disease Registry, U.S. Public Health Service, Atlanta, U.S., 1992.
[253] EPA, Treatability manual volume I, U.S. Environmental Protection Agency, Office of Research and Development, Washington, DC, 1980.
[254] EPA, Health effects assessment for nitrophenols, U.S. Environmental Protection Agency, Office of Research and Development, Cincinnati, OH, 1987.

3. OBJECTIVES

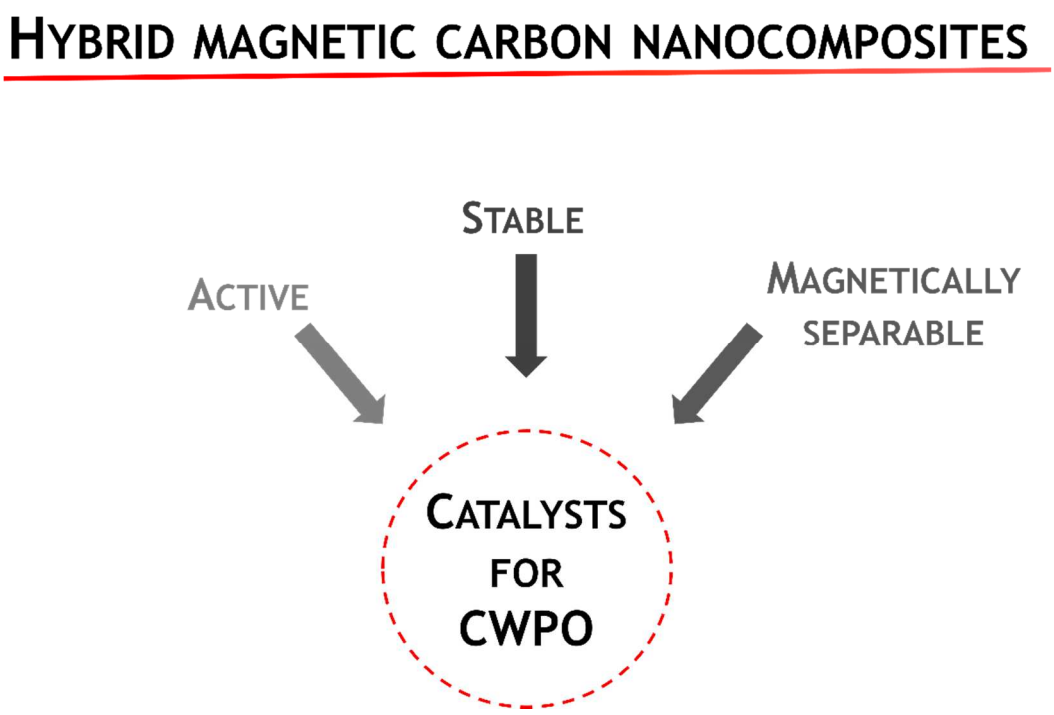

Catalyst design plays a crucial role in CWPO. Bearing this in mind, the main objective in the conducted Ph.D. studies was the synthesis of hybrid magnetic carbon nanocomposites with high activity and stability characteristics for the CWPO of bio-recalcitrant pollutants. More specifically, it was intended to explore the synergistic effects that arise from the combination of the high catalytic activity of iron species with that of other metal species in CWPO, and the easily tailoring characteristics of carbon-based materials, as detailed in Chapter 2. In addition, the magnetic properties of these nanocomposites enable the realization of the different stages of treatment in a single vessel, namely equalization and treatment of the polluted water, as well as catalyst separation, avoiding typical systems needed in CWPO for separation of the catalyst, such as filtration.

In order to accomplish these objectives, synthesis techniques were optimized to obtain shape-controlled, highly stable and well-defined hybrid magnetic carbon nanocomposites. For that purpose, the recently developed synthesis techniques listed in Chapter 2 were considered, so that the catalytic activity of the resultant nanostructured materials can be appropriate and kept as similar as possible during successive reuse sequencing operations and in semi-continuous operation, a crucial requisite regarding the potential industrial application of the catalysts.

H_2O_2 is the main reactant employed in the CWPO process and thus the main contributor to the global cost. Therefore, an excessive consumption of H_2O_2 may hinder the viability of this water/wastewater treatment technology. It is know that an inefficient usage of H_2O_2 can be the result of several parasitic and radical scavenging reactions occurring in the bulk (*cf*. Table 2.4). Although most CWPO applications typically deal with pollutants present in water at low concentrations (up to 0.1 g L^{-1}) [1-4], recent studies performed with metal-free carbon-based catalysts show that higher H_2O_2 usage efficiencies (close to 100%) can be obtained when operating at higher pollutant loads (up to 5 g L^{-1}), under a process intensification approach [5-9]. This approach also allows increasing the range of industrial wastewater treatment applications of CWPO. Bearing this in mind, the developed catalytic systems were studied in the CWPO of selected model pollutants, searching the optimization of these catalytic systems and further process optimization through the variation of process operating parameters, a special emphasis being given to the efficiency of H_2O_2 consumption, as well as to the understanding of the degradation mechanisms involved. Likewise, the influence of operating pH was also studied. In this case, the main objective is to avoid the generation of acidic waters, which is a typical drawback of the Fenton process.

Once optimized the catalytic systems and the CWPO process, the benefits of magnetic separation for the recovery of the catalyst in water treatments were explored, since catalyst separation and long-term stability are crucial aspects for the feasibility of the proposed

process in possible large scale applications. Thus, the final defined goal was to develop a sequencing CWPO reactor coupled with a magnetic separation device, combining the knowledge acquired in previous stages.

References

[1] J.A. Zazo, J.A. Casas, A.F. Mohedano, J.J. Rodríguez, Catalytic wet peroxide oxidation of phenol with a Fe/active carbon catalyst, Appl. Catal. B 65 (2006) 261-268.

[2] X. Hu, B. Liu, Y. Deng, H. Chen, S. Luo, C. Sun, P. Yang, S. Yang, Adsorption and heterogeneous Fenton degradation of 17α-methyltestosterone on nano Fe_3O_4/MWCNTs in aqueous solution, Appl. Catal. B 107 (2011) 274-283.

[3] A. Rodríguez, G. Ovejero, J.L. Sotelo, M. Mestanza, J. García, Heterogeneous Fenton catalyst supports screening for mono azo dye degradation in contaminated wastewaters, Ind. Eng. Chem. Res. 49 (2010) 498-505.

[4] J.H. Ramirez, F.J. Maldonado-Hódar, A.F. Pérez-Cadenas, C. Moreno-Castilla, C.A. Costa, L.M. Madeira, Azo-dye orange II degradation by heterogeneous Fenton-like reaction using carbon-Fe catalysts, Appl. Catal. B 75 (2007) 312-323.

[5] A. Dhaouadi, N. Adhoum, Heterogeneous catalytic wet peroxide oxidation of paraquat in the presence of modified activated carbon, Appl. Catal. B 97 (2010) 227-235.

[6] C.M. Domínguez, P. Ocón, A. Quintanilla, J.A. Casas, J.J. Rodríguez, Graphite and carbon black materials as catalysts for wet peroxide oxidation, Appl. Catal. B 144 (2014) 599-606.

[7] H.T. Gomes, S.M. Miranda, M.J. Sampaio, A.M.T. Silva, J.L. Faria, Activated carbons treated with sulphuric acid: catalysts for catalytic wet peroxide oxidation, Catal. Today 151 (2010) 153-158.

[8] R.S. Ribeiro, N.A. Fathy, A.A. Attia, A.M.T. Silva, J.L. Faria, H.T. Gomes, Activated carbon xerogels for the removal of the anionic azo dyes orange II and chromotrope 2R by adsorption and catalytic wet peroxide oxidation, Chem. Eng. J. 195-196 (2012) 112-121.

[9] R.S. Ribeiro, A.M.T. Silva, J.L. Figueiredo, J.L. Faria, H.T. Gomes, Removal of 2-nitrophenol by catalytic wet peroxide oxidation using carbon materials with different morphological and chemical properties, Appl. Catal. B 140 (2013) 356-362.

4. MATERIALS AND METHODS

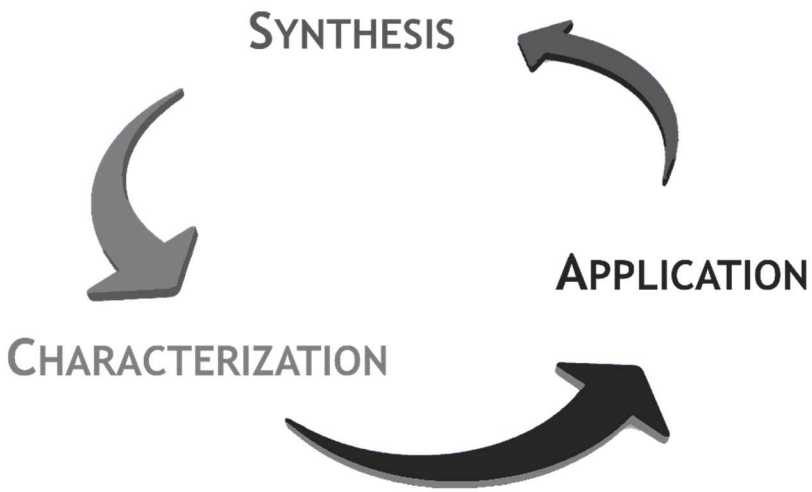

4.1. Synthesis procedures

The procedures employed for the preparation of all the materials considered in this Ph.D. dissertation are detailed in this Section.

4.1.1. Glycerol-based carbon materials

A glycerol-based carbon material (GBCM) was prepared by partial carbonization of glycerol (99 wt.%), adapting a procedure described elsewhere [1]. Briefly, a mixture of glycerol (10 g) and concentrated (95-97 wt.%) sulphuric acid (40 g) was gently heated to 180 ºC and left at that temperature for 20 min to allow *in-situ* partial carbonization. The resulting material, characterized as a strong solid acid carbon material, due to the presence of high amounts of sulphonic acid groups [1], was then ground to obtain particle sizes in the range 0.106-0.250 mm. Then, it was treated under a N_2 flow (100 cm^3 min^{-1}) at 120, 400 and 600 ºC during 60 min at each temperature, and afterwards at 800 ºC for 240 min (defining a heating ramp of 2 ºC min^{-1}) in order to stabilize the initial material (which by thermogravimetric analysis under N_2 atmosphere revealed to decompose about 50 wt.% up to 800 ºC). The treated material was named GBCM. Thereafter, GBCM was further thermally activated under oxidative atmosphere (air flow = 100 cm^3 min^{-1}) during 60 min at different temperatures, from 150 to 350 ºC, in order to produce several materials with different textural and surface chemistry properties, which were labelled as GBCM followed by a subscript number corresponding to the activation temperature in ºC (i.e., $GBCM_{150}$, $GBCM_{200}$, $GBCM_{300}$ and $GBCM_{350}$)[2]. In this temperature range, the weight loss (burn-off) due to the thermal activation under air atmosphere ranges from 9 to 20 wt.%.

4.1.2. Graphene-based carbon materials

Graphene oxide (GO) was synthesized from natural graphite (particle size ≤ 20 μm, from Sigma-Aldrich), by a modified Hummers method [2, 3] described elsewhere [4]. Concentrated sulphuric acid (50 mL) was added gradually with stirring to a 500 mL flask containing 2 g of graphite and immersed in an ice bath. 6 g of potassium permanganate was added slowly to the mixture, the suspension being continuously stirred for 2 h at 35 ºC. After that, it was allowed to cool in an ice bath and subsequently diluted with 350 mL of distilled water. Afterwards, H_2O_2 (30% w/v) was added in order to reduce residual permanganate to soluble manganese ions, a bright yellow colour appearing in the suspension. The oxidized material was purified with an hydrochloric acid solution (10 wt.%) and the suspension was

[2] The particular task of GBCM thermal activation under oxidative atmosphere was partially carried out by M.T. Pinho.

then filtered, washed several times with distilled water until the neutrality of the rinsing waters was reached, and dried at 60 ºC for 24 h to obtain graphite oxide. The resulting material was dispersed in a given volume of water and sonicated (ultrasonic processor UP400S, 24 kHz) for 1 h. The sonicated dispersion was centrifuged for 20 min at 3000 rpm to remove unexfoliated graphite oxide particles from the supernatant, GO being obtained in this way (ash content of ca. 0.06 wt.%, as determined by thermogravimetric analysis).

Reduced graphene oxide (rGO) samples were obtained by chemical reduction of GO using vitamin C (rGOV) [5], glucose (rGOG) [6] and hydrazine (rGOH) [7] as reducing agents and employing the aqueous dispersion of GO, as described elsewhere [8][3]. Briefly, the GO suspension (0.1 g L^{-1}) containing the reducing agent (2 mmol L^{-1}) was heated at 95 ºC for 3 h under vigorous stirring. Before reduction, the pH of the GO dispersion was adjusted to 9-10 with a 25% ammonia solution to promote the colloidal stability of the GO sheets through electrostatic repulsion.

4.1.3. Magnetic carbon xerogels

The magnetic carbon xerogels were obtained by inclusion of iron and/or cobalt precursors during the synthesis of the carbon xerogel by polycondensation of resorcinol with formaldehyde [9]. For that purpose, 9.91 g of resorcinol was dissolved in 18.8 mL of distilled water. Iron (III) chloride hexahydrate was added to the resorcinol solution (considering a Fe/resorcinol molar ratio of 0.05) and then stirred in an orbital shaker (160 rpm) during 2 h. 13.5 mL of formaldehyde solution was then added and the pH adjusted to 6.1 by means of NaOH solutions (1 and 0.02 mol L^{-1}). The gelation step was allowed to proceed freely, without catalyst, in a 100 mL beaker at 85 ºC during 3 days. The recovered gel was ground, dried in an oven (from 60 to 150 ºC, defining a heating ramp of 20 ºC day^{-1}) and annealed under a N_2 flow (100 cm^3 min^{-1}), in a tubular vertical furnace, at 120, 400 and 600 ºC during 60 min at each temperature, and then at 800 ºC for 240 min, defining a heating ramp of 2 ºC min^{-1}. Afterwards, the solid was washed with 1 L of a HCl solution (pH = 3) at 50 ºC and dried overnight at 60 ºC, resulting in the CX/Fe materials. This final step aims to wash out metal species that are not strongly embedded in the carbonaceous structure of the material, thereby increasing its stability and limiting the contamination of the water treated by CWPO. Likewise, CX/Co was obtained by adding cobalt (II) chloride hexahydrate (considering a Co/resorcinol molar ratio of 0.025). CX/CoFe was obtained by adding iron (III) chloride hexahydrate (Fe/resorcinol molar ratio of 0.05) and cobalt (II) chloride hexahydrate (Fe/Co molar ratio of 2, as previously reported for iron-copper bimetallic nanoparticles embedded

[3] Graphene-based materials were prepared by L.M. Pastrana-Martínez.

within ordered mesoporous carbon composite catalysts [10]). A carbon xerogel (CX) was prepared following the same procedure, but in the absence of metal precursors.

4.1.4. Magnetic nanoparticles

Magnetite (Fe_3O_4) was synthesised by co-precipitation of Fe^{2+} and Fe^{3+} in basic solution, at 30 ºC and under N_2 atmosphere. For that purpose, 13.44 mmol of iron (II) chloride tetrahydrate and 26.88 mmol of iron (III) chloride hexahydrate were dissolved in 250 mL of distilled water and transferred into a 500 mL glass reactor, equipped with a condenser and immersed in an oil bath with controlled temperature. When the desired temperature was reached, the mixture was deaerated during 10 min with N_2 under vigorous stirring, and further kept under inert atmosphere. At this point, 10 mL of ammonia solution (25 wt.%) was quickly added, and a black precipitate was instantly obtained. Afterwards, possible residues of the precursors were washed-out with distilled water, the sample being then dried in an oven at 60 ºC for 24 h, resulting in the Fe_3O_4 material.

Cobalt ferrite ($CoFe_2O_4$) was synthesized by co-precipitation of Co^{2+} and Fe^{3+} in basic solution at 75 ºC, adapting the procedure described elsewhere [11]. For that purpose, 67 mmol of cobalt (II) chloride hexahydrate and 134 mmol of iron (III) chloride hexahydrate were dissolved in 100 mL of distilled water and transferred into a 250 mL glass reactor, equipped with a condenser and immersed in an oil bath with controlled temperature. When the desired temperature was reached, 80 mL of ammonia solution (1 mol L^{-1}) was added dropwise using a peristaltic pump, under constant vigorous stirring. After the colour of the solution turned to dark-brown, the mixture was kept under vigorous stirring for additional 30 min, in order to ensure the complete formation of ferrite crystals. Possible residues of the precursors were washed-out with distilled water and absolute ethanol, the sample being then dried in an oven at 60 ºC for 24 h, ground into fine powder and treated under a purified air flow (100 cm^3 min^{-1}) at 500 ºC for 2 h with a heating ramp of 2 ºC min^{-1}, allowing crystallization of the materials with the inverse spinel structure [11, 12], and resulting in the $CoFe_2O_4$ sample[4].

4.1.5. Hybrid magnetic graphitic nanocomposites

The magnetic graphitic nanocomposites (MGNC) were prepared by hierarchical co-assembly of magnetic nanoparticles and carbon precursors, followed by thermal treatment, adapting the procedure described elsewhere [13]. For that purpose, 5 g of copolymer pluronic F127 was dissolved in 50 mL of H_2O, in a round bottom 500 mL glass reactor equipped with a condenser and immersed in an oil bath with temperature control.

[4] $CoFe_2O_4$ was prepared by R.O. Rodrigues.

Then, 5 mL of magnetic nanoparticles suspension (17 mg mL^{-1}, previously obtained by dispersion of Fe_3O_4 or $CoFe_2O_4$, in H_2O in an ultrasonic bath) was added, the resulting solution being stirred during 2 h at 66 ºC for homogenization. After that, ≈ 60 mL of a phenol/formaldehyde resol solution was added, the resulting mixture being kept under stirring (400 rpm) at 66 ºC for 72 h and then at 70 ºC for an additional period of 24 h. The phenol/formaldehyde resol solution was prepared by dissolution of 2.0 g of phenol in 7.0 mL of formaldehyde 37 wt.% solution, to which 50.0 mL of NaOH 0.1 mol L^{-1} was added, the solution being then kept under stirring at 70 ºC for 30 min.

In each case, the recovered solids were washed with distilled water in order to promote the washing-out of some possible residues of the precursors and then dried overnight in an oven at 60 ºC. Then, each sample was thermally treated under a N_2 flow (100 cm^3 min^{-1}) at 120, 400 and 600 ºC during 60 min at each temperature and then at 800 ºC for 240 min, defining a heating ramp of 2 ºC min^{-1}. Finally, each sample was washed with 1 L of distilled water at 50 ºC under vacuum filtration, and afterwards with 1 L of HCl solution (pH = 3), also at 50 ºC under vacuum filtration, being then dried overnight in an oven at 60 ºC, resulting in the Fe_3O_4/MGNC or $CoFe_2O_4$/MGNC materials.

4.2. Characterization techniques

Several techniques were used for the characterization of the materials reported in Section 4.1., in order to obtain deep information about their physical and chemical properties. A detailed experimental description of these techniques is provided in the following Sections.

4.2.1. Textural properties

The textural properties of the materials were determined from N_2 adsorption–desorption isotherms at -196 ºC, obtained in a Quantachrome NOVA 4200e adsorption analyser. Before the analysis, all samples were outgassed for 6 h at 130 ºC. The specific surface area (S_{BET}) was determined by applying the Brunauer-Emmett-Teller (BET) equation [14]. The micropore volume (V_{micro}) and the non-microporous surface area (S_{meso}) were determined by the t-method using an appropriate standard isotherm [15]. The total pore volume (V_{total}) was derived from the amount of N_2 adsorbed at a relative pressure close to unity, namely at p/p^o = 0.995 [16]. The average pore diameter (d_{pore}) was estimated from Eq. 4.1, assuming that the pores are of cylindrical shape and most of the surface area arises from the inner walls of the pores [17].

$$d_{pore} = \frac{4V_{total}}{S_{BET}} \qquad \textbf{(4.1)}$$

4.2.2. Topographical characterization

The topographical characterization of the materials was performed by transmission electron microscopy (TEM) and scanning electron microscopy (SEM).

4.2.2.1. Transmission electron microscopy

TEM was performed in a LEO 906E instrument operating at 120 kV, equipped with a 4 Mpixel 28 × 28 mm CCD camera from TRS. TEM micrographs were obtained in bright field and dark filed image modes[5]. ImageJ software was used in order to estimate the size of the materials. Specifically, at least 100 counts were performed for the determination of the magnetic nanoparticles size; and at least 65 counts were performed for the determination of the metal core size of the MGNC materials.

4.2.2.2. Scanning electron microscopy

SEM images in secondary electron (SE) and backscattered electron (BSE) detection modes were obtained using a FEI Quanta 400FEG ESEM/EDAX Genesis X4M instrument equipped with an Energy Dispersive Spectrometer (EDS)[6]. ImageJ software was used in order to estimate the size of the materials. At least 110 counts were performed for the determination of the size of the primary carbon microspheres of the carbon xerogel materials; and at least 65 counts were performed in order to estimate the size of the metal particles embedded in their structure.

4.2.3. Surface chemistry properties

The surface chemistry characterization comprised the determination of: pH at the point of zero charge (pH_{pzc}); concentration of acidic and basic sites; thermogravimetric analysis (TGA); X-ray diffraction (XRD); X-ray photoelectron spectroscopy (XPS); temperature programmed desorption (TPD); and atomic absorption spectroscopy. An experimental description of each technique is provided in the following Sections.

4.2.3.1. pH at the point of zero charge

The pH_{PZC} of the materials was determined by pH drift tests, adapting the procedures previously reported [18, 19]. For that purpose, solutions with varying initial pH (2-11) were prepared using HCl (1 mol L^{-1}) or NaOH (1 mol L^{-1}) and 20 mL of NaCl (0.01 mol L^{-1}) as electrolyte. Each solution was contacted with 0.05 g of the material and the final pH was measured after 48 h of continuous stirring (320 rpm) in an orbital shaker at room temperature. The pH_{PZC} was determined by intercepting the obtained final pH vs. initial pH curve with the straight line final pH = initial pH [20, 21].

[5] TEM micrographs were obtained by P.B. Tavares.
[6] SEM micrographs were obtained through an outsourced paid service.

4.2.3.2. Concentration of acidic and basic sites

The concentration of acidic sites at the surface of the materials was determined using a titration technique, adapting the procedure reported elsewhere [19]. For that purpose, 0.2 g of the material was contacted with 25 mL of a NaOH solution (0.02 mol L^{-1}) during 48 h under continuous stirring (320 rpm) in an orbital shaker at room temperature. Afterwards, the residual suspension was filtered, and the excess of OH^- was titrated with a HCl solution (0.02 mol L^{-1}) using phenolphthalein as indicator. Likewise, the concentration of basic sites at the surface of the materials was determined by contacting 0.2 g of the material with 25 mL of the HCl solution, the excess of H^+ being titrated with the NaOH solution.

4.2.3.3. Thermogravimetric analysis

TGA was performed using two different apparatus. The first was a Netzsch STA 490 PC/4/H Luxx thermal analyser, in which the sample was heated in a gas flow from 50 to 1000 ºC at 20 ºC min^{-1}; the second was a Netzsch TG 209 F3 Tarsus thermal analyser, the sample being heated from 30 to 950 ºC at 20 ºC min^{-1}. Both oxidative (air) and inert (N_2) gas flows were employed.

4.2.3.4. X-Ray diffraction

XRD analysis was performed in a PANalytical X'Pert MPD equipped with a X'Celerator detector and secondary monochromator (Cu Kα λ = 0.154 nm; data recorded at a 0.017º step size). The crystallographic phases were identified using the HighScore software and Crystallography Open Database. Rietveld refinement of the XRD diffraction patterns was performed using PowderCell software allowing phase quantification. Crystallite sizes were determined by the Williamson-Hall method[7].

4.2.3.5. X-Ray photoelectron spectroscopy

XPS analysis was performed in a Kratos Axis Ultra HAS equipment using a monochromatic Al X-ray source (1486.7 eV), powered at 15 kV (90 W), in lens hybrid mode. For the data analysis, the charge correction was based on the C 1s peak (285 eV). After a Shirley background subtraction, the C 1s, O 1s, Fe 2p and Co 2p peaks were fitted to Gaussian curves using the CasaXPS software[8].

4.2.3.6. Temperature programmed desorption

TPD was performed in a fully automated AMI-300 Catalyst Characterization Instrument (Altamira Instruments), equipped with a quadrupole mass spectrometer (Dymaxion, Ametek). For that purpose, the sample (0.10 g) was placed in a U-shaped quartz tube inside

[7] XRD analysis was performed by P.B. Tavares.
[8] XPS spectra were obtained through an outsourced paid service.

an electrical furnace and heated at 5 ºC min^{-1} up to 800 ºC using a constant flow rate of helium (25 cm^3 min^{-1}). The mass signals m/z = 28 and 44 were monitored during the thermal analysis, the corresponding TPD spectra being obtained. CO and CO_2 were calibrated at the end of each analysis with the respective gases [22].

The concentration of CO_2 and CO were obtained by integrating the area of the respective spectra. The percentage of oxygen in the sample was estimated from Eq. 4.2. Deconvolution analysis of the CO_2 and CO TPD spectra was performed as described elsewhere [22, 23]. For that purpose, the peaks in the CO_2 TPD spectra of the carbon materials were assigned to different functional groups, namely: strongly acidic carboxylic acids (SA; released in the range 230-280 ºC); less acidic carboxylic acids (LA; 300-350 ºC); carboxylic anhydrides (CAn; 480-540 ºC); and lactones (Lac; 610-720 ºC). Likewise, the peaks in the CO TPD spectra were assigned to: carboxylic anhydrides (Can; 480-540 ºC); phenols (Ph; 640-670 ºC); ethers (Eth; 700-720 ºC); and quinones (Qui; 820-850 ºC).

$$[O]/\ wt.\% = \left(\left([CO_2]/\ mol\ g^{-1} \times 2 + [CO]/\ mol\ g^{-1}\right) \times 16\ g\ mol^{-1}\right) \times 100 \qquad \textbf{(4.2)}$$

4.2.3.7. Atomic absorption spectroscopy

The total contents of Fe and Co were determined by atomic absorption analysis of the solution resulting from the acidic digestion of the solids. For this purpose, each sample was initially dispersed in distilled water (1 mg mL^{-1}). 1 mL of each dispersion was later added to 1 mL of aqua regia (mixture of pure nitric acid and hydrochloric acid, with a volume ratio of 1:3), the resulting solution being heated at 60 ºC for 48 h in order to promote the sample digestion. After being cooled down to room temperature, the digested samples were filtered (CA syringe filters, 0.45 μm) and the Fe and Co concentrations were determined by a PerkinElmer PinAAcle 900 atomic absorption spectrometer, using single and multi-element hollow cathode lamps (Lumina N3050126 and N3050214) for the determination of Fe and Co, respectively.

4.3. Catalytic wet peroxide oxidation

Batch CWPO experiments were performed in a well-stirred (600 rpm) glass reactor equipped with a condenser, a temperature measurement thermocouple, a pH measurement electrode and a sample collection port. The reactor was loaded with the aqueous solution of the model pollutant and heated by immersion in an oil bath at controlled temperature. Upon stabilization at the desired temperature, the solution pH was adjusted by means of H_2SO_4 and NaOH solutions (0.02 and 1 mol L^{-1}) when necessary, and the experiments were allowed to proceed freely, without further pH conditioning. A calculated volume of H_2O_2 (30% w/v) was injected into the system, in order to reach the desired concentration. The

catalyst was added after complete homogenization of the resulting solution, that moment being considered as t_0 = 0 min. Pure adsorption runs were also performed in order to assess the possible adsorption influence on the pollutant removal by CWPO, but, in this case, the amount of H_2O_2 was replaced by distilled water. Blank experiments, without any catalyst, were also carried out to assess possible non-catalytic oxidation promoted by H_2O_2.

In order to show the predominant role of heterogeneous catalysis promoted by Fe_3O_4/MGNC and $CoFe_2O_4$/MGNC, leaching tests were performed as proposed by Sheldon et al. [24], namely by removing the corresponding catalyst after 30 min of reaction at the reaction temperature, and allowing the reaction solution to progress further. The participation of $HO^{\bullet}$ radicals in the CWPO process was indirectly shown by adding *tert*-butanol (tBuOH) —a strong $HO^{\bullet}$ scavenger [25, 26].

4.4. Analytical methods

Several analytical methods were needed in order to evaluate the performance of the materials under study, as described in the following Sections.

4.4.1. 4-nitrophenol and possible oxidation by-products

The concentration of 4-nitrophenol (4-NP) was determined by high performance liquid chromatography (HPLC), adapting the procedure described elsewhere [27]. For that purpose, a Jasco HPLC system equipped with an UV/Vis detector (UV-2075 Plus), a quaternary gradient pump (PU-2089 Plus) for solvent delivery (1 mL min^{-1}) and a Kromasil 100-5-C18 column (15 cm x 4.6 mm; 5 μm particle size) was employed. The mobile phase consisted in an isocratic method of A:B (40:60) mixture of 3% acetic acid and 1% acetonitrile in methanol (A) and 3% acetic acid in ultrapure water (B). The absorbance of 4-NP peaked at 318 nm, as determined from the corresponding UV-Vis absorption spectrum (Jasco V530). Possible intermediates of 4-NP oxidation (e.g., hydroquinone, 1,4-benzoquinone, 4-nitrocatechol, catechol and phenol) were monitored using the same system, the absorbance wavelength being adjusted to 277 nm.

The formation and evolution of nitrates and carboxylic acids (e.g., formic, acetic, oxalic, malonic, maleic and malic acids) were also monitored using the same Jasco HPLC system, this time equipped with an YMC – Triart C18 column (25 cm x 4.6 mm; 5 μm particle size), adapting procedures reported elsewhere [28, 29]. The mobile phase consisted in an isocratic method of A:B (95:5) mixture of 1% sulphuric acid in ultrapure water (A) and acetonitrile (B), delivered to the system at 0.6 mL min^{-1}. The UV/Vis detector was set to 210 nm.

A thorough description of the HPLC methods used for the determination of the 4-NP parent compound and its possible oxidation by-products is provided in Appendix B, including

further details on the methods development and validation under the typical criteria for in-house pre-validations.

4.4.2. 2-nitrophenol

The concentration of 2-nitrophenol (2-NP) was determined using the HPLC method described for the quantification of 4-NP (*cf.* Section 4.4.1.), except that the absorbance wavelength was adjusted to 277 nm (the maximum absorbance, as determined by the analysis of the respective spectrum obtained by UV-Vis spectrophotometry).

4.4.3. Sulfamethoxazole

The concentration of sulfamethoxazole (SMX) was determined by HPLC, using an Alliance HPLC system equipped with a photodiode array detector (Waters 2996), a separation module including a gradient pump (Waters 2695) for solvent delivery (0.35 mL min^{-1}) and a Kinetex C18 100A column (150 mm × 3 mm; 2.6 μm particle size) maintained at 45 ºC. The mobile phase consisted in an isocratic method of ultrapure water (60%) and acetonitrile (40%). The absorbance of SMX peaked at 270 nm, as determined from the corresponding UV–Vis absorption spectrum (Waters 2996).

4.4.4. Hydrogen peroxide

The concentration of hydrogen peroxide (H_2O_2) was followed by a colorimetric method with titanium (IV) oxysulfate, adapted from the procedures described elsewhere [30, 31]. For that purpose, each sample was added to 1 mL of H_2SO_4 solution (0.5 mol L^{-1}) in a 20 mL volumetric flask, to which 0.1 mL of titanium oxysulfate was added. The resulting mixture was diluted with distilled water and further analysed by UV-Vis spectrophotometry (T70 spectrometer, PG Instruments, Ltd.) at 405 nm.

4.4.5. Total organic carbon

The determination of total organic carbon (TOC) was performed using three apparatus, namely: Shimadzu TOC-5000A (Chapter 5), Rosemount Analytical Dohrmann DC-190 (Chapter 6) and Shimadzu TOC-L CSN (Chapters 7 – 10).

4.4.6. Chemical oxygen demand

Chemical oxygen demand (COD) was determined by a closed reflux colorimetric method, adapting the procedure described elsewhere [32]. For that purpose, 2 mL of sample was mixed with 0.75 mL of potassium dichromate digestion solution (0.15 N) and 3.25 mL of sulphuric acid reagent. The mixture was kept at 150 ºC for 2 h, and, after cooling down, the

absorbance was measured at 436 nm. The sulphuric acid reagent solution was previously obtained by adding 6.6 g of silver sulphate to 1 L of concentrated sulphuric acid. A 10:1 weight ratio of $HgSO_4$:Cl^- was ensured in all the analysis in order to avoid the interference of chloride ion [32]. The apparent COD value obtained (COD_{app}) was then corrected considering the theoretical interference of residual H_2O_2, as described in Eq. 4.3, which was given elsewhere [33]. Nevertheless, the correction equation was experimentally confirmed in this study considering the concentration range $0 \leq [H_2O_2] \leq 692$ mg L^{-1}.

4.4.7. Absorbance spectra

Absorbance spectra in the range 200 – 660 nm were obtained with a 0.5 nm sampling interval, using a T70 spectrometer (PG Instruments, Ltd.).

4.4.8. Aromaticity

Aromaticity was estimated by measuring the absorbance at 254 nm —a wavelength at which most aromatic compounds typically present a maximum value of absorbance [34]. The contribution of residual H_2O_2 on aromaticity was experimentally determined using H_2O_2 standard solutions in the range 10 – 14000 mg L^{-1}. Afterwards, the apparent aromaticity value obtained ($Aromaticity_{app}$) was corrected considering the interference of residual H_2O_2, as described in Eq. 4.4.

4.4.9. 5-Day biochemical oxygen demand

The 5-day biochemical oxygen demand (BOD_5) was determined by the standardised respirometric OxiTop® method (WTW, Weilheim, Germany). For that purpose, an appropriate volume of sample was added into an amber glass bottle (nominal volume 510 mL) equipped with a magnetic stirrer and a carbon dioxide trap in the headspace (NaOH pellets). Each bottle was sealed with an OxiTop® head and then placed in an incubator box at constant temperature (20 ºC) during the five-day incubation period. The BOD_5 value was calculated from the pressure decrease in the closed vessel, as recorded via the piezoresistive electronic pressure sensors of the OxiTop® measuring system. In the samples collected after CWPO, the apparent BOD_5 value obtained ($BOD_{5,\ app}$) was then corrected considering the theoretical interference of residual H_2O_2, as described in Eq. 4.5.

$$COD = COD_{app} - 0.4706\ [H_2O_2]/\ mg\ L^{-1} \quad \textbf{(4.3)}$$

$$Aromaticity = Aromaticity_{app} - 0.0005\ [H_2O_2]/\ mg\ L^{-1} \quad \textbf{(4.4)}$$

$$BOD_5 = BOD_{5,\ app} + 0.4706\ [H_2O_2]/\ mg\ L^{-1} \quad \textbf{(4.5)}$$

4.4.10. Metal leaching

Dissolved iron content was determined by a colorimetric method using 1,10-phenantroline and measuring the absorbance at 510 nm, in accordance with ISO 6332 [35]. For that purpose, 4 mL of sample was mixed with 0.5 mL of ascorbic acid solution (12.6 g L^{-1}). After 30 min, 1 mL of acetate/acetic buffer and 0.5 mL of 1,10-phenantroline solution (2 g L^{-1}) were added, and the mixture developed a colour overnight. Afterwards, the absorbance was measured at 510 nm against a blank prepared in the same way, except that 1,10-phenantroline was replaced by ultrapure water. The acetate/acetic buffer was previously obtained by dissolving 12.5 g of ammonium acetate in a 50 mL volumetric flask, to which 35 mL of acetic acid was added. The resulting mixture was diluted with ultrapure water and further used. Dissolved nickel and cobalt contents were determined by atomic absorption spectroscopy with a PerkinElmer PinAAcle 900 apparatus using a multi-element hollow cathode lamp (Lumina N3050214).

4.4.11. Chlorides

The concentration of dissolved chlorides was determined by the Mohr method (titration with silver nitrate, using potassium chromate as indicator).

4.4.12. Microbiological assays

Heterotrophic plate count by the spread plate method was used in order to estimate the number of live heterotrophic bacteria in the liquid phase before and after treatment by CWPO [36]. For that purpose, 0.1 mL of starting sample and serial 10-fold dilutions were spread onto plate count agar (PCA) plates under aseptic conditions and incubated at 28 ºC during 5 days; counting was performed for plates displaying 10 – 100 colony-forming units (CFU), the results being reported as CFU per millilitre (CFU mL^{-1}). All the procedure was performed in triplicate.

The agar disk-diffusion method was used for the antimicrobial susceptibility testing of the liquid phase before and after treatment by CWPO [37]. *Klebsiella pneumoniae* (Gram negative) and *Bacillus cereus* (Gram positive) were selected as test microorganisms. In each case, the bacteria were initially grown overnight in nutrient broth (NB) at 37 ºC. Afterwards, Muller Hinton agar (MHA) plates were inoculated with standardized inocula of the test microorganisms (0.5 McFarland; corresponding to 10^8 CFU mL^{-1}). Then, antibiotics testing paper discs (6 mm diameter; Filtres Fioroni) containing 10 µL of the testing solution previously sterilized by filtration (0.2 µm), were placed on the agar surface. Finally, possible inhibition growth zones surrounding the paper discs were evaluated after 16 and 24 h of incubation at 37 ºC. The whole procedure was performed in triplicate.

4.4.13. Sampling and storage

For quantification purposes, small aliquots were periodically withdrawn from the reactor, and the solids were removed from the liquid phase by centrifugation (10000 rpm). In the case of 4-NP, 2-NP and TOC determinations, an excess of sodium sulphite was immediately added in order to consume residual H_2O_2 and to instantaneously stop the reaction [38-40]. The samples collected for the determination of H_2O_2, COD, absorbance spectra, aromaticity and BOD_5, as well as for the microbiological assays, were immediately placed in ice in order to stop the reaction, and kept at 3 ºC until the analysis. In the experiments performed with SMX, an excess of methanol - a known $HO^{\bullet}$ scavenger [41, 42], was immediately added in order to consume residual $HO^{\bullet}$ and to instantaneously stop the reaction, the resulting samples being then placed in ice. The samples were filtered (PVDF syringe filters, 0.2 μm) prior to analysis.

Appropriate dilutions were made when necessary.

4.5. Reproducibility, error and evaluation of the CWPO experimental results

Selected experiments were performed in duplicate and triplicate, in order to assess reproducibility and error of the CWPO experimental results. It was found that the standard deviation of the 2-NP, 4-NP and H_2O_2 concentrations was never superior to 1% in the experiments performed in duplicate with the nitrophenol aqueous model systems (Chapters 5, 6, 8 and 10). In the case of the results presented in Chapters 7 and 9, selected experiments were performed in triplicate. It was found that the standard deviation of the 4-NP and SMX determination was never superior to 3%. Appendix B provides additional details regarding the reproducibility and error of 4-NP experimental values obtained in three independent CWPO runs. Likewise, the standard deviation of the COD, TOC, H_2O_2 and aromaticity determinations was never superior to 2%, 1%, 4% and 1%, respectively, as determined in selected experiments performed in duplicate with the liquid effluent addressed in Chapter 10.

Four parameters were defined as described in Eqs. 4.6-9, in order to evaluate the performance of the CWPO process at a given time t, namely conversion of a specific compound/parameter (X_t), difference of a given pollutant removal due to H_2O_2 addition ($d_{\text{Removal},\, t}$; corresponding to the increase of pollutant removal obtained in CWPO experiments compared to that obtained in pure adsorption experiments), average pollutant mass removal rate ($m_{\text{Removal},\, t}$), and total organic carbon removal per unit of hydrogen peroxide decomposed

($\eta_{H_2O_2,\,t}$). $X_{CWPO,\,t}$ and $X_{Adsorption,\,t}$ represent the X_t obtained in CWPO and pure adsorption runs, respectively.

$$X_t\,/\,\% = \frac{[\text{pollutant/parameter}]_0 - [\text{pollutant/parameter}]_t}{[\text{pollutant/parameter}]_0} \times 100 \quad \textbf{(4.6)}$$

$$d_{Removal,\,t}\,/\,\% = X_{CWPO,\,t} - X_{Adsorption,\,t} \quad \textbf{(4.7)}$$

$$m_{Removal,\,t}\,/\,\text{mg g}^{-1}\,\text{h}^{-1} = \frac{\dfrac{[\text{pollutant/parameter}]_0 - [\text{pollutant/parameter}]_t}{[\text{Catalyst}]}}{t} \quad \textbf{(4.8)}$$

$$\eta_{H_2O_2,\,t}\,/\,\% = \frac{[TOC]_0 - [TOC]_t}{[H_2O_2]_0 - [H_2O_2]_t} \times 100 \quad \textbf{(4.9)}$$

References

[1] B.L.A. Prabhavathi Devi, K.N. Gangadhar, P.S. Sai Prasad, B. Jagannadh, R.B.N. Prasad, A Glycerol-based carbon catalyst for the preparation of biodiesel, ChemSusChem 2 (2009) 617-620.

[2] W.S. Hummers, R.E. Offeman, Preparation of graphitic oxide, J. Am. Chem. Soc. 80 (1958) 1339-1339.

[3] S. Stankovich, D.A. Dikin, R.D. Piner, K.A. Kohlhaas, A. Kleinhammes, Y. Jia, Y. Wu, S.T. Nguyen, R.S. Ruoff, Synthesis of graphene-based nanosheets via chemical reduction of exfoliated graphite oxide, Carbon 45 (2007) 1558-1565.

[4] L.M. Pastrana-Martínez, S. Morales-Torres, V. Likodimos, J.L. Figueiredo, J.L. Faria, P. Falaras, A.M.T. Silva, Advanced nanostructured photocatalysts based on reduced graphene oxide-TiO_2 composites for degradation of diphenhydramine pharmaceutical and methyl orange dye, Appl. Catal. B 123-124 (2012) 241-256.

[5] M.J. Fernández-Merino, L. Guardia, J.I. Paredes, S. Villar-Rodil, P. Solís-Fernández, A. Martínez-Alonso, J.M.D. Tascón, Vitamin C is an ideal substitute for hydrazine in the reduction of graphene oxide suspensions, J. Phys. Chem. C 114 (2010) 6426-6432.

[6] C. Zhu, S. Guo, Y. Fang, S. Dong, Reducing sugar: new functional molecules for the green synthesis of graphene nanosheets, ACS Nano 4 (2010) 2429-2437.

[7] S. Park, J. An, J.R. Potts, A. Velamakanni, S. Murali, R.S. Ruoff, Hydrazine-reduction of graphite- and graphene oxide, Carbon 49 (2011) 3019-3023.

[8] L.M. Pastrana-Martínez, S. Morales-Torres, V. Likodimos, P. Falaras, J.L. Figueiredo, J.L. Faria, A.M.T. Silva, Role of oxygen functionalities on the synthesis of photocatalytically active graphene-TiO_2 composites, Appl. Catal. B 158-159 (2014) 329-340.

[9] H.T. Gomes, B.F. Machado, A. Ribeiro, I. Moreira, M. Rosário, A.M.T. Silva, J.L. Figueiredo, J.L. Faria, Catalytic properties of carbon materials for wet oxidation of aniline, J. Hazard. Mater. 159 (2008) 420-426.

[10] Y. Wang, H. Zhao, G. Zhao, Iron-copper bimetallic nanoparticles embedded within ordered mesoporous carbon as effective and stable heterogeneous Fenton catalyst for the degradation of organic contaminants, Appl. Catal. B 164 (2015) 396-406.
[11] Y. Zhang, Z. Yang, D. Yin, Y. Liu, C. Fei, R. Xiong, J. Shi, G. Yan, Composition and magnetic properties of cobalt ferrite nano-particles prepared by the co-precipitation method, J. Magn. Magn. Mater. 322 (2010) 3470-3475.
[12] K. Maaz, S. Karim, A. Mumtaz, S.K. Hasanain, J. Liu, J.L. Duan, Synthesis and magnetic characterization of nickel ferrite nanoparticles prepared by co-precipitation route, J. Magn. Magn. Mater. 321 (2009) 1838-1842.
[13] R. Liu, L. Wan, S. Liu, Y. Yu, S. Li, D. Wu, Hierarchical co-assembly avenue to uniform rhombododecahedral magnetic mesoporous graphitic composites, J. Colloid Interface Sci. 414 (2014) 59-65.
[14] S. Brunauer, P.H. Emmett, E. Teller, Adsorption of gases in multimolecular layers, J. Am. Chem. Soc. 60 (1938) 309-319.
[15] F. Rodríguez-Reinoso, A. Linares-Solano, Physics of Carbon, Marcel Dekker Inc., New York, 1989.
[16] M. Thommes, K. Kaneko, A.V. Neimark, J.P. Olivier, F. Rodriguez-Reinoso, J. Rouquerol, K.S.W. Sing, Physisorption of gases, with special reference to the evaluation of surface area and pore size distribution (IUPAC Technical Report), Pure Appl. Chem. 87 (2015) 1051-1069.
[17] S. Lowell, J.E. Shields, M.A. Thomas, M. Thommes, Characterization of porous solids and powders: surface area, pore size and density, Springer Science + Business Media, New York, 2004.
[18] L.M. Pastrana-Martínez, S. Morales-Torres, S.K. Papageorgiou, F.K. Katsaros, G.E. Romanos, J.L. Figueiredo, J.L. Faria, P. Falaras, A.M.T. Silva, Photocatalytic behaviour of nanocarbon–TiO_2 composites and immobilization into hollow fibres, Appl. Catal. B 142–143 (2013) 101-111.
[19] H.T. Gomes, S.M. Miranda, M.J. Sampaio, A.M.T. Silva, J.L. Faria, Activated carbons treated with sulphuric acid: catalysts for catalytic wet peroxide oxidation, Catal. Today 151 (2010) 153-158.
[20] M.A. Ferro-García, J. Rivera-Utrilla, I. Bautista-Toledo, C. Moreno-Castilla, Adsorption of humic substances on activated carbon from aqueous solutions and their effect on the removal of Cr(III) Ions, Langmuir 14 (1998) 1880-1886.
[21] J. Rivera-Utrilla, I. Bautista-Toledo, M.A. Ferro-García, C. Moreno-Castilla, Activated carbon surface modifications by adsorption of bacteria and their effect on aqueous lead adsorption, J. Chem. Technol. Biotechnol. 76 (2001) 1209-1215.

[22] J.L. Figueiredo, M.F.R. Pereira, M.M.A. Freitas, J.J.M. Órfão, Modification of the surface chemistry of activated carbons, Carbon 37 (1999) 1379-1389.
[23] J.L. Figueiredo, M.F.R. Pereira, M.M.A. Freitas, J.J.M. Órfão, Characterization of active sites on carbon catalysts, Ind. Eng. Chem. Res. 46 (2007) 4110-4115.
[24] R.A. Sheldon, M. Wallau, I.W.C.E. Arends, U. Schuchardt, Heterogeneous catalysts for liquid-phase oxidations: philosophers' stones or trojan horses?, Acc. Chem. Res. 31 (1998) 485-493.
[25] A. Aguinaco, J.P. Pocostales, J.F. García-Araya, F.J. Beltrán, Decomposition of hydrogen peroxide in the presence of activated carbons with different characteristics, J. Chem. Technol. Biotechnol. 86 (2011) 595-600.
[26] W.H. Glaze, J.-W. Kang, D.H. Chapin, The chemistry of water treatment processes involving ozone, hydrogen peroxide and ultraviolet radiation, Ozone Sci. Eng. 9 (1987) 335-352.
[27] Â.C. Apolinário, A.M.T. Silva, B.F. Machado, H.T. Gomes, P.P. Araújo, J.L. Figueiredo, J.L. Faria, Wet air oxidation of nitro-aromatic compounds: reactivity on single- and multi-component systems and surface chemistry studies with a carbon xerogel, Appl. Catal. B 84 (2008) 75-86.
[28] R.P. Rocha, J.P.S. Sousa, A.M.T. Silva, M.F.R. Pereira, J.L. Figueiredo, Catalytic activity and stability of multiwalled carbon nanotubes in catalytic wet air oxidation of oxalic acid: the role of the basic nature induced by the surface chemistry, Appl. Catal. B 104 (2011) 330-336.
[29] L. Yang, L. Liu, B.A. Olsen, M.A. Nussbaum, The determination of oxalic acid, oxamic acid, and oxamide in a drug substance by ion-exclusion chromatography, J. Pharm. Biomed. Anal. 22 (2000) 487-493.
[30] C.N. Satterfield, A.H. Bonnell, Interferences in titanium sulfate method for hydrogen peroxide, Anal. Chem. 27 (1955) 1174-1175.
[31] W.C. Ketchie, Y.-L. Fang, M.S. Wong, M. Murayama, R.J. Davis, Influence of gold particle size on the aqueous-phase oxidation of carbon monoxide and glycerol, J. Catal. 250 (2007) 94-101.
[32] L.S. Clescerl, A.E. Greenberg, A.D. Eaton, Standard methods for the examination of water and wastewater, 20th ed., American Public Health Association, American Water Works Association, Water Environment Federation, Washington DC, 1999.
[33] Y.W. Kang, M.-J. Cho, K.-Y. Hwang, Correction of hydrogen peroxide interference on standard chemical oxygen demand test, Water Res. 33 (1999) 1247-1251.
[34] M. Mrkva, Evaluation of correlations between absorbance at 254 nm and COD of river waters, Water Res. 17 (1983) 231-235.

[35] ISO 6332:1988, Water quality - Determination of iron - Spectrometric method using 1,10-phenanthroline, International Organization for Standardization, 1988.
[36] G. Tchobanoglous, F.L. Burton, H.D. Stensel, Wastewater engineering: treatment and reuse, 4th ed., International Edition, Metcalf & Eddy, Inc., McGraw-Hill companies, New York, 2003.
[37] M. Balouiri, M. Sadiki, S.K. Ibnsouda, Methods for in vitro evaluating antimicrobial activity: a review, J. Pharm. Anal. 6 (2016) 71-79.
[38] F. Duarte, F.J. Maldonado-Hódar, L.M. Madeira, Influence of the characteristics of carbon materials on their behaviour as heterogeneous Fenton catalysts for the elimination of the azo dye orange II from aqueous solutions, Appl. Catal. B 103 (2011) 109-115.
[39] J.H. Ramirez, C.A. Costa, L.M. Madeira, G. Mata, M.A. Vicente, M.L. Rojas-Cervantes, A.J. López-Peinado, R.M. Martín-Aranda, Fenton-like oxidation of orange II solutions using heterogeneous catalysts based on saponite clay, Appl. Catal. B 71 (2007) 44-56.
[40] R.S. Ribeiro, A.M.T. Silva, J.L. Figueiredo, J.L. Faria, H.T. Gomes, Removal of 2-nitrophenol by catalytic wet peroxide oxidation using carbon materials with different morphological and chemical properties, Appl. Catal. B 140 (2013) 356-362.
[41] A. Rey, A. Bahamonde, J.A. Casas, J.J. Rodríguez, Selectivity of hydrogen peroxide decomposition towards hydroxyl radicals in catalytic wet peroxide oxidation (CWPO) over Fe/AC catalysts, Water Sci. Technol. 61 (2010) 2769-2778.
[42] R.S. Ribeiro, A.M.T. Silva, J.L. Figueiredo, J.L. Faria, H.T. Gomes, The influence of structure and surface chemistry of carbon materials on the decomposition of hydrogen peroxide, Carbon 62 (2013) 97-108.

PART II: METAL-FREE CARBON MATERIALS

The development of metal-free catalysts for the CWPO process is of great interest in order to avoid leaching, deactivation and use of high-cost metals. Bearing this in mind:

- In Chapter 5, a thermally stable and non-porous carbon material (GBCM), with low ash content and basic character, was produced by partial carbonization of glycerol with sulphuric acid followed by calcination under inert atmosphere. GBCM was further activated in air atmosphere at different temperatures. The results obtained with these materials highlight the importance of the interplay between chemical and textural properties when developing efficient carbon-based catalysts for CWPO;

- In Chapter 6, the unique structural and electronic transfer properties of graphene-based materials were explored. The results obtained emphasize the relevance of adsorptive interactions between the pollutant molecules and the surface of the catalysts when seeking highly efficient CWPO applications.

5. GLYCEROL-BASED CARBON MATERIALS

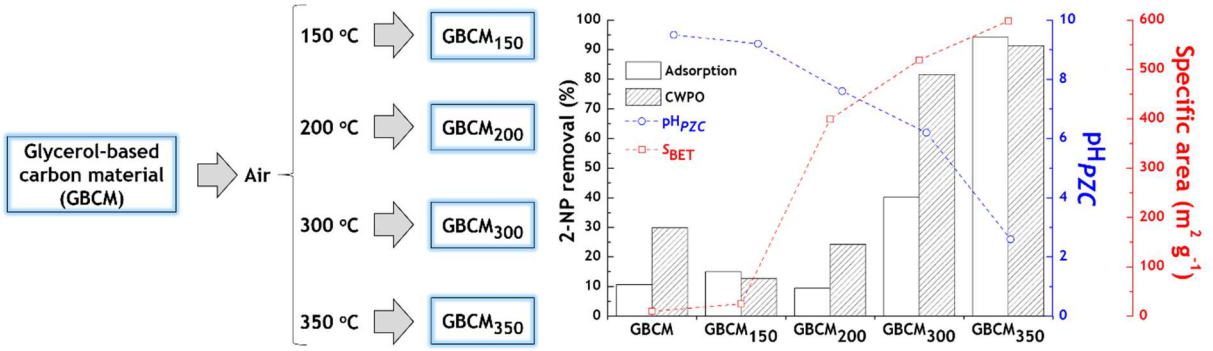

[9]

[9] Adapted from the graphical abstract of: Rui S. Ribeiro, Adrián M.T. Silva, Maria T. Pinho, José L. Figueiredo, Joaquim L. Faria, Helder T. Gomes, Development of glycerol-based metal-free carbon materials for environmental catalytic applications, Catal. Today 240, Part A (2015) 61-66
DOI: 10.1016/j.cattod.2014.03.048

Crude glycerol, resulting from the biodiesel production process, is being offered as an abundant and low cost feedstock [1]. As the worldwide biodiesel production increases, so does the production of this by-product, making the new markets for crude glycerol a focus of attention [2]. Seeking to explore new applications for this residue, a glycerol-based carbon material (GBCM) was prepared by partial carbonization of glycerol with sulphuric acid, followed by calcination under inert atmosphere. Materials with different properties were obtained by further thermal activation of GBCM in air atmosphere at different temperatures (from 150 to 350 ºC), as described in Section 4.1.1. The resulting materials, labelled as GBCM followed by a subscript number corresponding to the activation temperature in ºC, were explored as metal-free catalysts in the CWPO of 2-nitrophenol (2-NP) aqueous model solutions. In the following Sections the properties of the GBCM materials are fully characterized and the respective performance in CWPO is evaluated.

5.1. Textural and surface chemistry characterization

TGA analysis was initially performed with the non-activated GBCM (*cf*. Figure C.1, included as supplementary information in Appendix C). As observed, the results obtained under N_2 atmosphere reveal 3.1 wt.% of volatiles (decomposed upon heating), indicating that the material is thermally stable up to 900 ºC under inert atmosphere. On the other hand, a very low ash content (1.1 wt.%) was quantified by TGA analysis under air atmosphere.

The effects of the different thermal treatments on the textural and surface chemistry properties of the carbon materials were investigated by N_2 adsorption-desorption isotherms, pH_{PZC}, concentration of acidic and basic sites, and TPD.

The original GBCM is a non-porous material (V_{total} = 0.02 $cm^3\ g^{-1}$ and S_{BET} = 10 $m^2\ g^{-1}$), and the thermal activation of GBCM in air atmosphere leads to a considerable generation of porosity in the resulting materials, the S_{BET} increasing with the temperature applied as well as the V_{micro} (*cf*. Table 5.1). Higher activation temperatures lead to a significant development of microporosity. In fact, thermal activation of GBCM in air atmosphere at 350 ºC leads to a tremendous evolution of porosity (ca. 60-fold in S_{BET} and 13.5-fold in V_{total}), resulting in a material with a microporosity fraction (V_{micro}/V_{total} = 0.90) close to that reported for some activated carbons and carbon xerogels [3, 4]. This development of porosity, mostly within micropores, obtained through activation in air atmosphere, is clearly visible by SEM, as shown in Figure 5.1.

Regarding the surface chemistry, the original GBCM possesses a basic character, as reflected by the pH_{PZC} of 9.5 (*cf*. Table 5.1) and a concentration of basic functionalities higher than that of acidic functionalities (*cf*. Table 5.2). Overall, the amount of acidic functionalities of the resulting materials increases with the activation temperature, a

Table 5.1. Properties of the GBCM materials: specific surface area (S_{BET}), non-microporous specific surface area (S_{meso}), micropore volume (V_{micro}), total pore volume (V_{total}), average pore diameter (d_{pore}) and pH at the point of zero charge (pH_{PZC})

Material	Parameter					
	S_{BET} ($m^2\ g^{-1}$)	S_{meso} ($m^2\ g^{-1}$)	V_{micro} ($cm^3\ g^{-1}$)	V_{total} ($cm^3\ g^{-1}$)	d_{pore} (nm)	pH_{PZC}[a]
GBCM	10	10	0.00	0.02	8.0	9.5
$GBCM_{150}$	25	25	0.00	0.06	9.6	9.2
$GBCM_{200}$	400	70	0.16	0.22	2.2	7.6
$GBCM_{300}$	520	60	0.19	0.23	1.8	6.2
$GBCM_{350}$	600	30	0.24	0.27	1.8	2.6

[a] An ilustrative example of the pH drift tests performed for the determination of the pH_{PZC} of the materials included in this Ph.D. thesis is shown in Figure C.2.

markedly acidic material (pH_{PZC} = 2.6) being obtained at 350 ºC. As expected, this evolution is followed by the increase of oxygen-containing groups released during TPD analysis (*cf*. Figure 5.2 and Table 5.2). This effect is particularly observed for temperatures above 200 ºC, suggesting that the increase of acid functionalities is due to the incorporation of surface oxygen groups during thermal activation in air atmosphere [5].

Deconvolution analysis of the CO_2 and CO TPD spectra was performed as described in

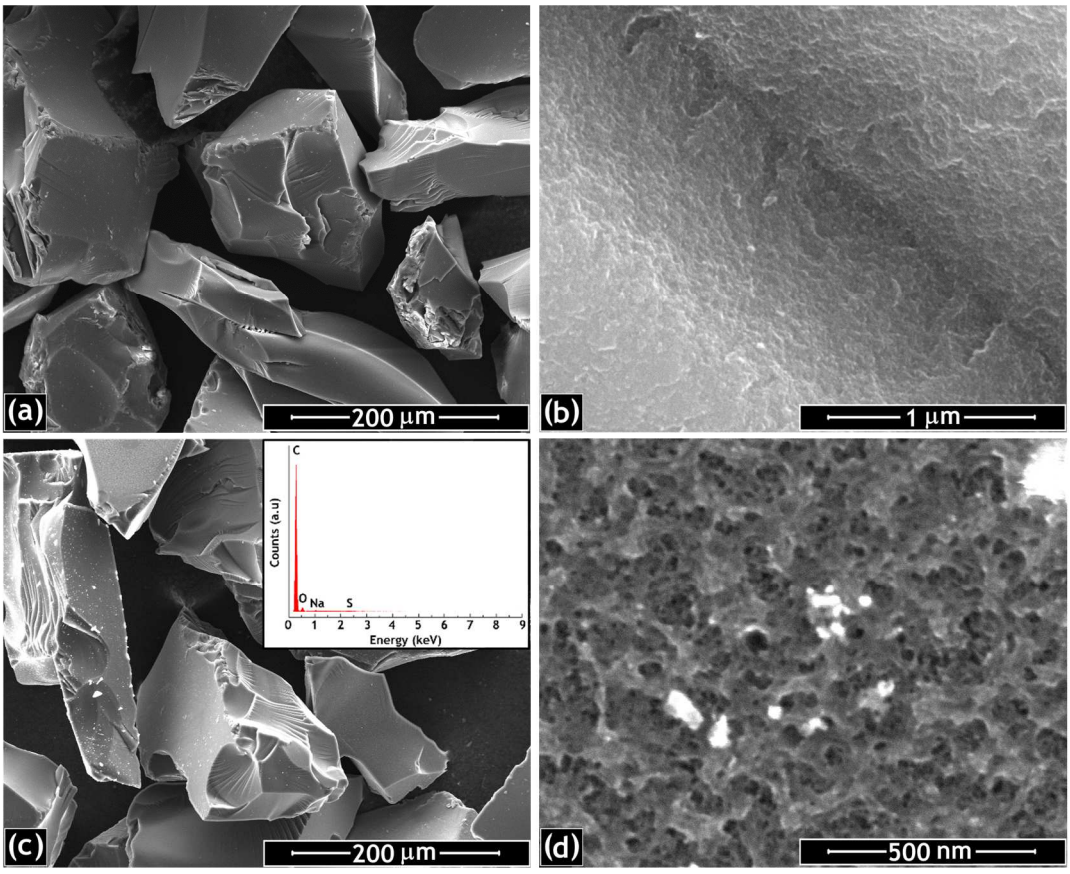

Figure 5.1. SEM micrographs of (a, b) GBCM and (c, d) $GBCM_{300}$. Inset of (c): EDS spectrum of $GBCM_{300}$.

Table 5.2. Properties of the GBCM materials: acid-base properties; amounts of CO_2 and CO, and percentage of oxygen (as obtained from the analysis of the TPD spectra)

Material	Parameter				
	Acidity (μmol g^{-1})	Basicity (μmol g^{-1})	CO_2 (μmol g^{-1})	CO (μmol g^{-1})	O (wt.%)
GBCM	380	590	213	385	1.3
$GBCM_{150}$	270	450	255	572	1.7
$GBCM_{200}$	310	500	524	940	3.2
$GBCM_{300}$	520	400	663	2843	6.7
$GBCM_{350}$	1250	250	955	3482	8.6

Section 4.2.3.6, in order to identify and quantify the amounts of the different functional groups originally present at the surface of GBCM and/or introduced during thermal activation under the oxidative atmosphere of air. Figures 5.3a and b illustrate the deconvolution of the CO_2 and CO peaks of $GBCM_{300}$, respectively. The amounts of the functional groups present at the surface of the different carbon materials are given in Table 5.3. From these results, it can be concluded that the increase of oxygen-containing groups previously commented (*cf*. Figure 5.2 and Table 5.2) is mainly due to the incorporation of lactones, phenols and quinones.

EDS analyses confirmed that the carbon materials produced from glycerol are mainly composed of carbon and oxygen, with some residual sulphur in the composition. The inset of Figure 5.1c is an example of these results. TPD analysis did not allow to identify the nature of possible sulphur containing functional groups, since no detectable signal was assigned to the release of SO_2 (normally associated with the decomposition of sulphonic acid groups or with other sulphur-containing functionalities [6]). However, since the increase of the acidity of the materials activated at higher temperatures cannot be fully explained by the incorporation of lactones, phenols and quinones, it should be reasonable to expect

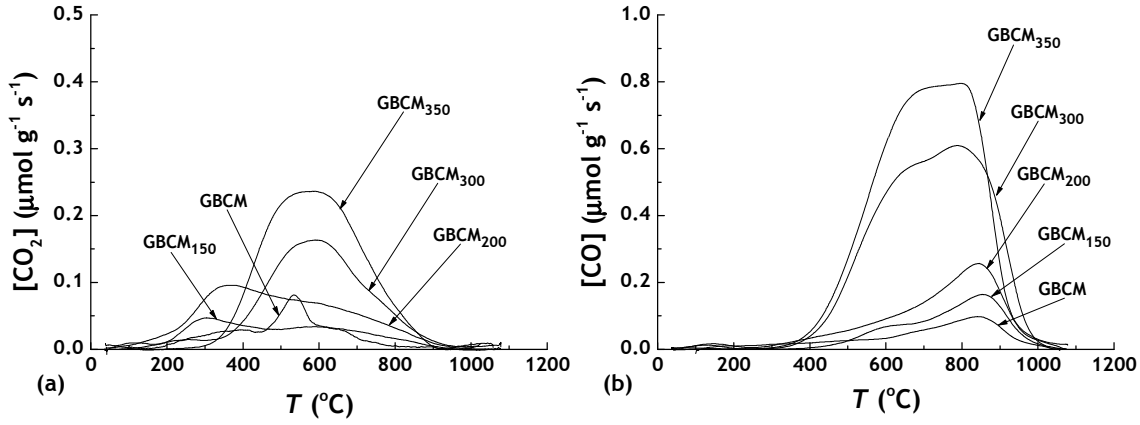

Figure 5.2. TPD spectra of the GBCM materials: (a) CO_2 and (b) CO evolution with temperature.

Table 5.3. Deconvolution of the TPD spectra using a multiple Gaussian function, considering peaks assigned to strongly acidic carboxylic acids (SA), less acidic carboxylic acids (LA), carboxylic anhydrides (Can), lactones (Lac), phenols (Ph), ethers (Eth) and quinones (Qui)

Material	CO_2		CO_2 and CO	CO		
	SA + LA (μmol g^{-1})	Lac (μmol g^{-1})	CAn (μmol g^{-1})	Ph (μmol g^{-1})	Eth (μmol g^{-1})	Qui (μmol g^{-1})
GBCM	66	48	72	0	100	176
$GBCM_{150}$	110	72	53	152	12	332
$GBCM_{200}$	220	225	53	298	20	482
$GBCM_{300}$	17	514	104	1391	70	1207
$GBCM_{350}$	0	762	164	1941	123	1132
$GBCM_{300,\ after\ CWPO}$	190	0	275	365	0	69
$GBCM_{300,\ regenerated}$	426	167	1260	379	935	444

that some acidic functionalities (not detected by TPD) may be present in the surface of the materials.

5.2. CWPO experiments

The ability of the carbon materials produced from glycerol to act as metal-free catalysts in the CWPO of 2-NP was evaluated through screening experiments performed under the conditions detailed in Table 5.4. The removals of 2-NP obtained in pure adsorption and CWPO runs performed during 4 h are given in Figure 5.4. The main conclusion withdrawn from this set of results is that carbon materials produced from glycerol have catalytic activity for this system. After appropriate activation conditions of the parent material, a marked increase of the 2-NP removal in the CWPO experiments compared to the pure adsorption experiments ($d_{Removal}$; determined as described in Eq. 4.7) is observed in the presence of some of the produced GBCM materials and, in particular, for the material treated under air atmosphere at 300 ºC. In fact, the difference of 2-NP removal due to H_2O_2 addition goes through a maximum, corresponding to a superior performance of $GBCM_{300}$ (2-fold higher when compared to the performance of the non-activated GBCM). Under these conditions, the non-catalytic removal of 2-NP amounts to ca. 12% of its initial content, which can be considered negligible when compared to the removals obtained in the presence of $GBCM_{300}$ (please refer to Figure C.3a for additional details on the non-catalytic experiment).

The highest removal of 2-NP is observed when using $GBCM_{350}$ but, in this case, pure adsorption experiments may indicate that significant adsorption of 2-NP occurs on the surface of this carbon material, reason why $GBCM_{300}$ was selected for further process intensification, reutilization and regeneration studies. In either case, it can be observed that very active catalysts can be produced from glycerol by selecting the proper temperature for the oxidative treatment under air atmosphere (300 ºC in the present study), a methodology

that allows the control of the textural and surface chemical properties of the carbon materials.

Taking into account that (i) the experiments were performed at pH = 3, (ii) the acid dissociation constant of 2-NP (pKa = 7.2, thus found in solution predominantly in the molecular form) and (iii) the pH_{PZC} of the materials, it can be concluded that electrostatic

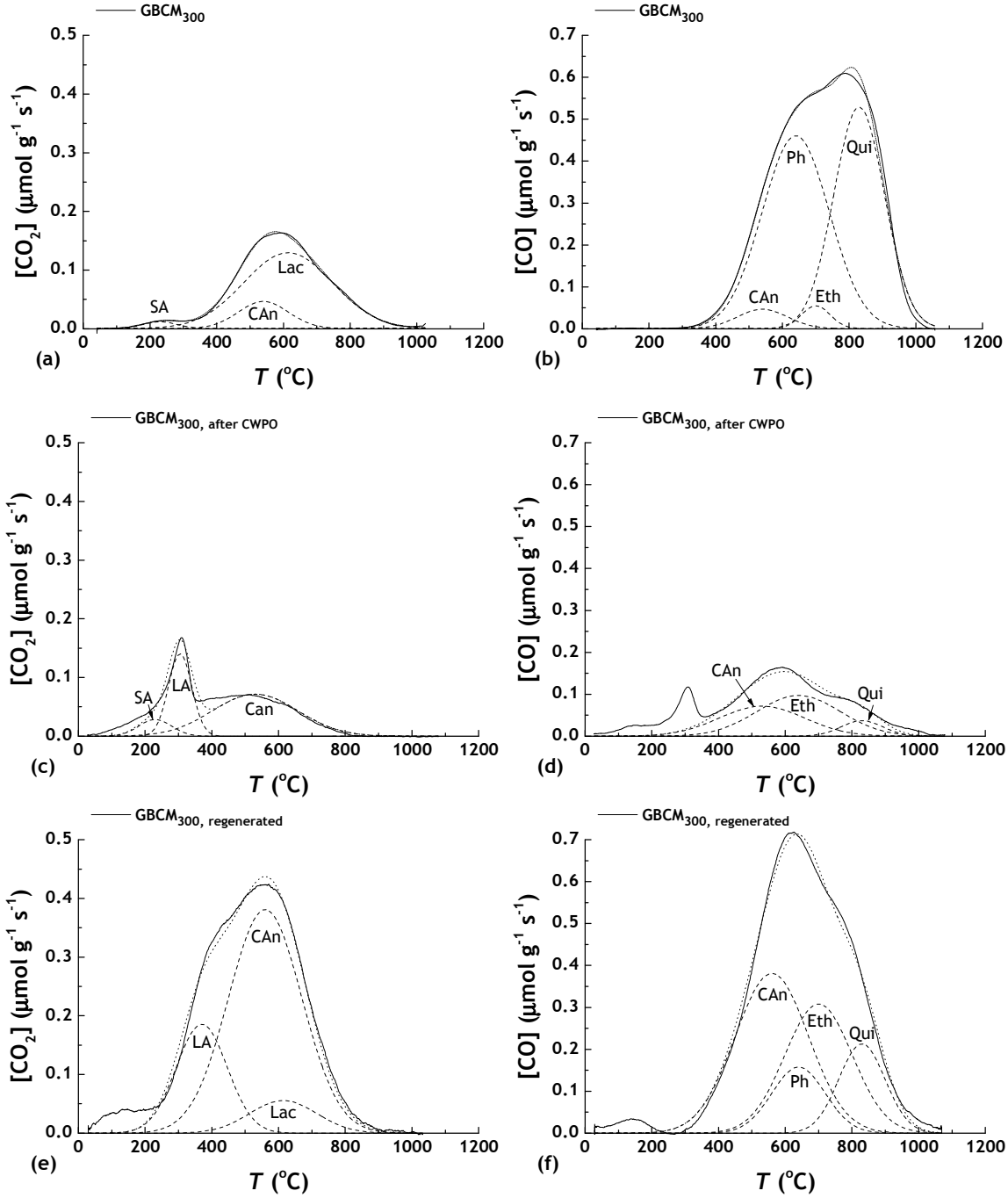

Figure 5.3. Deconvolution results of (a, c, e) CO_2 and (b, d, f) CO TPD spectra of $GBCM_{300}$ (a, b) prior and (c, d) after the first CWPO cycle performed under process intensification conditions (*cf.* Table 5.4, and (e, f) after oxidative thermal regeneration. Dashed lines represent peaks assigned to strongly acidic carboxylic acids (SA), less acidic carboxylic acids (LA), carboxylic anhydrides (Can), lactones (Lac), phenols (Ph), ethers (Eth) and quinones (Qui). Dotted lines represent cumulative peak fitting.

interactions between the surface of the carbon materials and the 2-NP molecules, by itself, shouldn't be the main driving force to explain the different adsorption behaviour of the materials [7, 8]. Considering the specific surface areas, the carbon material with the highest porous structure (i.e., $GBCM_{350}$, with S_{BET} = 598 m^2 g^{-1}) would be expected to show the best adsorption performance, which is confirmed by the adsorption results obtained.

CWPO is a much more complex process than pure adsorption. Several authors reported carbon materials with basic character as more active for H_2O_2 decomposition in CWPO processes [9-12] and that acidic oxygen-containing functionalities existing at the surface — having an electron withdrawal capacity—, limit their catalytic performance [11-13]. As observed, the material that better combines all of these properties is in fact $GBCM_{300}$, which shows the best catalytic activity in the removal of 2-NP by CWPO, corresponding to an average pollutant mass removal rate of 24.5 mg g^{-1} h^{-1} (determined as described in Eq. 4.8). This material possesses an interesting development of porosity (S_{BET} = 520 m^2 g^{-1}, S_{meso} = 60 m^2 g^{-1}, V_{micro} = 0.19 cm^3 g^{-1}), enabling the adsorption of the organic pollutant on its surface, and a basicity of 400 μmol g^{-1} (almost 2-fold higher than that of $GBCM_{350}$), which combined with an inferior oxygen content (6.7 wt.%) leads to higher activation of H_2O_2 molecules in close proximity of the 2-NP molecules. Hereupon, it is concluded that a balance between the textural and chemical properties is crucial in the synthesis of highly active catalysts for the CWPO process. Materials activated at lower temperatures have an important basic character (basicity > 450 μmol g^{-1}), with a lower oxygen content (< 3.2%), but also a very poor porous structure, while the material activated at the highest temperature (350 ºC) has a significant porosity, but a very high oxygen content (8.6%), combined with a low basicity (250 μmol g^{-1}).

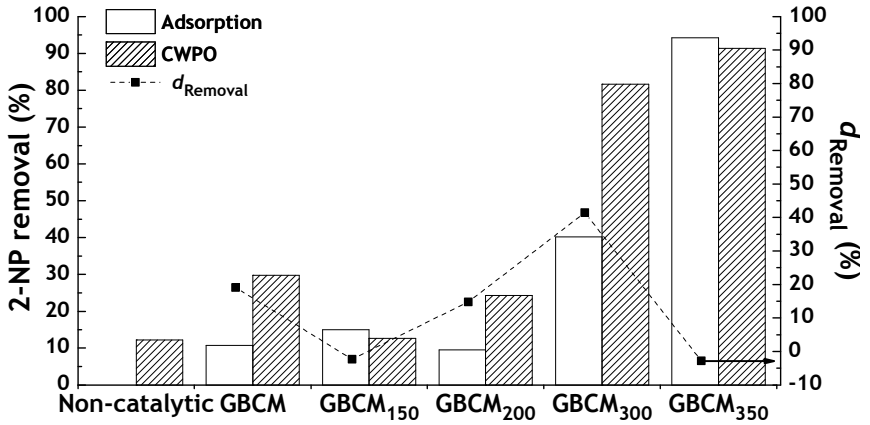

Figure 5.4. 2-NP removals in adsorption and CWPO runs (bars/left axis) after 4 h, and respective difference due to H_2O_2 addition [$d_{Removal}$ (squares/right axis)]. Experiments performed with $[2\text{-NP}]_0$ = 0.1 g L^{-1}, [Catalyst/adsorbent] = 1.0 g L^{-1}, $[H_2O_2]_0$ = 1.18 g L^{-1}, T = 50 ºC and pH = 3.

5.2.1. Process intensification

In order to assess the ability of $GBCM_{300}$ to act as catalyst in CWPO processes under intensified conditions, which may be potentially more attractive for industrial applications (i.e., to treat waste waters with higher pollutant concentrations and lower catalyst and H_2O_2 consumptions per mass of pollutant, thus increasing the efficiency of the catalyst and H_2O_2 usage), the concentration of 2-NP was increased to 0.5 g L^{-1}, the load of $GBCM_{300}$ was decreased to 0.25 g L^{-1}, and the dosage of H_2O_2 in the CWPO process was lowered to the stoichiometric amount theoretically needed to completely mineralise 2-NP. The 2-NP removals obtained as a function of time in adsorption and CWPO runs performed with $GBCM_{300}$ under these intensified operating conditions, together with the non-catalytic removal obtained in the same operating conditions, are collected in Figure 5.5. As observed, both adsorption and non-catalytic removals are negligible when compared to the 2-NP removal obtained by CWPO (please refer to Figure C.3b for additional details on the non-catalytic experiment). By comparing the average pollutant mass removal rate obtained under intensified conditions (67.6 mg g^{-1} h^{-1}) to that obtained under the conditions of Figure 5.4 (24.5 mg g^{-1} h^{-1}), it can be concluded that the efficiency of $GBCM_{300}$ usage is clearly increased (ca. 2.8-fold) when the CWPO process is implemented under intensified conditions.

5.2.2. Reusability cycles

The stability of $GBCM_{300}$ —a basic requirement for industrial scale applications— was tested in a series of three consecutive CWPO runs. For that purpose, after each run, the catalyst was filtered, washed and dried at 60 ºC overnight, and then reused in CWPO with a

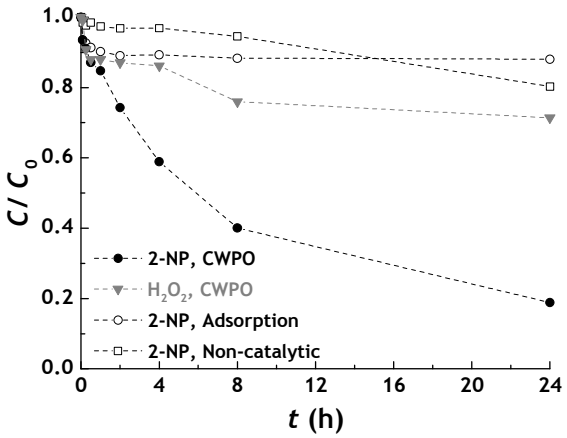

Figure 5.5. 2-NP and H_2O_2 normalized concentrations obtained as a function of time in the CWPO run performed with $GBCM_{300}$. Experiments performed with $[2\text{-NP}]_0$ = 0.5 g L^{-1}, $[GBCM_{300}]$ = 0.25 g L^{-1}, $[H_2O_2]_0$ = 1.78 g L^{-1} (stoichiometric amount), T = 50 ºC and pH = 3. 2-NP removals by adsorption are also shown for comparison.

fresh 2-NP solution. The 2-NP, TOC and H_2O_2 conversions obtained after 24 h of reaction in this series of experiments with successive reuse of $GBCM_{300}$ are given in Figure 5.6. As observed, the 2-NP and TOC removals obtained in the first cycle are higher when compared to the removals observed in the second cycle. This phenomenon was somehow expected due to the contribution of adsorption in the first use of the catalyst. However, a closer analysis reveals that adsorption, only by itself, is not enough to justify the difference between the 2-NP removals observed in the first and in the second runs. In fact, as recently shown in the CWPO of phenol over microporous activated carbon catalysts [14], this decrease of the catalytic activity of $GBCM_{300}$ may also be explained by deactivation of the carbon active sites responsible for hydrogen peroxide decomposition into $HO^{\bullet}$ radicals, due to reduction of the specific surface area caused by 2-NP reaction by-products adsorbed or deposited on the carbon surface. In order to confirm this hypothesis, the textural properties of $GBCM_{300}$ collected after the first CWPO cycle ($GBCM_{300,\ after\ CWPO}$) were determined: S_{BET} = 180 $m^2\ g^{-1}$, V_{micro} = 0.04 $cm^3\ g^{-1}$, V_{total} = 0.10 $cm^3\ g^{-1}$. By comparing these properties to those of $GBCM_{300}$ (*cf*. Table 5.1), a significant decrease of porosity is observed. For instance, the S_{BET} decreases from 520 $m^2\ g^{-1}$ to 180 $m^2\ g^{-1}$ upon application of $GBCM_{300}$ in the CWPO of 2-NP under intensified conditions. Likewise, the effect of CWPO on the surface chemistry properties of $GBCM_{300}$ was also evaluated. For that purpose, $GBCM_{300,\ after\ CWPO}$ was analysed by TPD (*cf*. Figure 5.3 and Table 5.3). As observed, CWPO leads to an increase of the amount of carboxylic acids (from 17 to 190 μmol g^{-1}) and carboxylic anhydrides (104 to 275 μmol g^{-1}) at the surface of $GBCM_{300}$, while the amounts of all the other surface groups are significantly decreased (some groups being completely removed). These observations point out two possible cumulative effects: on the one hand, (i) the number of available electron rich donating active sites is expected to decrease with the increase of acidic functionalities,

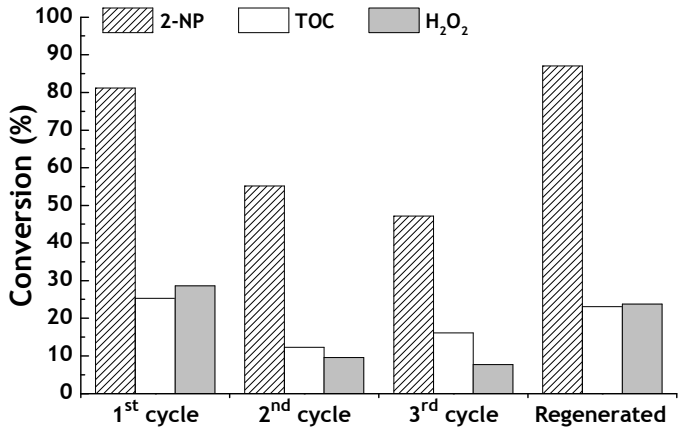

Figure 5.6. 2-NP, TOC and H_2O_2 conversions obtained after 24 h in a series of three CWPO runs performed with consecutive reuse of $GBCM_{300}$, and with $GBCM_{300}$ regenerated after the first cycle. Experiments performed under the operating conditions given in Figure 5.5.

since these functional groups are generated in the same active sites by capture of the available unpaired π electrons [13]; on the other hand, (ii) the decrease of electron donating species (i.e., reducing species) such as phenols and ethers containing alkyl groups, which is a necessary condition to promote the decomposition of H_2O_2 into $HO^{\bullet}$, through the reaction described by Eq. 2.8, is expected to hinder the efficiency of the catalytic decomposition of H_2O_2 during CWPO [9-12, 15, 16]. Indeed, a significant decrease of H_2O_2 decomposition was observed from the first to the second CWPO cycle (*cf*. Figure 5.6). At the same time, TOC removal is lower than 2-NP removal, suggesting the formation of oxidation by-products. From the second run to the third run only slight variations were observed. Nevertheless, the 2-NP and TOC removals are clearly decreased when compared to those obtained when using the fresh $GBCM_{300}$ material.

In order to study the possible impact of the effects described in (i) and (ii), a simple oxidative thermal regeneration of $GBCM_{300,\ after\ CWPO}$ was carried out, considering the same conditions used for its initial activation (i.e., treatment in air atmosphere at 300 ºC during 60 min). The weight loss due to the thermal regeneration amounts to 25 wt.%. The results obtained with the resulting material ($GBCM_{300,\ regenerated}$) are also shown in Figure 5.6. As observed, the catalyst activity is effectively recovered, the 2-NP and TOC removals obtained with $GBCM_{300,\ regenerated}$ being similar to those obtained with the fresh catalyst. Furthermore, the extent of H_2O_2 decomposition is also similar.

The textural properties of $GBCM_{300,\ regenerated}$ were also analysed. In this case, no significant variations in porosity were observed after the regeneration treatment (S_{BET} = 160 $m^2\ g^{-1}$, V_{micro} = 0.04 $cm^3\ g^{-1}$, V_{total} = 0.09 $cm^3\ g^{-1}$). However, significant changes in the surface chemistry were promoted, as observed by TPD analysis (*cf*. Figure 5.3 and Table 5.3). Specifically, it was observed an increase of the amount of all the oxygen-containing surface groups considered when compared to $GBCM_{300,\ after\ CWPO}$, including electron-withdrawing (e.g., carboxylic acids) and electron donating (e.g., phenols and ethers containing alkyl groups) species. Nevertheless, the higher increase was observed for the amount of ethers, namely from 0 ($GBCM_{300,\ after\ CWPO}$) to 935 μmol g^{-1} ($GBCM_{300,\ regenerated}$). It should be noted that the initial amount of ethers at the surface of the fresh $GBCM_{300}$ is 70 μmol g^{-1}. The recovery of the catalyst activity can thus be ascribed to the changes in the surface chemistry of the material promoted by the thermal regeneration procedure.

5.3. Conclusions

The results reported in this Chapter highlight the importance of the interplay between chemical and textural properties when developing efficient carbon-based catalysts for

Table 5.4. Experimental details of the CWPO experiments reported in Chapter 5

Aqueous model system	Reactor/solution volume	Operating conditions	H_2O_2 stoichiometric ratio[a]	[Pollutant]/ [catalyst]
2-nitrophenol (0.1 g L^{-1})	500 mL/ 250 mL	Screening experiments [Catalyst] = 1.0 g L^{-1} $[H_2O_2]_0$ = 1.18 g L^{-1} T = 50 ºC; pH_0 = 3 t = 4 h	3	0.1
2-nitrophenol (0.5 g L^{-1})	500 mL/ 250 mL	Process intensification [Catalyst] = 0.25 g L^{-1} $[H_2O_2]_0$ = 1.78 g L^{-1} T = 50 ºC; pH_0 = 3 t = 24 h	1	2

[a] Obtained by dividing the amount of H_2O_2 employed by the stoichiometric amount needed for the complete mineralization of the pollutant considered.

CWPO. The higher catalytic activity of $GBCM_{300}$ was ascribed to a combination of properties: the adequate development of porosity, enabling the adsorption of the organic pollutant on its surface, and a basicity of 400 μmol g^{-1} (almost twice higher than that of $GBCM_{350}$), which combined with lower oxygen content led to higher activity for the decomposition of H_2O_2 molecules in close proximity with adsorbed 2-NP molecules. Materials activated at lower temperatures have an important basic character (basicity > 450 μmol g^{-1}), with a low oxygen content (< 3.2%), but also a very poor porous structure, while the material activated at the highest temperature (350 ºC) has a significant porosity, but a very high oxygen content (8.6%) combined with a low basicity (250 μmol g^{-1}).

5.4. Experimental details

The CWPO experiments reported in Chapter 5 were performed under the conditions detailed in Table 5.4. Please refer to Chapter 4 for additional details on the experimental procedures.

References

[1] X. Fan, R. Burton, Y. Zhou, Glycerol (byproduct of biodiesel production) as a source for fuels and chemicals – mini review, Open Fuel Energ. Sci. J. 3 (2010) 17-22.

[2] F. Yang, M. Hanna, R. Sun, Value-added uses for crude glycerol – a byproduct of biodiesel production, Biotechnol. Biofuels 5 (2012) 13.

[3] H.T. Gomes, B.F. Machado, A. Ribeiro, I. Moreira, M. Rosário, A.M.T. Silva, J.L. Figueiredo, J.L. Faria, Catalytic properties of carbon materials for wet oxidation of aniline, J. Hazard. Mater. 159 (2008) 420-426.

[4] R.S. Ribeiro, N.A. Fathy, A.A. Attia, A.M.T. Silva, J.L. Faria, H.T. Gomes, Activated carbon xerogels for the removal of the anionic azo dyes Orange oII and chromotrope 2R by adsorption and catalytic wet peroxide oxidation, Chem. Eng. J. 195-196 (2012) 112-121.

[5] J.L. Figueiredo, M.F.R. Pereira, M.M.A. Freitas, J.J.M. Órfão, Modification of the surface chemistry of activated carbons, Carbon 37 (1999) 1379-1389.
[6] H.T. Gomes, S.M. Miranda, M.J. Sampaio, J.L. Figueiredo, A.M.T. Silva, J.L. Faria, The role of activated carbons functionalized with thiol and sulfonic acid groups in catalytic wet peroxide oxidation, Appl. Catal. B 106 (2011) 390-397.
[7] F. Rodríguez-Reinoso, The role of carbon materials in heterogeneous catalysis, Carbon 36 (1998) 159-175.
[8] F. Villacañas, M.F.R. Pereira, J.J.M. Órfão, J.L. Figueiredo, Adsorption of simple aromatic compounds on activated carbons, J. Colloid Interface Sci. 293 (2006) 128-136.
[9] L.B. Khalil, B.S. Girgis, T.A.M. Tawfik, Decomposition of H_2O_2 on activated carbon obtained from olive stones, J. Chem. Technol. Biotechnol. 76 (2001) 1132-1140.
[10] F. Lücking, H. Köser, M. Jank, A. Ritter, Iron powder, graphite and activated carbon as catalysts for the oxidation of 4-chlorophenol with hydrogen peroxide in aqueous solution, Water Res. 32 (1998) 2607-2614.
[11] R.S. Ribeiro, A.M.T. Silva, J.L. Figueiredo, J.L. Faria, H.T. Gomes, The influence of structure and surface chemistry of carbon materials on the decomposition of hydrogen peroxide, Carbon 62 (2013) 97-108.
[12] V.P. Santos, M.F.R. Pereira, P.C.C. Faria, J.J.M. Órfão, Decolourisation of dye solutions by oxidation with H_2O_2 in the presence of modified activated carbons, J. Hazard. Mater. 162 (2009) 736-742.
[13] P. Serp, J.L. Figueiredo, Carbon materials for catalysis, John Wiley & Sons, Inc., Hoboken, New Jersey, 2009.
[14] C.M. Domínguez, P. Ocón, A. Quintanilla, J.A. Casas, J.J. Rodríguez, Highly efficient application of activated carbon as catalyst for wet peroxide oxidation, Appl. Catal. B 140–141 (2013) 663-670.
[15] L.C.A. Oliveira, C.N. Silva, M.I. Yoshida, R.M. Lago, The effect of H_2 treatment on the activity of activated carbon for the oxidation of organic contaminants in water and the H_2O_2 decomposition, Carbon 42 (2004) 2279-2284.
[16] A. Rey, J.A. Zazo, J.A. Casas, A. Bahamonde, J.J. Rodríguez, Influence of the structural and surface characteristics of activated carbon on the catalytic decomposition of hydrogen peroxide, Appl. Catal. A 402 (2011) 146-155.

6. GRAPHENE-BASED MATERIALS

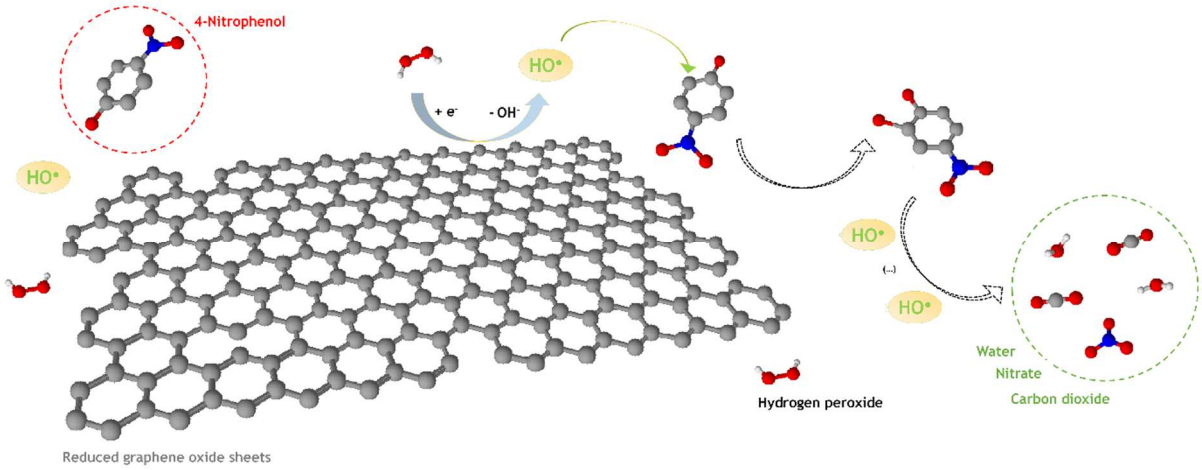

10

[10] Adapted from the graphical abstract of: Rui S. Ribeiro, Adrián M.T. Silva, Luisa M. Pastrana-Martínez, José L. Figueiredo, Joaquim L. Faria, Helder T. Gomes, Graphene-based materials for the catalytic wet peroxide oxidation of highly concentrated 4-nitrophenol solutions, Catal. Today 249 (2015) 204-212
DOI: 10.1016/j.cattod.2014.10.004

Graphene and its derivatives possess unique electronic, optical, thermal and mechanical properties, in addition to large theoretical specific surface areas and high adsorption capacities [1-3]. Graphene properties fascinated the scientific community, as recognized by a Nobel Prize in 2010. This two-dimensional honeycomb lattice, formed by hexagonally arrayed sp^2-bonded carbon atoms, can be considered as the basic building block for all other dimensionalities: 0D buckyballs, 1D nanotubes or 3D graphite [1, 4]. Specifically, it is known that the strong σ bonds work as the rigid backbone of the 2D honeycomb graphene structure, whereas the out-of plane π bonds control the interaction between the graphene sheets, allowing delocalized π electrons to be easily conducted through the basal plane [1]. Two distinct types of sites can be found in perfect graphene layers of carbon materials: (i) the basal plane sites, which are associated with the sp^2-hybridized aromatic carbon atoms forming the surface of the basal planes (i.e., within the graphene sheet) and (ii) the edge sites, which are the terminal sites of graphene layers [5, 6]. The latter are usually considered more electrochemically active than the former, due to the presence of higher amounts of delocalized unpaired π electrons [5, 6]. Structural defects may have been traditionally seen as imperfections in materials that could significantly decrease their performance [7]. However, at the nanoscale, defects can be extremely useful since they may be exploited to generate novel materials and applications [7].

One of the most popular and developed ways to produce graphene-based materials consists of the initial strong chemical oxidation of natural graphite to graphite oxide, followed by mechanical, chemical or thermal exfoliation of graphite oxide to graphene oxide (GO) sheets, which are finally chemically reduced, resulting in reduced graphene oxide (rGO) materials [1, 2]. In this way, three rGO samples were previously prepared elsewhere from GO [8], using different reducing agents (i.e., glucose, hydrazine and vitamin C), as described in Section 4.1.2. Aiming to explore the presence of electron donating active sites at the surface of graphene-based materials, and their unique structural and electronic transfer properties, these materials were explored as metal-free catalysts in the CWPO of 4-nitrophenol (4-NP) aqueous model solutions with high pollutant load (5 g L^{-1}). In the following Sections, the most relevant properties of the graphene-based materials are characterized and the respective performance in CWPO is evaluated.

6.1. Textural and surface chemistry characterization

All the graphene-based materials used in this work were extensively characterized in a previous publication related to the synthesis of graphene-based TiO_2 composites for photocatalysis [8]. Notwithstanding, the most relevant data are presented in this Section for the sake of discussion.

Table 6.1. Properties of the graphene-based materials: specific surface area (S_{BET}), non-microporous specific surface area (S_{meso}), micropore volume (V_{micro}) and pH at the point of zero charge (pH_{PZC}). Raman spectroscopy intensity ratios of the D bands relative to the G mode (I_D/I_G) are also included for the rGO samples

Material	Parameter					
	S_{BET} ($m^2\ g^{-1}$)	S_{meso} ($m^2\ g^{-1}$)	V_{micro} ($cm^3\ g^{-1}$)	pH_{PZC}[a]	I_D/I_G[a] 514.5 nm	I_D/I_G[a] 785 nm
GO	23	23	0	2.8	-	-
rGOG	94	90	0.004	5.2	1.85	4.00
rGOH	413	329	0.039	5.5	2.50	4.58
rGOV	29	0	0	5.1	2.16	4.26

[a] Data collected from [8].

The original GO is a non-porous material (S_{BET} = 23 $m^2\ g^{-1}$ and V_{micro} = 0 $cm^3\ g^{-1}$), and the textural properties of the rGO samples are affected differently by the type of reducing agent that is employed (*cf.* Table 6.1). For instance, rGOG and rGOH present some microporosity (V_{micro} of 0.004 $cm^3\ g^{-1}$ and 0.039 $cm^3\ g^{-1}$, respectively), while rGOV apparently maintains the non-porous character of GO (S_{BET} = 29 $m^2\ g^{-1}$ and V_{micro} = 0 $cm^3\ g^{-1}$). This effect can be attributed to the distinct extents of structural defects occurring with different reducing agents, as observed through Raman spectroscopy. Accordingly, the Raman intensity ratios of the D bands relative to the G mode (I_D/I_G) of the rGO samples, previously calculated from the areas of the corresponding Raman bands, at 514.5 and 785 nm, respectively [8], are also included in Table 6.1. As can be observed, rGOG presents the lowest I_D/I_G values, suggesting that it contains the lowest number of defects [8], followed by rGOV and rGOH.

As previously reported [8], and also shown in Table 6.1, an increase of the pH_{PZC} values was observed for the rGO samples (ranging from 5.1 to 5.5) compared to GO (2.8), showing that the carbon surface becomes less acidic after the chemical treatments with different

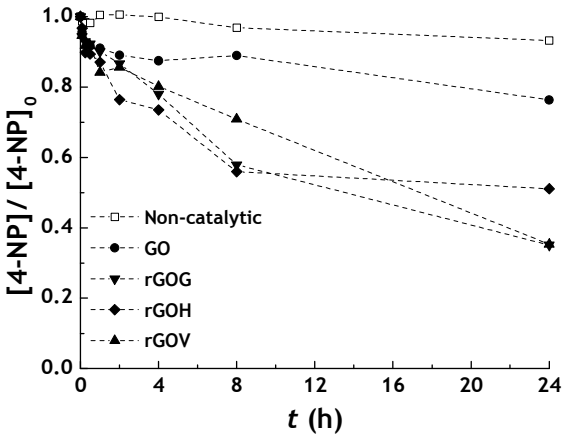

Figure 6.1. 4-NP removal obtained as a function of time in CWPO runs performed with the graphene-based materials. Experiments performed with $[4\text{-NP}]_0$ = 5.0 g L^{-1}, [catalyst] = 2.5 g L^{-1}, $[H_2O_2]_0$ = 17.8 g L^{-1} (stoichiometric amount), T = 50 ºC and pH = 3.

agents (also confirmed by the TPD results, which are not shown), due to the removal of acidic surface functional groups from GO.

6.2. CWPO experiments

The performance of the graphene-based materials in the CWPO of highly concentrated 4-NP aqueous model solutions (5 g L^{-1}) was evaluated in screening experiments performed under the operating conditions detailed in Table 6.2. The corresponding 4-NP removal curves are shown in Figure 6.1. As observed, the 4-NP removal obtained after 24 h in the non-catalytic experiment is below 7% of its initial content (please refer to Figure C.4a for additional details on the non-catalytic experiment), which is negligible when compared to that obtained in the presence of the graphene-based catalysts. In addition, these preliminary results suggest that the performances of the rGO samples are largely superior to the performance of their precursor (GO). However, the possible adsorption contribution on the removal of 4-NP by CWPO must be estimated. For that purpose, pure adsorption experiments were also carried out with all the graphene-based materials. As observed, all the graphene-based materials are unequivocally active catalysts for the CWPO of highly concentrated 4-NP solutions at mild conditions, since the removals of 4-NP obtained in CWPO runs are markedly superior to the removals obtained by pure adsorption (*cf*. Figure 6.2). In order to better assess the catalytic performance of the materials, the parameter $d_{Removal}$ was considered once again (*cf*. Eq. 4.7). Accordingly, it can be concluded that the catalytic activity of the graphene-based materials follows the sequence: rGOV > rGOH > rGOG > GO. Specifically, the use of rGOV as catalyst allows a 4-NP mass removal rate of 53.9 mg g^{-1} h^{-1} (*cf*. Eq. 4.8). The highest removal of 4-NP is observed when using rGOG (54.1 mg g^{-1} h^{-1}) but, in this case, pure adsorption experiments indicate that a larger

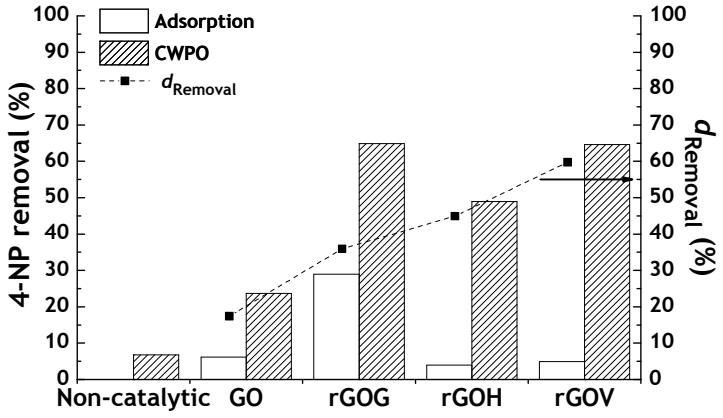

Figure 6.2. 4-NP removal in adsorption and CWPO runs (bars/left axis) after 24 h, and respective difference due to H_2O_2 addition [$d_{Removal}$ (squares/right axis)]. Experiments performed under the operating conditions given in Figure 6.1.

adsorption of 4-NP may occur on the surface of this carbon material during CWPO.

Given that the best performances in the CWPO of 4-NP were observed when the rGO samples were used as catalysts, only these graphene-based materials were selected for additional studies.

6.2.1. Efficiency of H_2O_2 consumption

TOC and H_2O_2 evolution were also monitored during the CWPO runs performed with the rGO samples. This methodology enables a more detailed analysis regarding their catalytic activity, based on the TOC and H_2O_2 removals (X_{TOC} and $X_{H_2O_2}$, respectively) obtained at the end of each CWPO run (24 h). Although the TOC removal was found to be quite similar ($23.0\% \leq X_{TOC} \leq 24.7\%$), $X_{H_2O_2}$ ranges from 30.4% (rGOG) to 54.7% (rGOH). These observations suggest that the products resulting from the decomposition of H_2O_2 catalysed by the rGO samples might proceed via distinct catalytic reaction pathways; for instance, it is known that H_2O_2 can be catalytically decomposed via formation of $HO^{\bullet}$ radicals with further efficient reaction of $HO^{\bullet}$ radicals with the organic pollutants; or end up with the formation of oxygen and water, resulting from non-efficient parasite reactions occurring between formed $HO^{\bullet}$ radicals and H_2O_2 molecules. In order to enquire about the quality of the H_2O_2 decomposition at the surface of the rGO samples, the parameter $\eta_{H_2O_2}$ was introduced – corresponding to the TOC removal per unit of H_2O_2 decomposed (obtained as described in Eq. 4.9). Values in the range of 45.2% to 75.6% were obtained through this approach, the $\eta_{H_2O_2}$ following the sequence: rGOG > rGOV > rGOH.

Clear relationships are found when $\eta_{H_2O_2}$ is analysed together with the apparent structural disorder (as inferred from the ratios I_D/I_G, *cf*. Table 6.1) and the 4-NP adsorption behaviour

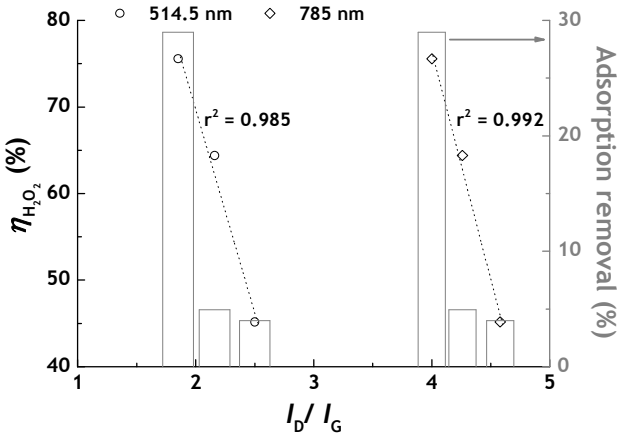

Figure 6.3. TOC removal per unit of H_2O_2 decomposed [$\eta_{H_2O_2}$ (symbols/left axis)] and adsorption removal (bars/right axis) as a function of the intensity ratios of the D bands relative to the G mode (I_D/I_G) for the rGO samples. Points represent experimental data, while dashed lines represent the linear fittings.

(*cf*. Figure 6.2) of the rGO samples. First, it is observed that, in the particular case of the rGO samples employed in this study, higher amounts of structural defects lead to lower values of $\eta_{H_2O_2}$, although graphene-based materials with higher amounts of structural defects resulted in increased catalytic decomposition of H_2O_2. The relationship becomes evident when $\eta_{H_2O_2}$ is plotted against the intensity ratios of the D bands relative to the G mode (I_D/I_G) for the rGO samples (*cf*. Figure 6.3). Although not directly supported by quantification of the HO• formed during the process, this effect may be explained by confinement of the electron rich regions caused by the structural defects, leading to an increase of electron density at those regions which act as active sites for the reaction, increasing the generation of HO• radicals. However, higher concentration of HO• radicals will not necessarily lead to higher efficiency of the CWPO process, since the amount of parasitic reactions is also expected to increase significantly, thus reducing $\eta_{H_2O_2}$. Second, it is also observed in Figure 6.3 that $\eta_{H_2O_2}$ follows the same order as the extent of 4-NP adsorption on the surface of the rGO samples. Thus, in the particular case of the rGO samples, the balance between a more controlled catalytic decomposition of H_2O_2, together with higher pollutant concentration nearby the generated HO• radicals, lead to the highest efficiency of the CWPO process. These observations suggest that $\eta_{H_2O_2}$ is favoured by higher pollutant concentrations at the surface of the catalysts, explained by a more efficient use of the HO• radicals formed nearby the adsorbed molecules leading to further oxidation. The two opposite reaction pathways are depicted in Figure 6.4.

6.2.2. Reusability cycles

Although in different extents, all the rGO samples (rGOV, rGOH and rGOG) exhibited

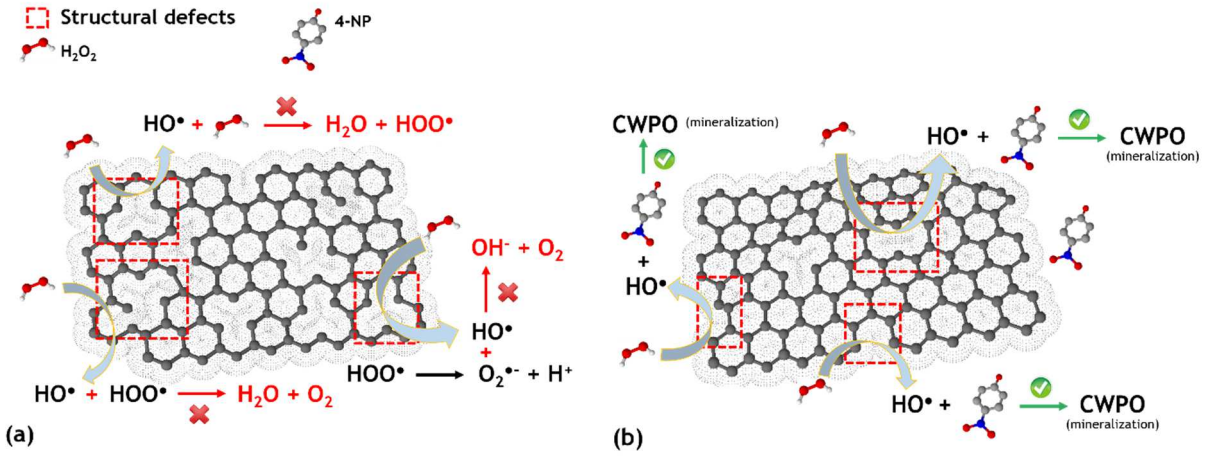

Figure 6.4. Representation of electron-rich regions caused by structural defects existing in reduced graphene oxide sheets, which act as active sites for the formation of HO• radicals: (a) in the absence of 4-NP molecules, and (b) in close proximity with adsorbed 4-NP molecules.

catalytic activity for the CWPO of highly concentrated 4-NP solutions. Thus, all these materials were selected for further studies on their catalytic stability in the CWPO process. For that purpose, after each run, the catalyst was filtered, washed and dried at 60 ºC overnight, and then reused in CWPO with a fresh 4-NP solution. The 4-NP, TOC and H_2O_2 conversions, as well as the corresponding $\eta_{H_2O_2}$ obtained after 24 h of reaction in this series of three experiments are given in Figure 6.5.

Different behaviours are observed in respect to the stability of the rGO catalysts. In the case of rGOG, the 4-NP mass removal rate decreases from 54.1 mg g^{-1} h^{-1}, in the first run, to 29.2 mg g^{-1} h^{-1} and 17.8 mg g^{-1} h^{-1}, in the second and third runs, respectively. Likewise, the TOC removal also decreases. In the opposite trend, the $\eta_{H_2O_2}$ obtained after 24 h of reaction in this series of three experiments performed with rGOG increases during its successive reuse, reaching a value as high as 98.1% in the third CWPO cycle. When rGOH is considered, it can be seen that the catalytic activity of this graphene-based material is kept without noteworthy variation during its successive reuse. Specifically, the 4-NP mass removal rate decreases from around 40.8 mg g^{-1} h^{-1}, in the first and second runs, to 35.0 mg g^{-1} h^{-1}, in the third run. Furthermore, the TOC mass removal rate reaches 10.7 mg g^{-1} h^{-1}, in the first run, decreasing to a still significant 5.8 mg g^{-1} h^{-1}. Finally, both 4-NP and TOC removals gradually decrease during the successive reuse of rGOV. Therefore, from a general point of view, the data given in Figure 6.5 allow to conclude that rGOH presents the highest catalytic stability among the tested graphene-based materials.

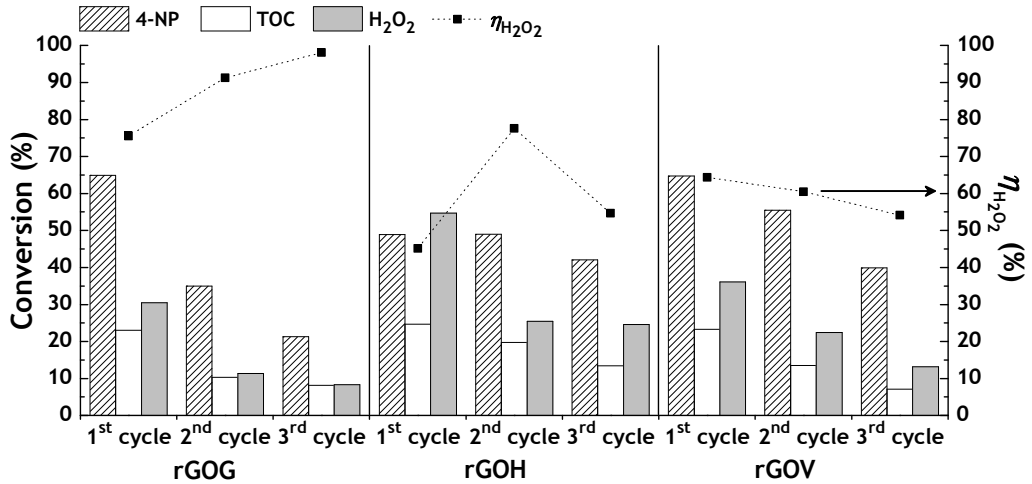

Figure 6.5. 4-NP, TOC and H_2O_2 conversions obtained after 24 h in a series of three CWPO runs performed with consecutive reuse of the rGO samples (bars/left axis), and respective TOC removal per unit of H_2O_2 decomposed [$\eta_{H_2O_2}$ (squares/right axis)]. Experiments performed under the operating conditions given in Figure 6.1.

6.2.3. Oxidation mechanism

In order to understand the oxidation/mineralization mechanism in the CWPO of highly concentrated 4-NP solutions, performed at mild conditions and using graphene-based materials as catalysts, the presence of some possible aromatic and non-aromatic by-products was explored. Since the highest catalytic activity was found for the rGOV sample (*cf*. Figure 6.2), the time-evolution of aromatic and non-aromatic compounds resulting from the CWPO of 4-NP performed with this material was followed, as given in Figures 6.6a and b, respectively. Based on the identified compounds, the mechanism depicted in Figure 6.7 was proposed.

It is well known that the reaction mechanism of HO$^{\bullet}$ radicals with aromatic compounds proceeds mainly through an electrophilic addition to the aromatic ring [9-11]. The phenolic –OH group is electron-donating for the electrophilic aromatic substitution, thus increasing the electron density both in the *ortho* and in the *para* positions [9]. On the other hand, the $-NO_2$ group is electron-withdrawing, thus being *meta* directing [9]. In the particular case of 4-NP (i.e., in the presence of both substituents), the electrophilic attack will occur preferably at the *ortho* position in respect to the –OH group, leading to the formation of 4-nitrocatechol [9, 11]. This mechanism is well evidenced in Figure 6.6a, since 4-nitrocatechol is the main aromatic intermediate of the 4-NP mineralization by CWPO.

Furthermore, an aromatic substitution of the $-NO_2$ group may occur due to an *ipso* attack of the HO$^{\bullet}$ radical at the *para* position in respect to the –OH group, hydroquinone being obtained [10, 11]. Hydroquinone was also identified as an intermediate of the 4-NP mineralization through CWPO (*cf*. Figure 6.6a), although in a smaller extent when compared to 4-nitrocatechol. On the other hand, hydroquinone is known to be very easily oxidized into

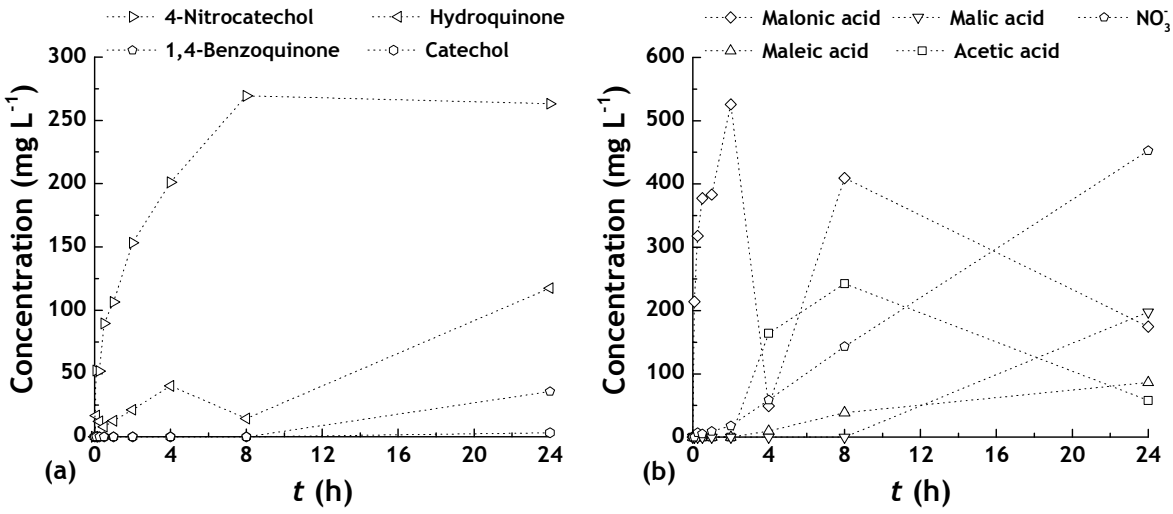

Figure 6.6. Evolution of (a) aromatic and (b) non-aromatic by-products of 4-NP oxidation, when using rGOV in the CWPO process developed under the operating conditions given in Figure 6.1.

benzoquinone [11]. Thus, benzoquinone formation would be expected from the reaction of hydroquinone with highly oxidizing species such as HO• radicals. As can be seen in Figure 6.6a, benzoquinone was effectively detected in the final stage of the experiment. Trace amounts of catechol were also detected, probably resulting from the cleavage of the $-NO_2$ group and subsequent electrophilic attack of the HO• radical at the *ortho* position.

Further attacks of HO• radicals on these aromatic intermediate compounds will eventually lead to the aromatic ring opening, and thus to the formation of a series of low molecular weight carboxylic acids, which subsequently are mineralized to carbon dioxide and water [10, 11]. In this study, several carboxylic acids were investigated (e.g., formic, acetic, oxalic, malonic, maleic and malic acids). Nevertheless, only four were effectively detected and quantified (*cf*. Figure 6.6b). Malonic acid was the main carboxylic acid detected.

Finally, nitrates can be produced from the $-NO_2$ group of the aromatic ring under the oxidation conditions employed [11]. From the concentration profile of nitrates given in Figure 6.6b, the effectiveness of the $-NO_2$ group subtraction from the main aromatic ring through the CWPO process is confirmed.

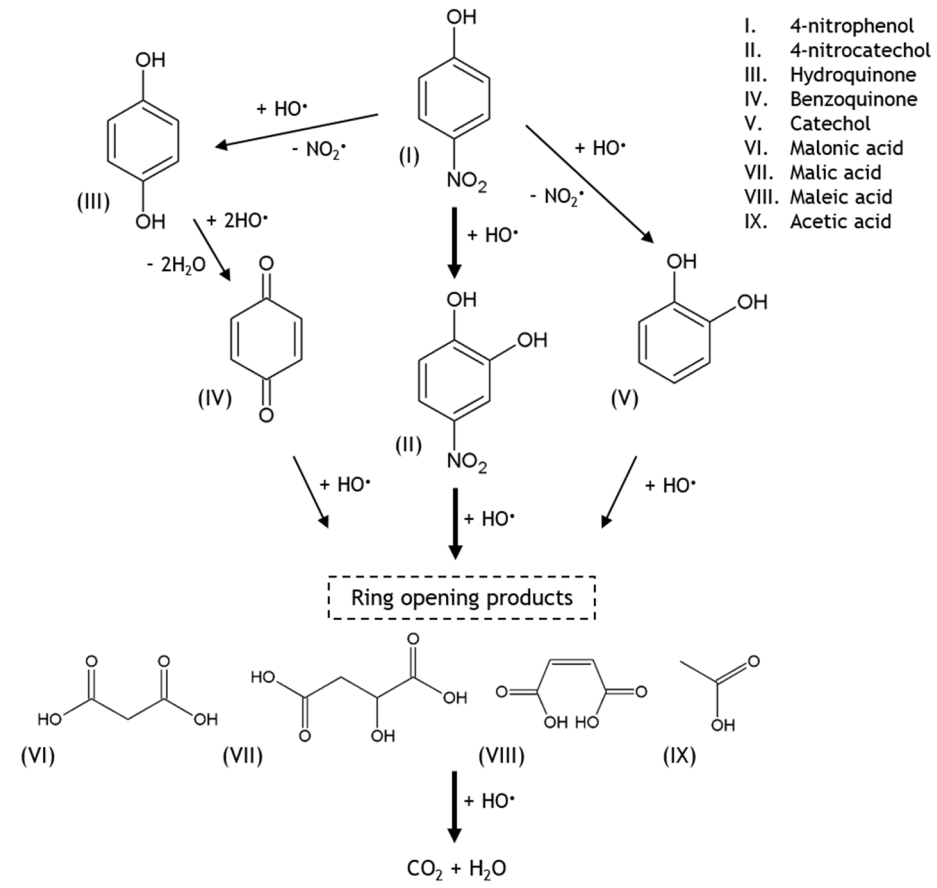

Figure 6.7. Mechanism proposed for the CWPO of 4-NP.

Table 6.2. Experimental details of the CWPO experiments reported in Chapter 6

Aqueous model system	Reactor/solution volume	Operating conditions	H_2O_2 stoichiometric ratio[a]	[Pollutant]/ [catalyst]
4-nitrophenol (5.0 g L^{-1})	250 mL/ 50 mL	[Catalyst] = 2.5 g L^{-1} $[H_2O_2]_0$ = 17.8 g L^{-1} T = 50 ºC; pH_0 = 3 t = 24 h	1	2

[a] Obtained by dividing the amount of H_2O_2 employed by the stoichiometric amount needed for the complete mineralization of the pollutant considered.

6.3. Conclusions

The number of defects in the structure of reduced graphene oxide was related with the enhanced H_2O_2 decomposition. Although not directly supported by quantification of the HO• formed during the process, this effect was ascribed to the confinement of electron-rich regions caused by structural defects, leading to an increased electron density at those regions, which act as active sites for the catalytic decomposition of H_2O_2, increasing the formation of HO•. However, this does not necessarily lead to higher efficiency of the CWPO process. Indeed, the balance between a more controlled catalytic decomposition of H_2O_2, together with higher pollutant concentration nearby the recently formed HO•, allows for the highest efficiency of H_2O_2 consumption during CWPO. Therefore, the results herein presented highlight the importance of adsorptive interactions between the pollutant molecules and the surface of the catalysts when developing efficient carbon-based catalysts for CWPO.

The 4-NP oxidation proceeds by initial aromatic hydroxyl oxidative attack followed by oxidative fragmentation, with release of nitrates, as confirmed by the identification of 4-nitrocatechol, hydroquinone, benzoquinone and catechol. Furthermore, several low molecular weight carboxylic acids were observed, including malonic, malic, maleic and acetic acids, allowing the mechanistic interpretation.

6.4. Experimental details

The CWPO experiments reported in Chapter 6 were performed under the conditions detailed in Table 6.2. Please refer to Chapter 4 for additional details on the experimental procedures.

References

[1] B.F. Machado, P. Serp, Graphene-based materials for catalysis, Catal. Sci. Technol. 2 (2011) 54-75.

[2] S. Morales-Torres, L.M. Pastrana-Martínez, J.L. Figueiredo, J.L. Faria, A.M.T. Silva, Design of graphene-based TiO_2 photocatalysts - a review, Environ. Sci. Pollut. Res. 19 (2012) 3676-3687.
[3] C.N.R. Rao, A.K. Sood, K.S. Subrahmanyam, A. Govindaraj, Graphene: the new two-dimensional nanomaterial, Angew. Chem. Int. Ed. 48 (2009) 7752-7777.
[4] A.K. Geim, K.S. Novoselov, The rise of graphene, Nat. Mater. 6 (2007) 183-191.
[5] W. Jiang, T. Tran, X. Song, K. Kinoshita, Thermal and electrochemical studies of carbons for Li-ion batteries: 1. Thermal analysis of petroleum and pitch cokes, J. Power Sources 85 (2000) 261-268.
[6] P. Serp, J.L. Figueiredo, Carbon materials for catalysis, John Wiley & Sons, Inc., Hoboken, New Jersey, 2009.
[7] H. Terrones, R. Lv, M. Terrones, M.S. Dresselhaus, The role of defects and doping in 2D graphene sheets and 1D nanoribbons, Rep. Prog. Phys. 75 (2012) 062501.
[8] L.M. Pastrana-Martínez, S. Morales-Torres, V. Likodimos, P. Falaras, J.L. Figueiredo, J.L. Faria, A.M.T. Silva, Role of oxygen functionalities on the synthesis of photocatalytically active graphene-TiO_2 composites, Appl. Catal. B 158-159 (2014) 329-340.
[9] A. Di Paola, V. Augugliaro, L. Palmisano, G. Pantaleo, E. Savinov, Heterogeneous photocatalytic degradation of nitrophenols, J. Photochem. Photobiol., A 155 (2003) 207-214.
[10] Y. Liu, H.L. Liu, Y. Li, Comparative study of the electrocatalytic oxidation and mechanism of nitrophenols at Bi-doped lead dioxide anodes, Appl. Catal. B 84 (2008) 297-302.
[11] M.A. Oturan, J. Peiroten, P. Chartrin, A.J. Acher, Complete destruction of p-nitrophenol in aqueous medium by electro-Fenton method, Environ. Sci. Technol. 34 (2000) 3474-3479.

PART III: CARBON EMBEDDED MAGNETIC COMPOSITES

Hybrid magnetic carbon composites can be regarded as the new generation of catalysts for CWPO. Within these composite materials, carbon structures decorated with magnetic particles were initially studied. For that purpose, as shown in Chapter 7, magnetic carbon xerogels consisting of interconnected carbon microspheres with iron and/or cobalt microparticles embedded in their structure were developed by a simple route. A carbon xerogel was selected as base material for this study since it inherently possesses a well-developed porosity and a non-acidic overall surface charge, which, as discussed in Part II, are fundamental requirements when designing efficient carbon-based catalysts for CWPO.

The results obtained in Chapter 7 revealed a clear synergy arising from the simultaneous inclusion of iron and cobalt species within carbon frameworks.

7. MAGNETIC CARBON XEROGELS

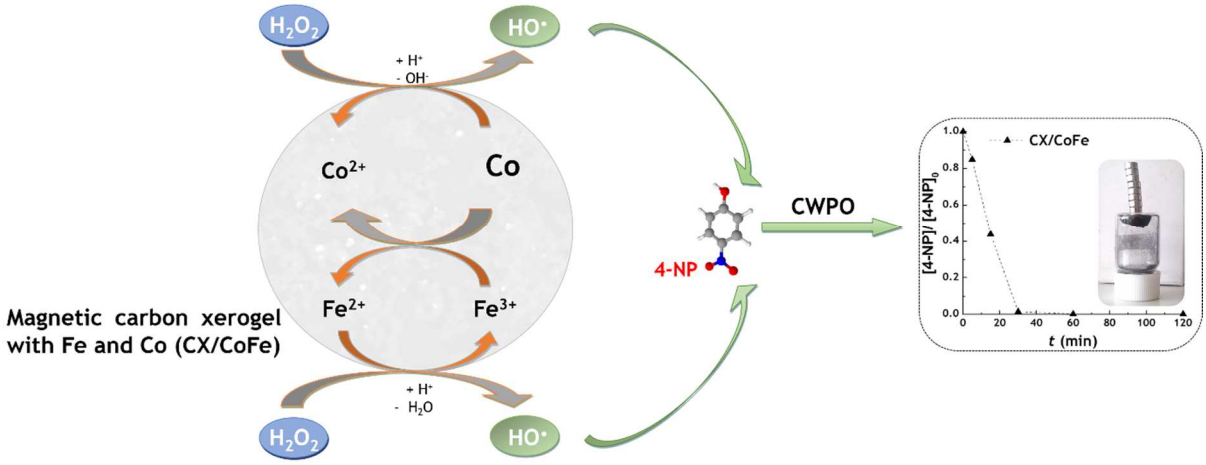

[11]

[11] Adapted from the graphical abstract of: Rui S. Ribeiro, Adrián M.T. Silva, José L. Figueiredo, Joaquim L. Faria, Helder T. Gomes, The role of cobalt in bimetallic iron-cobalt magnetic carbon xerogels developed for catalytic wet peroxide oxidation, Catal. Today 296 (2017) 66-75
DOI: 10.1016/j.cattod.2017.06.023

Three magnetic carbon xerogels, consisting of interconnected carbon microspheres with iron and/or cobalt microparticles embedded in their structure, were developed as described in Section 4.1.3. The monometallic catalysts containing only iron and cobalt were denoted as CX/Fe and CX/Co, while the bimetallic catalyst was denoted as CX/CoFe. A carbon xerogel prepared in the absence of metal precursors (CX) was also considered for comparison. As inferred from the characterization data, materials with distinctive properties may be directly obtained upon inclusion of iron and/or cobalt precursors during the sol-gel polymerization of resorcinol and formaldehyde, followed by thermal treatment. The unique electrochemical properties typically yielded by this type of carbon microstructures [1, 2] were explored in the CWPO of 4-NP aqueous model solutions with high pollutant load (5 g L^{-1}; considering a fixed pollutant/catalyst mass ratio of 2), together with the high catalytic activity of iron species. In the following Sections, the properties of the carbon xerogel materials are fully characterized and the respective performance in CWPO is evaluated. In addition, a detailed reaction mechanism is proposed for the surface catalytic reactions occurring over the iron-containing magnetic carbon xerogels.

7.1. Textural and surface chemistry characterization

Both CX and the magnetic carbon xerogels were extensively characterized. The main textural properties of the carbon xerogel materials are given in Table 7.1. As observed, all the carbon xerogel materials have a well-developed specific surface area, with S_{BET} values in the range 510 – 650 m^2 g^{-1}. CX is mainly a mesoporous material, with a ratio V_{mic}/V_{total} = 0.17 and d_{pore} = 6.7 nm. However, as observed from the corresponding values of S_{meso}, the inclusion of metal species leads to a substantial decrease of the mesoporous area, the resulting magnetic carbon xerogels being mainly microporous materials. This effect is particularly pronounced when Co is incorporated, with CX/CoFe and CX/Co having a strong microporous character (V_{mic}/V_{total} = 0.67 and 0.82, respectively, and d_{pore} of ca. 2 nm).

Regarding the surface chemistry, the inclusion of metal species, in particular Fe, leads to a slight decrease in the basicity of the resulting carbon xerogel materials when compared to that of CX, as observed from the corresponding values of pH_{PZC} also given in Table 7.1. The total Fe content in the bimetallic CX/CoFe catalyst is lower than that embedded in the structure of the monometallic CX/Fe; on the opposite, a higher total content of Co is observed in the bimetallic CX/CoFe when compared to the monometallic CX/Co (*cf.* Table 7.2).

The carbon xerogel materials were also analysed by SEM-EDS. As observed in Figure 7.1, the morphology of the materials helps to elucidate the differences observed in the textural

Table 7.1. Properties of the carbon xerogel materials: specific surface area (S_{BET}), non-microporous specific surface area (S_{meso}), micropore volume (V_{micro}), total pore volume (V_{total}), average pore diameter (d_{pore}) and pH at the point of zero charge (pH_{PZC})

Material	Parameter					
	S_{BET} ($m^2\ g^{-1}$)	S_{meso} ($m^2\ g^{-1}$)	V_{micro} ($cm^3\ g^{-1}$)	V_{total} ($cm^3\ g^{-1}$)	d_{pore} (nm)	pH_{PZC}
CX	650	240	0.19	1.09	6.7	9.2
CX/Fe	510	90	0.17	0.46	3.6	6.6
CX/Co	580	30	0.23	0.28	1.9	8.3
CX/CoFe	530	40	0.20	0.30	2.3	7.7

properties of the carbon xerogels with and without metal species embedded in their structures. Figures 7.1a and e correspond to CX, a typical carbon xerogel material, composed by large particles of carbon (153 ± 51 μm, as determined from SEM measurements). This is the result of the sol-gel polycondensation of resorcinol (R) and formaldehyde (F), in which two main reactions occur: (i) addition of F to the aromatic ring of R, leading to the formation of reactive R anions and hydroxymethyl derivatives; (ii) condensation of the hydroxymethyl derivatives to form methylene and methylene ether bridged compounds [3]. The condensation products form clusters whose aggregation leads to the formation of large particles. The concentration of F and R, as well as the pH, are the most important factors controlling the properties of the RF gels [3], and thus the properties of the resulting carbon xerogels after thermal annealing. On the opposite, the magnetic carbon xerogels are composed by aggregates of interconnected carbon microspheres (*cf*. Figures 7.1b-d) with iron and/or cobalt microparticles embedded in their structure (*cf*. Figures 7.1f-h). This observation suggests that the aggregation of clusters formed during the polycondensation of R and F is limited by both metals considered. Nevertheless, the size of the primary carbon microspheres and the size and distribution of the metal particles are different. Bearing this in mind, and since the magnetic carbon xerogels were prepared in the exactly same conditions as CX, except that iron and/or cobalt precursors were added during the sol-gel polycondensation of R and F, it can be concluded that the nature of the metal precursor affects the structure and morphology of the resulting carbon xerogel materials. As previously described elsewhere, the metal cations are expected to form bonds with the negatively charged functional groups of the RF gel, thus being able to catalyse the polymerization reaction and to influence the structure of the carbon xerogel [3].

A deeper analysis of Figures 7.1b-d suggests that CX/Fe possesses the biggest and more complex aggregates of interconnected primary carbon microspheres among the magnetic carbon xerogels, whereas CX/Co is at the opposite position, with the less extended aggregates; the bimetallic CX/CoFe possesses intermediate properties when compared to

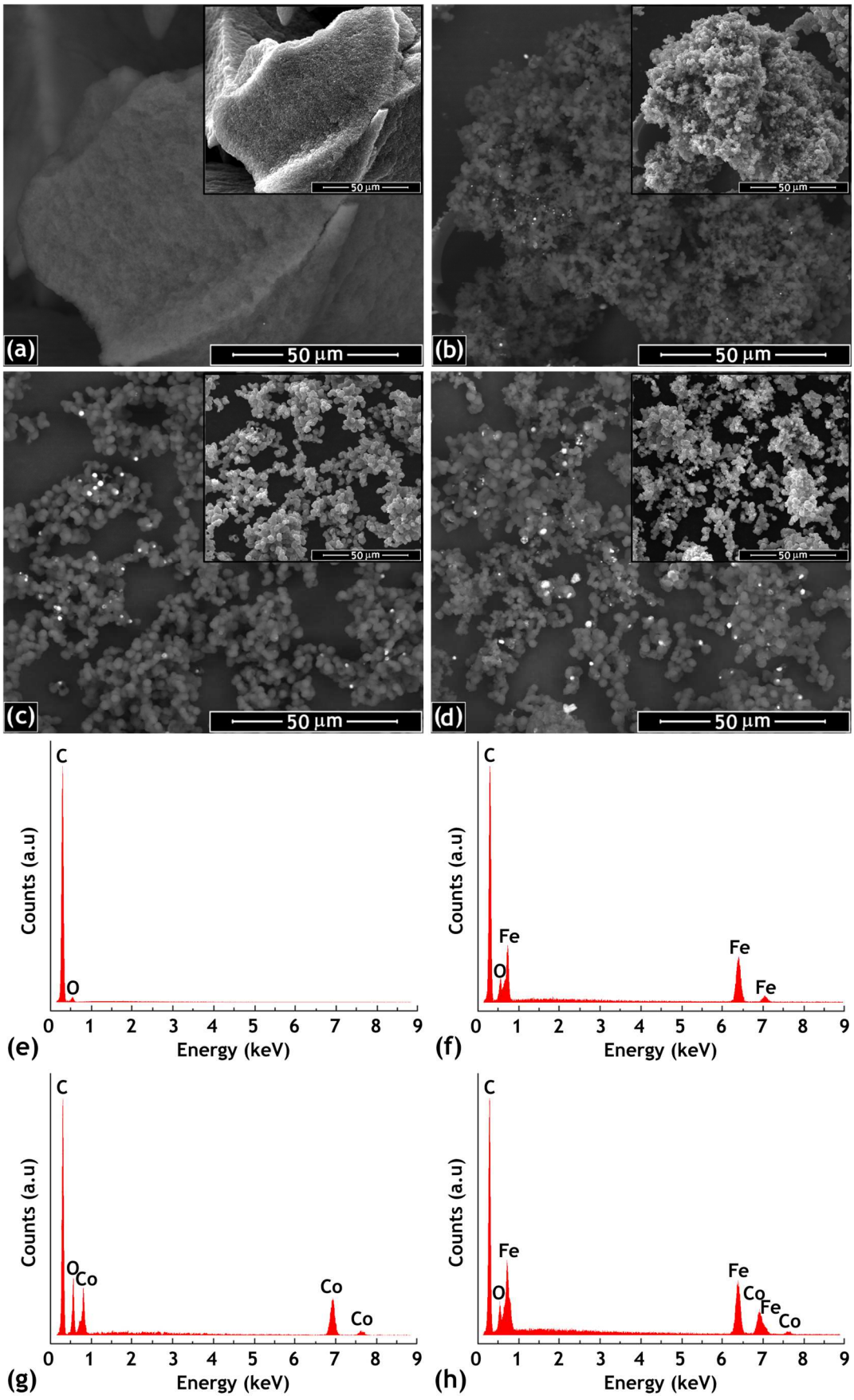

Figure 7.1. SEM micrographs of (a) CX, (b) CX/Fe, (c) CX/Co and (d) CX/CoFe, obtained in (main) BSE and (inset) SE mode. EDS spectra of (e) CX, (f) CX/Fe, (g) CX/Co and (h) CX/CoFe.

Table 7.2. Metal content of the magnetic carbon xerogels: total content of Fe and Co, as determined by atomic absorption analysis of the solutions resulting from the acidic digestion of the solids; and weight surface concentration of C, O, Fe and Co, as determined from XPS analysis

Material	Total content (wt.%)		Atomic surface concentration (wt.%)			
	Fe	Co	C	O	Fe	Co
CX/Fe	6.5	-	79.00	17.97	3.03	-
CX/Co	-	0.9	84.95	12.91	-	2.14
CX/CoFe	4.6	2.1	76.01	16.33	4.97	2.69

the monometallic materials. In addition, it is also observed that the distribution of metal particles at the surface of the magnetic carbon xerogels is more evident in the materials with Co embedded in their structure (i.e., CX/Co and CX/CoFe). This observation is even more relevant if the total content of Fe and Co in the magnetic carbon xerogels is considered. Specifically, although CX/Fe and CX/CoFe possess ca. the same total metal content (6.5% vs. 4.6% + 2.1%, i.e., 6.7%; *cf*. Table 7.2), the amount and distribution of metal particles at the surface of CX/CoFe (*cf*. Figure 7.1d) is more perceptible than that observed with CX/Fe (*cf*. Figure 7.1b).

In order to confirm the metal distribution at the surface of the magnetic carbon xerogels, these materials were also analysed by XPS. The corresponding XPS spectra and the atomic surface concentrations of C 1s, O 1s, Fe 2p and Co 2p are given in Figure C.5 and Table 7.2, respectively. As observed, the simultaneous incorporation of Fe and Co leads to an enhanced metal distribution at the surface of the bimetallic CX/CoFe (*cf*. Table 7.2), confirming the previous observations. In addition, if the surface weight concentrations given are compared to the total Fe and Co contents (*cf*. Table 7.2), it is suggested that some metal particles are surrounded by the organic phase during the synthesis of the monometallic CX/Fe and CX/Co catalysts, therefore being less accessible. In the opposite, when Co and Fe are simultaneously incorporated in the bimetallic CX/CoFe, the metals are preferentially located at the surface of the catalyst. The oxidation states of each component existing at the surface of the magnetic carbon xerogels were also determined by XPS analysis, as discussed in Section 7.3.

Further insights on the morphology and particle size distribution of the magnetic carbon xerogels are given in Figure 7.2, in which SEM images obtained with higher magnification (Figures 7.2a, c and e) are shown. During the synthesis procedure, the metal particles are expected to be anchored to the carbon structure, thus preventing their growth [3]. This mechanism is confirmed by the small size of the metal particles observed regardless of the magnetic carbon xerogel considered. Nevertheless, as detailed in Figures 7.2b, d and f, CX/Fe possesses the smallest primary carbon microspheres and metal particles, whereas

CX/Co is at the opposite position, with the biggest carbon microspheres and metal particles; once again, the bimetallic CX/CoFe possesses intermediate properties when compared to the monometallic materials.

The carbon xerogel materials were also characterized by XRD, the corresponding results being given in Figure 7.3. The absence of an identifiable crystallographic phase in the diffraction pattern of CX confirms the prevalence of amorphous carbon in its composition.

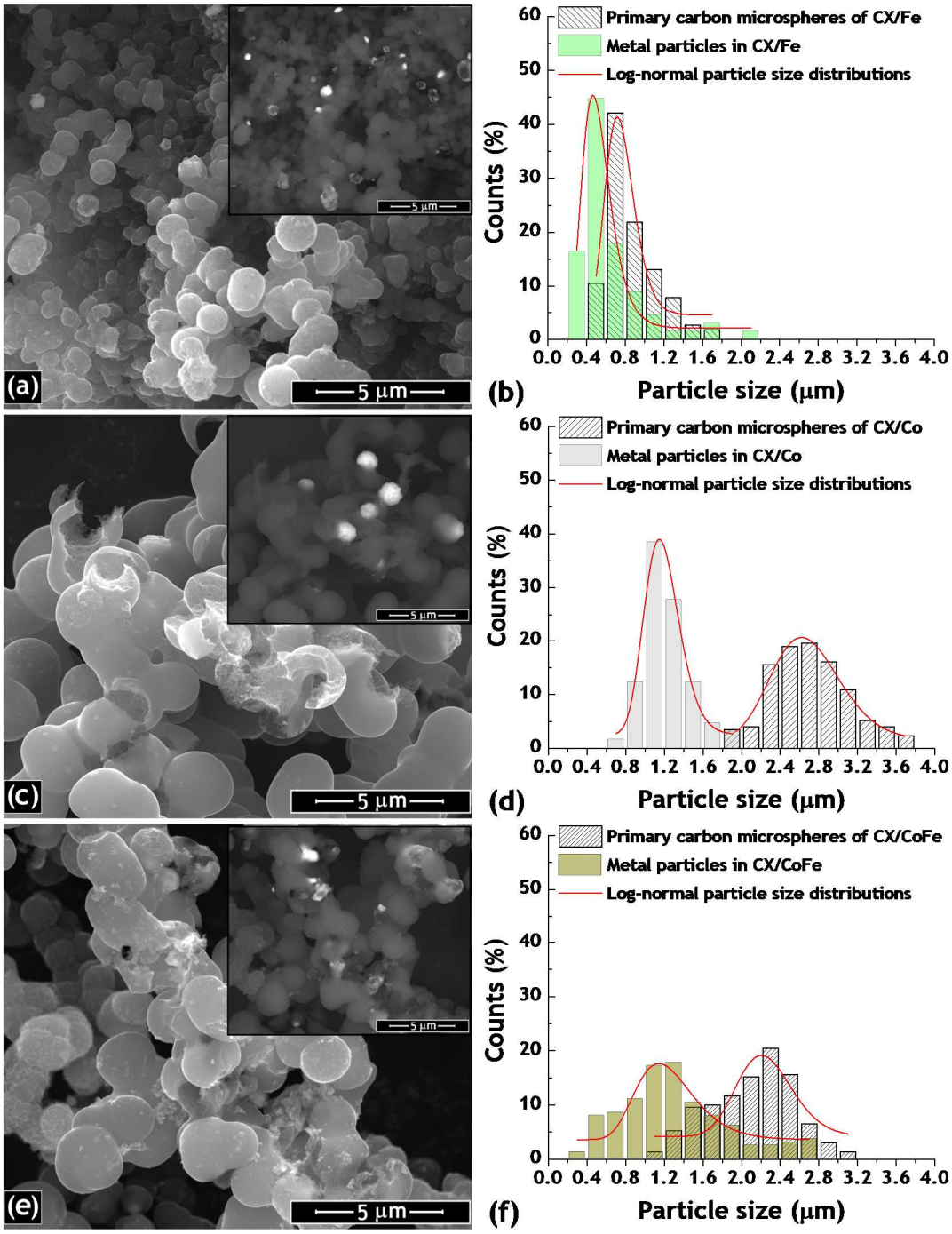

Figure 7.2. SEM micrographs, obtained in (main) SE and (inset) BSE mode, and histogram of particle size distribution of (a, b) CX/Fe, (c, d) CX/Co and (e, f) CX/CoFe.

On the other hand, the incorporation of iron and/or cobalt during the synthesis procedure promotes the formation of graphitic (i.e., more ordered) carbon, as observed in the diffraction patterns of the magnetic carbon xerogels. Magnetite (with a lattice parameter a = 8.380 Å) and metallic iron (a = 2.868 Å) were identified in the diffraction pattern of CX/Fe, in addition to graphite. The incorporation of Co during the synthesis of CX/Co leads to the formation of metallic cobalt (a = 3.544 Å), cobalt (II, III) oxide (a = 8.089 Å) and cobalt (II) oxide (a = 4.268 Å). The simultaneous incorporation of Co and Fe leads to the formation of cobalt ferrite (a = 8.388 Å) and metallic iron (a = 2.863 Å), in addition to graphite, as observed in the diffraction pattern of CX/CoFe.

If the values of pH_{PZC} obtained for the magnetic carbon xerogels (*cf*. Table 7.1) are compared with those recently reported in the literature for their main metal oxide constituents [4], it is observed that they follow the same order: CX/Fe (6.6) < CX/CoFe (7.7) < CX/Co (8.3), while Fe_3O_4 (6.5) < $CoFe_2O_4$ (7.5) < CoO (9.2) and Co_3O_4 (9.4). Therefore, the pH_{PZC} of the magnetic carbon xerogels can be partially explained by the different contributions of the main metal oxides detected by XRD.

7.2. CWPO experiments

The performance of the carbon xerogel materials in the CWPO of highly concentrated 4-NP aqueous model solutions (5 g L^{-1}) was evaluated in experiments performed under the operating conditions previously considered in Chapter 6 (please refer to Table 7.5 for additional details). The 4-NP removals obtained in pure adsorption and CWPO runs performed during 24 h are given in Figure 7.4. These results confirm the superior performance of the iron-containing materials, in particular that of the bimetallic magnetic carbon xerogel with cobalt and iron microparticles embedded in its structure (CX/CoFe). Further insights on this superior performance are provided in Figure 7.5, which shows the corresponding 4-NP

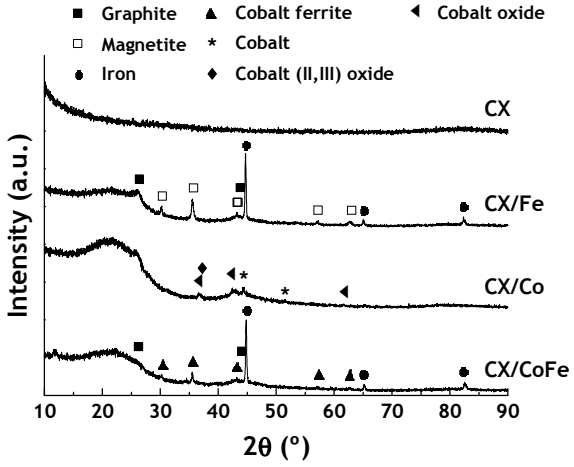

Figure 7.3. XRD diffraction patterns of the carbon xerogel materials.

removal curves as a function of time. Specifically, 98.5% of the initial 4-NP content is removed after 30 min in the presence of CX/CoFe, representing an average pollutant mass removal rate of 3940 mg g^{-1} h^{-1} —which is higher than the values reported in the literature at that time for carbon-based and magnetite-based catalysts [5, 6].

Given its potential catalytic activity (*cf*. Eqs. 2.1, 2.3 and 2.4), the iron leached to the treated water during the CWPO runs performed with CX/Fe and CX/CoFe (the magnetic carbon xerogels containing iron species) was determined. It was observed that the iron leached from CX/Fe amounts to 8.69 mg L^{-1}. On the opposite, CX/CoFe reveals a much better resistance to leaching, with an amount of iron leached of 0.67 mg L^{-1} at the end of the CWPO treatment, a value well below the limit of 2 mg L^{-1} allowed in Portugal for the discharge of treated waters into natural water bodies [7].

The results reported up to this point reveal a clear synergistic effect arising from the combination of Fe and Co in CX/CoFe, when its performance in CWPO is compared to that of the monometallic catalysts (CX/Fe and CX/Co). This effect may be partially explained by the enhanced accessibility to the highly active Fe species existing at the surface of CX/CoFe, promoted by the simultaneous incorporation of Co, as discussed in Section 7.1. However, the additional fact the iron leached is much lower for the catalyst CX/CoFe (0.67 mg L^{-1}), about 13-fold lower when compared to that obtained with CX/Fe (8.69 mg L^{-1}), under the same experimental conditions, cannot be explained only in terms of the bimetallic interaction during the synthesis. Bearing this in mind, additional experiments were conducted seeking to clarify the nature of the mechanisms and interactions between the different metallic phases, which can be held responsible for the superior performance of CX/CoFe, when compared to the monometallic catalysts.

The role of heterogeneous catalysis promoted by CX/CoFe was thus the object of a

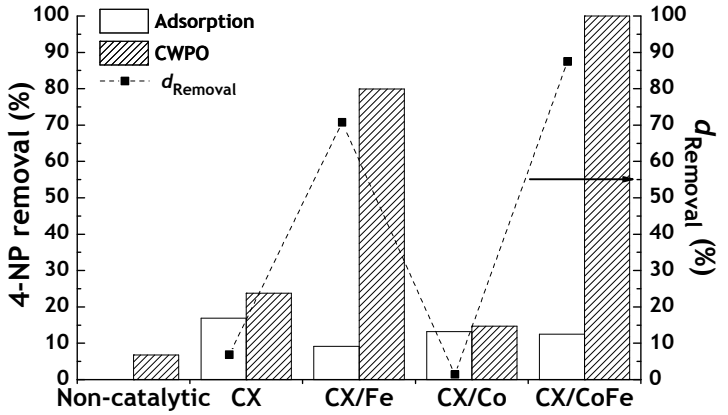

Figure 7.4. 4-NP removal in adsorption and CWPO runs (bars/left axis) after 24 h, and respective difference due to H_2O_2 addition [$d_{Removal}$ (squares/right axis)]. Experiments performed with $[4\text{-NP}]_0$ = 5.0 g L^{-1}, [catalyst/adsorbent] = 2.5 g L^{-1}, $[H_2O_2]_0$ = 17.8 g L^{-1} (stoichiometric amount), T = 50 ºC and pH = 3.

detailed study (Figure 7.6). The influence of adsorption in the global performance of CX/CoFe was evaluated in a pure adsorption run. As observed in Figure 7.6a, the removal of 4-NP by CWPO in the presence of CX/CoFe is markedly higher than the removal obtained by pure adsorption. Moreover, the removal of 4-NP in the absence of a catalyst (non-catalytic) is null after 2 h of reaction (please refer to Figure C.4a for additional details on the non-catalytic experiment). In order to understand if the iron leached to the solution could be responsible for the 4-NP removals observed, the effect of homogeneous catalysis promoted by the amount of iron leached during CWPO was simulated using a Fe^{2+} solution as catalyst. This solution contained the same concentration of iron as the iron leached in the CWPO experiment performed with CX/CoFe (i.e., 0.67 mg L^{-1}). This contribution represents 4-NP and TOC removals of only 9.4% and 2.3%, respectively (*cf*. Figure 7.6b). Likewise, the possible effect of cobalt leaching was also considered negligible (as discussed in detail in Section 7.3). Taking into consideration these results, it can be clearly established that the contributions of pure adsorption, non-catalytic and homogeneous catalytic removals are negligible when compared to the global 4-NP removal obtained by CWPO, confirming that CX/CoFe is very active as a heterogeneous catalyst for the CWPO of highly concentrated 4-NP solutions under mild operating conditions. In addition, the magnetic susceptibility of CX/CoFe (inset of Figure 7.6a) opens prospects for the development of *in-situ* magnetic separation systems.

Regarding the mineralization of 4-NP, ca. 57% of TOC removal is achieved upon application of the bimetallic CX/CoFe catalyst during 2 h —a value that increases up to ca. 67% when the CWPO experiment is allowed to proceed during 24 h. The efficiency of H_2O_2 consumption was also assessed. Values of $\eta_{H_2O_2}$ (obtained as described in Eq. 4.9) in the range 86 – 95% were obtained, the higher efficiency being achieved after 2 h of reaction. Therefore, it is possible to conclude that, in addition to the high performance of the catalyst,

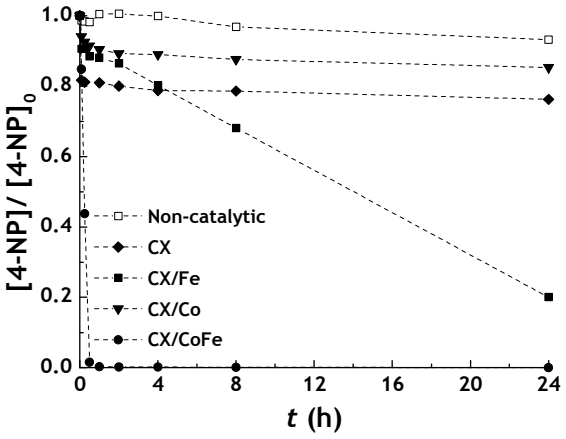

Figure 7.5. 4-NP removal obtained as a function of time in CWPO runs performed with the carbon xerogel materials. Experiments performed under the operating conditions given in Figure 7.4.

the H_2O_2 employed in the CWPO of highly concentrated 4-NP solutions with CX/CoFe is consumed with high efficiency.

7.2.1. Oxidation mechanism

In order to confirm the oxidation/mineralization mechanism proposed in Section 6.2.3, the evolution of possible aromatic by-products was assessed in the experiments performed with the two magnetic samples exhibiting the highest activity (*cf*. Figures 7.7a and b). Regardless of the catalyst employed, the mineralization of 4-NP by CWPO proceeds as expected, mainly via formation of 4-nitrocatechol; even if hydroquinone, 1,4-benzoquinone and catechol are also detected. However, the aromatic by-products of 4-NP CWPO are accumulated in solution when CX/Fe is applied (*cf*. Figure 7.7a); while, in the opposite, the aromatic by-products of 4-NP CWPO are readily mineralized in the presence of the bimetallic CX/CoFe catalyst (*cf*. Figure 7.7b). Therefore, it is possible to conclude that the superior performance previously evidenced by CX/CoFe regarding 4-NP removal is also reflected on the subsequent steps of 4-NP mineralization.

The evolution of possible non-aromatic by-products was assessed in the experiment performed with CX/CoFe, in order to confirm the formation of ring-opening products as the aromatic by-products are further attacked by $HO^{\bullet}$. As observed in Figure 7.7c, several low molecular weight carboxylic acids were detected. Nitrate produced from the $-NO_2$ group of the 4-NP aromatic ring was also detected, confirming the $-NO_2$ group abstraction from the main aromatic rings through CWPO in the presence of CX/CoFe.

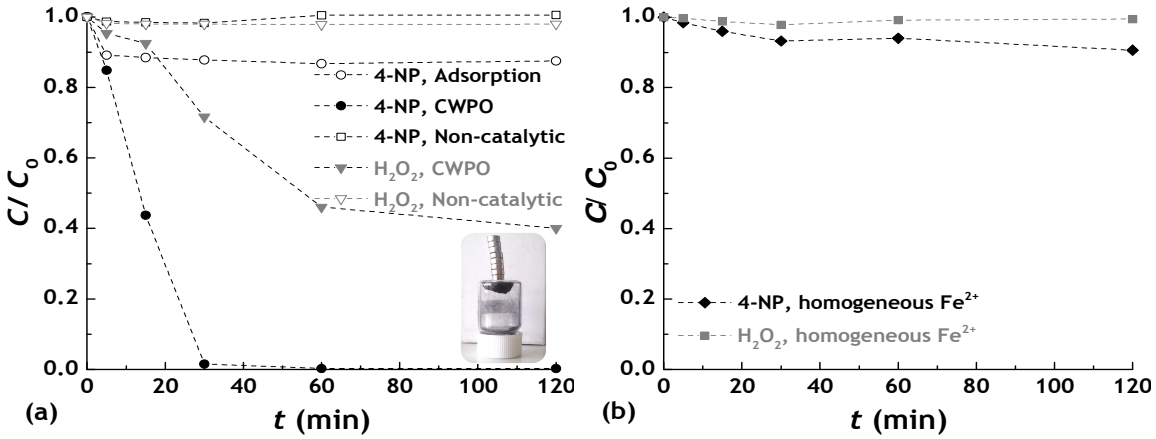

Figure 7.6. (a) 4-NP and H_2O_2 normalized concentrations as a function of time in the CWPO run performed with CX/CoFe (Inset: magnetic sensitivity of the bimetallic CX/CoFe catalyst); 4-NP removal by adsorption is also shown for comparison. (b) 4-NP and H_2O_2 conversions as a function of time in the homogeneous CWPO run performed with Fe^{2+} (0.67 mg L^{-1}, corresponding to the amount of iron leached during the CWPO of 4-NP in the presence of CX/CoFe). Experiments performed under the operating conditions given in Figure 7.4.

7.2.2. Reusability cycles

Two series of three CWPO runs were performed with consecutive reuse of CX/Fe and CX/CoFe, in order to evaluate the effect of the simultaneous incorporation of cobalt and iron on the stability of the catalysts. For that purpose, the catalyst was filtered after each run, washed and dried overnight at 60 ºC, and then reused in CWPO with a fresh 4-NP solution. As observed in Figure 7.8, both magnetic carbon xerogels undergo partial deactivation upon successive reuse in CWPO cycles. This phenomenon results from the water treatment process intensification approach used in this work. The CWPO experiments were performed with high pollutant load (5 g L^{-1}) and low catalyst dosage (2.5 g L^{-1}), allowing to promote very harsh conditions in the catalytic system, especially as several by-products of 4-NP oxidation are formed. After the initial adjustment, the experiments were allowed to proceed without further conditioning of pH. Therefore, the pH of the treated water dropped

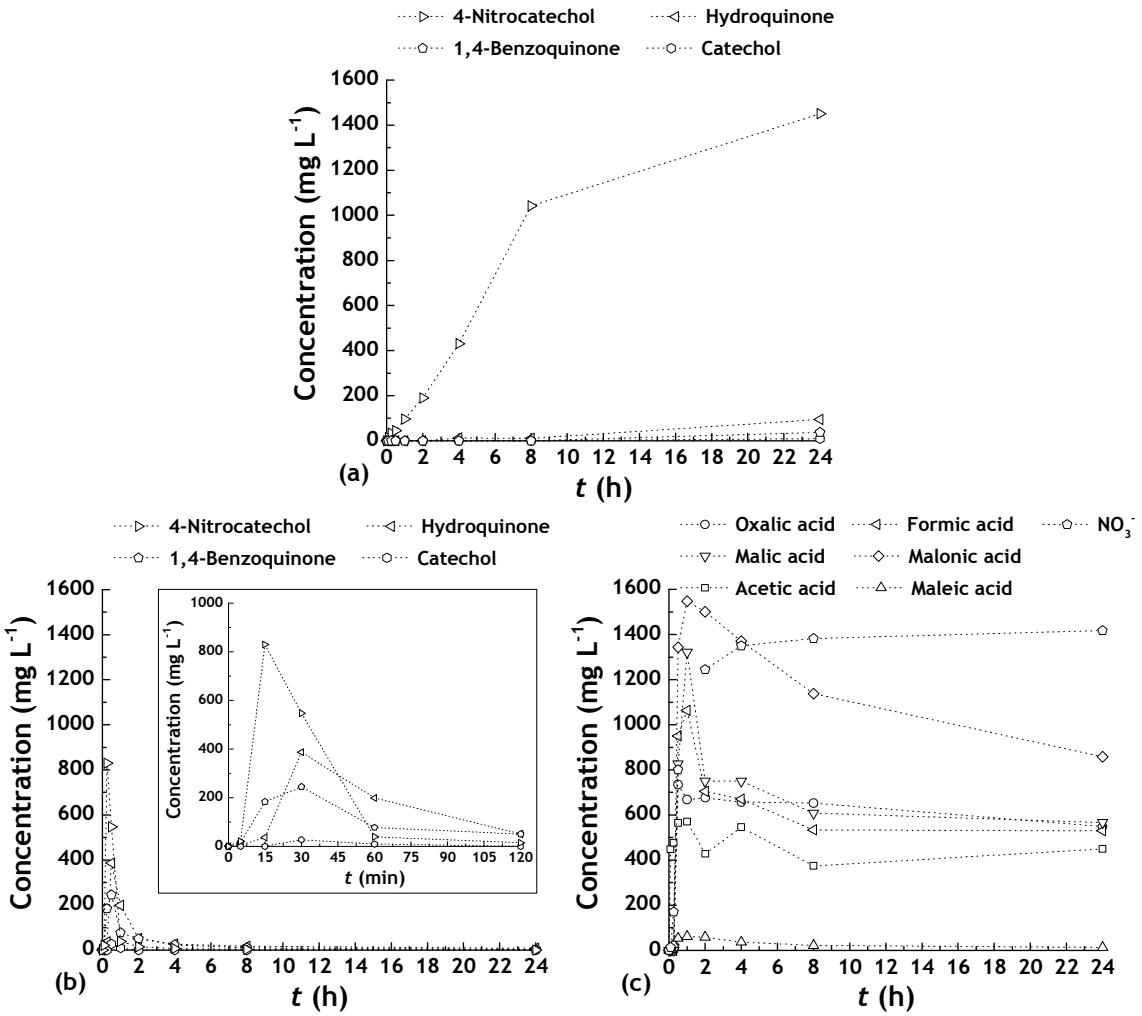

Figure 7.7. Evolution of aromatic by-products of 4-NP oxidation, when using (a) CX/Fe and (b) CX/CoFe (Inset: x-axis with maximum of 120 min = 2 h); and (c) evolution of non-aromatic by-products of 4-NP oxidation when using CX/CoFe in the CWPO process developed under the operating conditions given in Figure 7.4.

from 3.0 to 2.5 and 2.0, in the CWPO experiments performed with CX/Fe and CX/CoFe, respectively. In spite of the substantially higher decrease of the solution pH, the CX/CoFe catalyst reveals a much better resistance against the leaching of iron species to the treated water throughout the three reusability cycles considered (*cf*. Figure 7.8). Nevertheless, the performance of CX/CoFe also decreases in the series of three CWPO experiments. Aiming to explain the interactions between cobalt and iron species responsible for the superior performance of CX/CoFe, but also for the partial catalyst deactivation observed, a detailed reaction mechanism is proposed in the following Section.

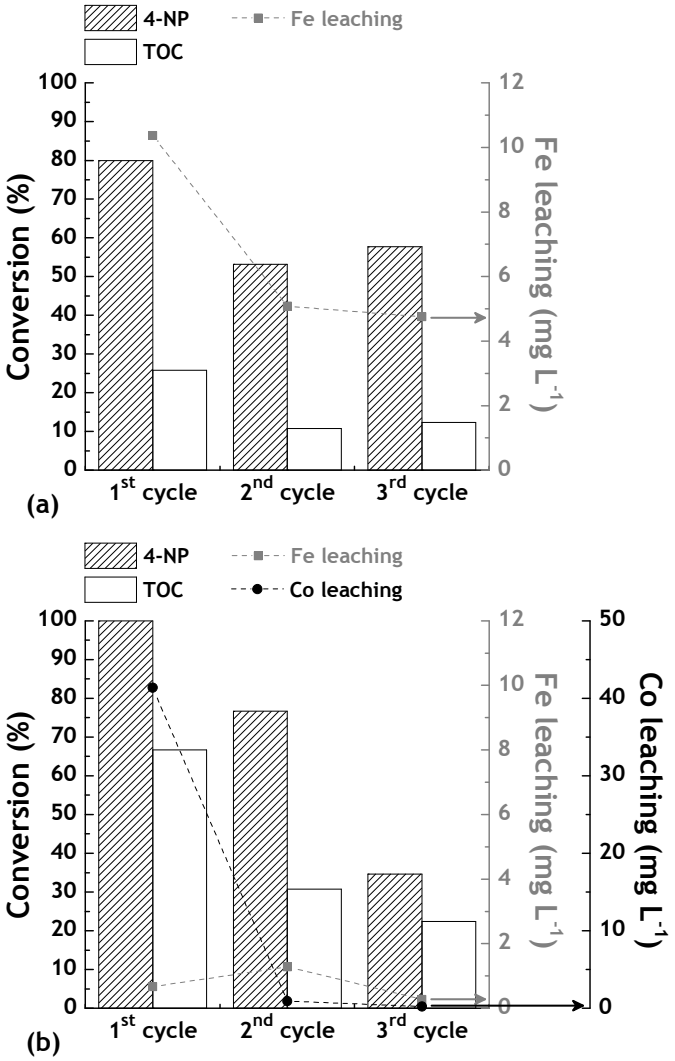

Figure 7.8. 4-NP and TOC conversions obtained after 24 h in a series of three CWPO runs performed with consecutive reuse of (a) CX/Fe and (b) CX/CoFe (bars/left axis), and respective iron and cobalt leaching (symbols/right axis). Experiments performed under the operating conditions given in Figure 7.4.

Table 7.3. Standard reduction potentials at 25 ºC (E^0) for some half-reactions of interest [8, 9]

Half-reaction			E^0 (V)	
H_2O_2	⇄	$O_2 + 2H^+ + 2e^-$	- 0.695	**(7.1)**
$Fe^{2+} + 2e^-$	⇄	Fe	- 0.447	**(7.2)**
$Co^{2+} + 2e^-$	⇄	Co	- 0.280	**(7.3)**
$Fe^{3+} + e^-$	⇄	Fe^{2+}	0.771	**(7.4)**
$H_2O_2 + H^+ + e^-$	⇄	$HO^\bullet + H_2O$	0.800	**(7.5)**
$Co^{3+} + e^-$	⇄	Co^{2+}	1.920	**(7.6)**

7.3. Interactions between cobalt and iron species at the surface of the bimetallic CX/CoFe catalyst

As detailed in Chapter 2, in CWPO, the H_2O_2 molecule is decomposed via $HO^\bullet$ radicals formation with the participation of reduced active sites/species (i.e., electron donor sites/species) existing at the surface of a catalyst. In this sense, the electron donating capacity of Fe^{2+} is well recognized in CWPO. For the current experiments, the catalytic cycle is thought to be initiated through the redox reaction described by Eq. 2.2. In a more complex system, in which several metal species are present, the overall catalytic cycle is expected to be influenced by the redox potentials of each metal. With this in mind, the standard reduction potentials at 25 ºC (E^0) for half-reactions involving the metal species embedded in the magnetic carbon xerogels are compiled in Table 7.3. The standard reduction potential of H_2O_2 decomposition via $HO^\bullet$ formation is also given. As observed, the redox properties of cobalt and iron species are determined by the oxidation state in which they are present. Therefore, the identification and quantification of the oxidation state of each component existing at the surface of the magnetic carbon xerogels was performed by XPS analysis. Accordingly, the results of Fe $2p_{3/2}$ and Co $2p_{3/2}$ spectral fitting are shown in Figure 7.9. Regarding iron, the fit suggests a mix of Fe^{2+} and Fe^{3+} species both in CX/Fe and CX/CoFe. In addition, the relative amount of each iron species is not particularly affected by the simultaneous inclusion of cobalt, as concluded from the inset of Figure 7.9a and c. For cobalt, the fit of the Co $2p_{3/2}$ region suggests a mix Co, Co^{2+} and Co^{3+} species, both in CX/CoFe and CX/Co. In this case, the relative amounts of each cobalt species are also not particularly affected by the simultaneous inclusion of iron, as concluded from the insets of Figure 7.9e and g. It should be noted that metallic Co was undetectable in the XRD pattern of CX/CoFe (*cf.* Figure 7.3). This phenomenon may be ascribed to the interference promoted by the presence of the graphitic and metallic Fe phases.

Once the composition of iron and cobalt species in each magnetic carbon xerogel is

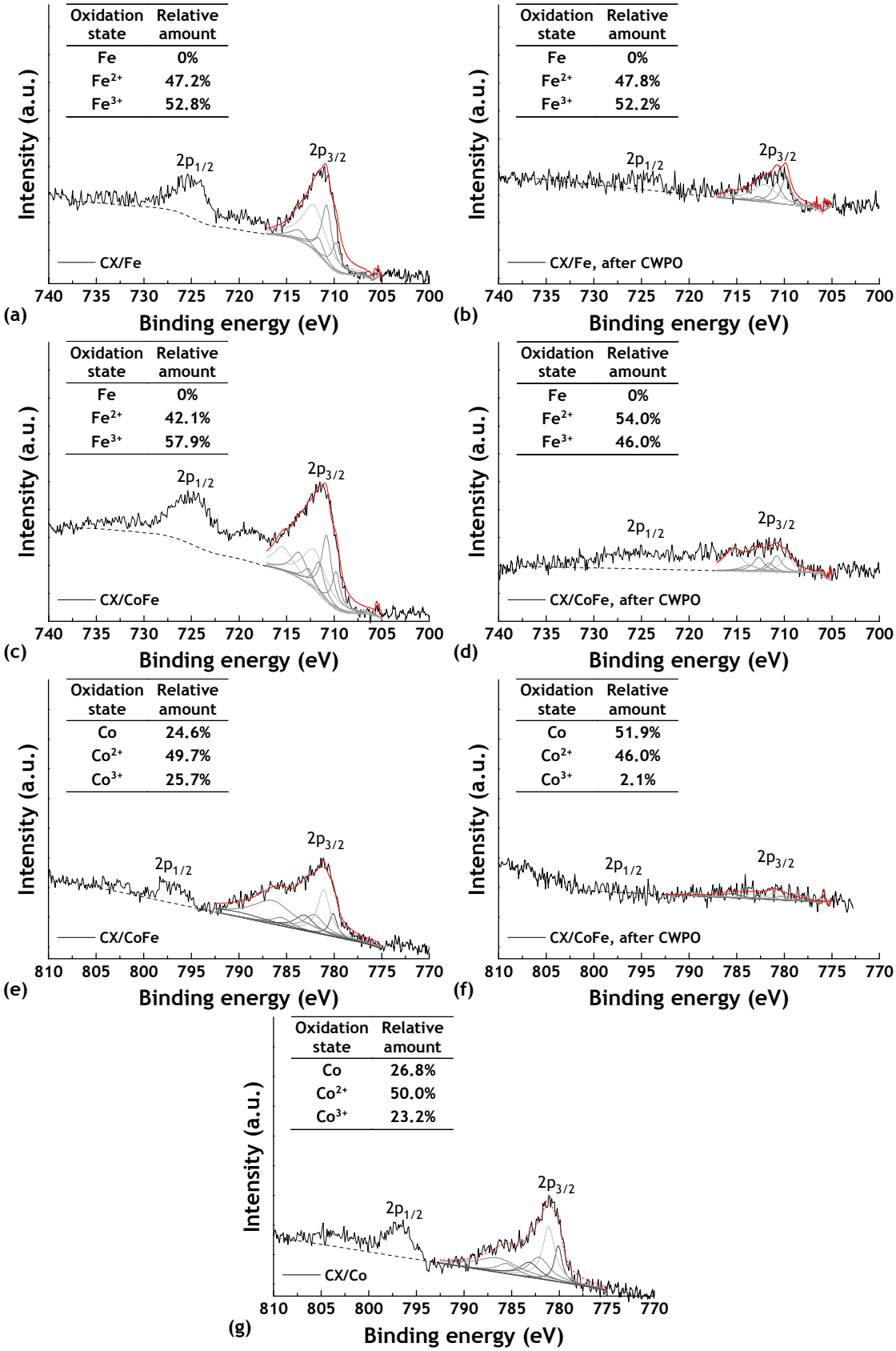

Figure 7.9. Detailed XPS spectra of Fe 2p region of (a, b) CX/Fe and (c, d) CX/CoFe; and detailed XPS spectra of Co 2p region of (e, f) CX/CoFe and (g) CX/Co. XPS spectra obtained (a, c, e, g) before and (b, d, f) after CWPO runs performed under the operating conditions given in Figure 7.4. Inset: oxidation state of iron and cobalt species obtained from Fe $2p_{3/2}$ and Co $2p_{3/2}$ spectral fitting, respectively.

Table 7.4. Reaction potentials at 25 ºC (*E*) for some reactions of interest

Reaction			*E* (V)	Comment	
$H_2O_2 + Fe + H^+$	→	$Fe^{2+} + HO^{\bullet} + H_2O + e^-$	1.247	Spontaneous	**(7.7)**
$H_2O_2 + Fe^{2+} + H^+$	→	$Fe^{3+} + HO^{\bullet} + H_2O$	0.029	Spontaneous	**(7.8)**
$H_2O_2 + Co^{2+} + H^+$	→	$Co^{3+} + HO^{\bullet} + H_2O$	- 1.120	Non-spontaneous	**(7.9)**
$H_2O_2 + Co + H^+$	→	$Co^{2+} + HO^{\bullet} + H_2O + e^-$	1.080	Spontaneous	**(7.10)**
$Fe^{3+} + Co^{2+}$	→	$Co^{3+} + Fe^{2+}$	- 1.149	Non-spontaneous	**(7.11)**
$Fe^{3+} + Co$	→	$Co^{2+} + Fe^{2+} + e^-$	1.051	Spontaneous	**(7.12)**

known, the half-reactions given in Table 7.3 were combined as shown in Table 7.4, aiming to obtain a reaction mechanism able to justify the superior performance of the bimetallic CX/CoFe in CWPO, when compared to the performance of the monometallic CX/Fe and CX/Co. In order to predict the feasibility of the proposed redox reactions, the reaction potentials at 25 ºC (*E*) are also given. As observed in Eq. 7.7, Fe is theoretically able to reduce H_2O_2 via $HO^{\bullet}$ formation. However, although Fe was detected by XRD analysis (*cf*. Figure 7.3), it was undetected by XPS analysis both in CX/Fe and CX/CoFe (*cf*. Figure 7.9a and c). This observation suggests that Fe particles are preferably surrounded by the organic phase during the synthesis of the magnetic carbon xerogels, therefore being less accessible to H_2O_2. As expected, the reaction potential obtained for the reaction described in Eq. 7.8 confirms the feasibility for the decomposition of H_2O_2 with the participation of reducing Fe^{2+} species. The $HO^{\bullet}$ radicals formed at the surface of the catalyst are afterwards expected to readily react with 4-NP molecules adsorbed nearby the $HO^{\bullet}$ radicals generation sites, resulting in the oxidation mechanism described in Section 7.2.1, and the high efficiency of TOC removal per unit of H_2O_2 decomposed previously shown. On the other hand, the potential obtained for the reaction described in Eq. 7.9 suggests that Co^{2+} species are not active species for CWPO. In order to confirm this hypothesis, an additional CWPO run was performed with homogeneous Co^{2+} under the operating conditions given in Figure 7.4. For that purpose, a relatively high amount of Co^{2+} was employed (126 mg L^{-1}, corresponding to the total amount of Co^{2+} in the cobalt precursor included during the synthesis of CX/Co and CX/CoFe). The 4-NP and H_2O_2 conversions were null after 2 h of reaction (*cf*. Figure C.4b), confirming the theoretical prediction given in Table 7.4. The ability of metallic Co species to promote the formation of $HO^{\bullet}$ from H_2O_2, as described by Eq. 7.10, was also considered. From a theoretical point of view, this reaction is spontaneous, with a high redox reaction potential. Nevertheless, when the results in Figure 7.5 are analysed together with the results in Figure 7.9, it is observed that the presence of metallic Co species cannot, by itself, explain the largely superior performance of CX/CoFe in the CWPO of 4-NP, when compared to CX/Fe and CX/Co. As discussed before, CX/CoFe possesses nearly the same amount of metallic Co

species as CX/Co; on the other hand, the phase composition of iron species in CX/CoFe is also about the same as in CX/Fe. However, the sum of the 4-NP removals obtained after 30 min of CWPO in the presence CX/Fe and CX/Co (i.e., 11.5% and 8.5%, respectively, corresponding to a combined 4-NP removal of 20%) is far below the 4-NP removal obtained in the presence of CX/CoFe (98.5%). These results suggest that the reaction described in Eq. 7.10 is not the main mechanism responsible for the superior performance of CX/CoFe in CWPO.

Since the synergy arising from the simultaneous incorporation of cobalt and iron in the CX/CoFe catalyst cannot be fully ascribed to the direct interactions of iron and cobalt species with H_2O_2, particular attention was given to the interactions between Fe and Co species. When there are only iron species, the Fe^{2+} regeneration from Fe^{3+} proceeds mainly through the reaction described by Eq. 2.5. However, several cobalt species are also present at the surface of the catalyst in addition to Fe^{2+} and Fe^{3+} when CX/CoFe is applied in CWPO. To evaluate the ability of Co^{2+} and Co species to promote Fe^{2+} regeneration from Fe^{3+}, the reactions described by Eqs. 7.11 and 7.12 were considered. As observed, Co^{2+} species are unable to regenerate Fe^{2+} by reduction of Fe^{3+} (*cf*. Eq. 7.11). On the other hand, the redox reaction of Co with Fe^{3+}, leading to the regeneration of Fe^{2+} (*cf*. Eq. 7.12), reveals a high reaction potential, thus being considered spontaneous. In order to confirm this hypothesis, both CX/Fe and CX/CoFe were collected after CWPO and characterized by XPS (*cf*. Figure 7.9). As observed in Figures 7.9a and b, the relative amount of iron species at the surface of CX/Fe is unaffected by CWPO although the overall iron surface content decreases. This result was expected, since when CX/Fe is applied in CWPO the catalytic cycle is mainly driven by Eq. 2.5. On the opposite, when in the presence of cobalt species, the relative amount of Fe^{2+} at the surface of CX/CoFe increases from 42.1 to 54.0% upon its application in CWPO (*cf*. Figure 7.9c and d), confirming the feasibility of the reaction described in Eq. 7.12. Therefore, it is possible to conclude that the reduction of Fe^{3+} in the CWPO process is more efficient when metallic Co is combined with iron species, such as in the surface of the bimetallic CX/CoFe catalyst. This feature offers an alternative route to the reactions described by Eqs. 2.3 and 2.4, which enables a faster regeneration of Fe^{2+} in the catalytic cycle and thus allows to overcome one limiting step of the CWPO cycle with Fe species.

Summarizing, it can be concluded that the synergy arising from the simultaneous incorporation of cobalt and iron in the magnetic carbon xerogel catalyst denoted as CX/CoFe can be ascribed to (i) the enhanced accessibility to the active iron species existing at the surface of CX/CoFe, (ii) the ability of metallic Co species to catalyse H_2O_2 decomposition via $HO^{\bullet}$ formation, and to (iii) the more efficient reduction of Fe^{3+} to Fe^{2+} promoted by Co species existing at the surface of CX/CoFe. The catalytic surface mechanism summarized in

Figure 7.10 accounts for the superior performance of the bimetallic iron-cobalt magnetic carbon xerogel (CX/CoFe) in the CWPO of 4-NP, when compared to that of the monometallic CX/Fe.

Regarding the stability of the catalysts, as discussed in Section 7.2.2., the bimetallic CX/CoFe material reveals a better resistance against leaching of iron species to the treated water when compared to monometallic CX/Fe. This increased stability of iron species can be ascribed to the presence of Co^{2+} in the structure of $CoFe_2O_4$ (i.e., the main iron oxide detected by XRD analysis; *cf*. Figure 7.3), rather than Fe^{2+} in Fe_3O_4 (i.e., in the case of CX/Fe). Briefly, magnetite possesses the chemical formula $Fe^{2+}Fe_2^{3+}O_4$; when Co^{2+} replaces Fe^{2+}, cobalt ferrite with the general formula $Co_xFe_{3-x}O_4$ is obtained [10]. Under this context, Sileo et al. showed that the iron dissolution rate decreases with increasing Co^{2+} content in cobalt ferrites, through a complex process approximately described by a second-order kinetic model [10]. This observation was thoroughly explained in terms of electronic effects within the solid framework, the most significant being the fast electron hopping between octahedral adjacent Fe^{2+}/Fe^{3+} pairs occurring preferentially in magnetite. In this case, inner vicinal lattice Fe^{2+} accelerates the rate of Fe^{3+} reductive dissolution via internal electron hopping, whereas the amount of adjacent Fe^{2+}/Fe^{3+} pairs is significantly lower in cobalt ferrite, thus yielding lower iron leaching rates. As depicted in Figure 7.10b, metallic Co is oxidized to Co^{2+} both during the regeneration of Fe^{2+} active sites and the formation of $HO^{\bullet}$ radicals from H_2O_2. The leaching of cobalt species to the treated water during the first CWPO cycle performed with CX/CoFe amounts to 41.36 mg L^{-1} (*cf*. Figure 7.8b) —representing ca.

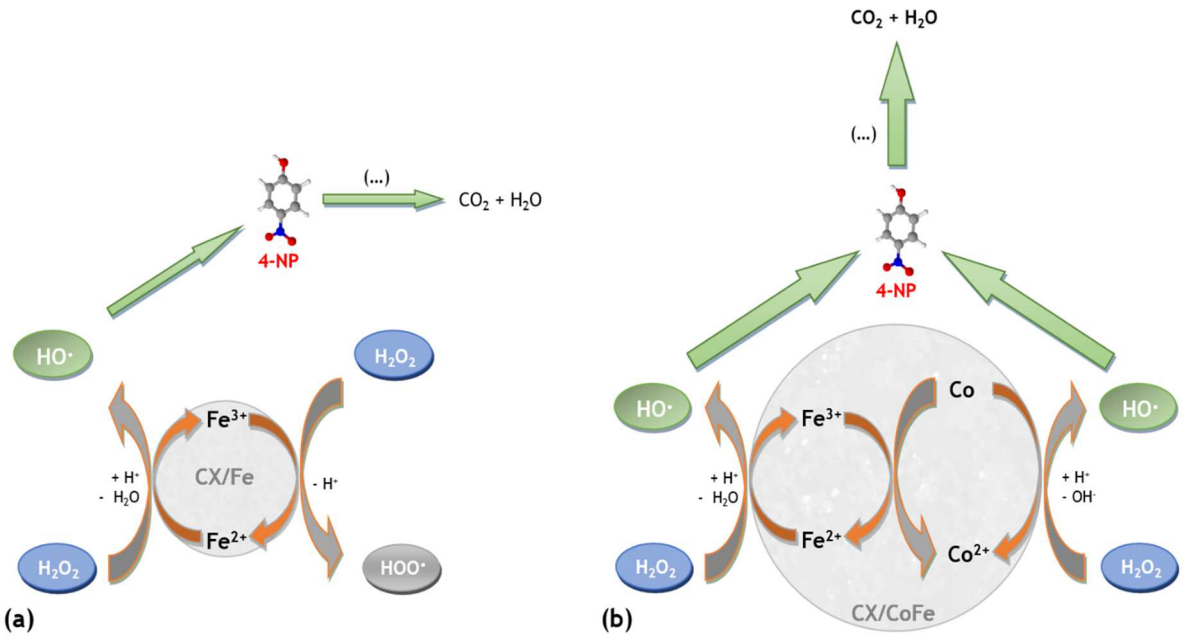

Figure 7.10. Mechanism proposed for the surface catalytic reactions occurring on (a) CX/Fe and (b) CX/CoFe. Bulk reactions between $HO^{\bullet}$ radicals and 4-NP are also represented.

Table 7.5. Experimental details of the CWPO experiments reported in Chapter 7

Aqueous model system	Reactor/solution volume	Operating conditions	H_2O_2 stoichiometric ratio[a]	[Pollutant]/ [catalyst]
4-nitrophenol (5.0 g L^{-1})	100 mL/ 50 mL	[Catalyst] = 2.5 g L^{-1} $[H_2O_2]_0$ = 17.8 g L^{-1} T = 50 ºC; pH_0 = 3 t = 24 h	1	2

[a] Obtained by dividing the amount of H_2O_2 employed by the stoichiometric amount needed for the complete mineralization of the pollutant considered.

79 wt.% of the total content of cobalt initially embedded in the CX/CoFe catalyst. On the other hand, the cobalt leaching in the second and third CWPO cycles is rather low (0.93 and 0.23 mg L^{-1}, respectively). These observations are in agreement with the mechanism proposed in Figure 7.10. However, it is suggested that the leaching of cobalt species is the main cause of the partial catalyst deactivation observed in CWPO cycles performed with consecutive reuse of CX/CoFe. In order to infer about the propensity of cobalt species to undergo leaching from the surface of CX/CoFe to the treated waters, the catalyst was collected after CWPO and analysed by XPS (*cf*. Figure 7.9f). In comparison with the fresh sample (Figure 7.9e), it was observed that the overall cobalt surface content decreases after CWPO. In addition, the relative amount of Co^{3+} species decreases significantly, maybe because they are preferably leached to water during CWPO; on the other hand, the relative amount of metallic Co increases substantially from 24.6 to 51.9%, suggesting a higher resistance to leaching.

7.4. Conclusions

The bimetallic magnetic carbon xerogel containing cobalt and iron species embedded in its structure (CX/CoFe) revealed a much higher catalytic performance in the CWPO of highly concentrated 4-NP solutions than that expected from the performances of the monometallic catalysts containing only iron (CX/Fe) or cobalt (CX/Co). A clear synergy arises from the simultaneous incorporation of cobalt and iron into the carbon xerogel matrix. This effect was ascribed to (i) the enhanced accessibility to the active iron species existing at the surface of CX/CoFe promoted by the simultaneous incorporation of cobalt, (ii) the ability of metallic Co species to catalyse the decomposition of H_2O_2 via $HO^{\bullet}$ formation, and to (iii) the more efficient reduction of Fe^{3+} to Fe^{2+} promoted by metallic Co species existing at the surface of CX/CoFe.

7.5. Experimental details

The CWPO experiments reported in Chapter 7 were performed under the conditions detailed in Table 7.5. Please refer to Chapter 4 for additional details on the experimental procedures.

References

[1] J. Chaichanawong, T. Yamamoto, S.-I. Kim, T. Ohmori, Preparation and characterization of nickel-modified carbon cryogel beads with uniform particle size, J. Non-Cryst. Solids 355 (2009) 1605-1612.

[2] X. Wang, X. Wang, L. Liu, L. Bai, H. An, L. Zheng, L. Yi, Preparation and characterization of carbon aerogel microspheres by an inverse emulsion polymerization, J. Non-Cryst. Solids 357 (2011) 793-797.

[3] C. Moreno-Castilla, F.J. Maldonado-Hodar, Carbon aerogels for catalysis applications: an overview, Carbon 43 (2005) 455-465.

[4] M. Kosmulski, The pH dependent surface charging and points of zero charge. VI. Update, J. Colloid Interface Sci. 426 (2014) 209-212.

[5] R.S. Ribeiro, A.M.T. Silva, J.L. Figueiredo, J.L. Faria, H.T. Gomes, Catalytic wet peroxide oxidation: a route towards the application of hybrid magnetic carbon nanocomposites for the degradation of organic pollutants. A review, Appl. Catal. B 187 (2016) 428-460.

[6] M. Munoz, Z.M. de Pedro, J.A. Casas, J.J. Rodríguez, Preparation of magnetite-based catalysts and their application in heterogeneous Fenton oxidation - A review, Appl. Catal. B 176-177 (2015) 249-265.

[7] Decreto-Lei n.º 236/98 de 1 de agosto, Diário da República - I Série - A, n.º 176 - 1-8-1998

[8] D.R. Lide, CRC Handbook of Chemistry and Physics, 84th ed., CRC Press, Boca Raton, 2003.

[9] A. Armstrong David, E. Huie Robert, H. Koppenol Willem, V. Lymar Sergei, G. Merényi, P. Neta, B. Ruscic, M. Stanbury David, S. Steenken, P. Wardman, Standard electrode potentials involving radicals in aqueous solution: inorganic radicals (IUPAC Technical Report), Pure Appl. Chem. 87 (2015) 1139-1150.

[10] E.E. Sileo, L. García Rodenas, C.O. Paiva-Santos, P.W. Stephens, P.J. Morando, M.A. Blesa, Correlation of reactivity with structural factors in a series of Fe(II) substituted cobalt ferrites, J. Solid State Chem. 179 (2006) 2237-2244.

PART IV: CARBON ENCAPSULATED MAGNETIC COMPOSITES

Hybrid magnetic carbon nanocomposites in which the magnetic phase is protected against the external environment by a carbonaceous shell were also considered in these Ph.D. studies. Unlike the magnetic carbon xerogels studied in Part III, in which the magnetic material is embedded to the carbon structure, without being protected against the environment by a carbonaceous shell, *the materials studied in Part IV are core-shell structures with a carbonaceous shell and a core made of magnetic materials. For that purpose, a hybrid magnetic graphitic nanocomposite catalyst —composed by a magnetite core and a graphitic shell, was prepared by a hierarchical co-assembly approach, followed by thermal annealing. The results obtained revealed a clear synergy arising from the encapsulation of magnetic nanoparticles within a graphitic structure.*

8. HYBRID MAGNETIC GRAPHITIC NANOCOMPOSITES

8. HYBRID MAGNETIC GRAPHITIC NANOCOMPOSITES

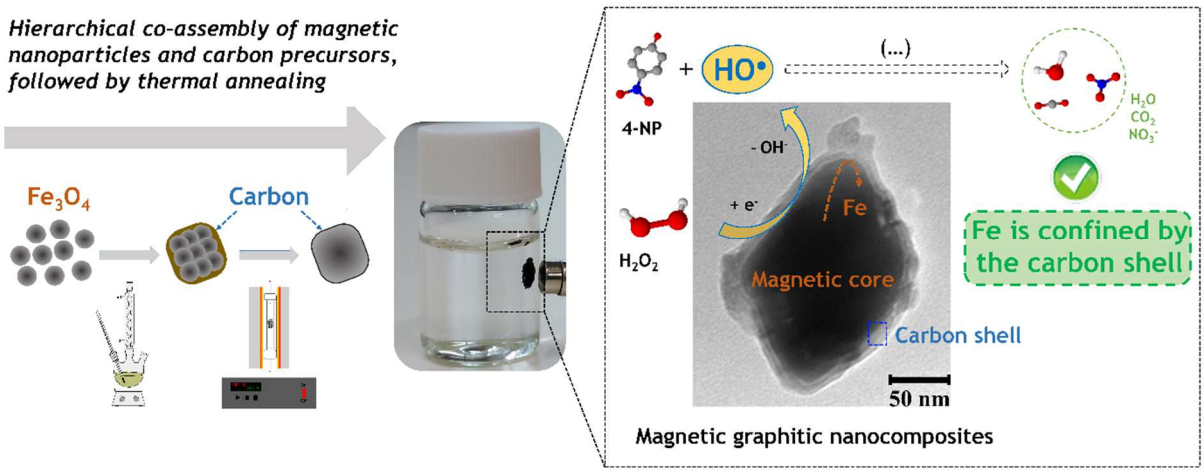

12

[12] Adapted from the graphical abstract of: Rui S. Ribeiro, Adrián M.T. Silva, Pedro B. Tavares, José L. Figueiredo, Joaquim L. Faria, Helder T. Gomes, Hybrid magnetic graphitic nanocomposites for catalytic wet peroxide oxidation applications, Catal. Today 280 (2017) 184-191
DOI: 10.1016/j.cattod.2016.04.040

Magnetite (Fe_3O_4) was prepared by the co-precipitation method described in Section 4.1.4, and encapsulated within a graphitic structure by a hierarchical co-assembly approach, followed by thermal annealing (*cf*. Section 4.1.5). The resulting hybrid magnetic graphitic nanocomposite was denoted as Fe_3O_4/MGNC. In the following Sections the properties of Fe_3O_4 and Fe_3O_4/MGNC are fully characterized and the respective performance in CWPO is evaluated using 4-NP aqueous model solutions in a very wide concentration range (0.2 – 5 g L^{-1}). In order to further optimize the efficiency of catalyst usage, the catalyst dosage was kept very low when compared to the pollutant concentration. Specifically, all the experiments were performed considering the mass ratio $[4\text{-NP}]_0/[Fe_3O_4]$ = 36.6, corresponding to a mass ratio $[4\text{-NP}]_0/[Fe_3O_4/\text{MGNC}]$ = 10 (27.3 wt.% of Fe_3O_4 in Fe_3O_4/MGNC, as determined by TGA). As a result of this approach, the operating temperature was increased from 50 to 80 ºC, which is in line with the current trend for the application of higher temperatures (up to 125 ºC) in CWPO [1, 2] and Fenton [3] processes. In addition, the individual effect of operating pH was evaluated.

8.1. Textural and surface chemistry characterization

Fe_3O_4 and Fe_3O_4/MGNC were characterized by XRD and TEM. The corresponding results are given in Figures 8.1 and 8.2, respectively. As observed in Figure 8.1, Fe_3O_4 exhibits the typical diffraction pattern of magnetite, with a lattice parameter a = 8.357 Å and a crystallite size of 16.6 ± 0.2 nm, which is near the average particle size of 12.5 ± 3.6 nm determined from TEM (*cf*. Figure 8.2e). Graphite, maghemite (a = 8.379 Å), iron (a = 2.868 Å) and traces of hematite (proto) were identified in the diffraction pattern of

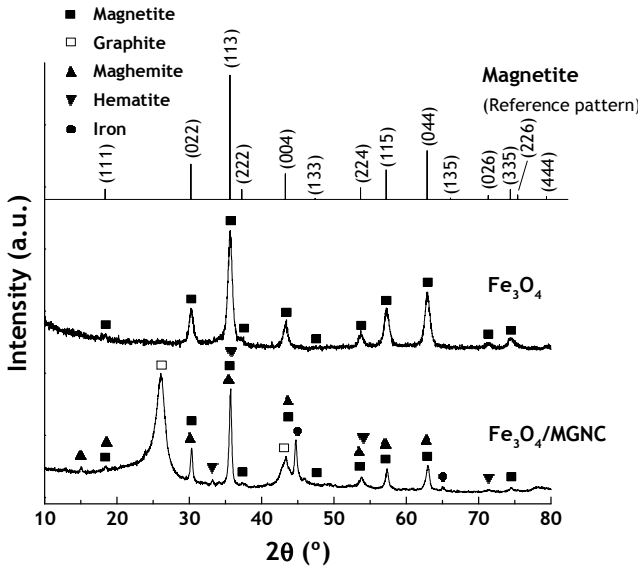

Figure 8.1. XRD diffraction patterns of Fe_3O_4 and Fe_3O_4/MGNC. Standard reference pattern of magnetite (crystallography open database code: 9005840) is also given for comparison.

Fe_3O_4/MGNC (*cf*. Figure 8.1), in addition to magnetite (a = 8.343 Å). This result suggests that Fe_3O_4 nanoparticles were successfully encapsulated within a graphitic structure during the synthesis of Fe_3O_4/MGNC, although with some changes in the magnetite phase. This fact is

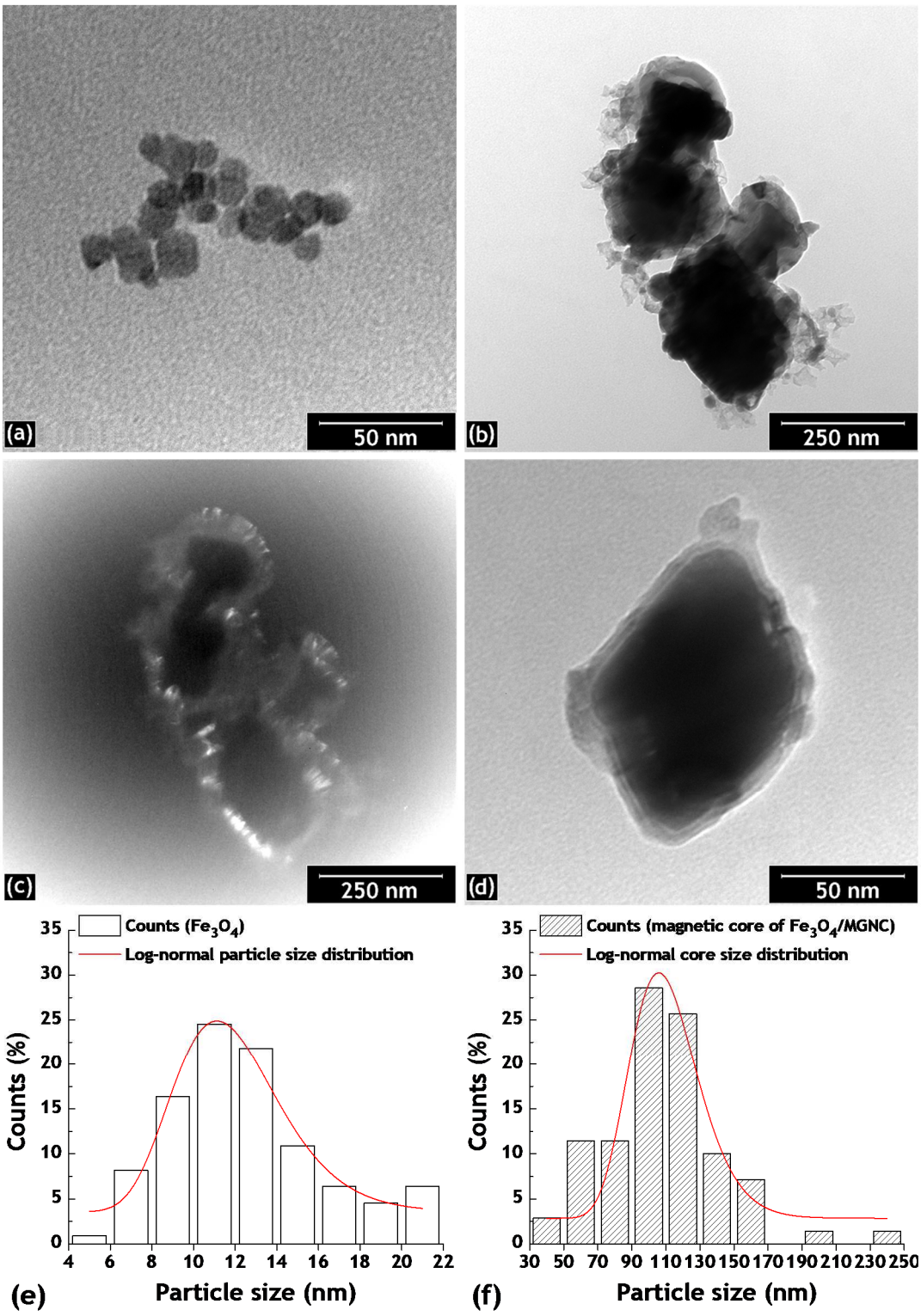

Figure 8.2. TEM micrographs of (a) Fe_3O_4 and (b-d) Fe_3O_4/MGNC: (b and d) and (c) were obtained in bright field and dark field image modes, respectively. Histogram of particle size distribution: (e) Fe_3O_4 and (f) magnetic core of Fe_3O_4/MGNC, as determined by TEM measurements.

Table 8.1. Properties of Fe_3O_4/MGNC: specific surface area (S_{BET}), non-microporous specific surface area (S_{meso}), micropore volume (V_{micro}), total pore volume (V_{total}), average pore diameter (d_{pore}) and pH at the point of zero charge (pH_{PZC})

Material	Parameter					
	S_{BET}[a] ($m^2\ g^{-1}$)	S_{meso}[a] ($m^2\ g^{-1}$)	V_{micro}[a] ($cm^3\ g^{-1}$)	V_{total}[a] ($cm^3\ g^{-1}$)	d_{pore}[a] (nm)	pH_{PZC}
Fe_3O_4/MGNC	330	170	0.07	0.31	3.75	7.1

[a] An ilustrative example of the N_2 adsorption-desorption isotherms at -196 ºC used for the determination of the textural properties of the materials included in this Ph.D. thesis is shown in Figure C.6b.

also supported by the TEM micrographs depicted in Figures 8.2b-d, in which the core-shell structure of Fe_3O_4/MGNC is unequivocally observed. In particular, the TEM micrograph obtained in dark field mode (*cf*. Figure 8.2c) confirms the existence of crystalline cores inside the carbon shells. The average size of the magnetic core of Fe_3O_4/MGNC, 109 ± 35 nm, as determined from TEM measurements (*cf*. Figure 8.2f), suggests that the cores are mainly composed by agglomerates of magnetic nanoparticles (with crystallite sizes in the range 23 – 165 nm, depending on the phase, as determined by XRD analysis). These observations are in accordance with the hierarchical co-assembly mechanism of the Fe_3O_4/MGNC synthesis, as detailed elsewhere [4]. During this procedure, Fe_3O_4 nanocrystals grow and spontaneously co-assemble by partially replacing F127/resol micelles; at the same time, carbon-carbon bonds are formed with the polymerization of resols and, upon thermal annealing, the copolymer F127 is eliminated, graphitic carbon frameworks being obtained with the participation of Fe_3O_4 as graphitization catalyst [4]. The main steps of the Fe_3O_4/MGNC synthesis are depicted in Figure 8.3.

The texture and surface chemistry of Fe_3O_4/MGNC were further characterized by TGA analysis, N_2 adsorption-desorption isotherms and pH_{PZC}. The TGA analysis of Fe_3O_4/MGNC (*cf*. Figure C.6a) reveals 27.3 wt.% of ashes, corresponding to the mass fraction of Fe_3O_4 encapsulated in Fe_3O_4/MGNC. It was also found that Fe_3O_4/MGNC is stable up to 400 ºC under

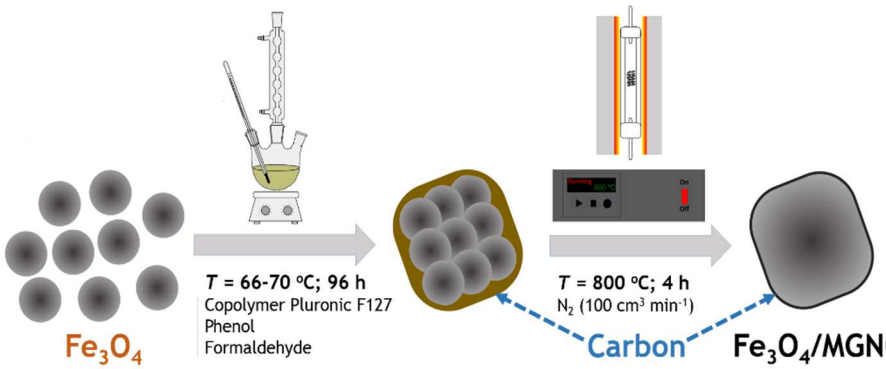

Figure 8.3. Synthesis of magnetic graphitic nanocomposites by hierarchical co-assembly of magnetite nanoparticles and carbon precursors, followed by thermal treatment.

oxidizing atmosphere. As observed in Table 8.1, Fe_3O_4/MGNC has a well-developed specific surface area, with a S_{BET} of 330 m^2 g^{-1}, and a micro-mesoporous character, which is particularly reflected by the ratio V_{mic}/V_{total} = 0.23, as well as by the average pore diameter of 3.75 nm. Regarding the surface chemistry, the pH_{PZC} of 7.1 (*cf.* Table 8.1) reveals that most of the acidic and basic functionalities were removed during the thermal annealing.

8.2. CWPO experiments

The performance of Fe_3O_4/MGNC in the CWPO of 4-NP aqueous model solutions was initially evaluated against that of bare Fe_3O_4, in experiments performed with $[4\text{-NP}]_0$ = 200 mg L^{-1} and a fixed mass ratio $[4\text{-NP}]_0/[Fe_3O_4]$ = 36.6, corresponding to a mass ratio $[4\text{-NP}]_0/[Fe_3O_4/\text{MGNC}]$ = 10 (27.3 wt.% of Fe_3O_4 in Fe_3O_4/MGNC, as determined by TGA). The 4-NP removals obtained after 1 h in pure adsorption and CWPO runs performed with Fe_3O_4 and Fe_3O_4/MGNC are given in Figure 8.4a. These results reveal the superior performance of Fe_3O_4/MGNC. Further insights are provided in Figure 8.4b, which shows the corresponding 4-NP removal curves as a function of time. The 4-NP removal obtained after 2 h in the non-catalytic experiment is not significant (representing a TOC removal of 0.6% only), while a fast removal of 4-NP is achieved in the presence of Fe_3O_4 (please refer to Figure C.7a for additional details on the non-catalytic experiment). In addition, the catalytic activity is enhanced when the Fe_3O_4 magnetic material is encapsulated within a carbon shell in the Fe_3O_4/MGNC catalyst. This behaviour may be explained by the presence of the carbon phase, which increases the adsorptive interactions between the surface of the catalyst and the pollutant molecules, attracting higher amounts of pollutant molecules to the vicinity of the active sites where highly oxidizing HO• radicals are generated, thus inhibiting

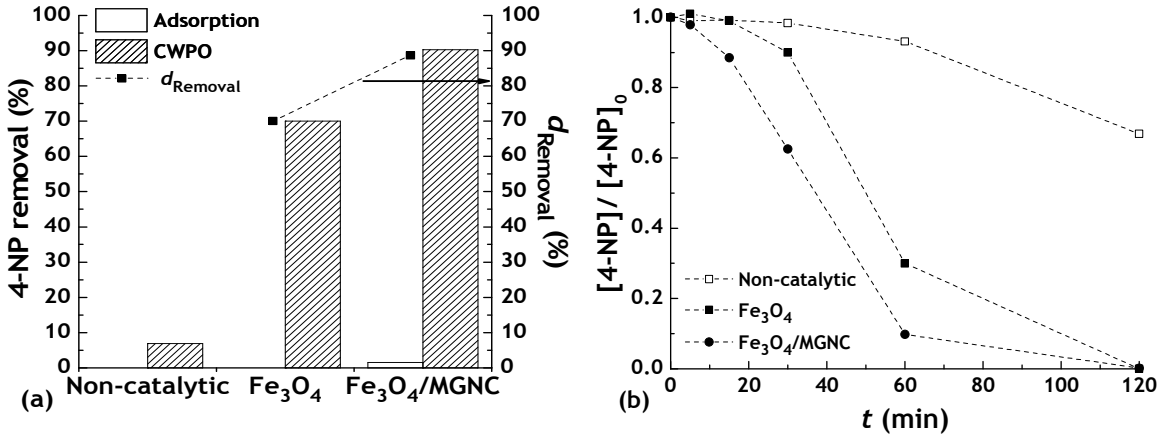

Figure 8.4. (a) 4-NP removal in adsorption and CWPO runs (bars/left axis) after 1 h, and respective difference due to H_2O_2 addition [$d_{Removal}$ (squares/right axis)]. (b) Removal of 4-NP obtained as a function of time in CWPO runs performed with Fe_3O_4 and Fe_3O_4/MGNC. Experiments performed with $[4\text{-NP}]_0$ = 0.2 g L^{-1}, $[Fe_3O_4/\text{MGNC}]$ = 0.02 g L^{-1}, $[Fe_3O_4]$ = 0.0055 g L^{-1} (corresponding to 27.3 wt.% of Fe_3O_4/MGNC), $[H_2O_2]_0$ = 0.712 g L^{-1} (stoichiometric amount), T = 80 ºC and pH = 3.

non-efficient parasitic reactions involving H_2O_2 and HO•, as discussed in Chapter 6. Specifically, it was found that the adsorption of 4-NP obtained with Fe_3O_4/MGNC amounts to 100.8 mg g^{-1} after 2 h, while there is no adsorption on Fe_3O_4 under the same conditions (data not shown). In addition, the electron transfer features of carbon-based materials, as well as their potential intrinsic catalytic activity in CWPO, may also contribute to enhance the catalytic decomposition of H_2O_2 and the subsequent oxidation of 4-NP molecules. Nevertheless, by comparing the leaching of Fe species at the end of the CWPO experiments performed with Fe_3O_4 (0.98 mg L^{-1}) and Fe_3O_4/MGNC (0.27 mg L^{-1}), the main synergistic effect arising from the inclusion of Fe_3O_4 nanoparticles into a carbon structure during the synthesis of Fe_3O_4/MGNC is unequivocally highlighted (as inferred from the ca. 4-fold decrease of iron leaching observed). These observations allow to conclude that the lower leaching of Fe species obtained with Fe_3O_4/MGNC is due to the confinement effect caused by the carbon shell, as depicted in Figure 8.5.

Complementary data for the CWPO of 4-NP with Fe_3O_4/MGNC are shown in Figure 8.6a. Regarding the mineralization of 4-NP, ca. 29% of TOC removal is achieved upon application of the Fe_3O_4/MGNC catalyst —a value that increases up to ca. 60% when the CWPO experiment is allowed to proceed during 8 h. At the same time, the consumption of H_2O_2 amounts to ca. 45% after 2 h and to ca. 60% after 8 h of reaction, which represents $\eta_{H_2O_2}$ in the range 64 – 100%. In addition, the removal of 4-NP obtained in the pure adsorption run suggests the wide prevalence of the catalytic activity in the 4-NP removal by CWPO. The predominant role of heterogeneous CWPO promoted by Fe_3O_4/MGNC is also well evidenced in Figure 8.6a, through the leaching test performed as described in Section 4.3. Specifically, when the Fe_3O_4/MGNC catalyst is removed after 30 min of reaction (ca. 37.5% 4-NP removal), negligible 4-NP and TOC removals were then observed. All these observations, together with the magnetic properties of Fe_3O_4/MGNC (*cf.* inset of Figure 8.6b) and the very high average pollutant mass removal rate obtained (5000 mg g^{-1} h^{-1}) —which was unprecedented when

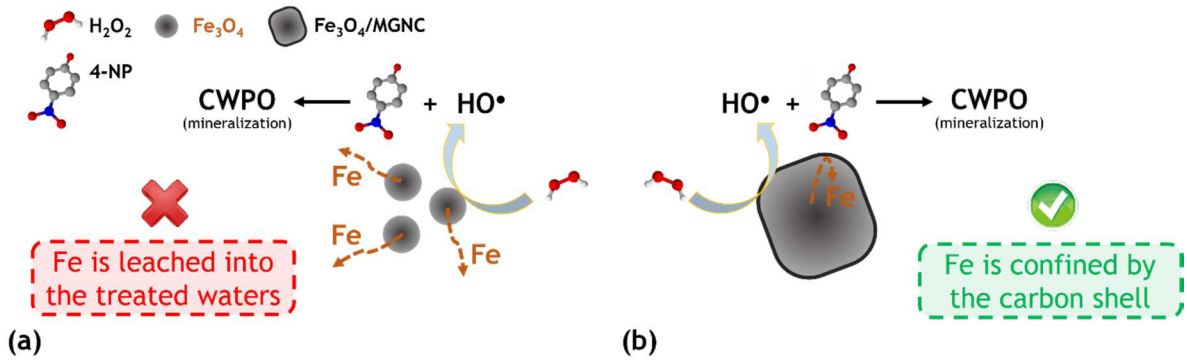

Figure 8.5. Representation of the CWPO process in the presence of (a) Fe_3O_4 nanoparticles, and (b) Fe_3O_4/MGNC, in which the confinement effect promoted by the carbon shell is highlighted.

compared to the values reported in the literature at that time for carbon-based and magnetite-based catalysts [5, 6]—, opened a window of opportunity, not only for the application of Fe_3O_4/MGNC in CWPO, but also for the development of *in-situ* magnetic separation systems. Therefore, Fe_3O_4/MGNC was object of additional studies.

The individual effect of the solution pH on the performance of Fe_3O_4/MGNC in CWPO was evaluated, as shown in Figure 8.6b. As observed, when CWPO is carried out without adjustment of the natural pH of the 4-NP solution (i.e., at pH = 6), Fe_3O_4/MGNC reveals some catalytic activity, with ca. 42% of the initial pollutant being removed. Although the complete abatement of 4-NP is not achieved under these conditions, the average pollutant mass removal rate obtained (2090 mg g^{-1} h^{-1}) is still higher than the values reported in the literature at that time for carbon-based and magnetite-based catalysts [5, 6]. Nevertheless, Fe_3O_4/MGNC loses most of its catalytic activity when the initial pH is increased to 9, with only ca. 11% of the parent pollutant being removed.

8.2.1. Process intensification

Following the trend reported in this Ph.D. dissertation, i.e., towards the application of CWPO for the treatment of 4-NP aqueous model solutions with high pollutant loads, the 4-NP concentration was increased 5-fold, to 1 g L^{-1}. The same mass ratio $[4\text{-NP}]_0/[Fe_3O_4/\text{MGNC}]$ = 10 was employed (corresponding to $[4\text{-NP}]_0/[Fe_3O_4]$ = 36.6, as previously discussed). Likewise, the H_2O_2 dosage was kept at the stoichiometric amount needed to completely mineralise 4-NP. As observed in Figure 8.7a, complete 4-NP removal is obtained after 4 h in experiments performed under these conditions, corresponding to an

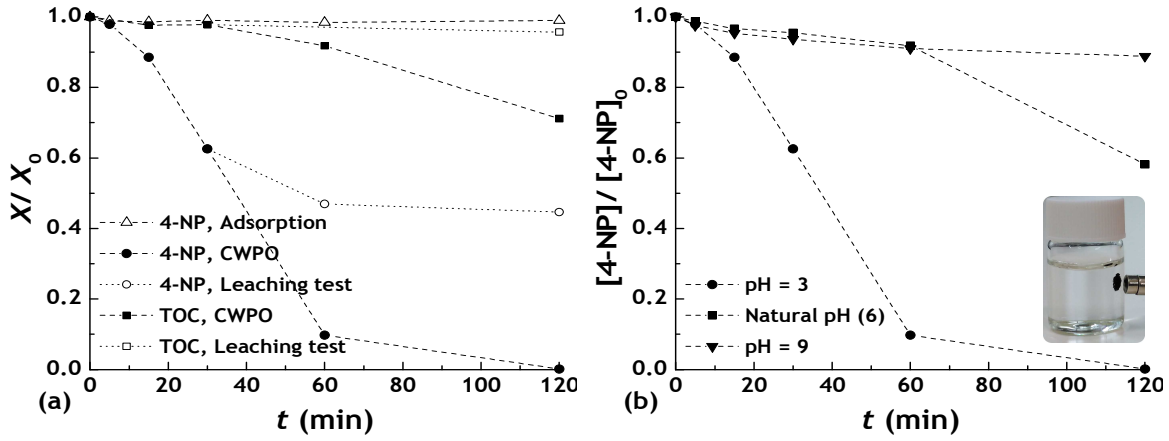

Figure 8.6. (a) 4-NP and TOC removals as a function of time in the CWPO run performed with Fe_3O_4/MGNC, as well as 4-NP and TOC removals obtained during the "leaching test" performed (i.e., where the catalyst was removed from the solution after 30 min of reaction); 4-NP removal by adsorption is also shown for comparison. (b) Effect of the initial pH on the 4-NP removal by CWPO, when using Fe_3O_4/MGNC (Inset: magnetic separation of the Fe_3O_4/MGNC catalyst in distilled water). Experiments performed under the operating conditions given in Figure 8.4.

average pollutant mass removal rate of 2500 mg g^{-1} h^{-1}. Afterwards, the initial 4-NP concentration was again increased 5-fold, reaching the concentration previously considered in Chapters 6 and 7 (5 g L^{-1}), while keeping the mass ratio $[4\text{-NP}]_0/[Fe_3O_4/\text{MGNC}]$ and feeding H_2O_2 at the stoichiometric amount needed for the complete 4-NP mineralisation. Complete 4-NP removal is also achieved even under these operating conditions, as long as the CWPO reaction is allowed to proceed during 8 h (*cf*. Figure 8.7a). In this case, the average pollutant mass removal rate amounts to 1250 mg g^{-1} h^{-1}, which is much higher than that reported at that time for carbon-based catalysts [5] and similar to the best results reported for magnetite-based catalysts operating with ca. 8-fold lower pollutant concentrations [6]. The 4-NP removal obtained in the non-catalytic experiment performed during 8 h under these operating conditions is not significant, representing a 4-NP removal of 13% (please refer to Figure C.7b for additional details on the non-catalytic experiment). For comparison purposes, the 4-NP removal curve obtained with T = 50 ºC is also shown in Figure 8.7a. Under these conditions, the average pollutant mass removal rate amounts to 267.5 mg g^{-1} h^{-1}, which puts in evidence the relevance of operating the CWPO process with T = 80 ºC.

It is noteworthy that after the initial pH adjustment, the experiments were allowed to proceed freely, without further conditioning of pH. Therefore, the initial 4-NP concentration in the experiment is expected to affect the final pH of the treated water, particularly when the aromatic ring of the 4-NP molecule is opened and carboxylic acids are formed (*cf*. Figure C.8). Bearing this in mind, the pH of the treated water was measured at the end of the CWPO experiments. It was observed that the final pH dropped from 3 to 2.79, 2.45 and

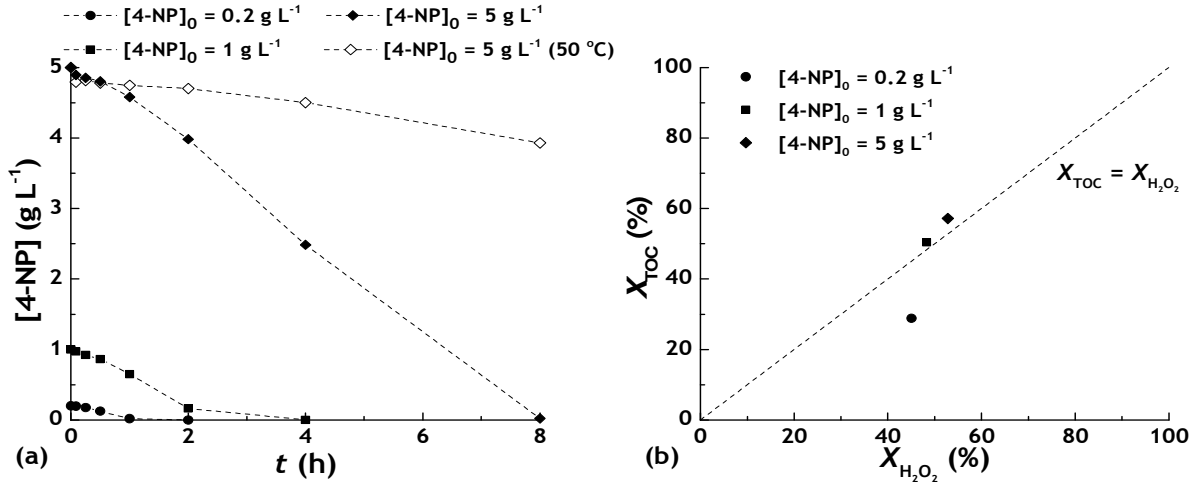

Figure 8.7. (a) 4-NP removal obtained as a function of time in CWPO runs performed with Fe_3O_4/MGNC under different operating conditions, and (b) corresponding TOC vs H_2O_2 conversions obtained after 2, 4 and 8 h, when considering $[4\text{-NP}]_0$ = 0.2 g L^{-1}, 1 g L^{-1} and 5 g L^{-1}, respectively. Experiments performed with a fixed mass ratio $[4\text{-NP}]_0/[Fe_3O_4/\text{MGNC}]$ = 10, T = 80 ºC, pH = 3 and stoichiometric amounts of H_2O_2. 4-NP (5 g L^{-1}) removal curve obtained by CWPO with T = 50 ºC is also shown in (a) for comparison.

1.79, when the initial 4-NP concentration was 0.2 g L^{-1}, 1 g L^{-1} and 5 g L^{-1}, respectively. Nevertheless, even with the most pronounced decrease of the solution pH, i.e., in the experiment performed with 5 g L^{-1} 4-NP, the iron leached to the treated water was 1.8 mg L^{-1} —a value still below the limit to discharge the treated water into natural receiving water bodies (2 mg L^{-1}).

In order to evaluate the efficiency of H_2O_2 consumption when Fe_3O_4/MGNC is applied in the CWPO of 4-NP aqueous model solutions in the concentration range studied, TOC and H_2O_2 evolution were also monitored. Accordingly, the TOC conversion (X_{TOC}) was plotted against the H_2O_2 conversion ($X_{H_2O_2}$) obtained in each experiment (*cf*. Figure 8.7b). The high $\eta_{H_2O_2}$ previously observed for $[4\text{-NP}]_0$ = 0.2 g L^{-1} is improved when higher pollutant concentrations are considered. Specifically, the values of X_{TOC} are similar to those of $X_{H_2O_2}$, suggesting $\eta_{H_2O_2}$ of ca. 100%. Therefore, it is possible to conclude that, in addition to the highly efficient usage of the catalyst, the H_2O_2 employed in the CWPO process with Fe_3O_4/MGNC is also consumed with rather high efficiency across the wide 4-NP concentration range studied.

8.2.2. Reusability cycles

The stability of the Fe_3O_4/MGNC catalyst was tested in two series of consecutive CWPO runs, performed with 0.2 g L^{-1} and 5 g L^{-1} 4-NP solutions. For that purpose, after each run, the catalyst was filtered, washed and dried at 60 ºC overnight, and then reused in CWPO with a fresh 4-NP solution. The 4-NP and TOC removals obtained in these two series of experiments are given in Figure 8.8. As observed, 4-NP removal slightly decreases from 100%, in the first run, to 96%, in the fourth run, in the experiments performed with 0.2 g L^{-1} 4-NP

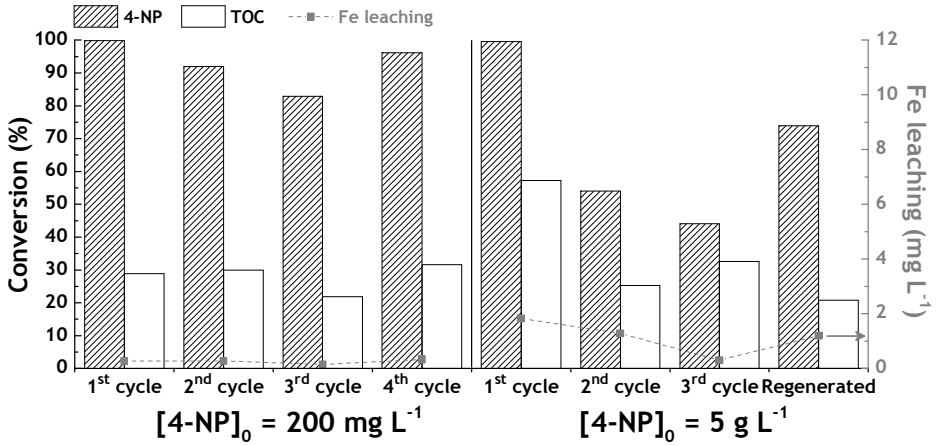

Figure 8.8. 4-NP and TOC conversions obtained in a series of CWPO runs performed with consecutive reuse of the Fe_3O_4/MGNC (bars/left axis) under the operating conditions given in Figure 8.7 and detailed in Table 8.2, and respective iron leaching (squares/right axis). Data obtained after 2 and 8 h of reaction, when considering $[4\text{-NP}]_0$ = 0.2 g L^{-1} and 5 g L^{-1}, respectively. Results obtained with Fe_3O_4/MGNC regenerated after the first CWPO run performed with $[4\text{-NP}]_0$ = 5 g L^{-1} are also given.

solutions. As previously discussed in Chapter 5, the decrease of the Fe_3O_4/MGNC catalytic activity may be partially caused by 4-NP reaction by-products adsorbed or deposited on the carbon surface, limiting the accessibility to the active sites. Nevertheless, the average pollutant mass removal rate obtained in the fourth CWPO cycle is still very high (4808 mg g^{-1} h^{-1}). Under these conditions, the TOC removal obtained after 2 h of reaction is not particularly affected by the successive reuse of the catalyst. Similar results, though with more pronounced effects, were observed in the reusability cycles performed with 5 g L^{-1} 4-NP solutions. In this case, the higher entropy of the system promotes harsher conditions, with higher concentration of by-products of 4-NP oxidation, which may result in the higher decrease of the catalytic performance of Fe_3O_4/MGNC upon successive reuse cycles. Nevertheless, the average pollutant mass removal rate obtained in the third CWPO cycle performed under these conditions (551 mg g^{-1} h^{-1}) is still quite good when compared to other catalysts [5, 6].

In order to demonstrate the influence of by-products deposition, a simple regeneration procedure of the Fe_3O_4/MGNC catalyst recovered from the first CWPO run was performed by H_2O_2 soaking, as detailed in Section 8.4. In this way, the oxidation of the by-products adsorbed at the surface of the Fe_3O_4/MGNC catalyst is promoted. As observed in Figure 8.8, the catalytic activity of Fe_3O_4/MGNC is partially restored through this simple regeneration approach. This observation confirms that the decrease of the catalyst performance in successive CWPO runs is in part explained by the adsorption or deposition of by-products of 4-NP oxidation on the carbon surface of Fe_3O_4/MGNC. In addition, Fe_3O_4/MGNC can be considered fairly stable against the leaching of Fe species to the treated water throughout the wide 4-NP concentration range studied (*cf.* Figure 8.8). For instance, the iron leached during the CWPO cycles performed with 0.2 g L^{-1} 4-NP solutions remains nearly constant (going from only 0.27 mg L^{-1}, in the first cycle, to 0.33 mg L^{-1} in the fourth cycle). Even in the experiments performed with intensified conditions, considering 5 g L^{-1} 4-NP solutions, the iron leached is always kept bellow the limits allowed by Portuguese and other EU Directives for treated water to be discharged into natural receiving water bodies (going from 1.8 mg L^{-1} in the first cycle, to only 0.3 mg L^{-1} in the third cycle).

8.3. Conclusions

The inclusion of Fe_3O_4 nanoparticles in a graphitic structure during the synthesis of Fe_3O_4/MGNC (i) enhances the catalytic activity in the CWPO of 4-NP when compared to that of bare Fe_3O_4, due to increased adsorptive interactions between the surface of the catalyst and the pollutant molecules, while (ii) strongly limiting the leaching of Fe species from Fe_3O_4 to the treated water, due to the confinement effect caused by the carbon shell. As a result

Table 8.2. Experimental details of the CWPO experiments reported in Chapter 8

Aqueous model system	Reactor/solution volume	Operating conditions	H_2O_2 stoichiometric ratio[a]	[Pollutant]/ [catalyst]
4-nitrophenol (0.2 g L^{-1})	500 mL/ 250 mL	Screening experiments [Fe_3O_4/MGNC] = 0.02 g L^{-1} [Fe_3O_4] = 0.0055 g L^{-1} $[H_2O_2]_0$ = 0.712 g L^{-1} T = 80 ºC; pH_0 = 3 t = 2 h	1	10[b]
4-nitrophenol (1 g L^{-1})	250 mL/ 100 mL	Intermediate experiments [Fe_3O_4/MGNC] = 0.1 g L^{-1} $[H_2O_2]_0$ = 3.56 g L^{-1} T = 80 ºC; pH_0 = 3 t = 4 h	1	10
4-nitrophenol (5 g L^{-1})	100 mL/ 50 mL	Process intensification [Fe_3O_4/MGNC] = 0.5 g L^{-1} $[H_2O_2]_0$ = 17.8 g L^{-1} T = 80 ºC; pH_0 = 3 t = 8 h	1	10

[a] Obtained by dividing the amount of H_2O_2 employed by the stoichiometric amount needed for the complete mineralization of the pollutant considered; [b] for Fe_3O_4/MGNC (a fixed 4-NP/Fe_3O_4 mass ratio of 36.6 was maintained regardless of the catalyst employed, considering that Fe_3O_4 corresponds to 27.3 wt.% of Fe_3O_4/MGNC).

of these effects, unprecedented pollutant mass removals were obtained. In addition, the Fe_3O_4/MGNC catalyst revealed activity for CWPO when operating at pH = 6.

8.4. Experimental details

Unless stated otherwise, the CWPO experiments reported in Chapter 8 were performed under the conditions detailed in Table 8.2. Please refer to Chapter 4 for additional details on the experimental procedures.

The regeneration of the Fe_3O_4/MGNC catalyst was performed using a simple H_2O_2 soaking technique, adapting the procedure described elsewhere [7]. For that purpose, the catalyst recovered from the first CWPO run performed with $[4\text{-NP}]_0$ = 5 g L^{-1} was contacted with H_2O_2 during 8 h under the same operation conditions used in the CWPO experiments, but in the absence of 4-NP (i.e., T = 80 ºC, pH = 3, [Fe_3O_4/MGNC] = 0.5 g L^{-1} and $[H_2O_2]_0$ = 17.8 g L^{-1}). The Fe_3O_4/MGNC catalyst after regeneration was washed and dried at 60 ºC overnight, and then reused in another CWPO run with a fresh 4-NP solution.

References

[1] C.M. Domínguez, A. Quintanilla, J.A. Casas, J.J. Rodríguez, Treatment of real winery wastewater by wet oxidation at mild temperature, Sep. Purif. Technol. 129 (2014) 121-128.
[2] Y. Yan, S. Jiang, H. Zhang, Efficient catalytic wet peroxide oxidation of phenol over Fe-ZSM-5 catalyst in a fixed bed reactor, Sep. Purif. Technol. 133 (2014) 365-374.

[3] G. Pliego, J.A. Zazo, P. Garcia-Muñoz, M. Munoz, J.A. Casas, J.J. Rodríguez, Trends in the intensification of the Fenton process for wastewater treatment: an overview, Crit. Rev. Environ. Sci. Technol. 45 (2015) 2611-2692.
[4] R. Liu, L. Wan, S. Liu, Y. Yu, S. Li, D. Wu, Hierarchical co-assembly avenue to uniform rhombododecahedral magnetic mesoporous graphitic composites, J. Colloid Interface Sci. 414 (2014) 59-65.
[5] R.S. Ribeiro, A.M.T. Silva, J.L. Figueiredo, J.L. Faria, H.T. Gomes, Catalytic wet peroxide oxidation: a route towards the application of hybrid magnetic carbon nanocomposites for the degradation of organic pollutants. A review, Appl. Catal. B 187 (2016) 428-460.
[6] M. Munoz, Z.M. de Pedro, J.A. Casas, J.J. Rodriguez, Preparation of magnetite-based catalysts and their application in heterogeneous Fenton oxidation – A review, Appl. Catal. B 176–177 (2015) 249-265.
[7] L.-X. Hu, D.-D. Xu, L.-P. Zou, H. Yuan, X. Hu, Heterogeneous Fenton oxidation of refractory dye rhodamine B in aqueous solution with mesoporous Fe/SBA-15, Acta Phys. Chim. Sin. 31 (2015) 771-782.

PART V: CASE STUDIES IMPLEMENTING MAGNETIC SEPARATION OF CATALYSTS

Due to the easier manipulation and simplicity, 2-NP and 4-NP aqueous model systems were used in the previous Chapters. Through this approach it was possible to ascribe superior performances in CWPO to specific features of the catalysts, which has enabled a continuous improvement of catalyst design during these Ph.D. studies. At this stage, seeking for more realistic and diversified applications:

- In Chapter 9, the ability of CWPO for the degradation of the antimicrobial agent sulfamethoxazole in environmentally relevant water matrices was evaluated using the magnetic carbon xerogels developed in Chapter 7;

- In Chapter 10, the ability of CWPO for the treatment of the liquid effluent from a mechanical biological treatment plant for municipal solid waste was evaluated. For that purpose, a high-performance hybrid magnetic graphitic nanocomposite —composed by a cobalt ferrite core and a graphitic shell, was designed based on the findings previously reported in this Ph.D. dissertation.

In addition, the magnetic susceptibility of the catalysts is explored for the development of in-situ magnetic separation systems for catalyst recovery.

9. MAGNETIC CARBON XEROGELS FOR THE CATALYTIC WET PEROXIDE OXIDATION OF SULFAMETHOXAZOLE IN ENVIRONMENTALLY RELEVANT WATER MATRICES

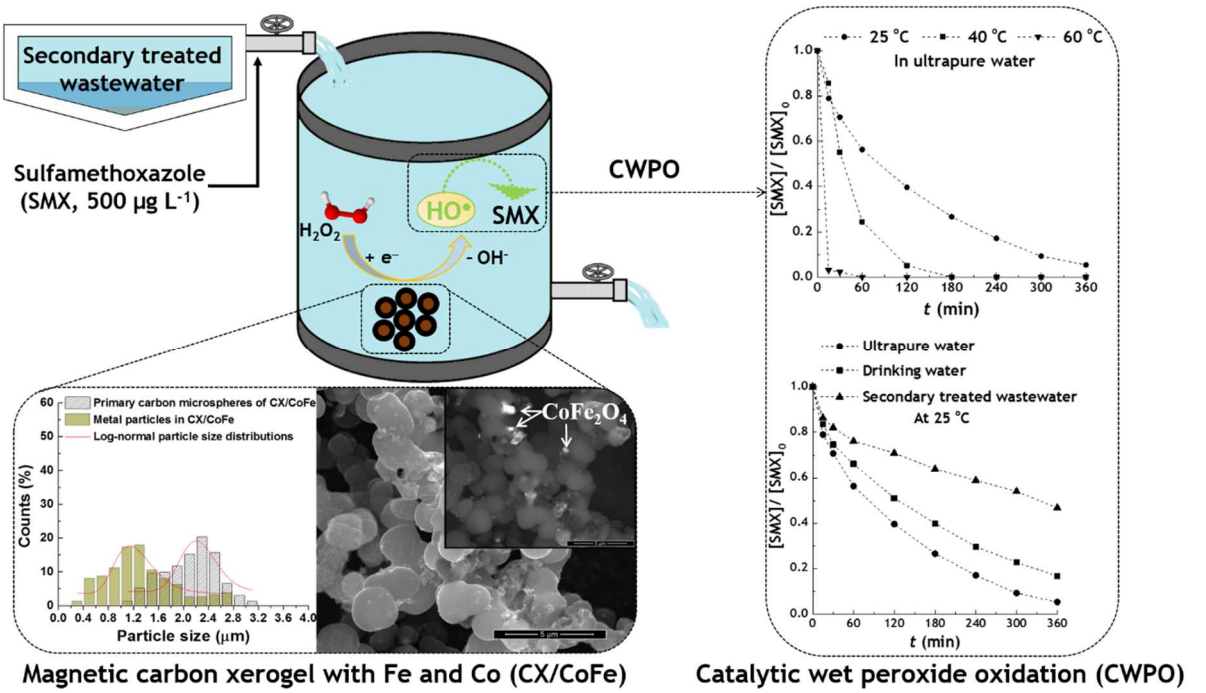

Magnetic carbon xerogel with Fe and Co (CX/CoFe) — Catalytic wet peroxide oxidation (CWPO)

[13]

[13] Adapted from the graphical abstract of: Rui S. Ribeiro, Zacharias Frontistis, Dionissios Mantzavinos, Danae Venieri, Maria Antonopoulou, Ioannis K. Konstantinou, Adrián M.T. Silva, Joaquim L. Faria, Helder T. Gomes, Magnetic carbon xerogels for the catalytic wet peroxide oxidation of sulfamethoxazole in environmentally relevant water matrices, Appl. Catal. B 199 (2016) 170-186
DOI: 10.1016/j.apcatb.2016.06.021

The increasing scarcity of clean water sources is driving several communities towards the reuse of treated wastewater, mainly for non-potable applications such as surface and groundwater replenishment, or agricultural and landscape irrigation —a practice already stablished in some places as an important component of sustainable wastewater management practices [1]. Recent improvements in several analytical techniques allowed the identification and quantification of an increasing number of micropollutants present in treated waste waters —also known as contaminants of emerging concern [2]. Among these, the antibiotics present in treated waste waters and their subsequent release into the environment have been receiving particular attention from the scientific community, mainly due to major public health concerns about the development of antibiotic resistant bacteria and/or resistance genes (ARB&ARG) [3].

Conventionally treated waste waters are often considered as one of the most important anthropogenic sources of antibiotics and ARB&ARG release into the environment [4-7]. Therefore, the development of efficient and economically viable advanced treatment technologies is presently of high priority in the policy agendas of the EU member states and many other countries around the world [1, 8, 9], as recently suggested by a National strategy in the US [10] and by the European COST Action ES1403 (New and emerging challenges and opportunities in wastewater reuse - NEREUS) [11]. These technologies should be able to reduce the propagation of microcontaminants typically present in treated waste waters (such as antibiotics), usually associated with the development of ARB&ARG in the urban water cycles, and to allow the reuse of treated waste waters as reliable alternative water sources.

Bearing this in mind, the ability of CWPO for the elimination of a persistent micropollutant was evaluated using the magnetic carbon xerogels developed in Chapter 7. Sulfamethoxazole (SMX) —an antimicrobial agent associated to the development of ARB&ARG [6] and typically found throughout the urban water cycle (in raw and in conventionally treated waste waters [12], in raw and in conventionally treated drinking waters [13], or in surface and ground waters [2])—, was used as model of persistent micropollutant at the ppb level (500 μg L^{-1}). In addition to ultrapure water and other synthetic waters, environmentally relevant water matrices were also considered, namely drinking water and a secondary treated wastewater collected from the wastewater treatment plant of the University of Patras, Greece. The main results are discussed in the following Sections.

9.1. CWPO experiments

The performance of the carbon xerogel materials developed in Chapter 7 in the CWPO of SMX solutions at the ppb level (500 μg L^{-1}) was evaluated in experiments performed under

the operating conditions detailed in Table 9.1. The SMX removals obtained in pure adsorption and CWPO runs performed during 6 h are given in Figure 9.1. The superior performance previously revealed by the bimetallic CX/CoFe catalyst in the CWPO of highly concentrated 4-NP aqueous model solutions (5 g L^{-1}; *cf*. Chapter 7) is also observed when the carbon xerogel materials are employed in the CWPO of 500 μg L^{-1} SMX solutions (*cf*. Figure 9.1). It should be noted that the SMX removal obtained when using CX is similar, but in this case ascribed to adsorption of the pollutant (and not to catalytic degradation). The non-catalytic removal of SMX is rather low, corresponding to ca. 13% of its initial content (please refer to Figure C.9a for additional details on the non-catalytic experiment).

Due to its superior performance, CX/CoFe was object of additional studies. In order to evaluate the participation of HO• radicals in the process, *tert*-butanol (tBuOH), a strong HO• radical scavenger [14, 15], was added before a CWPO experiment performed in the presence of CX/CoFe. When the SMX removal curves obtained in the presence and absence of tBuOH are compared (*cf*. Figure 9.2), it is observed that the removal of SMX is greatly suppressed by tBuOH. Although not directly supported by quantification of the HO• radicals formed during the process, this indirect result suggests the predominant role of HO• radicals in the CWPO of SMX. Therefore, the high catalytic performance of CX/CoFe in the CWPO of SMX is unequivocally highlighted.

Since CX/CoFe possesses Fe and Co in its structure (*cf*. Section 7.1), the leaching of metal species to the treated water was studied. The iron leached to the treated water during the CWPO experiment performed with CX/CoFe was 0.1 mg L^{-1}, i.e., 20-fold below the limit of 2 mg L^{-1} allowed for discharging treated water into natural receiving water bodies (and even below the maximum limits allowed for water intended for human consumption, 0.2 mg L^{-1}) [16]. Likewise, the leaching of Co was also rather low (0.2 mg L^{-1}), although in this case

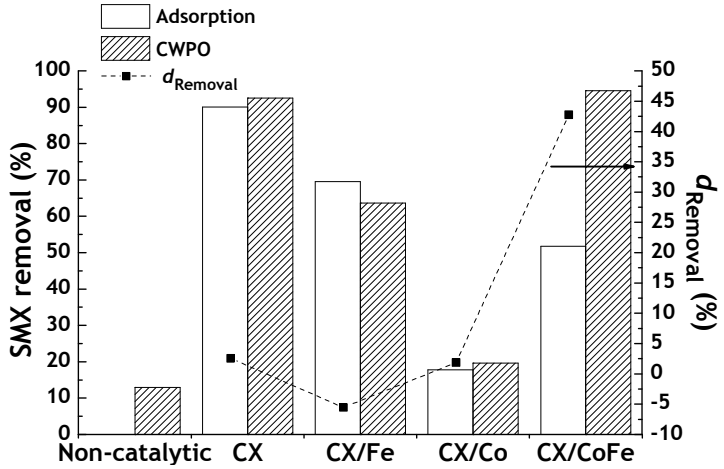

Figure 9.1. SMX removal in adsorption and CWPO runs (bars/left axis) after 6 h, and respective difference due to H_2O_2 addition [$d_{Removal}$ (squares/right axis)]. Experiments performed with $[SMX]_0$ = 500 μg L^{-1}, [catalyst/adsorbent] = 20 mg L^{-1}, $[H_2O_2]_0$ = 500 mg L^{-1}, T = 25 ºC and pH = 3.

there is a lack of standards for treated wastewater and even for drinking water [17].

In addition, it should be noted that the experiments depicted in Figure 9.2 were performed at room temperature and atmospheric pressure, putting in evidence the potential of this bimetallic hybrid magnetic carbon xerogel material with cobalt and iron embedded in its structure for economically viable CWPO applications.

9.1.1. Individual effects of the operating parameters

In order to investigate the operating conditions that maximize the performance of SMX removal by CWPO in the presence of CX/CoFe, the individual effect of several operating parameters was evaluated through the determination of apparent first order reaction rate constants (k_{app}). These include catalyst load, H_2O_2 dosage, SMX concentration, initial pH and temperature. The results obtained with the kinetic study are shown in Figure 9.3, while the corresponding SMX removal curves as a function of time are shown in Figures C.9a-e. As expected, the kinetics of the SMX removal increases with increasing catalyst dosage, and decreases with increasing operating pH. Regarding the H_2O_2 dosage, although the stoichiometric amount of H_2O_2 needed to completely mineralise SMX is ca. 1.3 mg L^{-1}, it is observed that SMX removal goes through a maximum, corresponding to $[H_2O_2]_0$ = 500 mg L^{-1}. The higher requirement of H_2O_2 may be explained by the operating conditions considered (mainly due to the low catalyst dosage and room temperature). In the opposite, when the H_2O_2 dosage is increased 2-fold up to 1000 mg L^{-1}, the SMX removal decreases. This observation suggests that under these conditions the formed HO$^{\bullet}$ radicals may react preferably with H_2O_2 molecules, through a series of non-efficient parasitic reactions that are more significant when low pollutant concentrations are considered [18]. The SMX removal apparently decreases when the initial SMX concentration increases; however, the average pollutant mass removal rate actually increases from 4.0 μg mg^{-1} h^{-1} up to 10.2 μg mg^{-1} h^{-1},

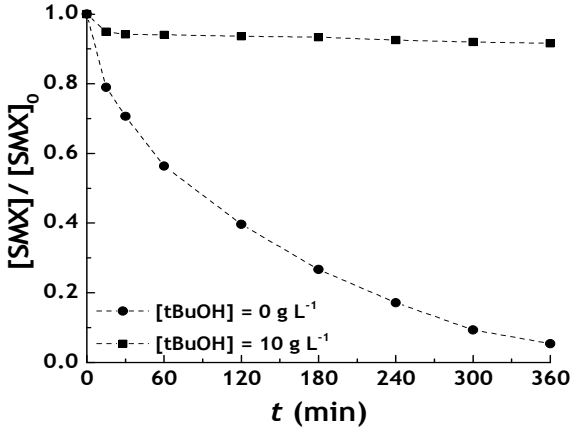

Figure 9.2. Effect of *tert*-butanol (tBuOH) on the SMX removal by CWPO when using CX/CoFe under the operating conditions given in Figure 9.1.

leading to a ca. 2.5-fold gain in the efficiency of catalyst usage when the concentration of SMX is increased from 500 to 2000 μg L^{-1}. It is also observed that the performance of CWPO for the elimination of SMX is substantially enhanced when the temperature is slightly increased from room temperature (25 ºC) up to mild temperatures (40-60 ºC). This effect is particularly observed at T = 60 ºC, with SMX being almost completely removed in 30 min (*cf*. Figure C.9e).

It should be noted that the majority of the experimental data are well described by the kinetic model considered. However, this is a pseudo first order kinetic model relative to the SMX concentration. Therefore, the effect of other contributions (mainly H_2O_2 dosage and catalyst concentration) is not accounted in the model. In addition, it is well known that the rate of advanced oxidation of organic contaminants depends on the substrate concentration. Usually the reaction obeys to a first order rate expression with respect to the substrate concentration at low concentrations, but it shifts towards zero order at higher concentrations [19]. This behaviour can be explained taking into account the rate-limiting step, where the reactive, oxidizing species (mainly $HO^{\bullet}$ radicals) become the limiting factor for the reaction. This might explains why k_{app} changes with the initial SMX concentration, while maintaining constant the initial values of the other operating parameters. In order to better understand the effect of temperature on the reaction rates, the Arrhenius plot (*cf*. Figure C.9f) was used to determine the apparent activation energy (E_a), a value of E_a = 69.8 kJ mol^{-1} being obtained.

9.1.2. Environmentally relevant water matrices

Ultrapure water may be considered an attractive matrix to conduct studies for the initial

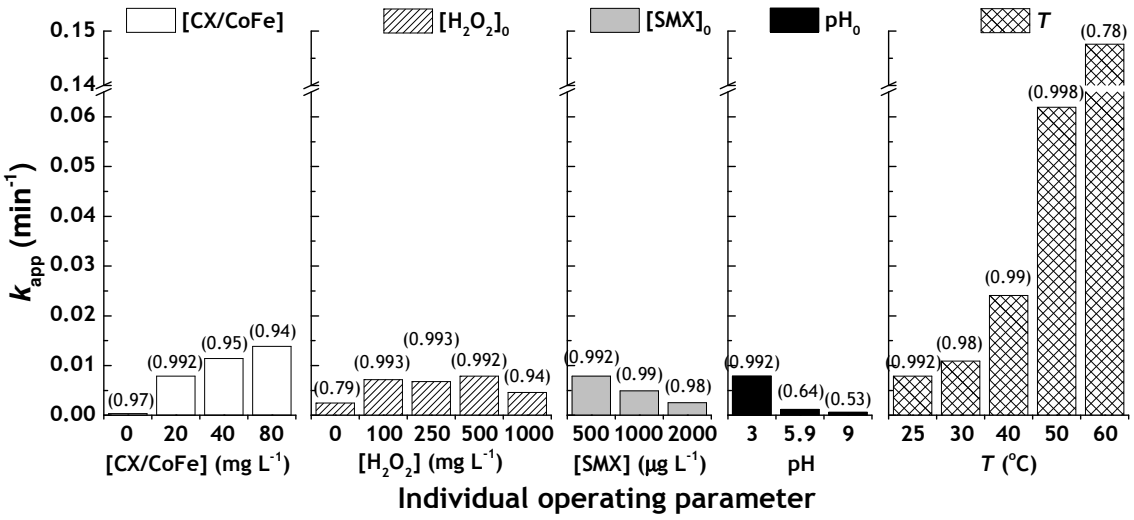

Figure 9.3. Apparent first order reaction rate constants (k_{app}) obtained after 6 h in experiments performed with CX/CoFe under different operating conditions. The numbers in brackets represent the regression coefficients of the linear fittings (r^2).

design and evaluation of advanced treatment technologies, mainly due to its ease of manipulation, simplicity and reproducibility of the experimental results. However, antimicrobial agents like SMX are typically released into the environment in much more complex water matrices, like conventionally treated wastewater [12]. Furthermore, SMX has also been found in drinking water [13], raising serious public health concerns. These environmentally relevant water matrices, in particular the treated wastewater, contain multiple natural and anthropogenic compounds [3], increasing their complexity and hindering the performance of treatment technologies.

Bearing this in mind, the influence of the water matrix on the performance of SMX removal by CWPO was assessed, using secondary treated wastewater and drinking water (*cf*. Section 9.3.1) spiked with SMX (500 μg L^{-1}). As observed in Figure 9.4a, the SMX removal decreases with the increasing complexity of the water matrix. Specifically, the values of k_{app} obtained after 6 h are 0.0079 min^{-1} (r^2 = 0.992), 0.0050 min^{-1} (r^2 = 0.98) and 0.0022 min^{-1} (r^2 = 0.87), when ultrapure water, drinking water and secondary treated wastewater are used, respectively. It is noteworthy that the lower value of r^2 obtained with secondary treated wastewater reflects the higher complexity of this water matrix, making the experimental results harder to predict. Nevertheless, the decrease of SMX removal may be ascribed to the presence of (i) dissolved organic matter and/or (ii) radical scavengers in the more complex water matrices, especially in the secondary treated wastewater. Since HO• radicals are non-selective oxidants [20], the presence of organic matter is expected to limit the SMX removal; while, at the same time, ion species (e.g., bicarbonates, chlorides and sulphates) may act as HO• scavengers, as previously shown for photocatalytic applications [21].

In order to better understand how the CWPO process is influenced by each of these

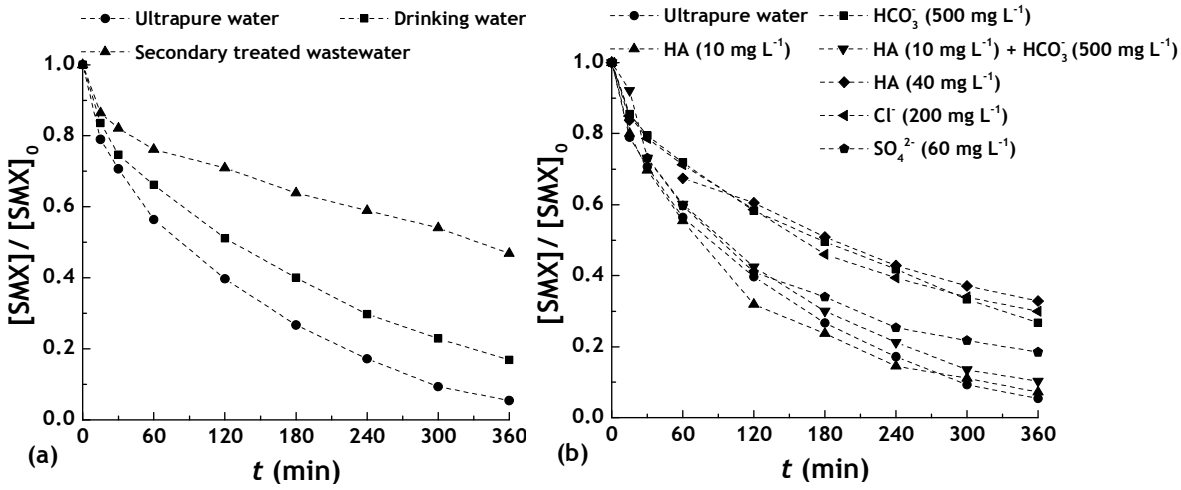

Figure 9.4. Effect of (a) environmentally relevant and (b) synthetic water matrices on the SMX removal by CWPO when using CX/CoFe under the operating conditions given in Figure 9.1.

components, additional experiments were performed using humic acid (HA) to mimic the presence of dissolved organic matter, and sodium bicarbonate (500 mg L^{-1} bicarbonates), sodium chloride (200 mg L^{-1} chlorides) and sodium sulphate (60 mg L^{-1} sulphates) to mimic the presence of the typical inorganic constituents of conventionally treated wastewater and drinking water. As observed in Figure 9.4b, the SMX removal obtained in the experiment performed with a 10 mg L^{-1} HA solution remains nearly the same when compared to that obtained with ultrapure water. However, when bicarbonates (500 mg L^{-1}) are added to the 10 mg L^{-1} HA solution, the SMX removal is affected; in this case, the value of *k* obtained after 6 h is 0.0065 min^{-1} (r^2 = 0.992), which represents a ca. 16.7% decrease when compared to that obtained with ultrapure water. Therefore, it is possible to conclude that the removal of SMX by CWPO in the presence of CX/CoFe is affected by dissolved organic matter corresponding to a HA concentration of 10 mg L^{-1}, although in a small extent. Nevertheless, when the concentration of HA is increased up to 40 mg L^{-1} —i.e., an overestimated amount if the total organic carbon of the secondary treated wastewater used in this work is considered (6.2 mg L^{-1})— the removal of SMX is greatly affected. Regarding the presence of inorganic species, it is observed that bicarbonates, chlorides and sulphates have a negative impact on the removal of SMX by CWPO. Therefore, it is possible to conclude that the decrease of pollutant removal is mainly due to the presence of sulphates (30 mg L^{-1}) and organic matter (18.9 mg L^{-1} chemical oxygen demand), but it is also affected by chlorides (0.44 mg L^{-1}) and, possibly, by other unidentified constituents of the secondary treated wastewater under study (*cf.* Section 9.3.1). Regarding the drinking water employed, if the results shown in Figure 9.4 are analysed together with the properties given in Section 9.3.1, it is possible to conclude that the removal of SMX in this water matrix is mainly affected by the presence of inorganic species, namely bicarbonates (211 mg L^{-1}), chlorides (9.8 mg L^{-1}) and sulphates (15 mg L^{-1}).

9.1.3. Reusability cycles implementing *in-situ* magnetic separation for catalyst recovery

The catalyst stability of CX/CoFe in the CWPO of SMX was assessed through reusability cycles performed by implementation of a simple *in-situ* magnetic separation procedure for catalyst recovery and reuse, as depicted in Figure 9.5. For that purpose, the treated water was recovered after the reaction stage, and the catalyst reused in another CWPO run upon the addition of a fresh SMX solution (500 μg L^{-1}). In this way, the reusability cycles are able to mimic real-scale applications. Both ultrapure water and secondary treated wastewater were used in this study (*cf.* Figure 9.6,). However, based on the previous results, the catalyst dosage employed for the CWPO of SMX in secondary treated wastewater was increased 4-

fold, up to 80 mg L^{-1}, in order to promote a SMX removal comparable to that obtained in ultrapure water. As observed, the removal of SMX in the presence of CX/CoFe decreases in the two series of three consecutive CWPO runs. When ultrapure water is used, the SMX removal decreases from 94.6%, in the first run, to 64.6% and 51.4%, in the second and third runs, respectively (*cf*. Figure 9.6a). A higher decrease from the first to the second run was expected, due to the contribution of adsorption in the first use of CX/CoFe. As observed in Figure 9.6b, this effect is more pronounced when secondary treated wastewater is employed, due to its higher complexity. Nevertheless, the ability of CWPO to eliminate SMX in secondary treated wastewater is unequivocally shown, with 96.8% of its initial content being removed after 6 h of reaction in the presence CX/CoFe (corresponding to k_{app} = 0.0102 min^{-1}; r^2 = 0.97). This achievement is even more relevant considering that the process was performed at room temperature and atmospheric pressure, thus opening a window of opportunity for the development of economically viable treatment options to reduce the propagation of SMX in the urban water cycles.

In order to better understand the deactivation phenomena responsible for the decrease of activity observed in the consecutive CWPO cycles, the textural properties of the CX/CoFe recovered after the first CWPO cycle performed with SMX in ultrapure water were analysed by N_2 adsorption-desorption isotherms. It was found that the textural properties of CX/CoFe are not significantly affected by its application in the CWPO of SMX under the operating conditions considered. Specifically, only a ca. 2% decrease of the S_{BET} was observed (from 530 m^2 g^{-1} in the fresh catalyst, to 520 m^2 g^{-1} in the used catalyst). Since the textural properties of CX/CoFe were not significantly affected following the application in the CWPO of SMX, it is possible to conclude that the blockage of the porous structure is not the main cause of the catalyst deactivation observed. Bearing this in mind, thermogravimetric analysis (TGA) under oxidative atmosphere was used in order to better elucidate the causes of

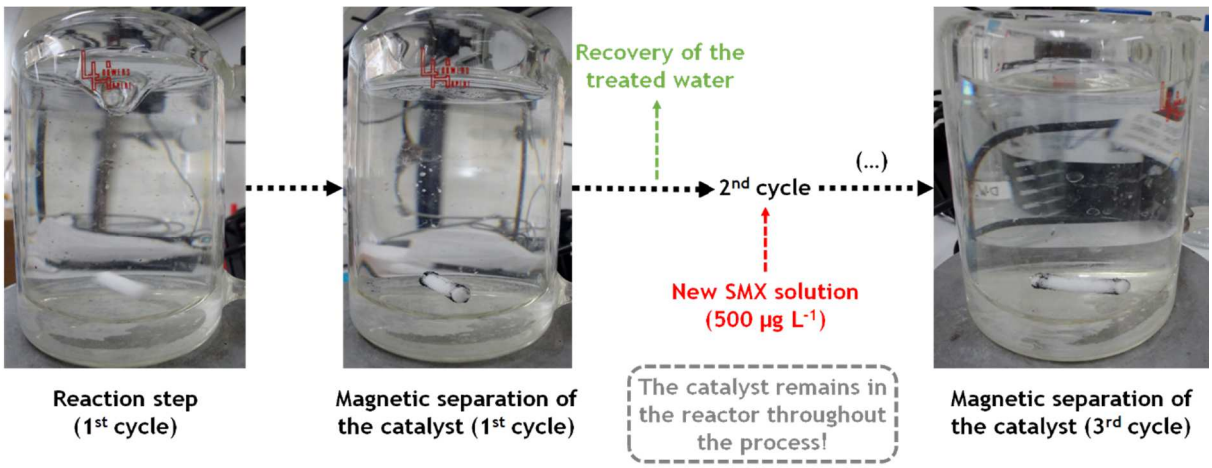

Figure 9.5. Experimental procedure during the CWPO reusability cycles performed with CX/CoFe.

catalyst deactivation. It was found that the ash content of CX/CoFe slightly decreases upon its application in the CWPO of SMX (from 11.0 wt.% in the fresh catalyst, to 8.9 wt.% in the used catalyst, representing a ca. 2% decrease). This fact suggests that the leaching of active metal species may contribute to the catalyst deactivation observed. Nevertheless, it should be noted that the experimental procedure used during the CWPO reusability cycles may also affect the results obtained. Since no catalyst is added during the successive CWPO cycles, this more realistic approach may lead to a loss of catalyst mass caused by the periodical withdrawn of samples from the reactor (to analyse SMX concentration against time). Therefore, the catalyst deactivation may be slightly overestimated.

9.2. Conclusions

The ability of the CWPO technology for the elimination of SMX in secondary treated wastewater and drinking water was shown. In addition, the magnetic susceptibility of the bimetallic magnetic carbon xerogel containing cobalt and iron species embedded in its structure (CX/CoFe) allowed for the application of an *in-situ* magnetic separation procedure for catalyst recovery and reuse.

9.3. Experimental details

Batch CWPO experiments were performed in a well-stirred (500 rpm) cylindrical jacketed glass reactor (internal diameter = 6 cm; height = 9.5 cm) connected to a thermostatic water bath with temperature control. The reactor was loaded with 250 mL of a SMX solution in different water matrices and, upon stabilization at the desired temperature, the solution pH was adjusted when necessary, using H_2SO_4 and NaOH solutions (1 mol L^{-1}), the experiments being then allowed to proceed freely, without further conditioning of pH. After

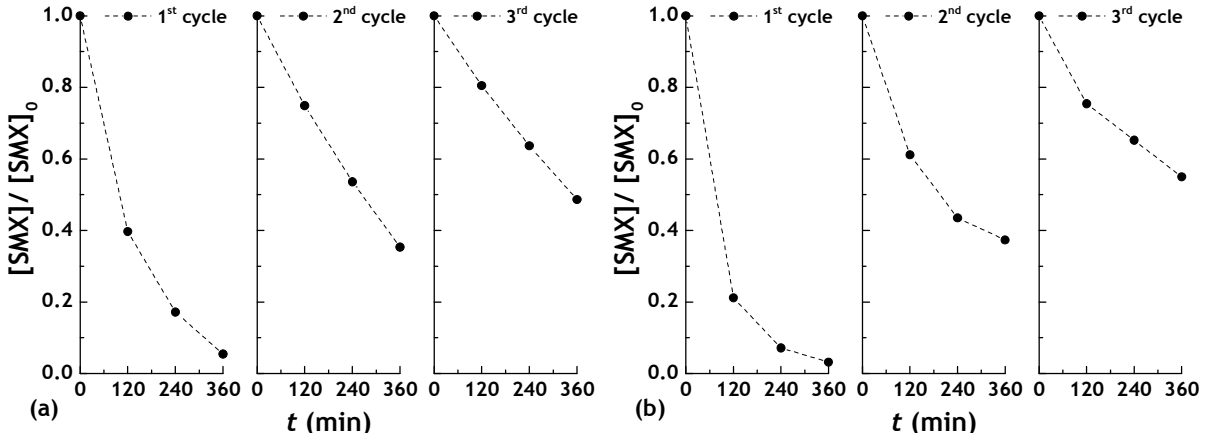

Figure 9.6. SMX removal in (a) ultrapure water and (b) secondary treated wastewater, obtained in a series of three CWPO runs performed with consecutive reuse of CX/CoFe. Experiments performed under the operating conditions given in Figure 9.1, except for the catalyst load of 80 mg L^{-1} in (b).

Table 9.1. Experimental details of the CWPO experiments reported in Chapter 9

Aqueous model system	Reactor/solution volume	Operating conditions	H_2O_2 stoichiometric ratio[a]	[Pollutant]/ [catalyst]
Sulfamethoxazole (500 μg L^{-1})	268 mL/ 250 mL	[catalyst] = 20 mg L^{-1} $[H_2O_2]_0$ = 500 mg L^{-1} T = 25 ºC; pH_0 = 3 t = 6 h	384.6	0.025

[a] Obtained by dividing the amount of H_2O_2 employed by the stoichiometric amount needed for the complete mineralization of the pollutant considered.

the initial pH adjustment, the catalyst was added and a calculated volume of H_2O_2 was injected into the system, in order to reach the desired concentration, that moment being considered as t_0 = 0 min. Pure adsorption runs were performed in order to estimate the possible contribution of adsorption in the removal of SMX by CWPO. In this case, the amount of H_2O_2 was replaced by ultrapure water. Blank experiments, without any catalyst, were also carried out to assess possible non-catalytic oxidation promoted by H_2O_2. In order to show the role of the $HO^{\bullet}$ radicals in the CWPO process, *tert*-butanol (tBuOH), a strong $HO^{\bullet}$ radical scavenger [14, 15], was added before reaction.

Unless stated otherwise, the CWPO experiments reported in Chapter 9 were performed under the conditions detailed in Table 9.1.

9.3.1. Water matrices

SMX solutions were prepared in (i) ultrapure water (pH = 6.5; 0.056 μS cm^{-1} conductivity); (ii) secondary treated wastewater (pH = 7.9; 6.2 mg L^{-1} total organic carbon; 1.07 mg L^{-1} total suspended solids; 18.9 mg L^{-1} chemical oxygen demand; 311 μS cm^{-1} conductivity; 30 mg L^{-1} sulphates; 0.44 mg L^{-1} chlorides) collected from the wastewater treatment plant of the University of Patras, Greece; and (iii) drinking water (pH = 7.5; 396 μS cm^{-1} conductivity; 211 mg L^{-1} bicarbonates; 15 mg L^{-1} sulphates; 9.8 mg L^{-1} chlorides) obtained from a bottle of the commercially available brand Avra®, Greece.

Six additional synthetic water matrices were used to prepare SMX solutions, namely ultrapure water in the presence of (i) humic acid (10 mg L^{-1}); (ii) sodium bicarbonate (500 mg L^{-1} bicarbonates); (iii) humic acid (10 mg L^{-1}) and sodium bicarbonate (500 mg L^{-1} bicarbonates); (iv) humic acid (40 mg L^{-1}); (v) sodium chloride (200 mg L^{-1} chlorides); and (vi) sodium sulphate (60 mg L^{-1} sulphates).

References

[1] I. Michael-Kordatou, C. Michael, X. Duan, X. He, D.D. Dionysiou, M.A. Mills, D. Fatta-Kassinos, Dissolved effluent organic matter: characteristics and potential implications in wastewater treatment and reuse applications, Water Res. 77 (2015) 213-248.

[2] D. Fatta-Kassinos, S. Meric, A. Nikolaou, Pharmaceutical residues in environmental waters and wastewater: current state of knowledge and future research, Anal. Bioanal. Chem. 399 (2011) 251-275.
[3] L. Rizzo, C. Manaia, C. Merlin, T. Schwartz, C. Dagot, M.C. Ploy, I. Michael, D. Fatta-Kassinos, Urban wastewater treatment plants as hotspots for antibiotic resistant bacteria and genes spread into the environment: a review, Sci. Total Environ. 447 (2013) 345-360.
[4] M.F. Ferreira da Silva, I. Tiago, A. Veríssimo, R.A.R. Boaventura, O.C. Nunes, C.M. Manaia, Antibiotic resistance of enterococci and related bacteria in an urban wastewater treatment plant, FEMS Microbiol. Ecol. 55 (2006) 322-329.
[5] V. Figueira, E. Serra, C.M. Manaia, Differential patterns of antimicrobial resistance in population subsets of Escherichia coli isolated from waste- and surface waters, Sci. Total Environ. 409 (2011) 1017-1023.
[6] K. Kümmerer, Antibiotics in the aquatic environment – A review – Part II, Chemosphere 75 (2009) 435-441.
[7] A. Lupo, S. Coyne, T.U. Berendonk, Origin and evolution of antibiotic resistance: the common mechanisms of emergence and spread in water bodies, Front. Microbiol. 3 (2012) 18.
[8] M.O. Barbosa, N.F.F. Moreira, A.R. Ribeiro, M.F.R. Pereira, A.M.T. Silva, Occurrence and removal of organic micropollutants: an overview of the watch list of EU Decision 2015/495, Water Res. 94 (2016) 257-279.
[9] A.R. Ribeiro, O.C. Nunes, M.F.R. Pereira, A.M.T. Silva, An overview on the advanced oxidation processes applied for the treatment of water pollutants defined in the recently launched Directive 2013/39/EU, Environ. Int. 75 (2015) 33-51.
[10] The White House, National strategy for combating antibiotic-resistant bacteria, Washington, DC, 2014.
[11] D. Fatta-Kassinos, C. Manaia, T.U. Berendonk, E. Cytryn, J. Bayona, B. Chefetz, J. Slobodnik, N. Kreuzinger, L. Rizzo, S. Malato, L. Lundy, A. Ledin, COST Action ES1403: New and Emerging challenges and opportunities in wastewater REUSe (NEREUS), Environ. Sci. Pollut. Res. 22 (2015) 7183-7186.
[12] Y. Luo, W. Guo, H.H. Ngo, L.D. Nghiem, F.I. Hai, J. Zhang, S. Liang, X.C. Wang, A review on the occurrence of micropollutants in the aquatic environment and their fate and removal during wastewater treatment, Sci. Total Environ. 473–474 (2014) 619-641.
[13] J. Benner, D.E. Helbling, H.-P.E. Kohler, J. Wittebol, E. Kaiser, C. Prasse, T.A. Ternes, C.N. Albers, J. Aamand, B. Horemans, D. Springael, E. Walravens, N. Boon, Is biological treatment a viable alternative for micropollutant removal in drinking water treatment processes?, Water Res. 47 (2013) 5955-5976.

[14] A. Aguinaco, J.P. Pocostales, J.F. García-Araya, F.J. Beltrán, Decomposition of hydrogen peroxide in the presence of activated carbons with different characteristics, J. Chem. Technol. Biotechnol. 86 (2011) 595-600.
[15] W.H. Glaze, J.-W. Kang, D.H. Chapin, The chemistry of water treatment processes involving ozone, hydrogen peroxide and ultraviolet radiation, Ozone Sci. Eng. 9 (1987) 335-352.
[16] Council Directive 98/83/EC of 3 November 1998 on the quality of water intended for human consumption, Official Journal of the European Communities, The Council of the European Union, 1998.
[17] E.P. Agency, Parameters of water quality: interpretation and standards, Environmental Protection Agency, Ireland, Wexford, Ireland, 2001.
[18] N. Inchaurrondo, J.O. Cechini, J. Font, P. Haure, Strategies for enhanced CWPO of phenol solutions, Appl. Catal. B 111-112 (2012) 641-648.
[19] D. Dimitrakopoulou, I. Rethemiotaki, Z. Frontistis, N.P. Xekoukoulotakis, D. Venieri, D. Mantzavinos, Degradation, mineralization and antibiotic inactivation of amoxicillin by UV-A/TiO_2 photocatalysis, J. Environ. Manage. 98 (2012) 168-174.
[20] S. Navalon, M. Alvaro, H. Garcia, Heterogeneous Fenton catalysts based on clays, silicas and zeolites, Appl. Catal. B 99 (2010) 1-26.
[21] O. Tsydenova, V. Batoev, A. Batoeva, Solar-enhanced advanced oxidation processes for water treatment: simultaneous removal of pathogens and chemical pollutants, Int. J. Environ. Res. Public Health 12 (2015) 9542-9561.

10. HYBRID MAGNETIC GRAPHITIC NANOCOMPOSITES TOWARDS CATALYTIC WET PEROXIDE OXIDATION OF THE LIQUID EFFLUENT FROM A MECHANICAL BIOLOGICAL TREATMENT PLANT FOR MUNICIPAL SOLID WASTE

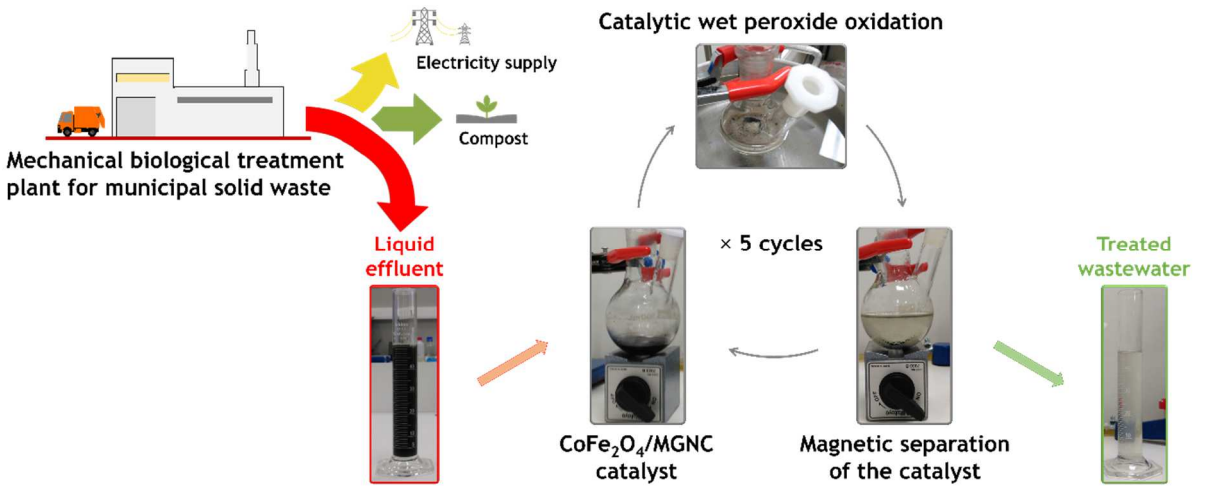

[14]

[14] Adapted from the graphical abstract of: Rui S. Ribeiro, Raquel O. Rodrigues, Adrián M.T. Silva, Pedro B. Tavares, Ana M.C. Carvalho, José L. Figueiredo, Joaquim L. Faria, Helder T. Gomes, Hybrid magnetic graphitic nanocomposites towards catalytic wet peroxide oxidation of the liquid effluent from a mechanical biological treatment plant for municipal solid waste, Appl. Catal. B 219 (2017) 645-657
DOI: 10.1016/j.apcatb.2017.08.013

The concept of hierarchical waste management is well-established nowadays, mechanical biological treatment (MBT) plants being a suitable alternative that is growing in popularity in many European countries as well as in other countries worldwide [1, 2]. MBT plants typically operate in two steps: the first step comprises residue preparation and sorting into different fractions using mechanical means; the second step envisages the biological treatment of the organic fraction of municipal solid waste (MSW) to produce a stabilised solid output for agronomical applications (compost) or ultimately for disposal to landfill [3]. Under this context, anaerobic digestion is an energy efficient biological treatment technique that allows using the organic fraction of MSW as renewable energy source (e.g. through biogas production) while reducing the environmental impact of its direct landfill disposal [4, 5]. Therefore, MBT plants allow reducing the waste stream going to landfill while benefiting from resources (e.g. recyclables and compost) and energy recovery [2]. In order to achieve optimum process conditions, the biodegradable fraction of the MSW going to anaerobic digestion must first be suspended in, or moistened with water, leading to significant freshwater requirements —from 0.4 to 0.6 m^3 per tonne of waste, for dry or wet fermentation, respectively [5]. In addition to the process water from (i) anaerobic digestion, the other main sources of process water streams requiring subsequent treatment are: (ii) leachate from intensive rotting, (iii) pressing water from digestate dewatering and (iv) condensates and/or scrubber water from the exhaust treatment [5].

Bearing this in mind, the ability of CWPO for the treatment of the liquid effluent from a MBT plant located in the Northeast region of Portugal (currently processing 50000 tonnes of MSW per year) was evaluated in Chapter 10. For that purpose, a high-performance hybrid magnetic graphitic nanocomposite —composed by a cobalt ferrite core and a graphitic shell ($CoFe_2O_4$/MGNC), was designed based on the findings reported in Chapters 5 – 8. In the following Sections the properties of $CoFe_2O_4$/MGNC are characterized and the respective performance in CWPO is evaluated against that of Fe_3O_4/MGNC using 4-NP aqueous model solutions (5 g L^{-1}, corresponding to a total organic carbon content similar to that of the liquid effluent considered in this Chapter). The best performing catalyst was employed in the treatment of the liquid effluent collected from the MBT plant. The treatment efficiency was thoroughly evaluated by systematic measurements of chemical oxygen demand (COD), total organic carbon (TOC), aromaticity, H_2O_2 consumption and dissolved metal species. 5-Day biochemical oxygen demand (BOD_5) was determined in order to estimate the effect of CWPO on the biodegradability of the liquid effluent. Total heterotrophic bacteria were estimated in order to assess the effect of CWPO on the autochthonous microbial population of the liquid effluent. Additional microbiological assays were performed in order to evaluate the antimicrobial activity of the liquid effluent before and after treatment by CWPO.

10.1. Textural and surface chemistry characterization

$CoFe_2O_4$ and $CoFe_2O_4$/MGNC were characterized by XRD and TEM. The corresponding results are given in Figures 10.1 and 10.2, respectively. As observed in Figure 10.1, an impure phase was found in the diffraction pattern of $CoFe_2O_4$ in addition to cobalt ferrite (a = 8.387 Å, crystallite size of 14.3 ± 0.2 nm), which was ascribed to the thermal treatment required for the crystallization of the amorphous materials with the inverse spinel structure. This additional phase was identified as hematite (a = 5.043 Å, c = 13.78 Å, crystallite size of 24.2 ± 0.5 nm), corresponding to 24 wt.% of $CoFe_2O_4$, as determined by XRD analysis. $CoFe_2O_4$/MGNC was prepared by the same procedure used for the synthesis of Fe_3O_4/MGNC, except that Fe_3O_4 was replaced by $CoFe_2O_4$ (*cf*. Section 4.1.5). Therefore, the encapsulation of these magnetic nanoparticles within a graphitic shell is expected to occur through a similar route to that reported in Section 8.1 for Fe_3O_4. As observed in Figure 10.2a, $CoFe_2O_4$ nanoparticles were successfully encapsulated within graphitic structures during the synthesis of $CoFe_2O_4$/MGNC, resulting in core-shell structures. Regarding the molecular structure, iron (a = 2.858 Å, crystallite size of 44 ± 1 nm) was identified in the diffraction pattern of $CoFe_2O_4$/MGNC, in addition to cobalt ferrite (a = 8.363 Å, crystallite size of 33 ± 2 nm) and graphite (*cf*. Figure 10.1). When the average size of the magnetic cores of $CoFe_2O_4$/MGNC (56 ± 18 nm, as determined from TEM measurements, *cf*. Figure 10.2b), is compared to the size of parent $CoFe_2O_4$ (14 ± 4 nm, *cf*. the inset of Figure 10.2b), it is suggested that the cores of this hybrid material are mainly composed by agglomerates of magnetic nanoparticles. This phenomenon is in agreement with the mechanism proposed in Chapter 8.1 for the synthesis of Fe_3O_4/MGNC, as depicted in Figure 8.3.

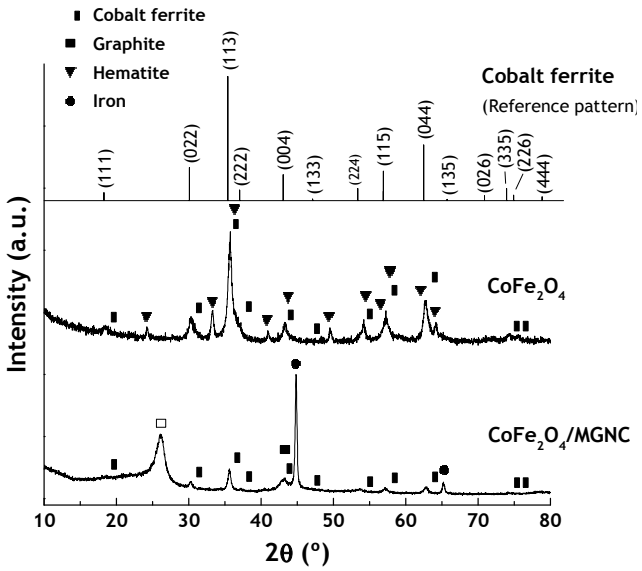

Figure 10.1. XRD diffraction patterns of $CoFe_2O_4$ and $CoFe_2O_4$/MGNC. Standard reference pattern of cobalt ferrite (crystallography open database code: 1535820) is also given for comparison.

Table 10.1. Properties of $CoFe_2O_4$/MGNC: specific surface area (S_{BET}), non-microporous specific surface area (S_{meso}), micropore volume (V_{micro}), total pore volume (V_{total}), average pore diameter (d_{pore}) and pH at the point of zero charge (pH_{PZC})

Material	Parameter					
	S_{BET} ($m^2\ g^{-1}$)	S_{meso} ($m^2\ g^{-1}$)	V_{micro} ($cm^3\ g^{-1}$)	V_{total} ($cm^3\ g^{-1}$)	d_{pore} (nm)	pH_{PZC}
$CoFe_2O_4$/MGNC	330	170	0.07	0.31	3.75	9.0

The texture and surface chemistry of $CoFe_2O_4$/MGNC were further characterized by TGA analysis, N_2 adsorption-desorption isotherms and pH_{PZC}. The TGA analysis of $CoFe_2O_4$/MGNC (results not shown) reveals 14.4 wt.% of ashes, corresponding to the mass fraction of $CoFe_2O_4$ encapsulated in $CoFe_2O_4$/MGNC. It was also found that $CoFe_2O_4$/MGNC is stable up to 400 °C under oxidizing atmosphere. As observed in Table 10.1, $CoFe_2O_4$/MGNC has a well-developed specific surface area, with a S_{BET} of 330 $m^2\ g^{-1}$, and a micro-mesoporous character, which is particularly reflected by the ratio V_{mic}/V_{total} = 0.23, as well as an average pore diameter of 3.75 nm. When the textural properties of $CoFe_2O_4$/MGNC are compared to that of Fe_3O_4/MGNC (*cf*. Table 8.1), it is observed that similar textural properties are obtained regardless of the composition of the magnetic core. Nevertheless, as reflected by the pH_{PZC} values given in Tables 8.1 and 10.1, the overall surface chemistry is slightly affected by the composition of the magnetic core. If the values of pH_{PZC} obtained for Fe_3O_4/MGNC (7.1) and $CoFe_2O_4$/MGNC (9.0) are compared with those recently reported in the literature for their main metal oxide constituents [6, 7], namely Fe_3O_4 (6.2 – 8.0) and $CoFe_2O_4$ (7.5 – 10.1), it is suggested that the pH_{PZC} of the MGNC materials are mainly determined by the different contributions of the metal oxides detected by XRD.

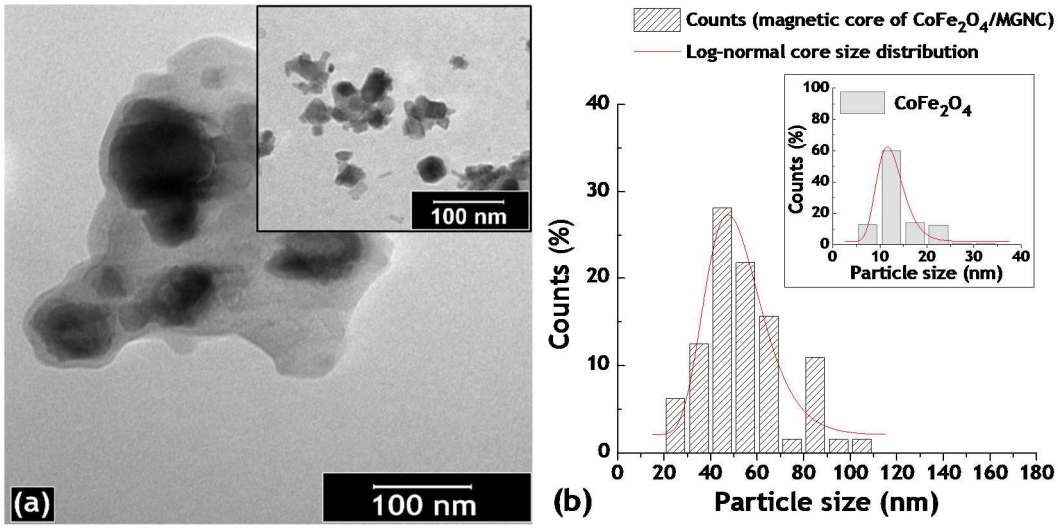

Figure 10.2. (a) TEM micrographs of (main) $CoFe_2O_4$/MGNC and (inset) $CoFe_2O_4$. (b) Histogram of particle size distribution of (main) $CoFe_2O_4$/MGNC and (inset) $CoFe_2O_4$.

10.2. CWPO screening experiments with 4-NP model solutions

The $CoFe_2O_4$/MGNC catalyst was prepared in order to further optimize the performance previously revealed by Fe_3O_4/MGNC in CWPO (*cf.* Chapter 8), through the replacement of the magnetic core. In order to evaluate the outcome of this approach, the performance of the MGNC materials in CWPO was initially evaluated through experiments performed with 4-NP aqueous model solutions with high concentration (5 g L^{-1}, corresponding to a TOC content similar to that of the liquid effluent considered in Section 10.4), under the operating conditions detailed in Table 10.2. In order to optimize the efficiency of catalyst usage, the catalyst dosage was kept very low when compared to the pollutant concentration, with a fixed pollutant/catalyst mass ratio as high as 10. As observed in Figure 10.3, the catalyst resulting from the inclusion of $CoFe_2O_4$ within a carbon shell ($CoFe_2O_4$/MGNC) reveals the highest activity for the CWPO of 4-NP. In this case, complete 4-NP conversion is obtained in 3 h, corresponding to a very high average pollutant mass removal rate of 3333 mg g^{-1} h^{-1}. The 4-NP removal obtained in the non-catalytic experiment is negligible when compared to that obtained in the presence of the MGNC catalysts (please refer to Figure C.7b for additional details on the non-catalytic experiment).

By comparing the leaching of Fe species at the end of the CWPO runs performed with Fe_3O_4/MGNC (1.8 mg L^{-1}) and $CoFe_2O_4$/MGNC (0.9 mg L^{-1}), it is observed that $CoFe_2O_4$/MGNC reveals an enhanced resistance to the leaching of Fe species, which can be ascribed to the presence of Co species, as detailed in Chapter 7. However, as Co is oxidized during CWPO, its susceptibility to undergo leaching to the treated waters is expected to increase (*cf.* Chapter 7). In order to confirm this hypothesis, the leaching of Co from $CoFe_2O_4$/MGNC was determined at the end of the CWPO run depicted in Figure 10.3. Although under these

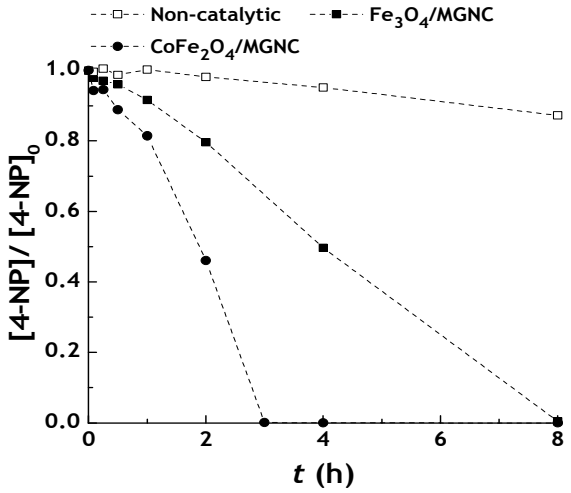

Figure 10.3. 4-NP removal obtained as a function of time in CWPO runs performed with the MGNC materials. Experiments performed with $[4\text{-NP}]_0$ = 5.0 g L^{-1}, [catalyst] = 0.5 g L^{-1}, $[H_2O_2]_0$ = 17.8 g L^{-1} (stoichiometric amount), T = 80 ºC and pH = 3.

conditions the leaching of Co amounts to 10.7 mg L^{-1}, there are a lack of standards for treated wastewater and even for drinking water [8].

Due to the best overall performance evidenced in the screening experiments, $CoFe_2O_4$/MGNC was object of additional studies. A pure adsorption run was performed in order to assess the possible adsorption influence on the removal of 4-NP by CWPO. As observed in Figure 10.4a, the removal of 4-NP obtained in the pure adsorption run performed with $CoFe_2O_4$/MGNC is negligible, corresponding to 0.7% of the initial content of 4-NP. This negligible percent adsorption removal of 4-NP can be ascribed to the very low $CoFe_2O_4$/MGNC dosage when compared to the pollutant concentration, as reflected by the 4-NP/catalyst mass ratio of 10. The evolution of COD, TOC and H_2O_2 consumption during the CWPO run performed with $CoFe_2O_4$/MGNC is also shown in Figure 10.4a. As observed, TOC and COD removals of 54.4% and 74.2% were respectively obtained. At the same time, the consumption of H_2O_2 amounts to 71.0%, representing high efficiencies of TOC and COD removals per unit of H_2O_2 decomposed.

A leaching test was performed in order to evaluate the heterogeneous nature of the $CoFe_2O_4$/MGNC catalyst, as described in Section 4.3. As observed in Figure 10.4b, when the $CoFe_2O_4$/MGNC catalyst is removed after 30 min of reaction, the reaction solution reveals negligible activity in the CWPO of 4-NP, considering both 4-NP and TOC removals. This observation confirms the predominant role of heterogeneous CWPO promoted by $CoFe_2O_4$/MGNC. In addition, the participation of HO• radicals in the process was indirectly evaluated by adding *tert*-butanol (tBuOH), a strong HO• radical scavenger [9, 10], before one reaction. When the CWPO runs performed in the presence and absence of tBuOH are compared (*cf*. Figure C.10), it is observed that the removal of 4-NP is greatly suppressed by tBuOH. Although not directly supported by quantification of the HO• radicals formed during

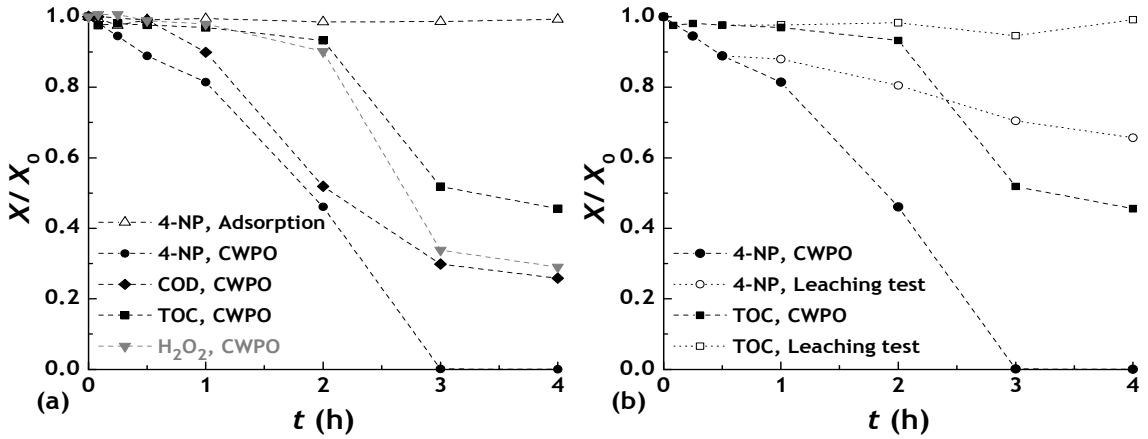

Figure 10.4. (a) 4-NP, COD, TOC and H_2O_2 normalized concentrations as a function of time in the CWPO run performed with $CoFe_2O_4$/MGNC; 4-NP removals by adsorption are also shown for comparison. (b) 4-NP and TOC removals obtained during the "leaching test" performed with $CoFe_2O_4$/MGNC (i.e., where the catalyst was removed from the solution after 30 min of reaction).

the process, this indirect result suggests the ability of $CoFe_2O_4$/MGNC to efficiently promote the decomposition of H_2O_2 via $HO^{\bullet}$ formation. Furthermore, the aromatic by-products detected during the CWPO of 4-NP in the presence of $CoFe_2O_4$/MGNC (*cf*. Figure C.11a) are in agreement with a reaction mechanism including the attack of the 4-NP molecule by $HO^{\bullet}$ radicals, as reported in Section 6.2.3. Further attack of $HO^{\bullet}$ radicals on the aromatic intermediate compounds leads to the opening of the aromatic ring, and thus to the formation of a series of low molecular weight carboxylic acids (*cf*. Figure C.11b). In addition, NO_3^- can be produced from the $-NO_2$ group subtraction from the 4-NP aromatic ring under the oxidation conditions employed. Based on the NO_3^- concentrations shown in Figure C.11b, it can be concluded that at least 50.8% of the total nitrogen initially present in the 4-NP aqueous model solution was effectively subtracted from the main aromatic ring after 4 h of CWPO in the presence of the $CoFe_2O_4$/MGNC catalyst.

10.3. Development of an *in-situ* magnetic separation system for catalyst recovery

In order to take advantage of the magnetic properties of $CoFe_2O_4$/MGNC, a lab-scale magnetic separation system was designed for *in-situ* catalyst recovery after the CWPO reaction stage. For that purpose, a switchable magnetic stand was coupled with the reactor after the reaction stage (as described in Section 10.6.2), allowing to perform reaction/separation sequential stages in a single vessel, thus avoiding the separation of the heterogeneous catalysts by filtration and/or centrifugation. As observed in Figure 10.5, this technique was successfully employed for the recovery of the $CoFe_2O_4$/MGNC catalyst after

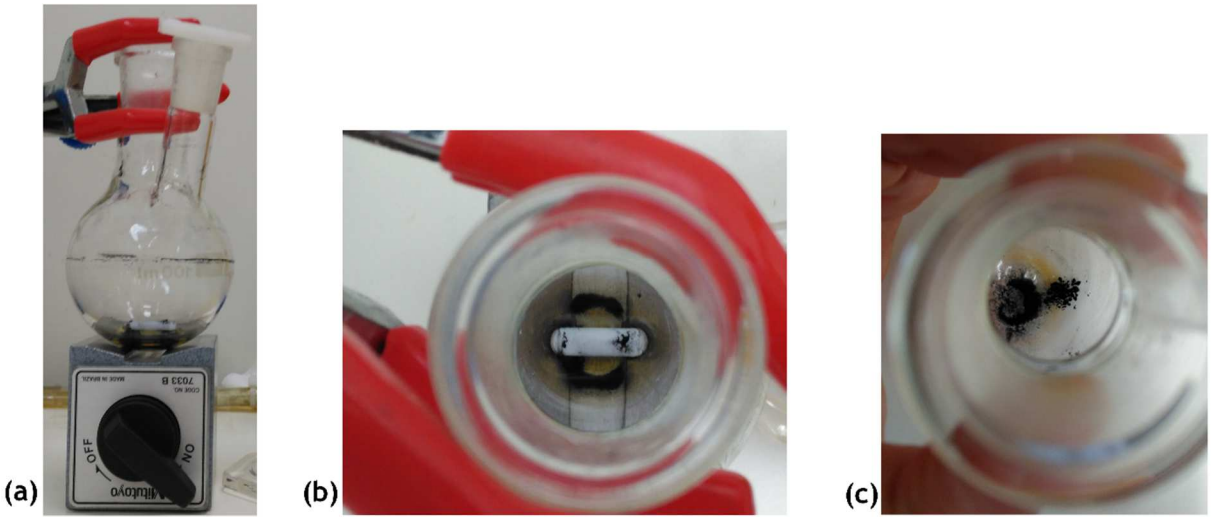

Figure 10.5. *In-situ* magnetic separation of $CoFe_2O_4$/MGNC at the end of the CWPO stage performed with the aid of a Mitutoyo 7033B switchable magnetic stand (clamping force 600 N); (a) front and (b) top view of the glass reactor immediately after the recovery of the treated water and (c) top view of the reactor after the drying process (60 ºC) for catalyst recovery.

the CWPO run performed with 4-NP (5 g L^{-1}), ca. 98% of the treated water being collected. An image of the glass reactor coupled with the magnetic separation device is provided in Figure 10.5a. In order to estimate the efficiency of catalyst recovery, the $CoFe_2O_4$/MGNC collected after the CWPO run was dried overnight at 60 ºC and then weighted. Reaction/separation sequential experiments performed in triplicate allowed to determine the percentage of catalyst recovery. It was found that 77.0 ± 6.1 wt.% of the initial $CoFe_2O_4$/MGNC load is recovered by implementing the proposed *in-situ* magnetic separation system, a value well above the 57.9 ± 2.4 wt.% recovered by conventional filtration. The direct benefit of magnetic separation for the recovery of the catalyst in the same unit that is used in the CWPO experiments is thus demonstrated. With this in mind, *in-situ* magnetic separation will be further explored in the reusability cycles performed in Section 10.4.3.

10.4. CWPO of the liquid effluent from a MBT plant for municipal solid waste

Herein, the suitability of the most active and stable catalytic system obtained in Section 10.2 for the CWPO of the liquid effluent collected from a MBT plant is evaluated. As detailed in Table 10.3, this effluent contains a high pollutant load, due to the presence of organic (9206 mg L^{-1} COD; 2046 mg L^{-1} TOC), inorganic (14350 mg L^{-1} bicarbonates; 2833 mg L^{-1} chlorides) and biological (14.7×10^4 CFU mL^{-1} total heterotrophic bacteria cultivable at 28 ºC) species. According to the BOD_5/COD ratio, which is widely used as an indicator of the biodegradability of liquid effluents, a wastewater is considered easily treatable by biological means if the BOD_5/COD ratio is 0.5 or larger [11]. On the opposite, a BOD_5/COD ratio below 0.3 suggests the presence of toxic components, the wastewater being not biodegradable or acclimated microorganisms being required for its biological treatment [11]. The liquid effluent considered in this work is not expected to be prone to degradation by conventional biological treatments, according to the low BOD_5/COD ratio of 0.21. It is also known that both bicarbonates and chlorides can act as $HO^{\bullet}$ radical scavengers. Although several reactions involving bicarbonate and chloride ions may occur in the bulk, the $HO^{\bullet}$ radical scavenging effect promoted by these inorganic species results mainly from their direct reaction with $HO^{\bullet}$ radicals. The reaction of bicarbonate ions with $HO^{\bullet}$ radicals can be described by Eq. 10.1 [12], while the reaction of chloride ions with $HO^{\bullet}$ radicals proceeds through the mechanism described by Eqs. 10.2 and 10.3 [13]. Therefore, the presence of these inorganic species is expected to hinder the performance of CWPO for the treatment of the liquid effluent considered in this work. Bearing this in mind, the operating conditions that maximize the performance of CWPO for the treatment of the liquid effluent from the MBT plant in the presence of $CoFe_2O_4$/MGNC were thoroughly investigated.

$$HO^{\bullet} + HCO_3^- \rightarrow CO_3^{\bullet-} + H_2O \quad \textbf{(10.1)}$$

$$HO^{\bullet} + Cl^- \rightarrow HOCl^{\bullet-} \quad \textbf{(10.2)}$$

$$HOCl^{\bullet-} + H^+ \rightarrow Cl^{\bullet} + H_2O \quad \textbf{(10.3)}$$

10.4.1. CWPO process optimization: the crucial role of the operating pH

The operating conditions used in Section 10.2 were initially employed in this Section, the catalyst dosage being kept very low when compared to the effluent COD. Taking into account the possible catalytic contribution of the Fe species present in the liquid effluent collected from the MBT plant (6.4 mg L^{-1}, *cf*. Table 10.3), a preliminary experiment was performed without added catalyst. In spite of the Fe content and the high complexity of the liquid effluent, the COD removal obtained after 24 h of reaction under these conditions was only 12.8%, representing less than a third of that obtained in the presence of $CoFe_2O_4$/MGNC (0.5 g L^{-1}). This result highlights the role of CWPO promoted by $CoFe_2O_4$/MGNC.

Seeking for CWPO process optimization, the influence of H_2O_2 dosage was then evaluated. Based on the results obtained in CWPO runs performed with H_2O_2 concentrations in the range 13.9 – 34.7 g L^{-1} (results not shown), it was found that the best performance is achieved when employing $[H_2O_2]_0$ = 27.7 g L^{-1} (corresponding to the stoichiometric amount theoretically needed to reduce the effluent COD and to neutralize the $HO^{\bullet}$ radical scavenging effect promoted by the chlorides dissolved in the effluent, as described by Eqs. 10.2 and 10.3). Therefore, additional experiments were performed with this H_2O_2 dosage.

It is noteworthy that the bicarbonate equilibrium concentration in water depends on the pH, as described by the acid ionization reactions, Eqs. 10.4 and 10.5, and corresponding acid-dissociation constants [14]. At the natural pH of the liquid effluent considered in this work (8.2) and given concentrations of dissolved matter and ions, the prevailing species is the bicarbonate ion (HCO_3^-). In addition to the $HO^{\bullet}$ radical scavenging described by Eq. 10.1, the negative effect of HCO_3^- is particularly significant in the case of CWPO, since H_2O_2 can be directly decomposed through the parasitic reaction described by Eq. 10.6 [15], even before $HO^{\bullet}$ formation. However, this parasitic reaction can be avoided by decreasing the solution pH to values below 6.35; in this case, HCO_3^- is converted to carbonic acid (H_2CO_3), which is subsequently decomposed into carbon dioxide (which escapes the solution for the gas phase) and water (*cf*. Eq. 10.7) [16]. Therefore, based on the presence of bicarbonate species (14350 mg L^{-1}), operating at pH < 6.35 is expected to favour the performance of CWPO for the treatment of the liquid effluent considered in this work.

$$H_2CO_3(aq) \leftrightarrows H^+(aq) + HCO_3^-(aq) \qquad pK_{a1} = 6.35 \quad \textbf{(10.4)}$$

$$HCO_3^-(aq) \leftrightarrows H^+ + CO_3^{2-}(aq) \qquad pK_{a2} = 10.33 \quad \textbf{(10.5)}$$

$$HCO_3^-(aq) + H_2O_2(aq) \leftrightarrows HCO_4^-(aq) + H_2O(aq) \quad \textbf{(10.6)}$$

$$H_2CO_3(aq) \leftrightarrows CO_2(g) + H_2O(l) \quad \textbf{(10.7)}$$

Nevertheless, the presence of chlorides should also be taken into account in this analysis. As discussed elsewhere for the H_2O_2/UV process, the solution pH can also affect the extent of the HO$^\bullet$ radical scavenging reaction described by Eq.10.2 [17]. Specifically, the rate constant for the reaction described by Eq. 10.2 is 4.3×10^9 M^{-1} s^{-1}; however, the hypochlorous radical ($HOCl^{\bullet-}$) formed by the reaction described by Eq. 10.2 is able to dissociate back to HO$^\bullet$ radical and chloride ion (Cl^-), the dissociation rate constant being 6.1×10^9 s^{-1} [17]. As described by Eq. 10.3, $HOCl^{\bullet-}$ can also be converted into chlorine radicals ($Cl^\bullet$) and water through a protonation reaction with the rate constant of 2.1×10^{10} M^{-1} s^{-1}, in this case the reverse rate reaction being much smaller (1.3×10^3 s^{-1}) [17]. Therefore, it is expected that the formation of $Cl^\bullet$ by the protonation reaction described by Eq. 10.3 increases as the solution pH decreases, thus promoting the scavenging reaction described by Eq. 10.2. In this case, the critical point affecting the extent of HO$^\bullet$ radical scavenging is the p*K*a of the reverse reaction (i.e., the deprotonation reaction) described by Eq. 10.3 (7.2). Thus, it can be concluded that $Cl^\bullet$ is the prevailing species at solution pH < 7.2, while $HOCl^{\bullet-}$ becomes the dominant species when pH > 7.2, thus decreasing the consumption of HO$^\bullet$ radicals by the reaction described by Eq. 10.2. Therefore, based on the presence of chloride species (2833 mg L^{-1}), operating pH > 7.2 is expected to favour the performance of CWPO for the treatment of the liquid effluent considered in this work.

Summarizing, the solution pH is expected to significantly affect the performance of CWPO for the treatment of the effluent from the MBT plant. On one hand, pH < 6.35 limits the negative effect of bicarbonates; while, on the other hand, pH > 7.2 limits the negative effect of chlorides. Therefore, the selection of the optimum pH may be considered as the crucial step to achieve the operating parameters that maximize the performance of the liquid effluent treatment by CWPO in the presence of $CoFe_2O_4$/MGNC.

Bearing this in mind, the individual effect of the operating pH on the efficiency of CWPO was evaluated in the range 2.5 – 8. For that purpose, COD, TOC, aromaticity and H_2O_2 conversions were determined, as shown in Figure 10.6a. The efficiency of CWPO for the treatment of the liquid effluent from the MBT plant tends to increase as the pH increases in the range 2.5 – 6, whereas it dramatically decreases for pH > 6. This phenomenon —ascribed to the presence of bicarbonates and chlorides— confirms the crucial role of the operating pH in the CWPO of the liquid effluent considered in this work, as previously discussed. At pH > 6, 97% of the initial H_2O_2 dosage is consumed within the first 30 min of reaction, most likely due to the fast reaction with HCO_3^-, as described by Eq. 10.6. At pH < 6, the HO$^\bullet$ radical scavenging by Cl^- is increasingly significant, thus hindering the efficiency of the CWPO process. Therefore, pH = 6 can be considered the optimum operating pH, since it allows to

maximize the performance of the liquid effluent treatment by CWPO in the presence of $CoFe_2O_4$/MGNC. Additional insights on the COD, TOC, H_2O_2 and aromaticity conversions, and absorbance spectra evolution as a function of time in the CWPO run performed under the optimized conditions are given in Figures 10.6b and c, respectively. As observed, fast conversions of COD, TOC, aromaticity and H_2O_2 are obtained in the first 8 h of CWPO. Up to that point, ca. 93% of the effluent aromaticity is already converted; while from 8 to 24 h of reaction, an increase of only ca. 2% is observed in the aromaticity conversion. However, the TOC content of the effluent decreases ca. 14% during the same period, while the absorbance spectra also evolved favourably (*cf.* Figure 10.6c), revealing that the treatment reactions still proceed, although at a lower rate. These observations suggest that recalcitrant by-products are formed when the aromatic compounds are attacked by HO• radicals (*cf.*

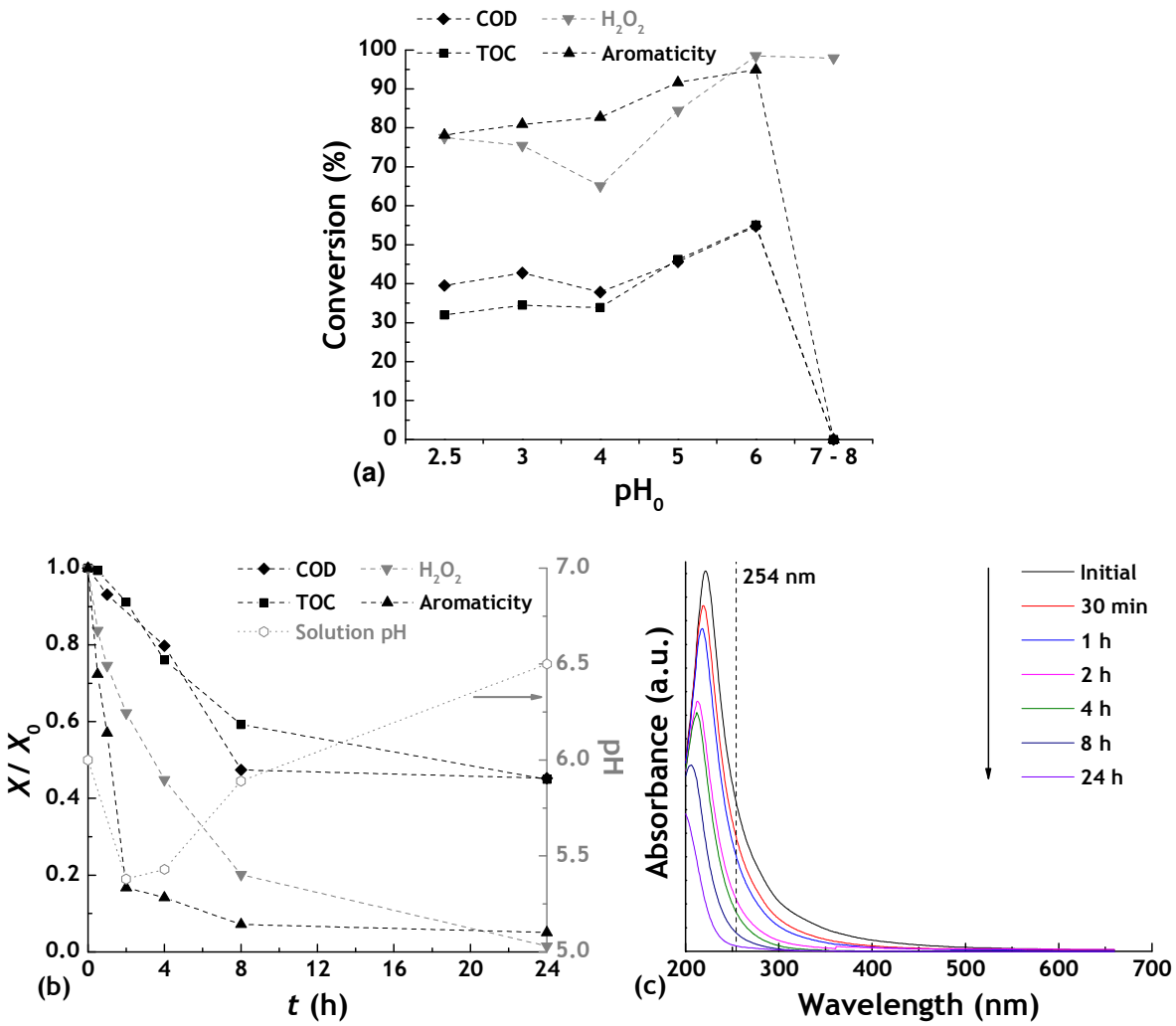

Figure 10.6. (a) Effect of pH on COD, TOC, H_2O_2 and aromaticity conversions obtained after 24 h in CWPO runs performed with $CoFe_2O_4$/MGNC. (b) COD, TOC, H_2O_2, aromaticity (left axis), solution pH (right axis) and (c) absorbance spectra evolution as a function of time in the CWPO run performed at pH = 6; Experiments performed with the liquid effluent collected from a MBT plant, [$CoFe_2O_4$/MGNC] = 0.5 g L^{-1}, $[H_2O_2]_0$ = 27.7 g L^{-1}, T = 80 ºC and pH = 6.

demonstrated in Section 10.2). This mechanism is also suggested by the changes in the solution pH observed during the treatment by CWPO (*cf.* Figure 10.6b). Specifically, pH decreases from 6 (i.e., the initial pH) to 5.4 in the first 2 h, suggesting the formation of low molecular weight carboxylic acids; afterwards the pH gradually increases up to 6.5 at the end of the reaction, suggesting that the CWPO treatment is able to mineralize most of these carboxylic acids although at an apparently lower rate when broad parameters, like COD and TOC are considered. After 24 h of CWPO, ca. 95% of the effluent aromaticity is converted under these operating conditions, while ca. 55% of the initial COD and TOC are effectively removed. The H_2O_2 consumption during the treatment represents ca. 98% of the initial dosage.

The BOD_5 of the treated water was also determined in order to estimate the effect of CWPO on the biodegradability of the liquid effluent. It was found that the BOD_5 is slightly affected during the process, a decrease from 1933 to 1760 mg L^{-1} being observed. At the same time the COD decreased from 9206 to 4164 mg L^{-1}. Accordingly, the BOD_5/COD ratio of the treated water is 0.42, representing a 2-fold increase when compared to the BOD_5/COD ratio of the liquid effluent (0.21). A BOD_5/COD ratio in the range 0.3 – 0.5 suggests that the wastewater is treatable by biological means [11]. It can be therefore concluded that the biodegradability of the liquid effluent is enhanced during the treatment by CWPO in the presence of $CoFe_2O_4$/MGNC.

In addition, the dissolved Fe content was measured at the end of the CWPO runs performed with operating pH in the range 2.5 – 6. The highest value was found in the experiment performed at pH = 2.5, corresponding to a Fe concentration of 1.04 mg L^{-1}; on the other hand, the lowest value was obtained in the experiment performed at pH = 6 (0.27 mg L^{-1}). However, it should be noted that the liquid effluent considered in this work is very complex. Although the total Fe content present in the effluent is 6.4 mg L^{-1}, the amount of dissolved Fe species, i.e., those obtained after filtration (0.2 μm), actually depends on the pH. For instance, the inherent dissolved Fe content of the effluent is 0.96 mg L^{-1} after 24 h at pH = 3, but this value decreases to 0.15 mg L^{-1} after 24 h at pH = 6. Therefore, the dissolved Fe content determined at the end of the CWPO runs cannot be fully ascribed to leaching from the $CoFe_2O_4$/MGNC catalyst. Likewise, the dissolved Co content at the end of the CWPO run performed at pH = 6 was also determined (0.58 mg L^{-1}); it can be considered very low, in particular when compared to the inherently dissolved Co content in the effluent (0.12 mg L^{-1}, *cf.* Table 10.3).

10.4.2. Disinfection and antimicrobial activity

Regarding the bacterial population, heterotrophic plate count is a procedure widely used to evaluate the performance of treatment processes, since it allows to estimate the number of live heterotrophic bacteria in a given water or wastewater [11]. As described in Section 4.4.12, the spread plate method was used in this work. The selected incubation temperature was 28 ºC, since it favours the growth of waterborne bacteria [18-20]. Under this context, total heterotrophic bacteria in the treated water were estimated in order to assess the effect of CWPO on the effluent autochthonous microbial population (14.7×10^4 CFU mL^{-1} total heterotrophic bacteria cultivable at 28 ºC). After incubation at 28 ºC during 5 days, not a single colony was found in the plate count performed in triplicate, even in the undiluted treated water samples. Therefore, although this was not the main goal of the treatment proposed, it can be concluded that disinfection of the effluent was achieved upon the CWPO treatment employed in the presence of $CoFe_2O_4$/MGNC under the optimum operating conditions considered (*cf.* Table 10.2).

Additional microbiological assays were performed in order to evaluate the antimicrobial activity of the liquid effluent before and after treatment by CWPO. As described in Section 4.4.12, the agar disk-diffusion method was used for the antimicrobial susceptibility testing. For that purpose, *Klebsiella pneumoniae* (Gram negative) and *Bacillus cereus* (Gram positive) were selected as test microorganisms. After 16 and 24 h of incubation at 37 ºC, the absence of inhibition growth zones surrounding the testing paper discs containing both the effluent and the treated water samples was observed. These qualitative results reveal that both selected microorganisms are resistant to the effluent, either before or after treatment by CWPO, suggesting that the toxicity of the liquid effluent from the MBT plant is not increased during its treatment by CWPO under the optimum operating conditions considered (*cf.* Table 10.2).

10.4.3. Reusability cycles implementing *in-situ* magnetic separation for catalyst recovery

Catalyst separation and long-term stability are crucial aspects for the feasibility of the proposed water treatment process in large scale applications. Therefore, once the catalytic system and the CWPO process were optimized, the benefits of magnetic separation for the recovery of the catalyst were explored by performing a series of five CWPO reaction/separation sequential experiments in the same vessel with consecutive reuse of the $CoFe_2O_4$/MGNC catalyst, as depicted in Figure 10.7. For that purpose, the *in-situ* magnetic separation system developed in Section 10.3 was employed for catalyst recovery at the end of each CWPO cycle, the treated water being collected afterwards. In order to

ensure equal catalyst dosage throughout all the reusability cycles (0.5 g L^{-1}), 23 wt.% of the initial catalyst load was added (i.e., 0.115 g L^{-1}; corresponding to the mass fraction lost due to sampling and treated water collection), and a new CWPO run was performed upon the addition of fresh liquid effluent. As observed in Figure 10.8, the efficiency of CWPO for the treatment of the liquid effluent from the MBT plant is maintained throughout the five cycles performed in the presence of $CoFe_2O_4$/MGNC under the optimum operating conditions determined in Section 10.4.1. Under these conditions, the COD, TOC, aromaticity and H_2O_2 conversions obtained after 24 h of reaction with $CoFe_2O_4$/MGNC are not particularly affected by the successive reuse of the catalyst, thus revealing its high stability for CWPO, and high potential for large scale applications. This stability feature for CWPO can be ascribed to the resistance of $CoFe_2O_4$/MGNC against the leaching of Fe, as highlighted by measuring the dissolved Fe content at the end of each CWPO cycle (*cf.* Figure 10.8). Specifically, the highest value was obtained in the first cycle, corresponding to 0.27 mg L^{-1}. From the second to the fifth cycle, the dissolved Fe content was in the range 0.13 – 0.17 mg L^{-1}. The dissolved Fe content obtained after the fifth CWPO cycle is similar to the dissolved Fe content inherent to the liquid effluent (0.15 mg L^{-1}; as discussed in Section 10.4.1), confirming the high resistance of $CoFe_2O_4$/MGNC to the leaching of Fe species. Regarding the leaching of Co species, the lowest value was obtained in the first CWPO cycle (0.58 mg L^{-1}), while the highest value was obtained in the third cycle (4.55 mg L^{-1}). The leaching of Co species in the remaining cycles was in the range 1.92 – 2.64 mg L^{-1}, the lowest value being obtained after the fifth cycle. These results suggest that Co species are more susceptible to undergo leaching from the catalyst to the treated waters than Fe species, which is in line with the

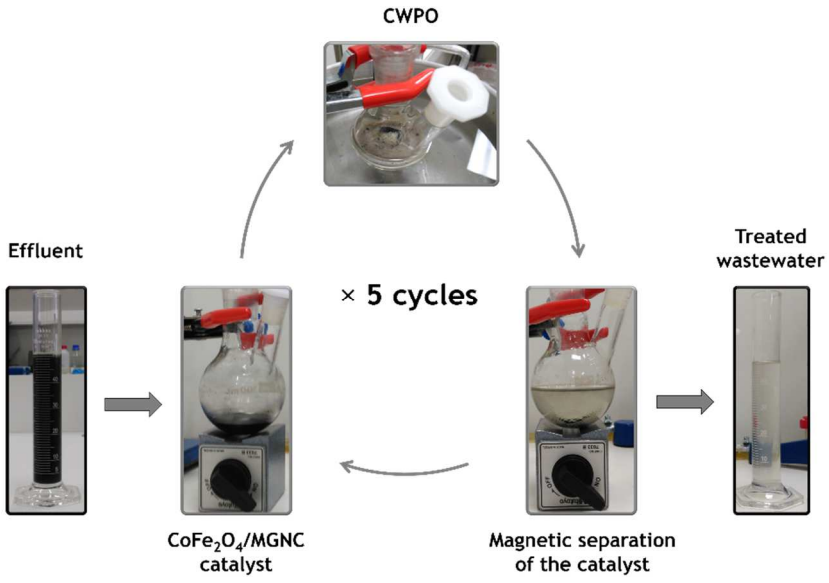

Figure 10.7. Experimental procedure during the CWPO reusability cycles performed with the liquid effluent collected from a MBT plant and $CoFe_2O_4$/MGNC.

results previously reported on the application of bimetallic iron-cobalt magnetic carbon xerogels in CWPO (*cf.* Chapter 7).

10.5. Conclusions

The ability of the developed catalytic system - resulting from the inclusion of $CoFe_2O_4$ into a graphitic structure during the synthesis of $CoFe_2O_4$/MGNC, to enable the treatment of the liquid effluent from a MBT plant for MSW by CWPO —in spite of its very high concentration of chlorides and bicarbonates, and in a wide range of operating pH— opens future prospects for the applicability of this wastewater treatment technology. A magnetic separation system was developed for the *in-situ* recovery of $CoFe_2O_4$/MGNC after the CWPO reaction stage. A series of five CWPO reaction/separation sequential experiments performed in the same vessel with consecutive catalyst reuse allowed to conclude about the high stability of $CoFe_2O_4$/MGNC for CWPO applications.

10.6. Experimental details

Unless stated otherwise, the CWPO experiments reported in Chapter 10 were performed under the conditions detailed in Table 10.2.

10.6.1. Liquid effluent from a mechanical biological treatment plant for municipal solid waste

The liquid effluent used in this Chapter was collected from a MBT plant for MSW located in Northern Portugal. The liquid effluent, whose properties are summarized in Table 10.3, gathers all the wastewater produced in the plant (mainly composed by a mechanical unit for

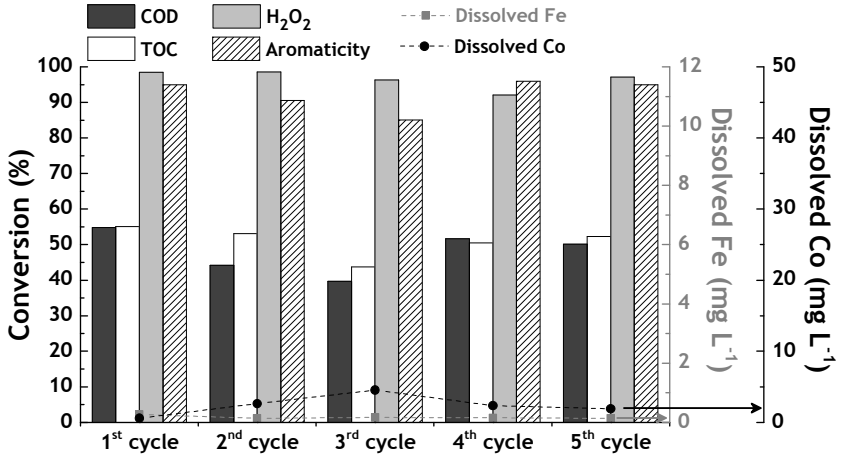

Figure 10.8. 4-NP, COD, TOC and H_2O_2 conversions obtained after 24 h in a series of five CWPO runs performed with consecutive reuse of $CoFe_2O_4$/MGNC (bars/left axis), and respective dissolved iron (squares/right axis) and cobalt (circles/right axis). Experiments performed with [$CoFe_2O_4$/MGNC] = 0.5 g L^{-1}, $[H_2O_2]_0$ = 27.7 g L^{-1}, T = 80 ºC and pH = 6.

Table 10.2. Experimental details of the CWPO experiments reported in Chapter 10

Aqueous model system	Reactor/solution volume	Operating conditions	H_2O_2 stoichiometric ratio[a]	[Pollutant]/ [catalyst]
4-nitrophenol (5.0 g L^{-1})	100 mL/ 50 mL	[Catalyst] = 0.5 g L^{-1} $[H_2O_2]_0$ = 17.8 g L^{-1} T = 80 ºC; pH_0 = 3 t = 8 h	1	10
Liquid effluent from the MBT plant for MSW	100 mL/ 50 mL	[Catalyst] = 0.5 g L^{-1} $[H_2O_2]_0$ = 27.7 g L^{-1} T = 80 ºC; pH_0 = 6 t = 24 h	1	Not applicable

[a] Obtained by dividing the amount of H_2O_2 employed by the stoichiometric amount needed for the complete mineralization of the pollutant considered; in the case of the liquid effluent from the MBT plant for MSW, this ratio was estimated based on the stoichiometric amount theoretically needed to reduce the effluent COD and to neutralize the $HO^{\bullet}$ radical scavenging effect promoted by the chlorides dissolved in the effluent, as described by Eqs. 10.2 and 10.3.

residue sorting, followed by an anaerobic digestion unit for biogas production from the organic fraction of the MSW). The liquid effluent was filtered (analytical filter paper, 25 μm) prior to its use in this work, in order to remove the suspended solids that would interfere in subsequent treatment and analytical steps.

10.6.2. Reusability cycles implementing *in-situ* magnetic separation for catalyst recovery

The *in-situ* magnetic separation of the catalyst was performed after the reaction stage, by coupling a Mitutoyo 7033B switchable magnetic stand (clamping force 600 N) with the glass reactor used for CWPO. Briefly, the magnetic separation device is composed by four parts: a non-ferrous metal spacer placed between two plates or iron, and the magnet at the centre; when the magnet poles are aligned with the ferrous plates the magnetic stand is ON, whereas the magnetic stand is OFF when the magnet poles are aligned with the non-ferrous spacer. When the round bottom glass reactor was placed on the magnetic separation device, it was immediately switched ON and the magnetic separation was allowed to proceed during 5 min. Afterwards, the treated water was collected with a pipette. In order to evaluate the stability of the $CoFe_2O_4$/MGNC catalyst in the CWPO of the liquid effluent from the MBT plant, reusability cycles were performed as described: after each run, *in-situ* magnetic separation was employed for catalyst recovery and the treated water was collected. Afterwards, 23 wt.% of the initial catalyst load was added (i.e., 0.115 g L^{-1}; corresponding to the mass fraction lost due to the sampling procedure and to the treated water collection) in order to ensure equal catalyst dosage throughout all the reusability cycles (0.5 g L^{-1}), and the catalyst was reused in CWPO upon the addition of fresh liquid effluent.

Table 10.3. Characterization of the liquid effluent from the MBT plant for MSW located in Northern Portugal, as determined in triplicate measurements

Parameter	Value	Units
Chemical oxygen demand (COD)	9206 ± 284	mg L^{-1}
Biochemical oxygen demand (BOD_5)	1933 ± 153	mg L^{-1}
Total organic carbon (TOC)	2046 ± 16	mg L^{-1}
Chlorides	2833 ± 14	mg L^{-1}
pH at 25 ºC	8.20 ± 0.01	Sørensen scale
Total Fe content	6.4 ± 0.1	mg L^{-1}
Dissolved Co content	0.12 ± 0.01	mg L^{-1}
Total heterotrophic bacteria cultivable at 28 ºC	14.7 ± 2.1	× 10^4 CFU mL^{-1}
Conductivity[a]	23933 ± 4554	µS cm^{-1}
Bicarbonates[a]	14350 ± 50	mg L^{-1}
Ammonia nitrogen[a]	2300 ± 285	mg L^{-1}
Total hydrocarbons[a]	4 ± 1	mg L^{-1}

[a] As determined in quarterly analysis provided by the intermunicipal company.

References

[1] M. Ragazzi, P. Tosi, E.C. Rada, V. Torretta, M. Schiavon, Effluents from MBT plants: plasma techniques for the treatment of VOCs, Waste Manage. 34 (2014) 2400-2406.

[2] J. Fang, H. Zhang, N. Yang, L. Shao, P. He, Gaseous pollutants emitted from a mechanical biological treatment plant for municipal solid waste: odor assessment and photochemical reactivity, J. Air Waste Manage. Assoc. 63 (2013) 1287-1297.

[3] Mechanical biological treatment of municipal solid waste, Department for Environment, Food & Rural Affairs, London, 2013.

[4] H. Shahriari, M. Warith, M. Hamoda, K.J. Kennedy, Anaerobic digestion of organic fraction of municipal solid waste combining two pretreatment modalities, high temperature microwave and hydrogen peroxide, Waste Manage. 32 (2012) 41-52.

[5] D. Weichgrebe, S. Maerker, T. Böning, H. Stegemann, Intended process water management concept for the mechanical biological treatment of municipal solid waste, Water Sci. Eng. 1 (2008) 78-88.

[6] M. Kosmulski, The pH dependent surface charging and points of zero charge. VI. Update, J. Colloid Interface Sci. 426 (2014) 209-212.

[7] M. Kosmulski, pH-dependent surface charging and points of zero charge. IV. Update and new approach, J. Colloid Interface Sci. 337 (2009) 439-448.

[8] E.P. Agency, Parameters of water quality: interpretation and standards, Environmental Protection Agency, Ireland, Wexford, Ireland, 2001.

[9] A. Aguinaco, J.P. Pocostales, J.F. García-Araya, F.J. Beltrán, Decomposition of hydrogen peroxide in the presence of activated carbons with different characteristics, J. Chem. Technol. Biotechnol. 86 (2011) 595-600.

[10] W.H. Glaze, J.-W. Kang, D.H. Chapin, The chemistry of water treatment processes involving ozone, hydrogen peroxide and ultraviolet radiation, Ozone Sci. Eng. 9 (1987) 335-352.

[11] G. Tchobanoglous, F.L. Burton, H.D. Stensel, Wastewater engineering: treatment and reuse, 4th ed., International Edition, Metcalf & Eddy, Inc., McGraw-Hill companies, New York, 2003.

[12] S. Parsons, Advanced oxidation processes for water and wastewater treatment, IWA Publishing, London, UK, 2004.

[13] J. De Laat, T.G. Le, Effects of chloride ions on the iron(III)-catalyzed decomposition of hydrogen peroxide and on the efficiency of the Fenton-like oxidation process, Appl. Catal. B 66 (2006) 137-146.

[14] D.R. Lide, CRC Handbook of Chemistry and Physics, 84th ed., CRC Press, Boca Raton, 2003.

[15] F.K. Attiogbe, W. Wang, A. McNeillie, R.C. Francis, The peroxymonocarbonate anions as pulp bleaching agents. Part 2. Mechanical pulp brightening and effects of metal ions, Bioresources 5 (2010) 2221-2231.

[16] C.H. Atwood, Survival guide for introductory chemistry, 1st ed., Brooks/Cole Cengage Learning, Belmont, CA, 2009.

[17] C.-H. Liao, S.-F. Kang, F.-A. Wu, Hydroxyl radical scavenging role of chloride and bicarbonate ions in the H_2O_2/UV process, Chemosphere 44 (2001) 1193-1200.

[18] M.J. Allen, S.C. Edberg, D.J. Reasoner, Heterotrophic plate count bacteria - what is their significance in drinking water?, Int. J. Food Microbiol. 92 (2004) 265-274.

[19] J. Bartram, J. Cotruvo, M. Exner, C. Fricker, A. Glasmacher, Heterotrophic plate counts and drinking-water safety: the significance of HPCs for water quality and the human health, Published on behalf of World Health Organization (WHO) by IWA Publishing, London, 2003.

[20] D.J. Reasoner, Heterotrophic plate count methodology in the United States, Int. J. Food Microbiol. 92 (2004) 307-315.

FINAL REMARKS

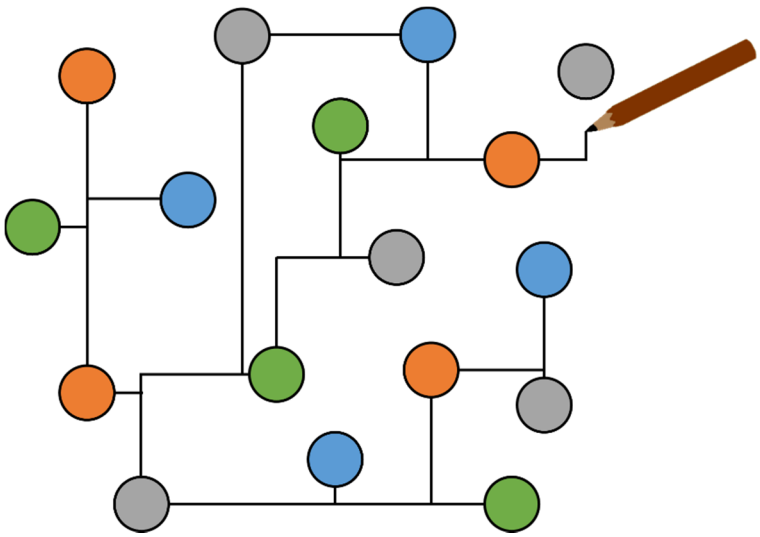

This work is about the application of chemical sciences and engineering to the design of hybrid magnetic carbon nanocomposites as catalysts for wet peroxide oxidation process. New insights into how the properties of carbon materials affect their performance in CWPO are gained in Chapters 5 and 6. In addition, the benefits of operating CWPO under intensified conditions (i.e., with higher pollutant concentrations, lower catalyst loads and stoichiometric amounts of H_2O_2, which may be potentially more attractive for industrial applications) became evident in terms of efficiency of catalyst usage and H_2O_2 consumption. The contribution of Chapters 5 and 6 towards this Ph.D. dissertation is of utmost importance. Although the overall performance of metal-free carbon materials in CWPO is significantly lower than that of the hybrid magnetic carbon nanocomposites (average pollutant mass removal rates in the range 53.9 – 67.6 mg g^{-1} h^{-1}, whereas values as high as 5000 mg g^{-1} h^{-1} were obtained with the metal-containing materials), the latter were prepared based on the assumptions that they were required to possess a well-developed porosity and a non-acidic overall surface charge. This is reflected by the S_{BET} (in the range 330 – 580 m^2 g^{-1}) and pH_{PZC} (6.6 – 9.0) of the hybrid materials reported in this Ph.D. dissertation. In addition, the experiments performed in the subsequent chapters were carried out with high pollutant/catalyst mass ratios, in the range 2 – 10, in order to increase the coverage of the catalyst surface by the pollutant molecules. Chapter 9 is an exception in this regard, since it reports the case-study on the removal of a micropollutant of emerging concern by CWPO, performed at the University of Patras under the framework of COST Action ES1403: NEREUS (as detailed in Chapter 1).

It should be noted that 2-nitrophenol (2-NP) was initially employed as model pollutant in Chapter 5, whereas 4-nitrophenol (4-NP) was used afterwards. Both these aqueous model systems are suitable for the preliminary evaluation of a given catalytic system, as detailed in Section 2.3. However, the higher solubility of 4-NP (*cf.* Table 2.5) enabled the preparation of solutions with higher concentrations, up to 5 g L^{-1}. Therefore, 4-NP aqueous model systems were selected for the subsequent studies.

The individual effects of the metal species employed in carbon embedded magnetic composites were studied in Chapter 7. For that purpose, three magnetic carbon xerogels were prepared by inclusion of iron and/or cobalt precursors during the sol-gel polymerization of resorcinol and formaldehyde, followed by thermal annealing.

In Chapter 8, a hybrid magnetic graphitic nanocomposite —composed by a magnetite core and a graphitic shell (Fe_3O_4/MGNC)—, was synthesized by hierarchical co-assembly of magnetite nanoparticles and carbon precursors, followed by thermal annealing.

Chapter 9 is an exception within the trend reported in these studies towards the application of CWPO under intensified conditions. In this case-study performed at the

University of Patras (*cf.* Chapter 1), the ability of CWPO for the degradation of an antimicrobial agent typically found throughout the urban water cycle —sulfamethoxazole (SMX)—, was evaluated using the magnetic carbon xerogels developed in Chapter 7.

The findings reported in Chapters 7 and 8 enabled the design of a high-performance hybrid magnetic graphitic nanocomposite —composed by a cobalt ferrite core and a graphitic shell ($CoFe_2O_4$/MGNC). In chapter 10, this new generation catalyst was used in order to evaluate the ability of CWPO for the treatment of the liquid effluent from a mechanical biological treatment plant for municipal solid waste.

CONCLUSIONS AND FUTURE WORK

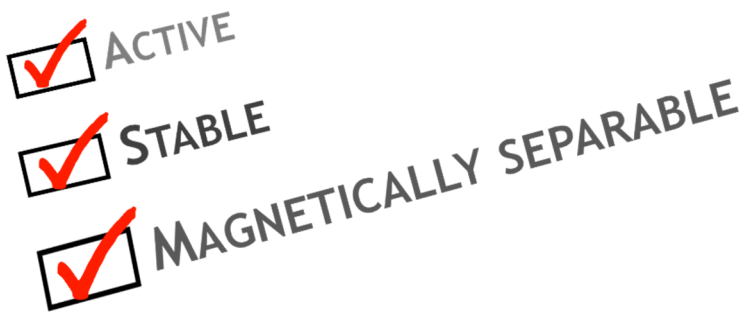

The importance of the balance between textural and surface chemistry properties of carbon-based catalysts for CWPO was demonstrated for the design and development of glycerol-based carbon materials (Chapter 5). Specifically, it was concluded that:

- the adequate development of porosity is crucial when designing efficient carbon-based catalysts for CWPO, as it enables increased adsorptive interactions between the pollutant molecules and the carbon surface;
- the presence of oxygen-containing acidic functionalities hinders the catalytic activity for the decomposition of H_2O_2 via $HO^{\bullet}$ radicals formation.

Regarding the graphene-based carbon materials (Chapter 6), the number of defects in the structure of reduced graphene oxides was related with enhanced H_2O_2 decomposition:

- It was shown that higher concentration of $HO^{\bullet}$ radicals does not necessarily leads to higher efficiency of the CWPO process —indeed, it can lead to a higher rate of non-efficient parasitic reactions occurring in the bulk;
- On the contrary, it was shown that higher pollutant concentrations at the surface of the catalysts enables a more intimate contact between the recently formed $HO^{\bullet}$ radicals and the pollutant, which promotes a more efficient use of the $HO^{\bullet}$ radicals formed nearby the adsorbed molecules, leading to further oxidation and thus increasing the efficiency of H_2O_2 consumption.

These observations highlight the relevance of adsorptive interactions between the pollutant molecules and the surface of carbon-based catalysts when seeking for highly efficient CWPO applications. In addition, a reaction mechanism was proposed for the CWPO of 4-NP.

The performance of three magnetic carbon xerogels was evaluated in Chapter 7. The bimetallic magnetic carbon xerogel catalyst (CX/CoFe) was more active than each of the monometallic catalysts (CX/Fe or CX/Co). This better performance in CWPO was explained in terms of a synergic association of factors arising from the simultaneous incorporation of cobalt and iron into carbon frameworks, as a result of:

- the enhanced accessibility to the active iron species existing at the surface of the catalyst;
- the ability of metallic Co species to catalyse the decomposition of H_2O_2 via $HO^{\bullet}$ radicals formation;
- the more efficient reduction of Fe^{3+} to Fe^{2+} promoted by metallic Co species existing at the surface of CX/CoFe.

The application of the developed carbon encapsulated magnetic composite (Fe_3O_4/MGNC) in CWPO allowed to conclude about the role of the carbon shell (Chapter 8). Specifically, it was shown that the encapsulation of magnetite nanoparticles within carbon frameworks has two effects:

- enhances the catalytic activity in CWPO when compared to bare magnetite;
- strongly prevents the leaching of iron species to the treated water.

The first effect was ascribed to the increased adsorptive interactions between the carbon phase and the pollutant molecules. The lower metal leaching obtained with the nanocomposite catalyst was ascribed to the confinement effect promoted by the carbon shell. As a result of these positive effects, very high pollutant mass removals were obtained with a rather high efficiency of H_2O_2 consumption, and the composite catalyst was active for operating pH in the range 3 – 6.

The ability of CWPO for the elimination of SMX in secondary treated wastewater and drinking water was shown in Chapter 9. Nevertheless, it was found that the performance of the treatment decreases when applied to more complex water and wastewater samples. In addition, an *in-situ* magnetic separation procedure was applied for catalyst recovery and reuse.

A high-performance hybrid magnetic graphitic nanocomposite was prepared by inclusion of $CoFe_2O_4$ into a graphitic structure ($CoFe_2O_4$/MGNC), as described in Chapter 10. In this way, the positive effects listed under the conclusions of Chapters 7 and 8 were potentially combined in the same nanocomposite material (except for the enhanced accessibility to the active iron species). It was found that the application of this new generation catalyst enables the treatment of waste waters with high pollutant loads, such as that from the MBT plant considered in this chapter. The biodegradability of the wastewater was enhanced during the treatment performed at pH = 6, regardless of its high organic and inorganic content; disinfection was achieved and the treated water revealed no toxicity against selected bacteria. In addition, a magnetic separation system was developed for the *in-situ* recovery of the $CoFe_2O_4$/MGNC catalyst after the CWPO reaction stage. The high stability of $CoFe_2O_4$/MGNC for CWPO was then demonstrated in a series of five CWPO reaction/magnetic separation sequential experiments performed in the same vessel.

Bearing this in mind, the conducted studies demonstrate the adequacy of CWPO as a water treatment technology for the elimination of bio-recalcitrant pollutants in aqueous phase. A detailed catalyst design, based on the understanding of the surface reactions and

interactions involved in the whole process, has allowed the development of hybrid magnetic carbon nanocomposites with increasingly improved activity and stability features for CWPO. Operating CWPO under intensified conditions (i.e., with higher pollutant concentrations, lower catalyst loads and stoichiometric amounts of H_2O_2) has enabled achieving high efficiency of H_2O_2 consumption throughout the treatment processes. The application of the developed catalytic systems has also allowed the treatment of waste waters at near-neutral operating pH. This approach was a step forward towards the treatment of a real industrial wastewater with high pollutant load —collected from a MBT plant for MSW.

The proper understanding of how the efficiency of this treatment technology is affected by the catalyst properties and the operating conditions is fundamental in order to design materials with potential to be an effective tool for real-scale CWPO applications. Nevertheless, as in all fields of nanomaterials application, large-scale production is still a major challenge. Studies on large-scale production of hybrid magnetic carbon nanocomposites for application in CWPO processes have never been reported in the literature. Therefore, possible limitations on reproducibility of the characteristics of these novel materials should be addressed in future works, in order to evaluate the feasibility of its large-scale use. However, much is yet to be done in order to move on from the design of materials with potential to be an effective tool for real-scale CWPO applications towards effective real-scale CWPO applications. The strategy herein proposed would ultimately allow producing materials in sufficient quantities to study the performance of CWPO in more realistic conditions. Once the legal requirements established by Municipal regulations for the discharge of industrial waste waters into the municipal wastewater collection system are met, the by-products formed during CWPO and, specially, the biodegradability (in subsequent conventional treatment plants for municipal waste waters) of the treated industrial waters should be thoroughly evaluated. Afterwards, the impact of the final water discharge on Flora, Fauna and Human health should also be addressed, including both the study of toxicity and proliferation of antibiotic resistant bacteria and/or resistance genes (ARB&ARG).

APPENDICES

Supplementary information to this Ph.D. dissertation is provided in the Appendices:

- A full list of the reagents used in this work is provided in Appendix A;

- In Appendix B, the research article published on the development and validation of the HPLC methods used for the determination of the 4-NP parent compound and its possible oxidation by-products is entirely reproduced in portable document format (pdf);

- Supplementary material to this Ph.D. dissertation is provided in Appendix C;

- Detailed lists of publications in peer reviewed journals and communications in scientific meetings directly related with the present Ph.D. dissertation are given in Appendices D and E, respectively.

A. REAGENTS

The main charactheristics of the chemicals used throughout this work are listed in Table A.1. All chemicals were used as received, without further purification. Distilled water was used throughout the work. Gases with high purity were used in all the procudures.

Table A.1. Main characteristics of the reagents used during the Ph.D. studies

Task	Reagent description	CAS registry number	Purity	Supplier
Synthesis of glycerol-based carbon materials	Glycerol	56-81-5	99 wt.%	Alfa Aesar
	Sulphuric acid	7664-93-9	95 wt.%	Fisher Chemical
Synthesis of graphene-based materials	Sulphuric acid	7664-93-9	96 wt.%	Riedel-de-Haën
	Potassium permanganate	7722-64-7	99 wt.%	Merck
	Hydrogen peroxide	7722-84-1	30% w/v	Fluka
	Hydrochloric acid	7647-01-0	37 wt.%	Sigma-Aldrich
	L-ascorbic acid	50-81-7	99 wt.%	Sigma-Aldrich
	D-(+)-glucose	50-99-7	99.5 wt.%	Sigma-Aldrich
	Hydrazine hydrate	10217-52-4	50 wt.%	Sigma-Aldrich
	Ammonia solution	1336-21-6	25 wt.%	Riedel-de Haën
Synthesis of magnetic carbon xerogels	Resorcinol	108-46-3	99 wt.%	Fisher Chemical
	Formaldehyde solution[a]	50-00-0	37 wt.%	Panreac
	Sodium hydroxide	1310-73-2	98.7 wt.%	Fisher Chemical
	Iron (III) chloride hexahydrate	10025-77-1	97 wt.%	Panreac
	Cobalt (II) chloride hexahydrate	7791-13-1	99 wt.%	Fisher Chemical
	Hydrochloric acid	7647-01-0	37 wt.%	Fisher Chemical
Synthesis of magnetic nanoparticles	Iron (II) chloride tetrahydrate	13478-10-9	99 wt.%	Sigma-Aldrich
	Iron (III) chloride hexahydrate	10025-77-1	97 wt.%	Panreac
	Ammonia solution	1336-21-6	25 wt.%	Panreac
	Cobalt (II) chloride hexahydrate	7791-13-1	99 wt.%	Fisher Chemical
	Ethanol absolute	64-17-5	99.99 wt.%	Fisher Chemical
Synthesis of magnetic graphitic nanocomposites	Copolymer pluronic F127	9003-11-6	Unavailable	Sigma-Aldrich
	Phenol	108-95-2	99.5 wt.%	Panreac
	Formaldehyde solution[a]	50-00-0	37 wt.%	Panreac
	Sodium hydroxide	1310-73-2	98.7 wt.%	Fisher Chemical
	Hydrochloric acid	7647-01-0	37 wt.%	Fisher Chemical
Determination of pH_{PZC}	Hydrochloric acid	7647-01-0	37 wt.%	Fisher Chemical
	Sodium hydroxide	1310-73-2	98.7 wt.%	Fisher Chemical
	Sodium chloride	647-14-5	99.8 wt.%	Sigma-Aldrich
Concentration of acidic and basic sites	Hydrochloric acid	7647-01-0	37 wt.%	Sigma-Aldrich
	Sodium hydroxide	1310-73-2	98 wt.%	Panreac
	Phenolphthalein	77-09-8	99 wt.%	Panreac
CWPO experiments[b]	4-nitrophenol	100-02-7	99 wt.%	Acros Organics
	2-nitrophenol	88-75-5	98 wt.%	Sigma-Aldrich
	Sulphuric acid	7664-93-9	95 wt.%	Fisher Chemical
	Sodium hydroxide	1310-73-2	98.7 wt.%	Fisher Chemical
	Hydrogen peroxide	7722-84-1	30% w/v	Fluka
Determination of 4-NP and oxidation by-products (and 2-NP)	Acetic acid	64-19-7	99.8 wt.%	Fisher Chemical
	Methanol	67-56-1	99.99 wt.%	Fisher Chemical
	Acetonitrile	75-05-8	99.99 wt.%	Fisher Chemical
	Sulphuric acid	7664-93-9	98 wt.%	LabKem

[a] In water, stabilized with 15 wt.% methanol; [b] except Chapter 9; n/a = not applicable.

Table A.1 (cont.). Main characteristics of the reagents used during the Ph.D. studies

Task	Reagent description	CAS registry number	Purity	Supplier
Determination of sulfamethoxazole	Acetonitrile	75-05-8	99.9 wt.%	Sigma-Aldrich
Determination of hydrogen peroxide[b]	Titanium (IV) oxysulfate in dilute sulphuric acid	13825-74-6	15 wt.%	Sigma-Aldrich
	Sulphuric acid	7664-93-9	95 wt.%	Fisher Chemical
Determination of COD	Mercury (II) sulphate	7783-35-9	99 wt.%	Panreac
	Potassium dichromate	7778-50-9	99.5 wt.%	Panreac
	Silver sulphate	10294-26-5	95 wt.%	Fisher Chemical
	Sulphuric acid	7664-93-9	95 wt.%	Fisher Chemical
Determination of BOD_5	Sodium hydroxide	1310-73-2	98.73 wt.%	Fisher Chemical
Dissolved iron content	1,10-phenantroline	5144-89-8	99 wt.%	Panreac
	L-ascorbic acid	50-81-7	99 wt.%	Fisher Chemical
	Ammonium acetate	631-61-8	98 wt.%	Pronalab
	Acetic acid	64-19-7	99.8 wt.%	Fisher Chemical
Microbiological assays	Plate count agar (PCA)	n/a	n/a	Liofilchem
	Muller Hinton agar (MHA)	n/a	n/a	Liofilchem
	Nutrient broth (NB)	n/a	n/a	Liofilchem
Sampling	Sodium sulphite	7757-83-7	98 wt.%	Panreac
	Methanol	67-56-1	99.9 wt.%	Fluka
Chapter 9	Sulfamethoxazole	723-46-6	Analytical standard	Sigma-Aldrich
	hydrogen peroxide	7722-84-1	30 wt.%	Sigma-Aldrich
	Acetic acid	64-19-7	99.8 wt.%	Sigma-Aldrich
	Humic acid	1415-93-6	Technical grade	Sigma-Aldrich
	Sodium bicarbonate	144-55-8	99.7 wt.%	Sigma-Aldrich
	Sodium chloride	7647-14-5	99.8 wt.%	Sigma-Aldrich
	Sodium hydroxide	1310-73-2	98 wt.%	Sigma-Aldrich
	Sodium sulphate	7757-82-6	99 wt.%	Sigma-Aldrich
	Sodium sulphite	7757-83-7	98 wt.%	Sigma-Aldrich
	Sulphuric acid	7664-93-9	95 wt.%	Sigma-Aldrich
	tert-Butanol	75-65-0	99 wt.%	Fluka
	L-ascorbic acid	50-81-7	99 wt.%	Chem-Lab NV
	1,10-phenantroline	5144-89-8	99 wt.%	Serva
	Ammonium acetate	631-61-8	98 wt.%	Penta Chemicals

[a] In water, stabilized with 15 wt.% methanol; [b] except Chapter 9; n/a = not applicable.

B. HIGH-PERFORMANCE LIQUID CHROMATOGRAPHY AS A TOOL TO EVALUATE THE PERFORMANCE OF THE CATALYTIC WET PEROXIDE OXIDATION OF 4-NITROPHENOL: PRE-VALIDATION OF ANALYTICAL METHODS

Rui S. Ribeiro, Adrián M.T. Silva, Helder T. Gomes, Joaquim L. Faria, High-performance liquid chromatography as a tool to evaluate the performance of the catalytic wet peroxide oxidation of 4-nitrophenol: pre-validation of analytical methods, U.Porto Journal of Engineering 1 (2015) 50-66
http://journalengineering.fe.up.pt/article/view/112

U.Porto Journal of Engineering, 1:1 (2015) 50-66
ISSN

Received: 23 January, 2015
Accepted: 14 February, 2015
Published: 1 October, 2015

High-performance liquid chromatography as a tool to evaluate the performance of the catalytic wet peroxide oxidation of 4-nitrophenol: pre-validation of analytical methods

Rui S. Ribeiro[1], Adrián M. T. Silva[2], Helder T. Gomes[3], Joaquim L. Faria[4]

[1]LCM - Laboratory of Catalysis and Materials - Associate Laboratory LSRE-LCM, Department of Chemical and Biological Technology, School of Technology and Management, Polytechnic Institute of Bragança, Campus de Santa Apolónia, 5300-857 Bragança, Portugal (rui.ribeiro@ipb.pt); [2]LCM - Laboratory of Catalysis and Materials - Associate Laboratory LSRE-LCM, Departamento de Engenharia Química, Faculdade de Engenharia da Universidade do Porto, Rua Dr. Roberto Frias, 4200-465 Porto, Portugal (adrian@fe.up.pt); [3]LCM - Laboratory of Catalysis and Materials - Associate Laboratory LSRE-LCM, Department of Chemical and Biological Technology, School of Technology and Management, Polytechnic Institute of Bragança, Campus de Santa Apolónia, 5300-857 Bragança (htgomes@ipb.pt); [4]LCM - Laboratory of Catalysis and Materials - Associate Laboratory LSRE-LCM, Departamento de Engenharia Química, Faculdade de Engenharia da Universidade do Porto, Rua Dr. Roberto Frias, 4200-465 Porto, Portugal (jlfaria@fe.up.pt)

Abstract

A high-performance liquid chromatography (HPLC) method capable to detect 4-nitrophenol (4-NP) in aqueous solutions with concentration in the range 0.0495-118.8 mg L-1 was developed and validated under the typical criteria for in-house pre-validations. Accordingly, linearity was demonstrated through the Fisher's exact probability test. Accuracy and precision were then assessed in three concentration levels over the linear range.

The reproducibility of the catalytic wet peroxide oxidation (CWPO) of 4-NP was evaluated together with the analytical error of 4-NP determination in independent experiments. In this case, the sum of both contributions to error never reached 3%.

Two multi-component HPLC methods were also developed for the determination of possible aromatic intermediates (hydroquinone, 1,4-benzoquinone, catechol, 4-nitrocatechol and phenol) and carboxylic acids (oxalic, formic, malic, malonic, acetic and maleic acids) resulting from the 4-NP degradation. The combination of these analytical methods already led to the proposal of an oxidation/mineralization mechanism for the CWPO of 4-NP.

Subject Headings. Chemical analysis, chromatography, water pollution.
Author Keywords. High-performance liquid chromatography (HPLC), catalytic wet peroxide oxidation (CWPO), 4-nitrophenol.

1. Introduction

Like other advanced oxidation processes, catalytic wet peroxide oxidation (CWPO) is a water treatment technology based on the in-situ generation of hydroxyl radicals ($HO^{\bullet}$) – very reactive species with high oxidizing potential (between +2.8 V and +2.0 V), known to be effective in the destruction of a huge range of organic pollutants (Gogate and Pandit 2004, Navalon, Alvaro and Garcia 2010). For that purpose, hydrogen peroxide (H_2O_2) is used as oxidation source, provided that a suitable catalyst is employed to decompose H_2O_2 into $HO^{\bullet}$ - according to a previously reported reaction mechanism (Ribeiro et al 2013a).

High-performance liquid chromatography as a tool to evaluate the performance of the catalytic wet peroxide oxidation of 4-nitrophenol
Rui S. Ribeiro, Adrián M.T. Silva, Helder T. Gomes, Joaquim L. Faria

In recent years, CWPO has been well established as a treatment option that is suitable for the degradation of a broad range of toxic and bio-recalcitrant pollutants in aqueous phase (Bautista et al 2010, Domínguez et al 2014b, Lücking et al 1998, Melero et al 2009, Neamţu et al 2004, Pinho et al 2015, Ramirez et al 2007a, Rey et al 2008, Ribeiro et al 2012, Ribeiro et al 2013b, Santos et al 2009, Taran et al 2010). Although several studies have been focused on the degradation of real industrial wastewaters (Bautista et al 2010, Domínguez et al 2014b, Melero et al 2009), most CWPO applications still deal with model pollutants such as dyes (Neamţu et al 2004, Ramirez et al 2007b, Ribeiro et al 2012, Santos et al 2009), phenol (Pinho et al 2015, Rey et al 2008, Taran et al 2010) or other phenolic compounds (Lücking et al 1998, Ribeiro et al 2013b, Ribeiro et al 2015a). Typically, real effluents are complex mixtures of several compounds; therefore, generic (lumped) parameters such as chemical oxygen demand (COD) and/or total organic carbon (TOC) are usually determined in order to assess the efficiency of the CWPO treatment process (Bautista et al 2010, Domínguez et al 2014b, Melero et al 2009). On the other hand, model pollutants are usually prepared by dissolution of the target compound in water; in this case, to monitor the concentration of the model pollutant during the CWPO experiments, very specific analytical methods are required (Lücking et al 1998, Neamţu et al 2004, Pinho et al 2015, Ramirez et al 2007b, Rey et al 2008, Ribeiro et al 2012, Ribeiro et al 2013b, Santos et al 2009, Taran et al 2010). For that purpose, dyes have been usually determined by UV-Vis spectrophotometry (Neamţu et al 2004, Ramirez et al 2007b, Ribeiro et al 2012, Santos et al 2009), whereas high-performance liquid chromatography (HPLC) has been found as the most suitable analytical technique for the determination of phenol or phenolic compounds (Pinho et al 2015, Rey et al 2008, Ribeiro et al 2013b, Taran et al 2010).

In addition to the determination of the model compounds, HPLC techniques have been also used successfully in several works for the identification and quantification of reaction intermediates and by-products resulting from the degradation of the model pollutants by CWPO, allowing the identification of the oxidation/mineralization mechanisms that are involved in these processes (Domínguez et al 2013, 2014a, Inchaurrondo et al 2012, Rey et al 2008, Ribeiro et al 2015a).

The main goal of the present work is the development of a single-component HPLC analytical method suitable for the determination of 4-nitrophenol (4-NP), a compound chosen as model pollutant for the screening of new catalysts for CWPO. Once validated, this single-component method will allow to follow the 4-NP abatement during the CWPO experiments.

Furthermore, to perform the identification and quantification of reaction intermediates and by-products resulting from the degradation of 4-NP by CWPO, two other multi-component HPLC analytical methods were developed. Specifically, one of these multi-component methods is devoted to the determination of possible aromatic intermediates (i.e., hydroquinone, 1,4-benzoquinone, catechol, 4-nitrocatechol and phenol), whereas the other is focused on the determination of carboxylic acids (i.e., oxalic, formic, malic, malonic, acetic and maleic acids). Once validated, these multi-component methods allow the identification of the oxidation/mineralization mechanisms involved in the CWPO of 4-NP. Finally, in order to assess reproducibility and error of the 4-NP determinations in real applications, a suitable catalyst was synthesized and used in three consecutive CWPO runs.

2. Materials and Methods

2.1. Chemicals

Catechol (99 wt.%), 4-nitrocatechol (98 wt.%), D-(+)-malic acid (99 wt.%), maleic acid (99 wt.%), sulfuric acid (H_2SO_4, 95–97 wt.%) and hydrogen peroxide (H_2O_2, 30% w/v) were obtained from Fluka. 4-nitrophenol (4-NP, 99 wt.%) and 1,4-benzoquinone (99 wt.%) were purchased from Acros Organics. Phenol (99.5 wt.%), formic acid (98 wt.%) and sodium hydroxide (NaOH, 98 wt.%) were obtained from Panreac. Hydrochloric acid (HCl, 37 wt.%), oxalic acid (99 wt.%) and malonic acid (99 wt.%) were purchased from Sigma-Aldrich and hydroquinone (99 wt.%) was obtained from Merck. Methanol (HPLC grade, 99.99 wt.%), glacial acetic acid (99.83 wt.%) and acetonitrile (HPLC grade, 99.99 wt.%) were obtained from Fisher Chemical.

All chemicals were used as received without further purification. Distilled water was used throughout the work.

2.2. Standards

The experimental work required for the development and validation of the analytical methods was performed using standard samples (Std.) with previously known concentrations. All the Std. were prepared considering the purity of each compound (cf. Section 2.1) and injected in triplicate. The accurate concentration of each Std. is given in Table 1.

2.3. Analytical methods

UV-Vis absorption spectra were obtained using a T70 Spectrophotometer (PG Instruments, Ltd.) in the wavelength range of 200-660 nm, with a scan interval of 1 nm.

The amount of 4-NP was determined by HPLC, adapting the procedure described elsewhere (Apolinário et al 2008). For that purpose, a Jasco HPLC system equipped with an UV-Vis detector (UV-2075 Plus), a quaternary gradient pump (PU-2089 Plus) for solvent delivery (1 mL min^{-1}) and a Kromasil 100-5-C18 column (15 cm x 4.6 mm; 5 μm particle size; reversed-phase) was employed. Mobile phase consisted in an isocratic method of A:B (40:60) mixture of 3% acetic acid and 1% acetonitrile in methanol (A) and 3% acetic acid in ultrapure water (B). The 4-NP absorbance peaked at 318 nm, as determined from the corresponding UV-Vis absorption spectrum. Possible intermediates of 4-NP oxidation (e.g., hydroquinone, 1,4-benzoquinone, 4-nitrocatechol, catechol and phenol) were determined using the same system, the absorbance wavelength being adjusted to 277 nm.

The amount of the carboxylic acids (e.g., formic, acetic, oxalic, malonic, maleic and malic acids) was also determined using the same Jasco HPLC system, but in this case using an YMC – Triart C18 column (25 cm x 4.6 mm; 5 μm particle size; reversed-phase), adapting procedures reported elsewhere (Rocha et al 2011, Yang et al 2000). Mobile phase consisted in an isocratic method of A:B (95:5) mixture of 1% sulfuric acid in ultrapure water (A) and acetonitrile (B), delivered to the system at 0.6 mL min^{-1}. The UV/Vis detector was set to 210 nm.

2.4. Synthesis of the catalyst

The catalyst used in the CWPO experiments was prepared by polycondensation of resorcinol with formaldehyde (with a molar ratio of 1:2), adapting a procedure previously reported (Gomes et al 2008). Namely, 9.91 g of resorcinol were added to 18.8 mL of deionized water in a glass flask, to which a calculated mass of iron (III) chloride hexahydrate was added (Fe/resorcinol molar ratio of 0.05). After complete dissolution, 13.5 mL of formaldehyde solution were also added. In order to achieve the desired initial pH of the precursor solution (6.1), sodium hydroxide solution was added dropwise under continuous stirring and pH

monitoring. The gelation step was allowed to proceed at 85 °C during 3 days. After this period the gel was dried in oven during several days from 60 to 150 °C, defining a heating ramp of 20°C day^{-1}. After drying, the gel was calcined under a nitrogen flow (100 cm^3 min^{-1}) at 120, 400 and 600 °C during 60 min at each temperature and then at 800 °C for 240 min, defining a heating ramp of 2 °C min^{-1}. Finally, the calcined materials were washed with 1 L of deionized water at 50 °C under vacuum filtration, and then with 1 L of HCl solution (pH = 3), also at 50°C under vacuum filtration, being afterwards dried overnight in an oven at 60 °C, resulting in the material named CX/$Fe_{0.05}$.

Analyte	Std. concentration (mg L^{-1})							
	#1	#2	#3	#4	#5	#6	#7	#8
4-NP	0.0495[a]	19.8	39.6[b]	79.24	118.8[c]	-	-	
Hydroquinone	0.0449[a]	4.49	22.4	89.7[b]	179[c]	-	-	-
1,4-Benzoquinone	0.0892[a]	0.892	44.6	89.2[b]	178	357[c]	-	-
Catechol	0.0468	0.0936[a]	0.936	9.36	46.8	93.6[c]	-	-
4-Nitrocatechol	0.0445	0.0890[a]	8.90	44.5	89.0[b]	178	356[c]	-
Phenol	0.0456	0.0911[a]	0.911	9.11	45.6	91.1[c]	-	-
Oxalic acid	10.2[a]	20.3	40.7	81.4	163[c]	-	-	-
Formic acid	10.1[a]	20.2	40.3	80.7	161[b]	323[c]	-	-
Malic acid	20.7[a]	41.4	82.8	166	332[b]	663[c]	1327	-
Malonic acid	22.7[a]	45.5	182	364[b]	728[c]	1456	-	-
Acetic acid	13.5[a]	26.9	53.9	108	216[b]	431[c]	-	-
Maleic acid	0.0989	0.198[a]	0.989	1.98	3.96	7.92	15.8[b]	31.7[c]

Table 1: Concentration of the standard samples (Std.) used throughout the work. a, b and c Standards used in the validation studies: (a) low, (b) medium and (c) high concentration levels over the working range

2.5. CWPO experiments

Batch CWPO experiments were performed as previously described (Ribeiro et al 2015a), in a 250 mL well-stirred (600 rpm) glass reactor equipped with a condenser, a temperature measurement thermocouple, a pH measurement electrode and a sample collection port. The reactor was loaded with 50 mL of a 4-NP aqueous solution (5.0 g L^{-1}) and heated by immersion in an oil bath at controlled temperature. Upon stabilization at the desired temperature, the solution pH was adjusted to 3 by means of H_2SO_4 and NaOH solutions, and the experiments were allowed to proceed freely, without further pH adjustment. A calculated volume of H_2O_2 (30% w/v) was injected into the system, in order to reach the stoichiometric amount of H_2O_2 needed to completely mineralize 4-NP (17.8 g L^{-1}). The catalyst (CX/$Fe_{0.05}$, cf. Section 2.4) was added after complete homogenization of the resulting solution, that moment being considered as t_0 = 0 min. The experiments were conducted during 24 h, at T = 50 °C, pH = 3 and catalyst load = 2.5 g L^{-1}.

3. Acceptance criteria for methods validation

Based on a literature survey, acceptance criteria were established for each one of the parameters that were considered in this in-house validation (cf. Table 2). Individual expressions and requirements for each parameter are detailed in the next subsections.

It should be noted that the ruggedness of the analytical methods was not assessed since the experimental work was fully performed by the same operator and using the same equipment.

3.1. Accuracy

The difference between the true value (X_{true}) and the measured value ($X_{measured}$) was assessed through the analysis of bias values obtained as described in Eq. 1 (Taverniers, De Loose and Van Bockstaele 2004). The values of $X_{measured}$ were given by the average result obtained by

three replicate measurements of three samples over the working range, representing high, medium and low concentration levels (cf. Table 1), as typically required (Snyder, Kirkland and Glajch 1997, Taverniers, De Loose and Van Bockstaele 2004).

In the particular case of bias, the results obtained should be compared with a second validated reference method (Taverniers, De Loose and Van Bockstaele 2004). Therefore, since no validated reference methods were found, the acceptance criterion was established as 20%, i.e., the accuracy of the analytical method is accepted if the absolute value of bias is ≤ 20% (Peters and Maurer 2005, UNODC 2009, USEPA 1997).

$$\text{bias, \%} = \frac{(X_{measured} - X_{true})}{X_{true}} \times 100 \quad (1)$$

3.2. Precision

During the pre-validation of the methods, only repeatability precision and intermediate precision were assessed, since these are the levels of precision that are usually related to measurements performed within the same laboratory (Snyder, Kirkland and Glajch 1997, Taverniers, De Loose and Van Bockstaele 2004). Both levels of precision were expressed in terms of relative standard deviation (RSD, also known as coefficient of variation) of a data set, as usually performed (Snyder, Kirkland and Glajch 1997, Taverniers, De Loose and Van Bockstaele 2004). In repeatability precision (i.e., intra-run precision) conditions, three samples over the working range, representing high, medium and low concentration levels (cf. Table 1), were independently measured in triplicate assays during one day; in intermediate precision (i.e., inter-run precision) conditions, that same three samples were independently measured in triplicate assays during three consecutive days, as typically required (Snyder, Kirkland and Glajch 1997, Taverniers, De Loose and Van Bockstaele 2004). Afterwards, the RSD associated to repeatability precision (RSD_r) was obtained as described in Eq. 2, while RSD associated to intermediate precision (RSD_{int}) was obtained as described in Eq. 3 (Taverniers, De Loose and Van Bockstaele 2004). SD_r is the standard deviation (SD) obtained in repeatability precision conditions and SD_{int} is the SD obtained in intermediate precision conditions; $\tilde{X}$ is the average of the measured values.

$$RSD_r, \% = \frac{SD_r}{\tilde{X}} \times 100 \quad (2)$$

$$RSD_{int}, \% = \frac{SD_{int}}{\tilde{X}} \times 100 \quad (3)$$

Nowadays, the so-called Horwitz ratio (HorRat) is widely recognized as a suitable acceptance criterion for the evaluation of the precision of an analytical method, namely by several research groups (Brown and Yu 2013, Indyk et al 2014, Sasaki et al 2014) and organizations worldwide (Horwitz and Albert 2006, Latimer 2012). Specifically, the HorRat is a normalized performance parameter indicating the acceptability of the precision of an analytical method, which is obtained by the ratio between the observed RSD and the predicted relative standard deviation (PRSD) calculated from the Horwitz equation, as described in Eq. 4 (Horwitz and Albert 2006). PRSD is obtained as described in Eq. 5, where C is the concentration of a given analyte, expressed as a dimensionless mass fraction (Horwitz and Albert 2006, Latimer 2012).

$$\text{HorRat} = \frac{RSD}{PRSD} \quad (4)$$

$$PRSD = 2C^{-0.15} \quad (5)$$

Based on recommendations made by AOAC International - Association of Official Analytical Chemists, regarding standard method performance requirements, the optimum target for

HorRat values should be set to 0.5 in validations performed within the laboratory (Latimer 2012). Nevertheless, a broader acceptance criterion has been defined by the same organization considering HorRat values of 0.3 and 1.3 as the minimum and maximum acceptance values, respectively (Latimer 2012). Therefore, these values were used to set the HorRat acceptance criterion used in this work for repeatability precision ($HorRat_r$) and intermediate precision ($HorRat_{int}$).

Parameter	Requirement/ description
Accuracy	|bias| ≤ 20%
Precision	HorRat ≤ 1.3
Linearity	$P(H_{0,2nd}) > 0.05$
Range	Lower and upper analyte concentrations for which the analytical method has adequate accuracy, precision and linearity
LOD	Determined based on the average peak area of 10 independent blank samples, plus 3 times the corresponding standard deviation
LOQ	Determined based on the average peak area of 10 independent blank samples, plus 10 times the corresponding standard deviation

Table 2: Acceptance criteria considered in this work

3.3. Linearity and range

Statistical tests, such as the Lack-of-fit test, the Mandel's fitting test or the Fisher's exact test, are the more suitable options for the validation of a linear calibration model (Fisher 1934, Loco et al 2002). In this work, Fisher's exact probability test was used to assess the linearity of the calibration curves (Fisher 1934). Specifically, the data was adjusted to a second-degree polynomial model ($y = \beta_0 + \beta_1 x + \beta_2 x^2$), and then the statistical significance of the null value of the second-degree coefficient was tested through its p-value [$P(H_{0,2nd})$], with a significance level of $P \leq 0.05$. Therefore, the acceptance criterion for the linearity of the calibration curve was set to $P(H_{0,2nd}) > 0.05$.

The question of whether to force the regression line through the origin (i.e., $\beta_0 = 0$) has been the subject of several debates on linear regression (Meier and Zünd 2000). Although theory can justify the $\beta_0 = 0$ assumption, the reality may be somewhat more complex (Meier and Zünd 2000). Taking this into account, the statistical significance of the null value of the y-intercept was tested through its p-value [$P(H_{0,int})$], with a significance level of $P \leq 0.05$. Therefore, a linear model with y-intercept ($y = \beta_0 + \beta_1 x$) was used when $P(H_{0,int}) \leq 0.05$, whereas a linear model without y-intercept ($y = \beta_1 x$) was used when $P(H_{0,int}) > 0.05$.

All the linear and polynomial regressions were performed using R Software (version 3.1.2), Copyright © 2014, The R Foundation for Statistical Computing.

The range of each method was defined as the lower and upper analyte concentrations for which the analytical method has adequate accuracy, precision and linearity (Snyder, Kirkland and Glajch 1997).

3.4. Limit of detection

The determination of the limit of detection (LOD) of each analyte was based on a signal-to-noise ratio of 3, as suggested by Eurachem and IUPAC (Snyder, Kirkland and Glajch 1997, Taverniers, De Loose and Van Bockstaele 2004). The practical assessment of these values was performed as previously described (Taverniers, De Loose and Van Bockstaele 2004). Namely, 10 independent blank samples were analyzed, in order to determine the average peak area of

that samples (x_{bl}) and the corresponding standard deviation (s_{bl}). Afterwards, the LOD value was obtained as described in Eq. 6, where β_1 is the slope of the linear regression performed for the quantification of each component.

$$LOD = \frac{x_{bl} + 3\, s_{bl}}{\beta_1} \quad (6)$$

3.5. Limit of quantification

The limit of quantification (LOQ) of each analyte was determined exactly as in the case of the LOD, except that it was based on a signal-to-noise ratio of 10, as described in Eq. 7 (Snyder, Kirkland and Glajch 1997, Taverniers, De Loose and Van Bockstaele 2004).

$$LOQ = \frac{x_{bl} + 10\, s_{bl}}{\beta_1} \quad (7)$$

4. Results and discussion

4.1. Development and validation of the analytical methods

In this Section, the development of three distinct and independent analytical methods will be described and discussed. Furthermore, the resulting methods will undergo in-house validation studies.

4.1.1. Selection of the HPLC method

The first task of the development process was the choice of the most accurate HPLC method. Accordingly, taking into account that 4-NP, the aromatic intermediates and carboxylic acids considered in this work are non-ionic compounds soluble in water, reversed-phase HPLC was found the most appropriate solution (Lindsay 1992). For each particular analytical method, the choice of the most suitable reversed-phase HPLC column was made based on procedures previously reported elsewhere. Namely, a Kromasil 100-5-C18 column was used for 4-NP and for aromatic intermediates determinations (Apolinário et al 2008), whereas a YMC – Triart C18 column was used for carboxylic acids determination (Rocha et al 2011).

4.1.2. Selection of the detector

The next step in the development process was the selection of the most appropriate detector. It is known that UV-Vis detectors are by far the most used in HPLC (Christian 1994, Lindsay 1992), mainly due to their high sensitivity, relatively low cost and robustness towards slight temperature changes (Christian 1994). Furthermore, UV-Vis detectors are selective, since they only detect compounds that absorb a specific UV or visible radiation (Lindsay 1992). Keeping these assumptions in mind, an UV-Vis detector was chosen (Jasco UV-2075 Plus). Afterwards, UV-Vis absorbance spectra were obtained for each component, using a spectrophotometer (cf. Section 2.3). UV-Vis detector settings (i.e., appropriate absorbance wavelengths) were then selected based on the resulting spectra, which are shown in Figure 1.

It should be mentioned that the three analytical methods will be employed to the analysis of complex samples containing 4-NP, and possibly several aromatic intermediates and carboxylic acids. Therefore, the wavelength of each method should be set to a value in which potential interferences have minimal absorbance (Snyder, Kirkland and Glajch 1997). Keeping this in mind, it is observed in Figure 1a that the absorbance spectrum of 4-NP has a very well pronounced maximum at 318 nm. On the opposite, the aromatic intermediates and the carboxylic acids all have negligible absorbance at that wavelength, except 4-nitrocatechol, as it can be seen in Figures 1b and c. Therefore, the UV-Vis detector wavelength was set to 318 nm in the analytical method developed for the determination of 4-NP. The analysis of the UV-Vis absorbance spectra of the aromatic intermediates is more complex, since several

compounds must be simultaneously determined. As observed in Figure 1b, several of these aromatic intermediates have their maximum absorbance peak around 220 nm and/or around 277 nm. On the other hand, as seen in Figure 1c, most of the carboxylic acids also show maximum absorbance around 220 nm, but negligible absorbance at 277 nm. Therefore, in order to minimize possible interferences from carboxylic acids, the UV-Vis detector wavelength was set to 277 nm in the analytical method developed for the determination of aromatic intermediates. Finally, the UV-Vis detector wavelength was set to 210 nm in the analytical method developed for the determination of carboxylic acids, in this way minimizing possible interferences from aromatic intermediates. Nevertheless, it should also be mentioned at this point that possible interferences only occur with overlapped compounds (i.e. compounds leaving the HPLC column with the same retention time). Therefore, the selection of the mobile phase for the determination of carboxylic acids also takes this into consideration.

4.1.3. Selection of the mobile phase

Once the detector settings were selected, the mobile phase and the way the mobile phase is supplied to the system were also selected. A combination of mobile phase and mobile phase rate, which was initially reported for the determination of dinitrophenol and trinitrophenol (Apolinário et al 2008) was successfully adapted for the determination of 2-nitrophenol by our group (Ribeiro et al 2013b, Ribeiro et al 2015b). That adaptation was used with success in a preliminary run for the determination of 4-NP, thus being selected for the analytical method used for the determination of 4-NP. Specifically, the mobile phase consists in an isocratic method of A:B (40:60) mixture of 3% acetic acid and 1% acetonitrile in methanol (A) and 3% acetic acid in ultrapure water (B), delivered at 1 mL min^{-1}. Furthermore, this mobile phase also showed good performance when applied to the determination of aromatic intermediates. In this case, complete separation of the individual components in the mixture was achieved, as observed by the high resolution of the resulting chromatographic peaks (as confirmed by the retention times given in Table 3). On the other hand, the development of a combination of mobile phase and mobile phase rate, suitable for carboxylic acids determination, was slightly more complex. Both the mobile phase and the mobile phase rate had to be optimized through a systematic approach in which each parameter was individually assessed. In a first preliminary run, the mobile phase consisted in a sulfuric acid solution (4 mmol L^{-1}) delivered at flow rate of 0.6 mL min^{-1} (Rocha et al 2011). This combination did not allowed proper separation of the mixture components. Therefore, different sulfuric acid concentrations (in the range 4-200 mmol L^{-1}) and delivery rates (in the range 0.4-1 mL min^{-1}) were tested. None of the tested combinations resulted in a suitable separation of the mixture components. In the second approach, a mobile phase consisting in an isocratic method of A:B (95:5) mixture of 1% sulfuric acid in ultrapure water (A) and acetonitrile (B), delivered to the system at 0.8 mL min^{-1} (Yang et al 2000), was tested. This time, the resulting separation of the mixture components was better. Thus, distinct sulfuric acid concentrations (in the range 20-200 mmol L^{-1}) and delivery rates were tested (in the range 0.4-1 mL min^{-1}). The best separation was obtained when using a delivery rate of 0.6 mL min^{-1} and the composition which was previously reported by Yang et al. (Yang et al 2000). As observed by the retention times given in Table 3, complete separation of the individual components in the mixture was achieved in this way.

4.1.4. Quantitative determination

Assuming that the separation conditions were fully optimized for each analytical method, the next step was the quantitative analysis of each component. Within this scope, the peak area

was used in order to provide a value in terms of detector signal; this signal being then related to the concentration of the respective analyte through linear calibration curves (Snyder, Kirkland and Glajch 1997). The number of standards that were used for each calibration, the retention times, the linear ranges, the linear fitting parameters, the statistical significance of the null value of the y-intercepts [$P(H_{0,int})$], and the statistical significance of the null value of the second-degree coefficients [$P(H_{0,2nd})$], are given in Table 3. As detailed in Section 3.1.3, a linear model without y-intercept was used when $P(H_{0,int}) > 0.05$ and the non-linearity of the calibration curve was found insignificant when $P(H_{0,2nd}) < 0.05$. Therefore, the linear range was demonstrated for all the analytes.

4.1.5. Limit of detection and limit of quantification

The limit of detection (LOD) and the limit of quantification (LOQ) of each analyte, obtained as described in Sections 3.4 and 3.5, respectively, are given in Table 4. As observed, 4-NP presents the lowest LOD and LOQ values, whereas the carboxylic acids have the highest limits.

4.1.6. Precision and bias studies

Precision and bias studies may be considered the most important criteria for the validation of analytical methods (Taverniers, De Loose and Van Bockstaele 2004). Therefore, bias was determined for three concentration levels over the linear range, as recommended (Snyder, Kirkland and Glajch 1997, Taverniers, De Loose and Van Bockstaele 2004). The corresponding results are also given in Table 4. For more details on the exact concentrations that were used for bias determinations, please refer to Table 1. As observed in Table 4, all the values of bias are in accordance with the acceptance criterion that was established in Section 3.1 (i.e., absolute value of bias ≤ 20%).

As described in Section 3.2, repeatability precision (i.e., intra-run precision) and intermediate precision (i.e., inter-run precision) were assessed in three concentration levels over the linear range, through the so-called Horwitz ratio (HorRat). For more details on the exact concentrations that were used in the precision studies, please refer to Table 1. The results obtained in repeatability precision conditions ($HorRat_r$) and in intermediate precision conditions ($HorRat_{int}$), are shown in Figures 2 and 3, respectively. As observed, all the $HorRat_r$ and $HorRat_{int}$ values are below the maximum acceptable value that was defined in Section 3.2.

Summarizing, the accuracy and precision criteria were met in all the concentration levels that were considered. Therefore, considering the criteria established in Section 3.3 for the definition of the range of each analytical method, it can be concluded that all the analytical methods were validated in the linear range of each analyte.

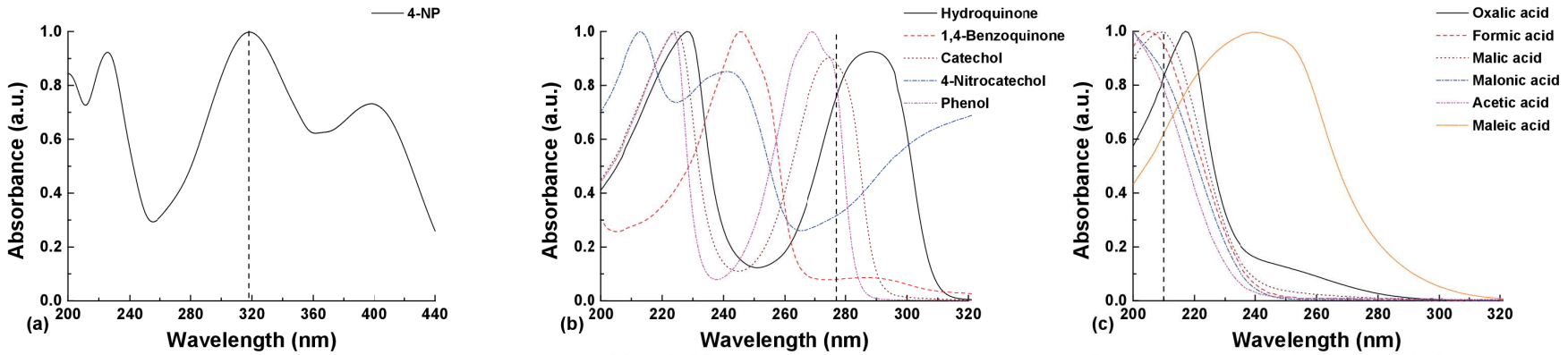

Figure 1: UV-VIS absorbance spectra of (a) 4-nitrophenol (4-NP), (b) aromatic intermediates (hydroquinone, 1,4-benzoquinone, catechol, 4-nitrocatechol and phenol) and (c) carboxylic acids (oxalic, formic, malic, malonic, acetic and maleic acids), obtained as described in Section 2.3. Vertical line points out the wavelengths selected for each determination: (a) 318 nm, (b) 277 nm and (c) 210 nm

Analyte	Retention time (min)	Std.	Linear range (mg L^{-1})	Linear fitting				$P(H_{0,2nd})$
				y-intercept	$P(H_{0,int})$	Slope	r^2	
4-NP	8.6 ± 0.1	5	0.0495 - 118.8	0	0.615	71692.6	1	0.170
Hydroquinone	1.981 ± 0.007	5	0.0449 – 179	0	0.288	17829.3	0.9993	0.063
1,4-benzoquinone	2.64 ± 0.01	6	0.0892 – 357	0	0.149	4696.3	0.9997	0.134
Catechol	3.19 ± 0.02	6	0.0468 – 93.6	0	0.308	24851.8	1	0.388
4-nitrocatechol	5.17 ± 0.09	7	0.0445 – 356	0	0.136	15410.8	1	0.245
Phenol	5.61 ± 0.07	6	0.0456 – 91.1	0	0.434	15148.4	1	0.919
Oxalic acid	5.45 ± 0.02	5	10.2 – 163	-7925.3	0.006	11992.8	1	0.170
Formic acid	5.79 ± 0.01	6	10.1 – 323	0	0.593	2043.2	0.9999	0.104
Malic acid	6.25 ± 0.04	7	20.7 – 1327	0	0.974	1674.1	0.9998	0.105
Malonic acid	7.13 ± 0.05	6	22.7 - 1456	16389.5	0.007	1716.6	1	0.419
Acetic acid	7.54 ± 0.02	6	13.5 – 431	0	0.065	729.1	0.9997	0.401
Maleic acid	9.6 ± 0.1	8	0.0989 – 31.7	-3166.7	0.007	109423.4	1	0.804

Table 3: Retention times and calibration data of each analyte (number of standards used throughout the linear range, linear fitting parameters and p-values calculated using the Fisher's exact test)

High-performance liquid chromatography as a tool to evaluate the performance of the catalytic wet peroxide oxidation of 4-nitrophenol
Rui S. Ribeiro, Adrián M.T. Silva, Helder T. Gomes, Joaquim L. Faria

Analyte	LOD (mg L^{-1})	LOQ (mg L^{-1})	bias (%)		
			Low	Medium	High
4-NP	0.0018	0.0049	10.39	-0.47	0.36
Hydroquinone	0.0082	0.023	14.98	3.22	-1.02
1,4-benzoquinone	0.031	0.086	-15.55	4.02	-0.63
Catechol	0.0059	0.016	-0.15	n.a.	-0.04
4-nitrocatechol	0.0095	0.026	-19.25	0.50	-0.04
Phenol	0.0097	0.027	-0.60	n.a.	0.00
Oxalic acid	0.19	0.60	11.32	n.a.	0.04
Formic acid	1.1	3.5	0.24	1.44	-0.36
Malic acid	1.4	4.3	-11.24	4.54	0.86
Malonic acid	1.3	4.2	0.62	0.44	-0.72
Acetic acid	3.2	9.9	8.56	0.57	0.13
Maleic acid	0.021	0.066	1.29	0.03	0.00

Table 4: Limit of detection (LOD), limit of quantification (LOQ) and bias obtained for each analyte, in low, medium and high concentration levels over the linear range

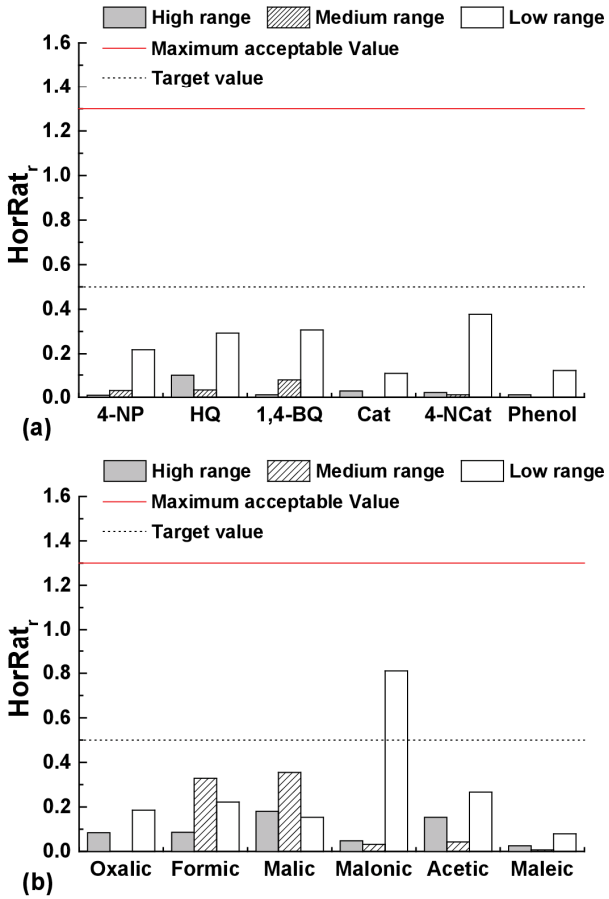

Figure 2: Horwitz ratios obtained in repeatability precision conditions (HorRatr), considering low, medium and high concentration levels over the linear range of (a) 4-nitrophenol (4-NP) and aromatic intermediates [hydroquinone (HQ), 1,4-benzoquinone (1,4-BQ), catechol (Cat), 4-nitrocatechol (4-NCat) and phenol], and (b) carboxylic acids

High-performance liquid chromatography as a tool to evaluate the performance of the catalytic wet peroxide oxidation of 4-nitrophenol
Rui S. Ribeiro, Adrián M.T. Silva, Helder T. Gomes, Joaquim L. Faria

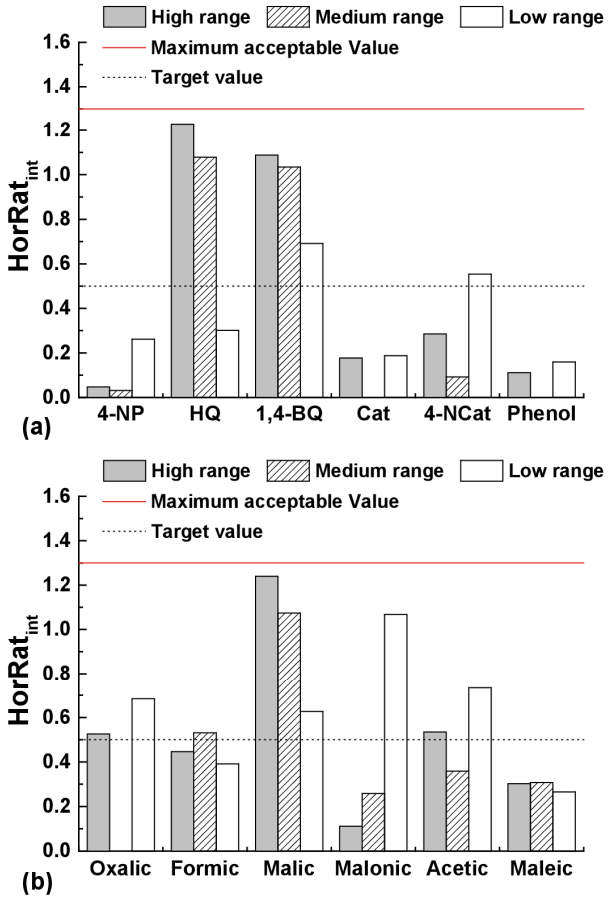

Figure 3: Horwitz ratios obtained in intermediate precision conditions (HorRatint), considering low, medium and high concentration levels over the linear range of (a) 4-nitrophenol (4-NP) and aromatic intermediates [hydroquinone (HQ), 1,4-benzoquinone (1,4-BQ), catechol (Cat), 4-nitrocatechol (4-NCat) and phenol], and (b) carboxylic acids

4.2. Application of the analytical methods

So far, a single-component HPLC analytical method suitable for the determination of 4-NP was developed and validated throughout its linear range. Although the proficiency of this particular method has already been shown in the assessment of 4-NP abatement during CWPO experiments (Ribeiro et al 2015a), further studies were now performed. Specifically, three CWPO runs were carried out under the same operating conditions, in order to assess reproducibility and error of the 4-NP determinations. Through this approach, both the analytical error and CWPO process reproducibility were evaluated. The results obtained in this study are shown in Figure 4, where it is observed that the RSD of the individual measurements never reaches 3%.

Likewise, the suitability of the two multi-component methods – one of which is devoted to the determination of possible aromatic intermediates, whereas the other is devoted to the determination of carboxylic acids – was already demonstrated in a previous work (Ribeiro et al 2015a). Figure 5 shows the oxidation/mineralization mechanism resulting from the CWPO of 4-NP, as previously proposed (Ribeiro et al 2015a), based on the application of the two analytical methods that were developed in this work.

High-performance liquid chromatography as a tool to evaluate the performance of the catalytic wet peroxide oxidation of 4-nitrophenol
Rui S. Ribeiro, Adrián M.T. Silva, Helder T. Gomes, Joaquim L. Faria

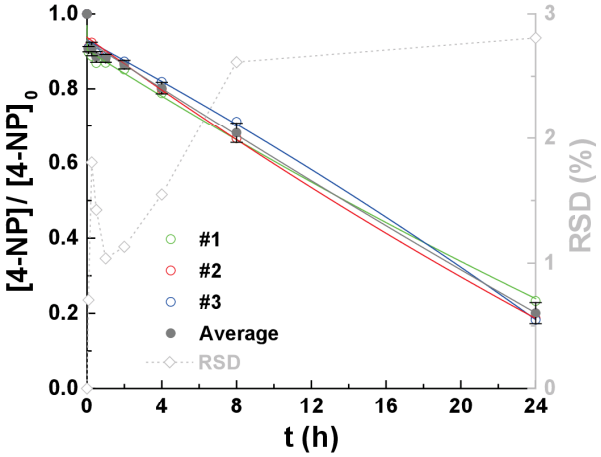

Figure 4: Reproducibility and error of 4-nitrophenol (4-NP, 5 g L^{-1}) experimental values obtained in three independent CWPO runs performed with CX/$Fe_{0.05}$ (2.5 g L^{-1}), considering T = 50 °C, pH = 3 and $[H_2O_2]_0 = [H_2O_2]_{Stoichiometric}$ = 17.8 g L^{-1}, as described in Section 2.5

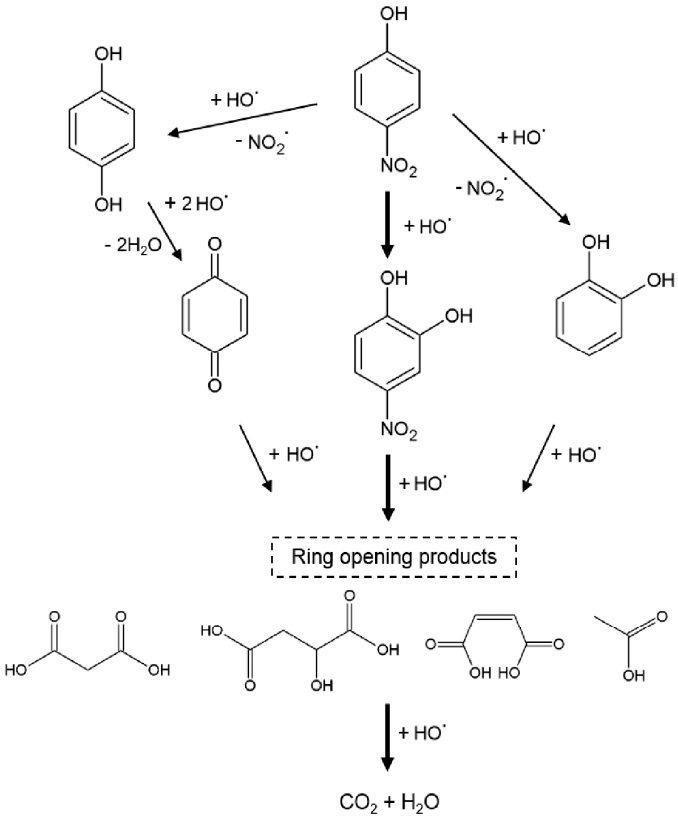

Figure 5: Mechanism proposed for the CWPO of 4-NP. Reprinted from (Ribeiro et al 2015a), Copyright © 2014, with permission from Elsevier [License number: 3554781266494]

5. Conclusions

The main conclusion withdrawn from this work is that an analytical HPLC method for the determination of the 4-NP concentration in aqueous solutions was successfully developed and validated under the acceptance criteria that were previously established for this in-house pre-

validation. The linearity of the calibration curve used for the determination of 4-NP was demonstrated through the Fisher's exact probability test. Accuracy studies have shown that the bias of this method is in the range 0.4-10%, depending on the concentration level of the analyte. Repeatability precision and intermediate precision were also assessed in three concentration levels over the linear range, through the so-called Horwitz ratio (HorRat). In this case, HorRat values never exceeded 0.26, the maximum acceptable value being 1.3. Taking all this into account, the range of the analytical method developed for the determination of 4-NP was 0.0495 - 118.8 mg L^{-1}. The CWPO process reproducibility was evaluated together with the analytical error of 4-NP determination. In this case, the sum of both contributions to error never reached 3%.

Furthermore, two multi-component HPLC analytical methods were successfully developed for the determination of possible aromatic intermediates (i.e., hydroquinone, 1,4-benzoquinone, catechol, 4-nitrocatechol and phenol) and carboxylic acids (i.e., oxalic, formic, malic, malonic, acetic and maleic acids). These methods were validated in the linear range of each analyte, under the acceptance criteria that were previously established for this in-house pre-validation. In addition, the combination of these two analytical methods already led to the proposal of an oxidation/mineralization mechanism for the CWPO of 4-NP.

References

Apolinário, Ângela C., Adrián M.T. Silva, Bruno F. Machado, Helder T. Gomes, Paulo P. Araújo, José L. Figueiredo, and Joaquim L. Faria. 2008. "Wet air oxidation of nitro-aromatic compounds: Reactivity on single- and multi-component systems and surface chemistry studies with a carbon xerogel." *Applied Catalysis B: Environmental* no. 84 (1-2):75-86. DOI: 10.1016/j.apcatb.2007.12.018.

Bautista, Patricia, Ángel F. Mohedano, Nieves Menéndez, José A. Casas, and Juan J. Rodríguez. 2010. "Catalytic wet peroxide oxidation of cosmetic wastewaters with Fe-bearing catalysts." *Catalysis Today* no. 151 (1-2):148-152. DOI: 10.1016/j.cattod.2010.01.023.

Brown, Paula N., and Ronan Yu. 2013. "Determination of ginsenoside content in panax ginseng C.A. meyer and panax quinquefolius L. root materials and finished products by high-performance liquid chromatography with ultraviolet absorbance detection: Interlaboratory study." *Journal of AOAC International* no. 96 (1):12-19. DOI: 10.5740/jaoacint.12-153.

Christian, Gary D. 1994. *Analytical chemistry*. 5th ed. New York: John Wiley & Sons, Inc.

Domínguez, Carmen M., Pilar Ocón, Asunción Quintanilla, José A. Casas, and Juan J. Rodriguez. 2013. "Highly efficient application of activated carbon as catalyst for wet peroxide oxidation." *Applied Catalysis B: Environmental* no. 140–141:663-670. DOI: 10.1016/j.apcatb.2013.04.068.

Domínguez, Carmen M., Pilar Ocón, Asunción Quintanilla, José A. Casas, and Juan J. Rodriguez. 2014a. "Graphite and carbon black materials as catalysts for wet peroxide oxidation." *Applied Catalysis B: Environmental* no. 144:599-606. DOI: 10.1016/j.apcatb.2013.07.069.

Domínguez, Carmen M., Asunción Quintanilla, José A. Casas, and Juan J. Rodriguez. 2014b. "Treatment of real winery wastewater by wet oxidation at mild temperature." *Separation and Purification Technology* no. 129:121-128. DOI: 10.1016/j.seppur.2014.04.003.

Fisher, R.A. . 1934. *Statistical methods for research workers*. Edited by F. A. E. Crew and D. Ward Cutler. 5th ed, *Biological monographs and manuals*. Edinburgh: Oliver and Boyd Ltd.

Gogate, Parag R., and Aniruddha B. Pandit. 2004. "A review of imperative technologies for wastewater treatment I: oxidation technologies at ambient conditions." *Advances in Environmental Research* no. 8 (3-4):501-551. DOI: 10.1016/S1093-0191(03)00032-7.

Gomes, Helder T., Bruno F. Machado, Andreia Ribeiro, Ivo Moreira, Márcio Rosário, Adrián M.T. Silva, José L. Figueiredo, and Joaquim L. Faria. 2008. "Catalytic properties of carbon materials for wet oxidation of aniline." *Journal of Hazardous Materials* no. 159 (2-3):420-426. DOI: 10.1016/j.jhazmat.2008.02.070.

Horwitz, William, and Richard Albert. 2006. "The Horwitz ratio (HorRat): a useful index of method performance with respect to precision." *Journal of AOAC International* no. 89 (4):1095-1109. PMID: 16915851.

Inchaurrondo, Natalia, Jorge O. Cechini, Josep Font, and Patricia Haure. 2012. "Strategies for enhanced CWPO of phenol solutions." *Applied Catalysis B: Environmental* no. 111-112:641-648. DOI: 10.1016/j.apcatb.2011.11.019.

Indyk, Harvey E., Brendon D. Gill, Jane M. Broughton, and David C. Woollard. 2014. "Application of an LC–UV method to estimate lutein recovery during infant formula manufacture." *International Dairy Journal* no. 37 (2):82-86. DOI: 10.1016/j.idairyj.2014.02.010.

Latimer, George W. 2012. "Appendix F: guidelines for standard method performance requirements." In *Official methods of analysis of AOAC International*. ISBN: 0-935584-83-8: AOAC International.

Lindsay, Sandie 1992. *High performance liquid chromatography*. Edited by John Barnes. 2nd ed, *Analytical chemistry by open learning*. Chichester: John Wiley & Sons Inc.

Loco, Joris Van, Marc Elskens, Christophe Croux, and Hedwig Beernaert. 2002. "Linearity of calibration curves: use and misuse of the correlation coefficient." *Accreditation and Quality Assurance* no. 7 (7):281-285. DOI: 10.1007/s00769-002-0487-6.

Lücking, F., Heinz Köser, Manfred Jank, and Anika Ritter. 1998. "Iron powder, graphite and activated carbon as catalysts for the oxidation of 4-chlorophenol with hydrogen peroxide in aqueous solution." *Water Research* no. 32 (9):2607-2614. DOI: 10.1016/S0043-1354(98)00016-5.

Meier, Peter C., and Richard E. Zünd. 2000. *Statistical methods in analytical chemistry*. Edited by J. D. Winefordner. 2nd ed, *A series of monographs on analytical chemistry and its applications*. New York: John Wiley & Sons, Inc.

Melero, Juan A., Fernando Martínez, Juan A. Botas, Raúl Molina, and M. Isabel Pariente. 2009. "Heterogeneous catalytic wet peroxide oxidation systems for the treatment of an industrial pharmaceutical wastewater." *Water Research* no. 43 (16):4010-4018. DOI: 10.1016/j.watres.2009.04.012.

Navalon, Sergio, Mercedes Alvaro, and Hermenegildo Garcia. 2010. "Heterogeneous Fenton catalysts based on clays, silicas and zeolites." *Applied Catalysis B: Environmental* no. 99 (1-2):1-26. DOI: 10.1016/j.apcatb.2010.07.006.

Neamţu, Mariana, Carmen Zaharia, Cezar Catrinescu, Ayfer Yediler, Matei Macoveanu, and Antonius Kettrup. 2004. "Fe-exchanged Y zeolite as catalyst for wet peroxide oxidation of reactive azo dye Procion Marine H-EXL." *Applied Catalysis B: Environmental* no. 48 (4):287-294. DOI: 10.1016/j.apcatb.2003.11.005.

Peters, Frank T. , and Hans H. Maurer. 2005. "Bioanalytical method validation and its implications for forensic and clinical toxicology - A review." In *Validation in chemical measurement*. Berlin: Springer.

Pinho, Maria T., Helder T. Gomes, Rui S. Ribeiro, Joaquim L. Faria, and Adrián M.T. Silva. 2015. "Carbon nanotubes as catalysts for catalytic wet peroxide oxidation of highly concentrated phenol solutions: towards process intensification." *Applied Catalysis B: Environmental* no. 165:706-714. DOI: 10.1016/j.apcatb.2014.10.057.

Ramirez, J. Herney, Carlos A. Costa, Luis M. Madeira, Guiomar Mata, Miguel A. Vicente, María L. Rojas-Cervantes, Antonio J. López-Peinado, and Rosa M. Martín-Aranda. 2007a. "Fenton-like oxidation of Orange II solutions using heterogeneous catalysts based on saponite clay." *Applied Catalysis B: Environmental* no. 71 (1-2):44-56. DOI: 10.1016/j.apcatb.2006.08.012.

Ramirez, J. Herney, Francisco J. Maldonado-Hódar, Agustín F. Pérez-Cadenas, Carlos Moreno-Castilla, Carlos A. Costa, and Luis M. Madeira. 2007b. "Azo-dye Orange II degradation by heterogeneous Fenton-like reaction using carbon-Fe catalysts." *Applied Catalysis B: Environmental* no. 75 (3-4):312-323. DOI: 10.1016/j.apcatb.2007.05.003.

Rey, Ana, Marisol Faraldos, Ana Bahamonde, José A. Casas, Juan A. Zazo, and Juan J. Rodríguez. 2008. "Role of the activated carbon surface on catalytic wet peroxide oxidation." *Industrial & Engineering Chemistry Research* no. 47 (21):8166-8174. DOI: 10.1021/ie800538t.

Ribeiro, Rui S., Nady A. Fathy, Amina A. Attia, Adrián M.T. Silva, Joaquim L. Faria, and Helder T. Gomes. 2012. "Activated carbon xerogels for the removal of the anionic azo dyes Orange II and Chromotrope 2R by adsorption and catalytic wet peroxide oxidation." *Chemical Engineering Journal* no. 195-196:112-121. DOI: 10.1016/j.cej.2012.04.065.

Ribeiro, Rui S., Adrián M.T. Silva, José L. Figueiredo, Joaquim L. Faria, and Helder T. Gomes. 2013a. "The influence of structure and surface chemistry of carbon materials on the decomposition of hydrogen peroxide." *Carbon* no. 62:97-108. DOI: 10.1016/j.carbon.2013.06.001.

Ribeiro, Rui S., Adrián M.T. Silva, José. L Figueiredo, Joaquim L. Faria, and Helder T. Gomes. 2013b. "Removal of 2-nitrophenol by catalytic wet peroxide oxidation using carbon materials with different morphological and chemical properties." *Applied Catalysis B: Environmental* no. 140:356-362. DOI: 10.1016/j.apcatb.2013.04.031.

Ribeiro, Rui S., Adrián M.T. Silva, Luisa M. Pastrana-Martínez, José L. Figueiredo, Joaquim L. Faria, and Helder T. Gomes. 2015a. "Graphene-based materials for the catalytic wet peroxide oxidation of highly concentrated 4-nitrophenol solutions." *Catalysis Today*, in press. DOI: 10.1016/j.cattod.2014.10.004.

Ribeiro, Rui S., Adrián M.T. Silva, Maria T. Pinho, José L. Figueiredo, Joaquim L. Faria, and Helder T. Gomes. 2015b. "Development of glycerol-based metal-free carbon materials for environmental catalytic applications." *Catalysis Today* no. 240, Part A:61-66. DOI: 10.1016/j.cattod.2014.03.048.

Rocha, Raquel P., Juliana P.S. Sousa, Adrián M.T. Silva, Manuel F.R. Pereira, and José L. Figueiredo. 2011. "Catalytic activity and stability of multiwalled carbon nanotubes in catalytic wet air oxidation of oxalic acid: The role of the basic nature induced by the surface chemistry." *Applied Catalysis B: Environmental* no. 104 (3-4):330-336. DOI: 10.1016/j.apcatb.2011.03.009.

Santos, Vera P., Manuel F.R. Pereira, P.C.C. Faria, and José J.M. Órfão. 2009. "Decolourisation of dye solutions by oxidation with H_2O_2 in the presence of modified activated carbons." *Journal of Hazardous Materials* no. 162 (2-3):736-742. DOI: 10.1016/j.jhazmat.2008.05.090.

Sasaki, Kazunori, Tomoyuki Oki, Toru Kobayashi, Yumi Kai, and Shigenori Okuno. 2014. "Single-laboratory validation for the determination of caffeic acid and seven caffeoylquinic acids in sweet potato leaves." *Bioscience, Biotechnology, and Biochemistry* no. 78 (12):2073-2080. DOI: 10.1080/09168451.2014.942253.

Snyder, Lloyd R., Joseph J. Kirkland, and Joseph L. Glajch. 1997. *Practical HPLC method development*. 2nd ed. Hoboken: John Wiley & Sons, Inc.

Taran, Oxana, Elena Polyanskaya, Olga Ogorodnikova, Vladimir Kuznetsov, Valentin Parmon, Michèle Besson, and Claude Descorme. 2010. "Influence of the morphology and the surface chemistry of carbons on their catalytic performances in the catalytic wet peroxide oxidation of organic contaminants." *Applied Catalysis A: General* no. 387 (1-2):55-66. DOI: 10.1016/j.apcata.2010.08.001.

Taverniers, Isabel, Marc De Loose, and Erik Van Bockstaele. 2004. "Trends in quality in the analytical laboratory. II. Analytical method validation and quality assurance." *Trends in Analytical Chemistry* no. 23 (8):535-552. DOI: 10.1016/j.trac.2004.04.001.

UNODC. 2009. Guidance for the validation of analytical methodology and calibration of equipment used for testing of illicit drugs in seized materials and biological specimens. New York: United Nations Office on Drugs and Crime (UNODC).

USEPA. 1997. Recommended guidelines for measuring organic compounds in puget sound water, sediment and tissue samples. Seattle: U. S. Environmental Protection Agency (USEAP).

Yang, Libo , Li Liu, Bernard A. Olsen, and Mark A. Nussbaum. 2000. "The determination of oxalic acid, oxamic acid, and oxamide in a drug substance by ion-exclusion chromatography." *Journal of Pharmaceutical and Biomedical Analysis* no. 22 (3):487-493. DOI: 10.1016/S0731-7085(00)00230-2.

Acknowledgments

Work supported by project PEst-C/EQB/LA0020/2013, co-financed by FEDER through COMPETE, QREN and ON2, and by FCT – Fundação para a Ciência e a Tecnologia. Rui S. Ribeiro acknowledges financial support from the FCT individual Ph.D. grant SFRH/BD/94177/2013. Adrián M.T. Silva acknowledges the FCT Investigator 2013 Programme (IF/01501/2013), with financing from the European Social Fund and the Human Potential Operational Programme.

C. SUPPLEMENTARY INFORMATION

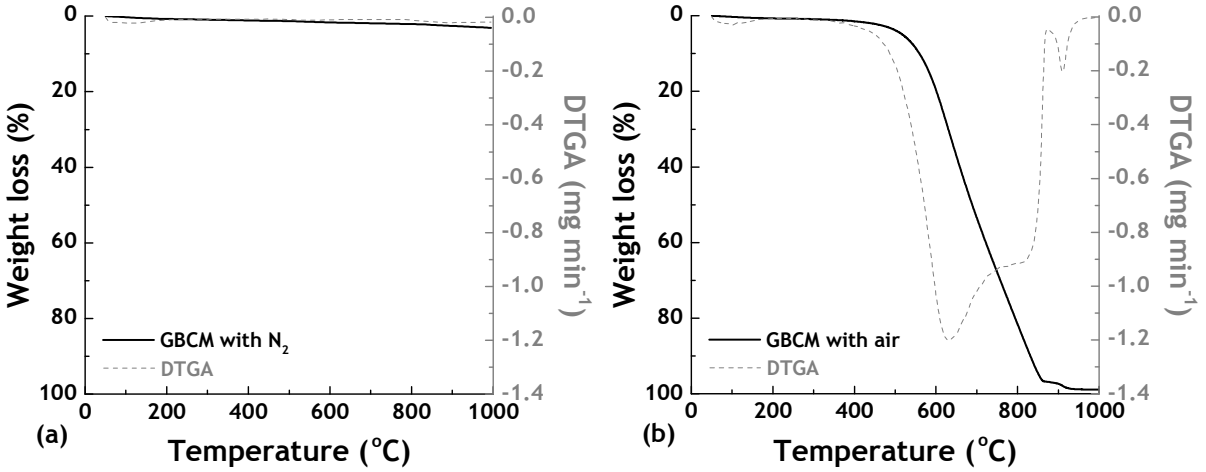

Figure C.1. Thermogravimetric analysis (TGA) of GBCM in (a) N_2 and (b) air atmosphere.

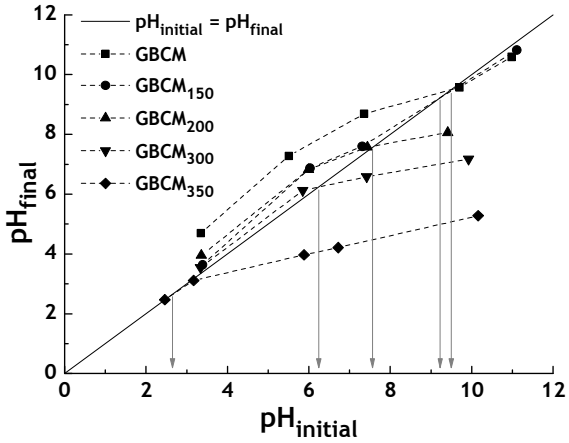

Figure C.2. pH drift tests performed for the determination of the pH at the point of zero charge (pH_{PZC}) of the GBCM materials.

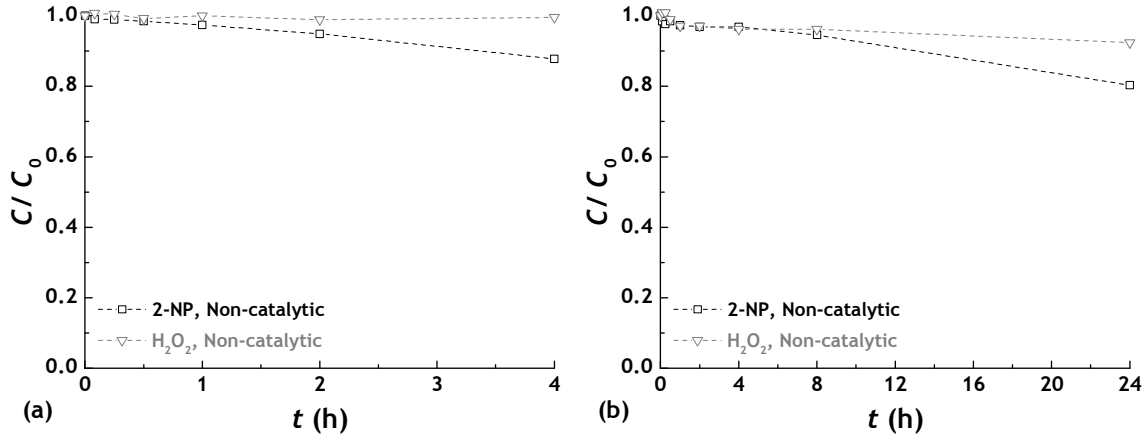

Figure C.3. 2-NP and H_2O_2 conversions obtained as a function of time in non-catalytic (blank) experiments performed with T = 50 ºC, pH = 3, and (a) $[2\text{-NP}]_0$ = 0.1 g L^{-1} and $[H_2O_2]_0$ = 1.18 g L^{-1}; and (b) $[2\text{-NP}]_0$ = 0.5 g L^{-1} and $[H_2O_2]_0$ = 1.78 g L^{-1}.

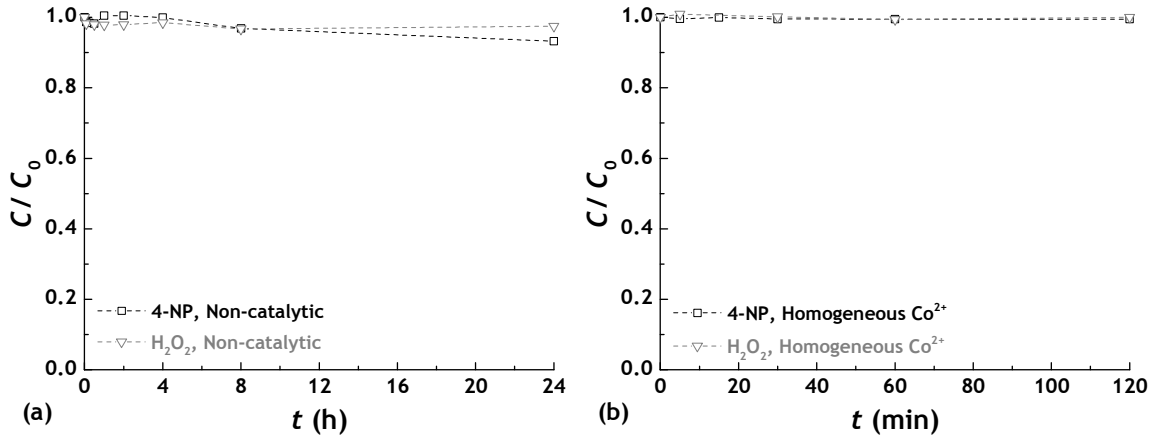

Figure C.4. 4-NP and H_2O_2 conversions obtained as a function of time in a (a) non-catalytic (blank) experiment and (b) homogeneous CWPO run performed with Co^{2+} (126 mg L^{-1}). Experiments performed with $[4\text{-NP}]_0$ = 5.0 g L^{-1}, $[H_2O_2]_0$ = 17.8 g L^{-1} , T = 50 ºC and pH = 3.

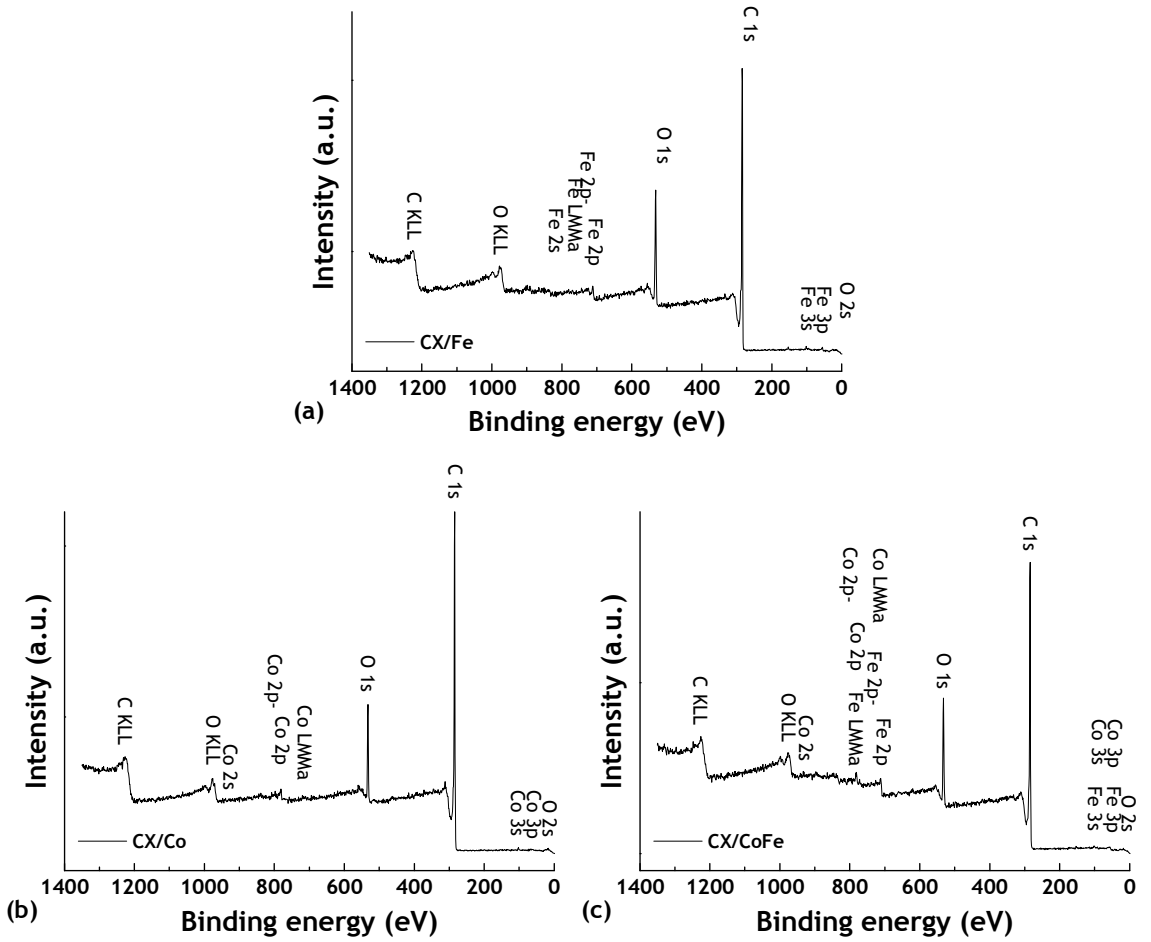

Figure C.5. XPS spectra of (a) CX/Fe, (b) CX/Co and (c) CX/CoFe.

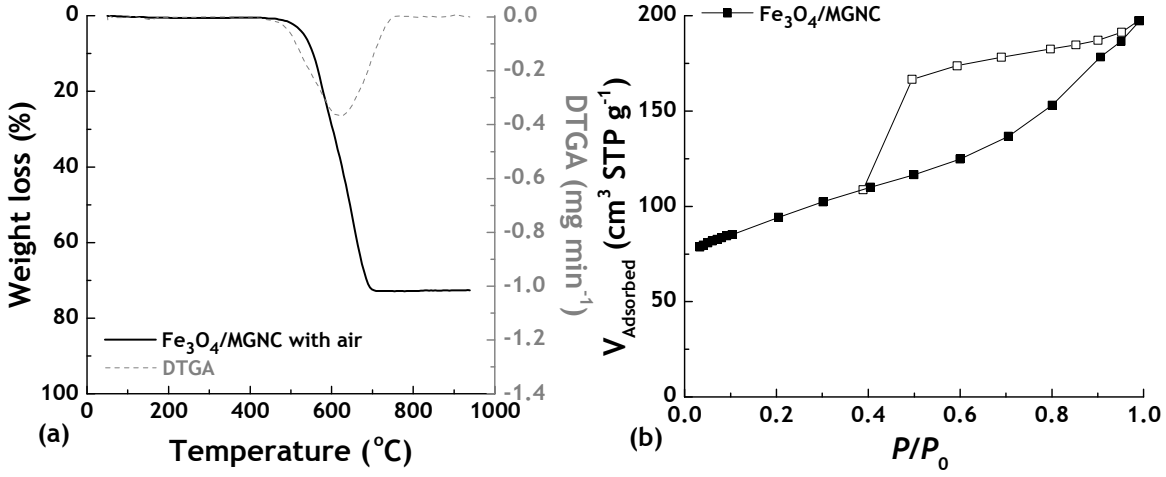

Figure C.6. (a) Thermogravimetric analysis (TGA) of Fe_3O_4/MGNC in air atmosphere; (b) N_2 adsorption-desorption isotherm at -196 ºC of Fe_3O_4/MGNC.

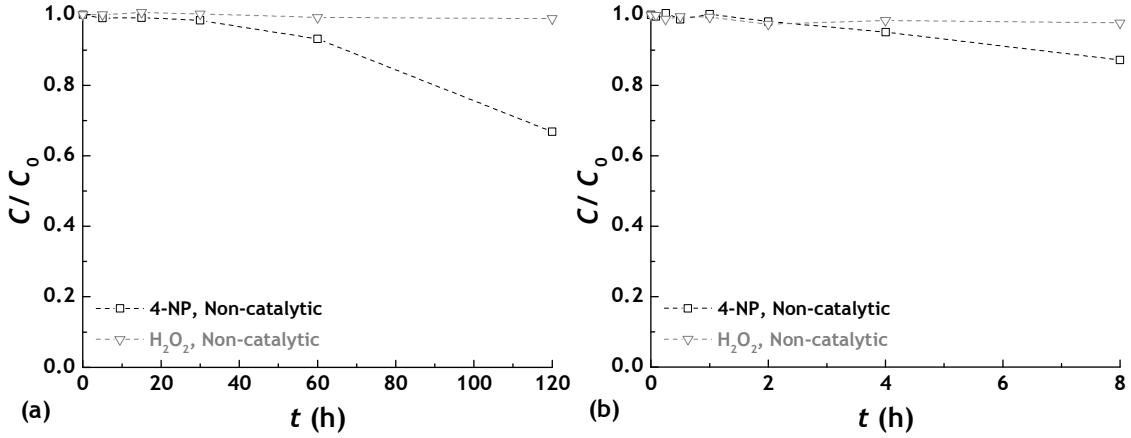

Figure C.7. 4-NP and H_2O_2 conversions obtained as a function of time in non-catalytic (blank) experiments performed with T = 80 ºC, pH = 3 and (a) $[4\text{-NP}]_0$ = 0.2 g L^{-1} and $[H_2O_2]_0$ = 0.712 g L^{-1}, and (b) $[4\text{-NP}]_0$ = 5.0 g L^{-1} and $[H_2O_2]_0$ = 17.8 g L^{-1}.

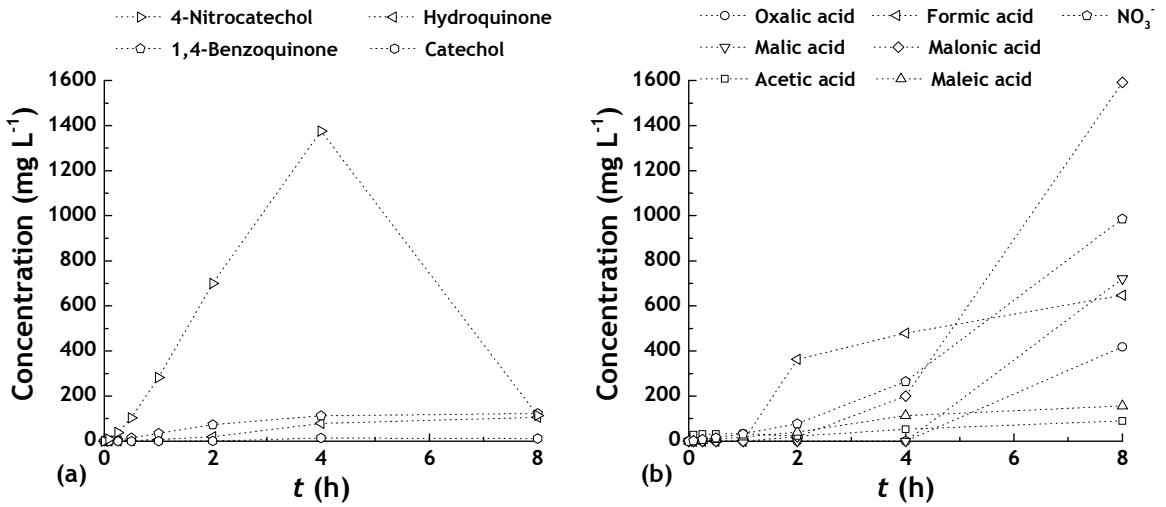

Figure C.8. Evolution of (a) aromatic and (b) non-aromatic by-products of 4-NP oxidation, when using Fe_3O_4/MGNC in the CWPO process developed with $[4\text{-NP}]_0$ = 5.0 g L^{-1}, $[Fe_3O_4/MGNC]$ = 0.5 g L^{-1}, $[H_2O_2]_0$ = 17.8 g L^{-1} (stoichiometric amount), T = 80 ºC and pH = 3.

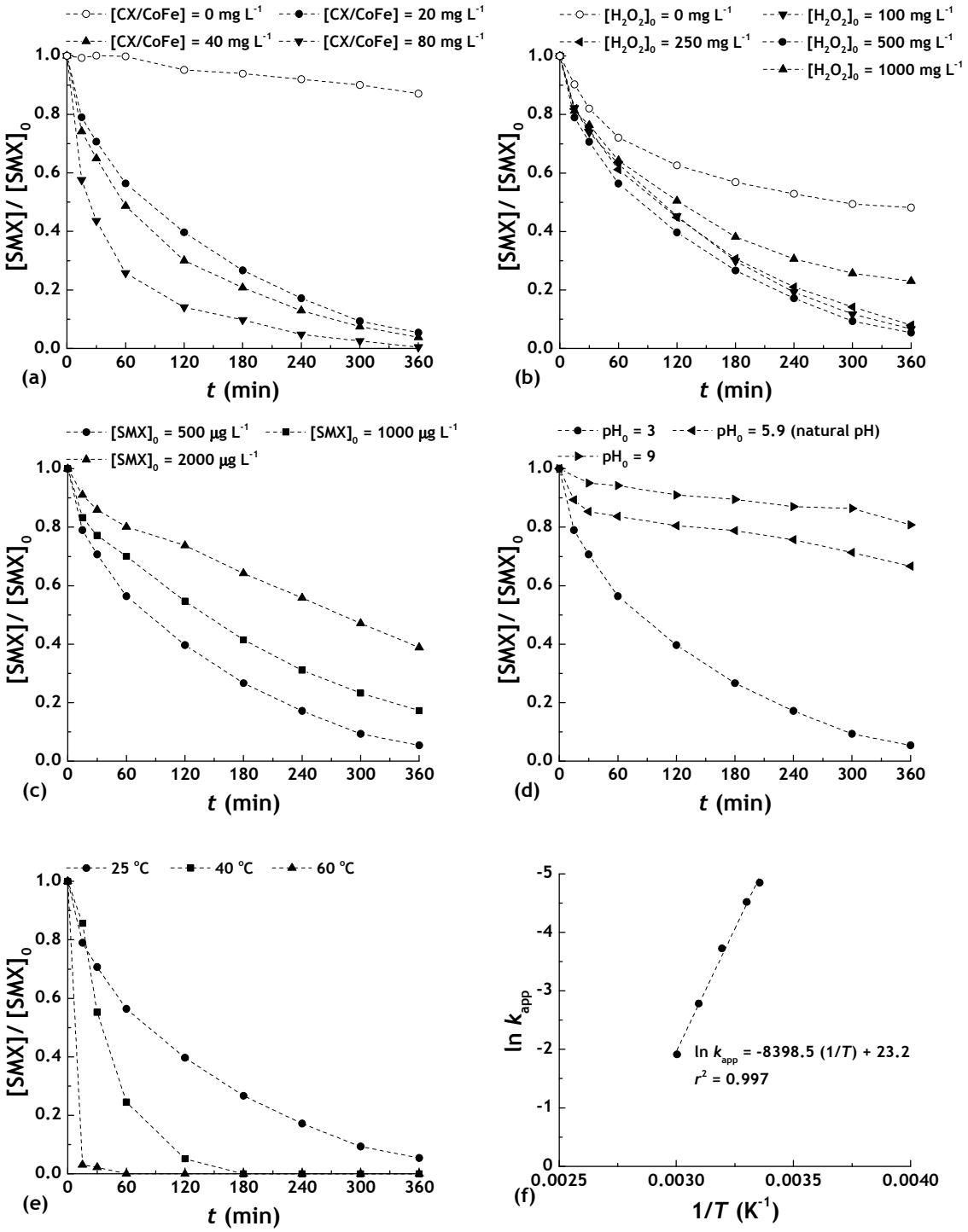

Figure C.9. Effect of (a) catalyst load, (b) $[H_2O_2]_0$, (c) $[SMX]_0$, (d) pH_o and (e) temperature, on the removal of SMX when using CX/CoFe. (f) Arrhenius plot of the k_{app} values obtained at T = 25, 30, 40, 50 and 60 ºC.

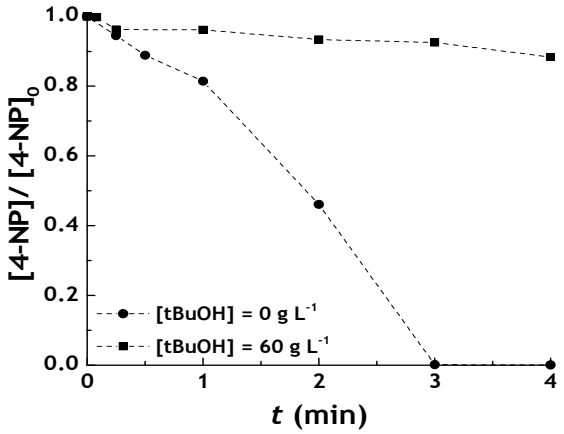

Figure C.10. Effect of *tert*-butanol (tBuOH) on the 4-NP removal by CWPO, when using $CoFe_2O_4$/MGNC. Experiments performed with $[4\text{-NP}]_0$ = 5.0 g L^{-1}, $[CoFe_2O_4/MGNC]$ = 0.5 g L^{-1}, $[H_2O_2]_0$ = 17.8 g L^{-1} (stoichiometric amount), T = 80 ºC and pH = 3.

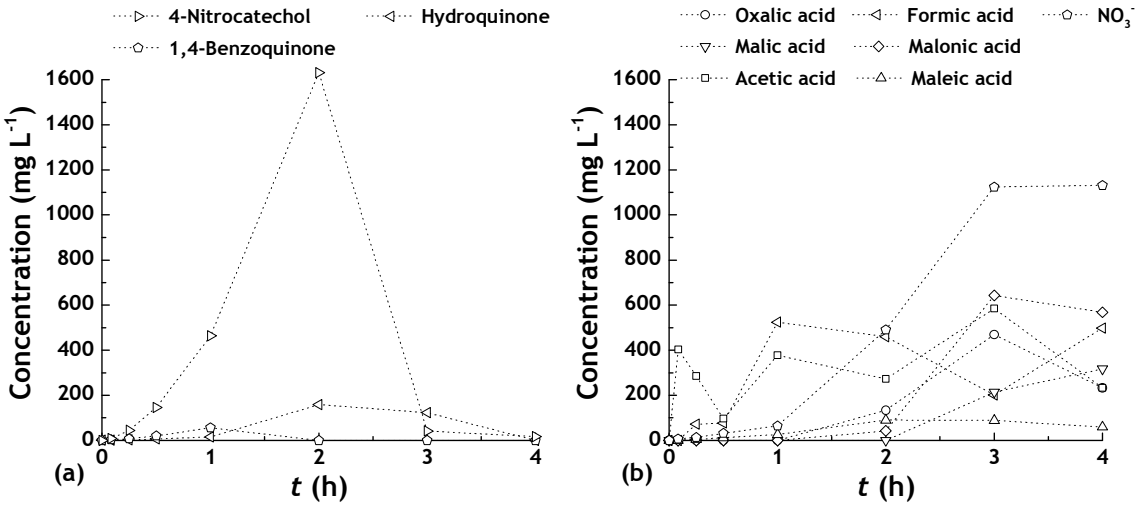

Figure C.11. Evolution of (a) aromatic and (b) non-aromatic by-products of 4-NP oxidation, when using $CoFe_2O_4$/MGNC in the CWPO process developed with $[4\text{-NP}]_0$ = 5.0 g L^{-1}, $[CoFe_2O_4/MGNC]$ = 0.5 g L^{-1}, $[H_2O_2]_0$ = 17.8 g L^{-1} (stoichiometric amount), T = 80 ºC and pH = 3.

D. PUBLICATIONS

D.1. International peer reviewed ISI indexed journals

[7] **Rui S. Ribeiro**, Raquel O. Rodrigues, Adrián M.T. Silva, Pedro B. Tavares, Ana M.C. Carvalho, José L. Figueiredo, Joaquim L. Faria, Helder T. Gomes, Hybrid magnetic graphitic nanocomposites towards catalytic wet peroxide oxidation of the liquid effluent from a mechanical biological treatment plant for municipal solid waste, Appl. Catal. B 219 (2017) 645-657
DOI: 10.1016/j.apcatb.2017.08.013

[6] **Rui S. Ribeiro**, Adrián M.T. Silva, José L. Figueiredo, Joaquim L. Faria, Helder T. Gomes, The role of cobalt in bimetallic iron-cobalt magnetic carbon xerogels developed for catalytic wet peroxide oxidation, Catal. Today 296 (2017) 66-75
DOI: 10.1016/j.cattod.2017.06.023

[5] **Rui S. Ribeiro**, Adrián M.T. Silva, Pedro B. Tavares, José L. Figueiredo, Joaquim L. Faria, Helder T. Gomes, Hybrid magnetic graphitic nanocomposites for catalytic wet peroxide oxidation applications, Catal. Today 280 (2017) 184-191
DOI: 10.1016/j.cattod.2016.04.040

[4] **Rui S. Ribeiro**, Zacharias Frontistis, Dionissios Mantzavinos, Danae Venieri, Maria Antonopoulou, Ioannis K. Konstantinou, Adrián M.T. Silva, Joaquim L. Faria, Helder T. Gomes, Magnetic carbon xerogels for the catalytic wet peroxide oxidation of sulfamethoxazole in environmentally relevant water matrices, Appl. Catal. B 199 (2016) 170-186
DOI: 10.1016/j.apcatb.2016.06.021

[3] **Rui S. Ribeiro**, Adrián M.T. Silva, José L. Figueiredo, Joaquim L. Faria, Helder T. Gomes, Catalytic wet peroxide oxidation: a route towards the application of hybrid magnetic carbon nanocomposites for the degradation of organic pollutants. A review, Appl. Catal. B 187 (2016) 428-460
DOI: 10.1016/j.apcatb.2016.01.033

[2] **Rui S. Ribeiro**, Adrián M.T. Silva, Luisa M. Pastrana-Martínez, José L. Figueiredo, Joaquim L. Faria, Helder T. Gomes, Graphene-based materials for the catalytic wet peroxide oxidation of highly concentrated 4-nitrophenol solutions, Catal. Today 249 (2015) 204-212
DOI: 10.1016/j.cattod.2014.10.004

[1] **Rui S. Ribeiro**, Adrián M.T. Silva, Maria T. Pinho, José L. Figueiredo, Joaquim L. Faria, Helder T. Gomes, Development of glycerol-based metal-free carbon materials for environmental catalytic applications, Catal. Today 240, Part A (2015) 61-66
DOI: 10.1016/j.cattod.2014.03.048

D.2. National peer reviewed journals

[1] **Rui S. Ribeiro**, Adrián M.T. Silva, Helder T. Gomes, Joaquim L. Faria, High-performance liquid chromatography as a tool to evaluate the performance of the catalytic wet peroxide oxidation of 4-nitrophenol: pre-validation of analytical methods, U.Porto Journal of Engineering (Portugal) 1 (2015) 50-66
http://journalengineering.fe.up.pt/article/view/112

D.3. Papers in conference proceedings

[2] **Rui S. Ribeiro**, Adrián M.T. Silva, José L. Figueiredo, Joaquim L. Faria, Helder T. Gomes, Desenvolvimento de xerogéis de carbono magnéticos para o processo de oxidação catalítica com peróxido de hidrogénio, in: "CICAT 2016 – XXV Congreso Iberoamericano de Catálisis", 18 – 23 September 2016, Montevideo, Uruguay
http://opc.cicat2016.org/tl/236_rui_s._ribeiro.pdf. 236

[1] **Rui S. Ribeiro**, Adrián M.T. Silva, José L. Figueiredo, Joaquim L. Faria, Helder T. Gomes, Hybrid magnetic graphitic nanocomposites for catalytic wet peroxide oxidation applications, in: "EAAOP4 – 4th European Conference on Environmental Applications of Advanced Oxidation Processes", 21 – 24 October 2015, Athens, Greece
https://cloud.ipb.pt/f/6f673414094b4a4c813a/?dl=1

E. COMMUNICATIONS IN SCIENTIFIC MEETINGS

E.1. Oral presentations

[9] **Rui S. Ribeiro***, Adrián M.T. Silva, Joaquim L. Faria, Helder T. Gomes, From nano- to macro-scale: hybrid magnetic carbon nanocomposites as a tool for catalytic wet peroxide oxidation, invited keynote lecture in: "Carbon 2018", 1 – 6 July 2018, Madrid, Spain

[8] **Rui S. Ribeiro**, Raquel O. Rodrigues, Ana M.C. Carvalho, Adrián M.T. Silva, José L. Figueiredo, Joaquim L. Faria, Helder T. Gomes*, Catalytic wet peroxide oxidation as a solution for the treatment of liquid effluents from mechanical biological treatment plants for municipal solid waste, in: "EuropaCat 2017 – 13th European Congress on Catalysis", 27 – 31 August 2017, Florence, Italy

[7] **Rui S. Ribeiro***, Adrián M.T. Silva, Joaquim L. Faria, Helder T. Gomes, Development of bimetallic iron-cobalt hybrid magnetic carbon composites for catalytic wet peroxide oxidation, a student short oral communication in: "2nd Summer School on Environmental Applications of Advanced Oxidation Processes and Training School on Advanced Treatment Technologies and Contaminants of Emerging Concern (NEREUS COST Action ES1403)", 10 – 14 July 2017, Porto, Portugal

[6] **Rui S. Ribeiro***, Raquel O. Rodrigues, Ana M.C. Carvalho, Adrián M.T. Silva, José L. Figueiredo, Joaquim L. Faria, Helder T. Gomes, Optimization of magnetic graphitic nanocomposites for the catalytic wet peroxide oxidation of liquid effluents from a mechanical biological treatment plant for municipal solid waste, a student paper communication in: "EAAOP5 – 5th European Conference on Environmental Applications of Advanced Oxidation Processes", 25 – 29 June 2017, Prague, Czech republic

[5] **Rui S. Ribeiro***, Zacharias Frontistis, Dionissios Mantzavinos, Adrián M.T. Silva, Joaquim L. Faria, Helder T. Gomes, The influence of the water matrix on the performance of sulfamethoxazole removal by catalytic wet peroxide oxidation, in: "XXII Encontro Luso-Galego de Química", 9 – 11 November 2016, Bragança, Portugal

[4] **Rui S. Ribeiro**, Adrián M.T. Silva, José L. Figueiredo, Joaquim L. Faria, Helder T. Gomes*, Desenvolvimento de xerogéis de carbono magnéticos para o processo de oxidação catalítica com peróxido de hidrogénio, in: "CICAT 2016 – XXV Congreso Iberoamericano de Catálisis", 18 – 23 September 2016, Montevideo, Uruguay

[3] **Rui S. Ribeiro***, Adrián M.T. Silva, Pedro B. Tavares, José L. Figueiredo, Joaquim L. Faria, Helder T. Gomes, Core-shell nanocomposites prepared by hierarchical co-assembly: the role of the carbon shell in catalytic wet peroxide oxidation processes, in: "Carbocat VII – 7th International Symposium on Carbon for Catalysis", 12 – 16 June 2016, Strasbourg, France

[2] Helder T. Gomes, **Rui S. Ribeiro***, Adrián M.T. Silva, Luisa M. Pastrana-Martínez, José L. Figueiredo, Joaquim L. Faria, The influence of carbon material properties in the efficiency of catalytic wet peroxide oxidation processes, in: "Carbon 2015", 12 – 17 July 2015, Dresden, Germany

[1] **Rui S. Ribeiro***, Adrián M.T. Silva, Luisa M. Pastrana-Martínez, José L. Figueiredo, Joaquim L. Faria, Helder T. Gomes, Key parameters when developing carbonaceous materials for catalytic wet peroxide oxidation, in: "XX Encontro Luso-Galego de Química", 26 – 28 November 2014, Porto, Portugal

*Presenting Author

E.2. Poster presentations

[10] **Rui S. Ribeiro***, Adrián M.T. Silva, Joaquim L. Faria, Helder T. Gomes, High-performance liquid chromatography in routine environmental analysis: in-house validation of analytical methods, in: "10.º Encontro Nacional de Cromatografia", 4 – 6 December 2017, Bragança, Portugal

[9] **Rui S. Ribeiro***, Adrián M.T. Silva, Joaquim L. Faria, Helder T. Gomes, Development of bimetallic iron-cobalt hybrid magnetic carbon composites for catalytic wet peroxide oxidation, in: "2nd Summer School on Environmental Applications of Advanced Oxidation Processes and Training School on Advanced Treatment Technologies and Contaminants of Emerging Concern (NEREUS COST Action ES1403)", 10 – 14 July 2017, Porto, Portugal

[8] **Rui S. Ribeiro***, Adrián M.T. Silva, Joaquim L. Faria, Helder T. Gomes, Hybrid magnetic carbon nanocomposites: a tool for environmental catalytic applications, in: "Ciência 2017 – Encontro com a Ciência e Tecnologia em Portugal", 3 – 5 July 2017, Lisboa, Portugal

[7] **Rui S. Ribeiro***, Raquel O. Rodrigues, Ana M.C. Carvalho, Adrián M.T. Silva, José L. Figueiredo, Joaquim L. Faria, Helder T. Gomes, Optimization of magnetic graphitic nanocomposites for the catalytic wet peroxide oxidation of liquid effluents from a mechanical biological treatment plant for municipal solid waste, in: "EAAOP5 – 5th European Conference on Environmental Applications of Advanced Oxidation Processes", 25 – 29 June 2017, Prague, Czech republic

[6] **Rui S. Ribeiro***, Raquel O. Rodrigues, Adrián M.T. Silva, Pedro B. Tavares, José L. Figueiredo, Joaquim L. Faria, Helder T. Gomes, Core-shell magnetic carbon nanocomposites for catalytic wet peroxide oxidation, in: "I Reunião do Grupo do Carbono", 12 – 13 June 2017, Porto, Portugal

[5] **Rui S. Ribeiro***, Adrián M.T. Silva, José L. Figueiredo, Joaquim L. Faria, Helder T. Gomes, Development of magnetic carbon xerogels for catalytic wet peroxide oxidation, in: "X ENCMP – 10.º Encontro Nacional de Catálise e Materiais Porosos" 19 – 20 May 2016, Lisboa, Portugal

[4] **Rui S. Ribeiro**, Zacharias Frontistis, Dionissios Mantzavinos, Adrián M.T. Silva, Joaquim L. Faria, Helder T. Gomes*, Novel hybrid magnetic carbon xerogels for the catalytic wet peroxide oxidation of the antimicrobial agent sulfamethoxazole, in: "XXI Encontro Galego-Portugués de Química", 18 – 20 November 2015, Pontevedra, Spain

[3] **Rui S. Ribeiro***, Adrián M.T. Silva, José L. Figueiredo, Joaquim L. Faria, Helder T. Gomes, Hybrid magnetic graphitic nanocomposites for catalytic wet peroxide oxidation applications, in: "EAAOP4 – 4th European Conference on Environmental Applications of Advanced Oxidation Processes", 21 – 24 October 2015, Athens, Greece

[2] **Rui S. Ribeiro**, Adrián M.T. Silva, Joaquim L. Faria*, Helder T. Gomes, Magnetic carbon xerogels for the catalytic wet peroxide oxidation of 4-nitrophenol solutions, in: "EuropaCat 2015 – 12th European Congress on Catalysis", 30 August – 4 September 2015, Kazan, Russia

[1] **Rui S. Ribeiro***, Adrián M.T. Silva, José L. Figueiredo, Joaquim L. Faria, Helder T. Gomes, Development of magnetically recoverable carbon nanocomposites for the catalytic wet peroxide oxidation of 4-nitrophenol solutions, in: "Carbon 2015", 12 – 17 July 2015, Dresden, Germany

*Presenting Author